NOTICE

The quality of this microform is heavily dependent upon the quality of the original thesis submitted for microfilming. Every effort has been made to ensure the highest quality of reproduction possible.

If pages are missing, contact the university which granted the degree.

Some pages may have indistinct print especially if the original pages were typed with a poor typewriter ribbon or if the university sent us an inferior photocopy.

Reproduction in full or in part of this microform is governed by the Canadian Copyright Act, R.S.C. 1970, c. C-30, and subsequent amendments.

AVIS

La qualité de cette microforme dépend grandement de la qualité de la thèse soumise au microfilmage. Nous avons tout fait pour assurer une qualité supérieure de reproduction.

S'il manque des pages, veuillez communiquer avec l'université qui a conféré le grade

La qualité d'impression de certaines pages peut laisser à désirer, surtout si les pages originales ont été dactylographiées à l'aide d'un ruban usé ou si l'université nous a fait parvenir une photocopie de qualité inférieure.

La reproduction, même partielle, de cette microforme est soumise à la Loi canadienne sur le droit d'auteur, SRC 1970, c. C-30, et ses amendements subséquents.

ISBN 0-315-56062-2

Techniques for Improving the Performance of a Simplified Electronic Fuel Controller with Incremental Actuation for Small Gas Turbine Engines

Antonios Ioannou Georgantas

A Thesis

in

The Department

of

Mechanical Engineering

Presented in Partial Fulfillment of the Requirements
for the Degree of Doctor of Philosophy at
Concordia University
Montreal, Quebec, Canada

April 1990

ABSTRACT

Techniques for Improving the Performance of a Simplified Electronic Fuel Controller with Incremental Actuation for Small Gas Turbine Engines

Antonios Ioannou Georgantas, PH.D
Concordia University, 1990

This work introduces concepts which improve the performance of an inexpensive electronic fuel control unit for small gas turbine engines. A conventional hydromechanical fuel control unit is modified and adapted for digital electronic control. The conversion involves the replacement of the pneumatic computing/actuating mechanism with digital computation and incremental electronic actuation of a flow metering valve.

A mathematical model of the unit is developed, implemented and validated. The model is used for simulation and study of the system dynamics. Some new methods are applied in the design and development of a digital controller. An optimization scheme for tuning the controller is formulated and implemented experimentally.

As a next step towards improvement of the simple electronic fuel controller, a concept of two electronic actuators, one operating the metering valve and the other a by-pass valve, is introduced and investigated. Higher flexibility and faster transient response, as compared to

the conventional system and the single actuator unit, are demonstrated. The possibility of a back-up scheme in case of failure of one of two actuating mechanisms is also discussed.

ACKNOWLEDGEMENT

The author is deeply indebted to Dr. T. Krepec, his supervisor, for his constant enthusiasm and help throughout the course of this work. Thanks are extended to Dr. R.M.H. Cheng for his invaluable support and advice.

The help of the machine shop technical staff for the construction of several parts needed for the electronic control unit prototypes, is greatly appreciated. Special thanks go to my colleagues and friends Mr. Gino Carrese and Mr. Carmine Lisio for many valuable discussions we had while working at the Fuel Controls Laboratory.

The author also wishes to express his gratitude to his family for their encouragement and understanding.

Finally, thanks go to the Natural Science and Engineering Research Council of Canada for their financial support without which the present work would not have been possible. Also the interest and support of Bendix Avelex Inc. is very much appreciated.

TABLE OF CONTENTS

CHAPTER 5

EXPERIMENTAL STUDY - CONCEPT FEASIBILITY

CHAPTER 6

MATHEMATICAL MODEL OF METERING SECTION

CHAPTER 7

VALIDATION OF MATHEMATICAL MODEL

CHAPTER 8

DESIGN OF A DIGITAL CONTROLLER

CHAPTER 9

EXPERIMENTAL TUNING OF THE DIGITAL CONTROLLER

CHAPTER 10

ELECTRONIC FUEL CONTROL UNIT WITH TWO DIGITAL ACTUATORS

CHAPTER 11

CHAPTER 12

LIST OF FIGURES

NOMENCLATURE

a_1, a_2, a_3	- metering valve flow area coefficients
A	- flow area
A_{De}	- by-pass effective valve diaphragm area
A_e	- flow force coefficient
A_f	- pressure area in lower end of by-pass valve
A_1	- minimum pressurizing valve downstream pressure area
A_2	- minimum pressurizing valve upstream pressure area
A_3	- minimum pressurizing valve return line pressure area
b_1, b_2, b_3	- by-pass valve flow area constants
B	- damping coefficient
C_d	- flow coefficient
CLP	- rotor collective pitch
c_1, c_2	- minimum pressurizing valve flow area constants
C_1	- pump displacement
C_2	- pump leakage coefficient
C_3	- pump flow constant
D	- diameter
D_{bo}	- by-pass valve orifice diameter
D_{po}	- pressurizing valve orifice diameter
e	- error signal
E	- numerical error in S
f	- actuator triggering frequency

F - force

$f(\underline{X})$ - objective function

$F(\underline{x})$ - set of non-linear equations

$\underline{g}$ - gradient vector

G - constraint function

GH - Pulse transfer function

g_i - partial derivative of objective function with with respect to k_i

g_{i1} - discretized partial derivative of objective function with respect to k_i with $\Delta k_i = 0.1\ k_i$

g_{i2} - discretized partial derivative of objective function with respect to k_i with $\Delta k_i = 0.2\ k_i$

g_{i3} - discretized partial derivative of objective function with respect to k_i with $\Delta k_i = 0.3\ k_i$

$G(s)$ - process transfer function

k - spring rate

K - constant, plant gain constant, penalty multiplier

KH - Pulse transfer function of closed loop

$K(s)$ - closed loop transfer function

K_{f1} - by-pass valve flow force rate

K_{f2} - by-pass valve flow force constant

k_1 - proportional controller gain

k_2 - integral controller gain

k_3 - derivative controller gain

$J(\underline{x})$ - Jacobian of $F(\underline{x})$

J_1 - penalized ISE index

J_2 - penalized ITAE index

J_3 - penalized IAE index

m - digital controller output

M - valve mass

n - iteration number

N_p - pump speed

N_1 - gas generator speed

N_2 - output shaft speed

P - pressure

P_r - nozzle pressure overshoot/undershoot

P_s - nozzle pressure demand

S - change of solution vector $\underline{x}$ during consecutive iterations

S_{bv} - by-pass valve actuator step size

S_{mv} - metering valve actuator step size

t - time

T - sampling period, temperature

t_o - transport delay

u_i - unit vector in the the k_i direction

Q - fuel flow rate

V - volume

$\dot{W}_f$ - fuel mass flow rate

x - metering valve position

$\underline{x}$ - vector of system parameters

$\underline{X}$ - design vector

X_f - governor flapper valve position

y - by-pass valve position

z - minimum pressurizing valve position

Greek Symbols

α_1 - throttle lever angle

α_2 - CLP pilot input

β - effective bulk modulus of fuel

θ - valve cone angle

θ_f - fuel flow angle

λ - tuning parameter, gradient vector multiplier

ρ - density

Subscripts

a - ambient

b - by-pass valve

c - combustor

f - flow force

g - power turbine governor reset lever

k - iteration number

ℓ - nozzle manifold pressure loss, by-pass valve leakage

n - fuel manifold

o - preload

p - pump, pressurizing valve, pressure

s - spring

w - valve stop

0 - return line

1 - metering valve upstream side

2b - by-pass valve low pressure side

2m - metering valve downstream side

3 - compressor discharge

CHAPTER 1

INTRODUCTION

The Fuel Control Unit (FCU) is one of the most complicated and important components of the gas turbine engine. It meters fuel to the engine at different operating modes and prevents the engine from exceeding its operating limits.

Fuel control units vary in complexity from simplified designs to sophisticated ones. Supervision required by the pilot is related to the degree of automation. A totally manual system, which would essentially be an adjustable flow orifice, would require constant supervision. A fully automated one, on the other hand, would receive commands specifying a desired action and would perform the fuel flow scheduling based on a set of sensed engine parameters. Manual controls are still employed in parallel configurations and are needed in emergency situations to bring the aircraft to the nearest base. In many cases, the emergency (back-up) system may be semi-automatic or even fully automatic in order to reduce the pilot's supervision. This is critical in military aircraft, where combat operations would not allow for the full supervision of the fuel flow controls.

The fuel flow metering can be performed by maintaining

a constant pressure difference across an adjustable orifice, or by varying the pressure difference across an orifice of constant flow area. Both approaches simplify the control of the fuel flow since one of the variables is eliminated. The constant pressure control is more widely used because it provides fuel flow proportional to the metering valve travel. In conventional units, mechanical components such as springs, levers, bellows and cams are used to operate the metering valve and thus to control the fuel supply to the engine.

Hydromechanical fuel control units have been studied and developed over several decades. They have become very reliable and versatile. Their most significant drawback, however, is that they are not very flexible. Every mechanism usually performs only a single function. Improved performance requires additional hardware.

The basic requirements for the metered fuel flow are defined by the acceleration/deceleration schedules and the engine speed governing characteristics. The engine acceleration is usually required to occur in the shortest time possible without exceeding gas temperature limits. Excessive temperatures could damage the turbine blades and should therefore be avoided. High fuel flow could also produce very high pressure in the compressor discharge end, thus reducing the air delivery and subsequently resulting in compressor stall. The acceleration fuel schedule should

be maintained somewhere between the steady state flow schedule and the compressor stall limit. Since there are no measuring devices available to detect the onset of compressor stall, the fuel delivery must be limited with respect to some engine operational parameter. Such a relationship can be obtained experimentally from engine testing. The steady state flow line is known as the "Required To Run" curve (RTR) and indicates the rate of fuel flow required to maintain a particular speed under nominal load.

During engine deceleration, the fuel flow rate should not decrease below the minimum fuel flow limit which would result in engine flame-out, also known as "lean die-out". The minimum fuel flow can be associated to some engine parameter, such as the compressor speed. "Minimum flow" and "maximum flow" stops are used in all fuel control units.

Fuel flow adjustments at steady state engine operation are made through the mechanical speed governor. A shift in the operating point occurs when inlet air conditions, or the engine load, change. An engine speed offset results from these disturbances. The characteristic of the engine speed versus load is known as "speed droop" or regulation and is the result of the proportional action of the controller. This is typical in the case of mechanical speed governors. More sophisticated mechanisms and control methods are sometimes employed to avoid speed droop. These

include: speed operating point resetting, speed governors with springs of lower rate, metering valves with variable area gain or mechanisms for readjusting the differential pressure across the metering valve. This leads to "isochronous" control which maintains the speed constant, despite large load variations. Nevertheless, in many applications, the engine-governor operation is more stable when a proportional speed governor is used. The fuel control should also avoid large overshoots or undershoots of the engine speed during transient processes. This could be achieved by anticipatory control action which position the metering valve in advance of the engine response. The mechanical speed governor cannot perform this task since it must first sense the engine speed error before taking corrective action.

With the advent of microprocessor technology, fuel control systems went through revolutionary changes affecting every level of system hardware. The digital computer has made possible a substantial leap in the computational and logical capabilities of modern engine control systems. Conventional controllers are being replaced by digital equivalents.

The aircraft industry has a special interest in electronic controls because of their flexibility and potential to respond better to the fuel demands of sophisticated modern engines. Electronic controls are

expected to improve the engine performance, prolong engine life and reduce pilot workload. However, the transition from the hydromechanical to electronic systems is hampered by the lack of satisfactory reliability records regarding electronic circuits and components. This is especially important when electronics are intended for use in the commercial aviation industry. Redundant control is required to improve the safety factor. Two schemes for electronic controls with back-up capability have emerged recently.

In the first, used in the Boeing 757 airliners and military aircraft, a multi-channel electronic controller is interfaced with a metering servo valve (1)*. If one channel fails, another takes over. Up to four-channel systems are being used. The higher cost of such a control system is compensated by the permanent readiness of the aircraft. In the event of failure, there is no need to interrupt the flight schedule and run into high cost penalties. A second channel takes over and the repair can wait until the next scheduled overhaul.

In the second scheme, used in smaller gas turbine engines, a conventional fuel control is equipped with electronic trimming (2). In case of electronic control failure, the unit operates in its conventional mode,

*Numbers in parentheses designate references at end of Thesis

providing the aircraft with "bring-home" capability.

The attempts made recently to implement digital electronic controls in the management of small gas turbine engines do not represent anything new regarding other types of combust on engines. This includes spark ignition engines for cars (3), or large gas turbine engines for airliners and for military applications where electronic controllers have been used for a number of years (4). However, in small gas turbine engines as well as in diesel engines, digital electronic control is not yet widely accepted. This is mainly due to relatively higher costs resulting from the need for parallel back-up systems in the former case and to the need for larger actuators in the latter. These setbacks have yet to be overcome (5).

Electronic Fuel Control Units (EFCU) for small gas turbine engines could achieve fuel control by very simplified hardware. Some examples are presented below:

- A variable displacement fuel pump with small internal leakage driven at constant speed. The fuel delivered could be controlled by varying electronically the angle of the pump plate which operates the concentrically located pumping elements. The number of pumping cylinders and the duration of their stroke has to be high enough so that a semi-continuous fuel flow is obtained.

- A metering valve with constant differential pressure maintained across the metering flow area by a second valve, such as a by-pass valve. The position of the metering valve, operated by a digital actuator, would control the fuel flow rate. This is a concept similar to that in the conventional Bendix DP-F2 fuel control unit.

- A constant displacement pump, with small internal leakage, driven by a digitally controlled electric motor at a speed proportional to the required fuel delivery rate.

A control strategy has to be based on signals from the engine, such as engine speed, torque or compressor pressure. These signals indicate indirectly the fuel flow delivered by the fuel control unit. The engine speed signal is fully satisfactory for speed governing at steady state. It might also be acceptable for the control of the engine during acceleration and deceleration. For more accurate control and faster response, the fuel flow rate could be sensed directly by transducers mounted on the fuel control unit. The fuel flow rate can be computed from the flow equation based on information about the metering valve opening and the differential pressure across the metering valve. A low inertia flowmeter, such as a turbine

flowmeter, can also be used. This, however, is not a preferred solution because accurate flowmeters are expensive.

If a digital linear actuator is used to operate the metering valve, a fuel flow feedback might not be needed because the position of the valve (and thus the fuel flow) could be obtained from the number of steps performed. During acceleration, the fuel schedule can be achieved by simply counting the steps triggered to the stepper motor, which are pre-scheduled as a function of engine speed. This approach is sufficiently accurate and reliable for short time periods. When operating for longer periods, the step count may be in error due to possible non-execution of steps ("lost" steps) or false triggering. This may result in wrong fuel scheduling during acceleration or deceleration. To avoid such problems, position feedback of the stepper motor is needed. Metering valve position transducers, such as LVDTs, special potentiometer types or linear position encoders (resolvers), that could withstand the harsh environment of the engine, could be used. Inexpensive solutions are not available yet. An alternate control strategy based only on the engine speed signal, is known as the "N-Dot control law". The controller delivers the fuel flow to the engine and maintains a safe engine acceleration, pre-scheduled as a function of rotor speed and altitude. This control has the advantage of using a

minimum of engine sensors. Only the compressor inlet pressure and the engine speed signals are required.

It has to be underlined that the electronic fuel controls schemes, discussed here, do not exhaust all the possibilities. The ones introduced are considered particularly suitable for small engines used in Remotely Piloted Vehicles (RPV), Auxiliary Power Units (APUs), in small aircraft and helicopter applications. The use of electronics is more justifiable in the case of RPVs and APUs where failure safeguards and back-up requirements are more relaxed.

CHAPTER 2

ELECTRONIC CONTROL SYSTEMS FOR GAS TURBINE ENGINES - LITERATURE SURVEY

The importance of electronics in the development of more sophisticated and flexible fuel controls was recognized with the advent of the monolithic component technology in the early 1960's (6), (7), (8). Simple microcircuit modules, employed to perform arithmetic operations such as multiplication or division, were much larger than the ones available today; however, considerably smaller than their analog equivalent at that time. There were many difficulties in interfacing the computing elements with analog sensors because of the unavailability of simple analog to digital converters. The interface was rather limited to digital type sensors. Analog computation was recognized as a prime candidate for electronic control due to the ease with which it could be interfaced to the majority of sensing elements. However, the set-up for fuel flow scheduling and other simple functions was very elaborate and time consuming. Another disadvantage of analog control was signal degradation caused by environmental variations. Digital information, on the other hand, could be stored in the form of binary numbers and was not influenced by environmental changes.

The weight of the electric controllers was reduced by a factor of about two. The mean time between overhauls was increased due to the smaller number of moving parts. Also, time to repair was lowered because built-in test circuitry for fault isolation became possible. Moreover, the low cost of electronic modules allowed the user to discard rather than repair faulty circuit blocks.

In 1965, Peck (6) from the Electronics Division of the United Aircraft Corporation, reported on a microelectronic fuel control unit for an airborne gas turbine engine. The fuel flow to the engine was metered by a servo-controlled metering valve operated by a torque motor. Solid state electronics were used for the electronic module which was attached directly on top of the hydromechanical unit and was cooled by the fuel.

Ronald Falk (7), in 1965, introduced digital pulse width modulated techniques which employed basic electronic circuit modules such as NOR gates, binary counters, and one-shot multivibrators, to demonstrate the effectiveness of simple digital devices in the design of electronic controllers. Using combinations of these elementary circuits, he was able to design a simple gas generator speed governor with adjustable speed, employing engine speed and actuator position feedback. His technique demonstrated that the "scheduling" (open loop) type of control used in the hydromechanical units could be replaced

by "closed loop" control. The idea of using digital and semi-digital techniques with a variety of actuators such as torque motors, electrohydraulic servo motors and incremental actuators (stepper motors) was discussed.

Ferre and Lenkaitis (8), in 1965, performed analog computer simulation of an engine control system with electronic fuel control. They demonstrated a new control philosophy in which the engine acceleration and speed were used as feedback signals to control an electronically operated metering valve. Their control strategy was similar to what is referred today as the N-dot control, applied successfully in electronic fuel controllers for helicopters and small aircraft.

In 1974, Keck et al (9) of the AiResearch Manufacturing Co. of Arizona, a division of The Garrett Corp., were the first to report on developments of a full authority electronic fuel control system for a small gas turbine aircraft engine. This work was initiated in recognition of a need for improved engine and aircraft operation. An electronic controller was developed for use in the Garrett model TFE731-2 turbofan engine intended for use in business-type aircraft. The TFE731-2 controller was originally an analog electronic system, using mainly operational amplifiers. The system had entered the production phase in August, 1972 and throughout the development program (up to 1974), 19,000 engine operating

hours had been accumulated. Subsequently, in 1981, Garrett Turbine Engine Co., also a division of The Garrett Corp., developed an analog electronic fuel control system for use in the model TPE331 turboprop engine manufactured by Garrett. This new design was a result of the experience gained with the previous analog electronic control system used in the turbofan engine. Most of the TFE circuits were used with minor or no modifications. The new system reduced the complexity of the hydromechanical fuel control unit and cut down on aircraft linkage and engine control components. Main features of that system were: automatic starting, acceleration fuel scheduling, fuel governing, power setting, engine torque limiting, isochronous propeller governing, overspeed protection and various monitor functions to detect system failure.

In both of the above systems, the computer used was an analog device receiving inputs from various sensors mounted on the engine and on the fuel control unit. It performed complex computations and produced output signals to drive the actuating devices (torque motors etc.). The Garret research program finally resulted in the development of the FFT731-5 electronic controller for use in executive jet aircraft (10).

Interest in analog electronic control systems started to decline with the new developments in the digital electronic technology in the early 1970's. Digital

electronic controllers were superior to their analog counterparts mainly because of their higher flexibility and ability to execute complex control functions without significant computational errors. Also, the digital systems operated on the input signals sequentially and could test each signal for irregularities between sampling intervals. In addition, the mathematical model of a process could be used to synthesize a missing or faulty signal. For example, if the fuel flowmeter was producing an unrealistic signal, the fuel flow could be evaluated from the pressure and valve displacement signals.

A program was initiated by the Hamilton Standard Division of the United Technologies Corporation in the late 1960's, in which a digital minicomputer was introduced in the military Pratt & Whitney F-100 engine to assist the hydromechanical fuel control unit in performing complex fuel delivery functions (11). Due to the success of the program and because of the extensive crew workload and related performance difficulties experienced at the time with the management of the newly developed engines, (the JT9D, RB211 and CF-6, in particular) a supervisory control program was initiated in 1972. The control program was first applied to the commercial JT10D engine. Subsequently, Boeing, Pratt & Whitney and Hamilton Standard conducted a joint demonstration program in order to evaluate the potential of a full-authority digital electronic control.

The program resulted in a system known as the Electronic Propulsion Control System (EPCS). There were no hydromechanical computational elements in this controller, except for the mechanical overspeed governor. During 1974-1975, EPCS was built, and late in 1975, it was installed and run on a JT8D engine in a test facility in Boardman, Oregon.

Studies related to the EPCS have shown that a higher frequency of maintenance actions were required, as compared to the hydromechanical fuel controls, due to the fact that EPCS had a failure rate about four times higher. However, when parallel processing and fault compensation techniques were applied, the operational reliability increased by a factor of three. This was achieved only at a cost of adding a few inexpensive coprocessing Integrated Circuits (I.C.). Moreover, since 1977, there has been an impressive increase in the functional capacity and reliability of semiconductor devices and most of the problems experienced in the early stages of the digital electronic systems have been solved today.

In 1980, Kniat and Bluish (12) reported on the continuation of the EPCS program as Bendix (Energy Controls Division), Hamilton Standard and Pratt & Whitney joined forces in 1980 to conduct a flight demonstration of the program. The EPCS controller for these tests was developed by Bendix. It incorporated two full authority electronic

control channels completely redundant and independent from each other. One channel operated the engine while the second was always active, ready to take over in case the primary channel failed. This control system was flight tested on a Boeing 747 research aircraft and effectively demonstrated that the technology to build advanced electronic control systems for commercial transport engines was available.

In 1978, Evans and Cusson (13) of Aviation Electric Limited (a subsidiary of the Bendix Corp.), in Montreal, Canada, reported on the development of hybrid simulation techniques for the evaluation of a Full Authority Digital Fuel Control (FADC) for a twin gas turbine engine installation used in helicopters. A validated engine simulator was used as a design tool and interfaced with the real time digital controller. The FADC electronic hardware was based on the Intel 8080A three chip microprocessor. The memory consisted of 4096 words of Programmable Read Only Memory (PROM) and 256 words of Random Access Memory (RAM). For analog signal input, a 12-bit successive approximation A/D converter was used. The digital output signal used to position an electronically controlled metering valve was processed by a 10-bit D/A converter. "Checking" circuits were created to monitor the "health" of the system and reduce the possibility of failure. The electronic circuits were contained on three double layer printed circuit

boards.

Around 1980, a second generation of digital electronic controls for small gas turbines started. AVCO Lycoming and Lucas Aerospace jointly developed a highly integrated electronic control for the LTS101 turboshaft engine (14). This system simplified the hydromechanical fuel control by minimizing the number of moving parts. The Central Processing Unit (CPU) was an Intersil IM6100 12-bit processor of moderate speed, low power consumption and 4 K words of memory. Only half of this memory was used and divided into Read Only Memory (ROM), Erasable Programmable Read Only Memory (EPROM) and Random Access Memory (RAM). This was the first full authority digital electronic control system proposed for FAA certification for a helicopter application.

Hawes and Evans (15), (16) presented a second generation of the FADC, the Speed Digital Electronic Control (NDEC) which employed a completely different control mode known as N-dot control. This innovative control had been applied in 1978 by Lucas Aerospace (17), in the SDS-100 and SDS-200 full authority electronic controls for helicopter powerplants. It was an unconventional control philosophy because it used the engine acceleration, instead of the fuel flow, to control the engine acceleration schedule. The advantage of the N-dot system was that it was more reliable and

cost-effective because it used simple hardware. The need for the delivery pressure measurement was eliminated. In essence, the control produced whatever fuel flow was necessary to achieve the scheduled acceleration rate. In the Lucas unit, an Active Remote Module (ARM) was used to establish communication with the cockpit (17). A simple serial data highway using fiber optics was proposed which would eventually replace the existing link consisting of 50 individual wires for each engine.

In 1976, Pratt & Whitney Aircraft had initiated the Full Authority Digital Electronic Control (FADEC) program, sponsored by the Naval Air Systems Command and directed by the Naval Air Propulsion Center (19), (20), (21). The objective of the program was to fabricate and test an engine-mounted digital electronic control for advanced aircraft gas turbine engines for military and commercial applications. The FADEC system demonstrated satisfactory reliability and fault tolerance capability through the use of redundant sensing, computation, parameter synthesis and self-test techniques. It showed satisfactory operation with fuel temperatures from 218 K to 516 K, vibrations up to 20 G's, 2 KHz and Electro-Magnetic Interference (EMI) levels over 130 volts/meter (frequencies up to 10 GHz). In addition to the advanced electronic circuitry, the FADEC was the first system to use optical communication with engine-mounted equipment. Most of the FADEC circuitry has

been built on multilayer ceramic modules (MCM) with circuit materials having low and well matched thermal expansion coefficients in order to avoid differential expansion stresses. This design proved superior to the design of systems with conventional packaging materials.

The FADEC system has since improved and has increased in sophistication. Its sensor Failure Indication and Corrective Action (FICA) feature uses mathematical model of the engine to generate outputs which are compared with the sensed parameter inputs. In case of a sensor failure, the remaining sensors continue to update the engine model while the control strategy continues to receive input data from the engine model.

The possible payoffs resulting from the FADEC program, prompted the Air Force to initiate in 1981 its Full Authority Fault Tolerant Electronic Engine Control (FAFTEEC) program (22). The main objective of this program was to identify the basic redundancy requirements of the control system in order to achieve high levels of mission reliability. Seven alternative system configurations with various degrees of redundancy were examined. High levels of failure coverage were attained using dual electronic systems. The intent of this program was mainly to examine the possibility of completely eliminating the need for hydromechanical back-up fuel control.

In 1980, Newirth and Bosco (23) reported on a

reliability evaluation program for a Hamilton Standard Engine Electronic Controller, the EEC-102. This project was undertaken jointly by Pratt & Whitney, Boeing Commercial Airplane Company, Hamilton Standard and the Bendix Energy Division, with the collaboration of many major airline carriers. The program was very successful. At the time of reporting (1980) there were no electronic failures for 70,000 hrs of reliability flight testing. During testing, the controller was functioning electronically but was not performing active control. It was only interacting with a monitor unit, located inside the aircraft, which read the outputs, provided inputs and recorded performance. The EEC-103 was a generic electronic engine controller intended for supervisory control on the JT9D-7R4 engine. The controller provided output for the operation of three torque motors, five solenoids, one potentiometer and three resolvers.

The EEC system was based on experience gained, while working with the EEC-90 supervisory fuel control used on the Pratt & Whitney F-100 military engine, in the early 1970's. Also the success of the EPCS joint program greatly contributed to the development of the design and manufacturing techniques used in the EEC-103 system. The EEC controller was interfaced with the Hamilton Standard JFC68 hydromechanical fuel control to achieve high levels of reliability. The electronic unit consisted of four

multilayer printed circuit boards enclosed in a cast aluminum housing. Computation was performed by a Hamilton Standard 16-bit processor, specifically developed for this application. Software was included in the Programmable Read Only Memory (PROM) and data to be processed was stored temporarily in the Random Access Memory (RAM). An Electrically Alternate Read Only Memory (AEPROM) was used to store codes for faults of the system's internal circuitry. Hamilton Standard, next, put into service the EEC-103, which was representative of a new generation of airborne electronic equipment.

In September 1982, the EEC-103 was installed on the Pratt & Whitney JT9D-7R4 turbofan engine powering a Boeing 767 of the United Airlines. The engine remained under hydromechanical control with the EEC operating a torque motor for speed governing. As of 1984 that controller had completed two years of commercial service and had been installed in 73 aircraft including the Airbus A310. The next generation of the EEC system included the EEC-104, EEC-131 and EEC-150 used in the Pratt & Whitney PW4000 family of engines. The EEC-104 was used in the Pratt & Whitney PW2037 powering the Boeing 757. This was a full authority engine control. It used two channels for redundancy and fault tolerance. Each channel had independent access to all sensors and actuators. The second channel was always in a standby mode with all actuators

disengaged. In case of failure of both channels, all actuators would revert to a fail safe state. The electronics were protected against direct lightning hits and high levels of EMI by an enclosing structure which served as a Faraday Shield (24), (25).

In 1982, a new digital Multi-Application Control System (MACS) was developed and flight tested by Hamilton Standard for use in small aircraft gas turbine engines (26). Turboprop, turbofan and turboshaft versions of that control system were developed and later introduced into production. The MACS design combined the computing power of modern digital electronic technology with the reliability of a simplified hydromechanical unit which served also as a manual backup. The MACS system did not provide the sophisticated failure logic and redundancy features of the digital systems in the large engines but offered the possibility of introducing these features in future versions of the system.

Other recent research programs exploring the advantages of the digital electronic controls in the general aviation industry, include; the joint NASA/Air Force Integrated Propulsion Control System (IPCS) program for the F-111 aircraft, the Air Force's Digital Electronic Engine Control (DEEC) program, the Highly Integrated Digital Electronic Control (HIDEC) pursued by NASA Ames-Dryden and among others the digital control used on

the Highly Maneuverable Aircraft Technology (HIMAT) remotely piloted vehicle (27), (28), (29).

In 1986, Georgantas et al converted the Bendix DP-F2 hydromechanical fuel control unit to an electronic one by replacing the pneumatic computing section with digital computation and the actuation of the metering valve by incremental actuation provided by a linear digital actuator (stepper motor) (30). That work proved the feasibility of such a concept and provided some novel control strategies for improving the transient response of the unit (31), (32), (33).

Parallel to the research and development of electronic controls for manned aircraft, interest was also focused on unmanned vehicle applications. This included Remotely Piloted Vehicles (RPV) and missiles which were characterized by short life and low cost. Full authority electronic fuel control was generally more acceptable because of the less stringent requirements to obtain certification for power plants for unmanned aircraft. Hence, lower levels of of redundancy and back-up were required (36). New possibilities for low cost electronic fuel control units for unmanned flying vehicles, employing existing automotive components were presented by Krepec et al in 1985, (35), (36), (37). Bendix Avelex Inc., showed interest in this work and a joint effort to develop a low cost electronic fuel control unit for small gas turbine

engines was initiated in 1987, (38), (39), (40), (41). This project is still under progress and upon its completion in 1990, a family of low cost electronic fuel control units with wide range of application would be available (42), (43), (44), (45).

Research and development on low cost fuel systems for expendable gas turbine engines used in drones, RPVs and missiles, was also undertaken by Teledyne CAE and the Wright Research and Development Center (46). Many components, such as fuel pumps, actuators, sensors, electronic hardware as well as different control strategies were thoroughly investigated.

South Bend Controls Inc., demonstrated the simplicity that digital electronic controls offer, by designing a fuel metering valve operated by a linear proportional solenoid (47), (48). Some applications of this design included airborne or ground based Auxiliary Power Units (A.P.U.), Missile Propulsion systems and Surveillance and Target Drones.

With regard to software development, there are still major problems to be overcome mainly because of the rapid updating of fuel schedules as engines develop to new applications. Continuous modification of the software development processes is required.

A control strategy is implemented using software which takes care of the basic program operation, various modes of

operation, updating the control signals, formulas, input/output, memory and timing. High level or machine level languages or combination of the two, may be used. Utility functions such as control of input or output, self-test, and communication with data from the physical processes are also part of the software development. Programming is done by different programmers using different computer languages. This avoids common mode failures and improves reliability significantly. Software is verified and refined at steady state and transient operation using a computer real time engine model. Verification of software involves simulated steady-state and transient engine operation and simulated failure of a single or of combination of sensors.

For each software development phase, problems are reported and documented. Certification requirements are very stringent especially for engines used in manned aircraft. For large and small engines alike, the methodology and guidelines set forth in the Radio Technical Commission for Aeronautics (RTCA) document DO-178, "Software Considerations in Airborne Systems and Equipment Certification", are followed (1), (10). Certification procedures cover bench and flight testing. On the test bench, operation during icing, bird injection and blade out are receiving special attention. Also, a series of closed loop control fault testing is conducted. Flight

certification testing includes thrust setting characteristics and demonstration of engine stability over a wide range of flight.

If changes are introduced in the software after certification, the affected modules, module interfaces, hardware/software, and in general all parts affected by the changes must be retested (1).

CHAPTER 3

OBJECTIVE - THESIS OUTLINE AND METHODOLOGY

3.1 Objective

The purpose of this thesis is to investigate different control strategies for the development of simple electronic fuel control units for small gas turbine engines. Linear incremental motion actuators under digital control are to be used instead of conventional hydromechanical mechanisms.

The development of the proposed concepts can eventually lead to a full authority electronically controlled system with back-up capability which could provide the performance required for the modern small gas turbine engines for remotely piloted vehicles and small manned aircraft.

3.2 Thesis Outline and Methodology

Two versions of an electronic fuel control unit are used for the investigation. In the first, a digital linear actuator is operating a metering valve while a by-pass valve is operated conventionally by a diaphragm actuator. In the second, the system is equipped with a second digital actuator which operates the by-pass valve. To investigate these concepts, a hydromechanical fuel control unit is

modified in stages and used as a prototype.

In Chapter 4, the operation and the basic functional requirements of a fuel control unit are described. The concept of an electronic fuel control unit is presented. Unit prototypes are described and digital controller hardware proposed.

In Chapter 5, preliminary semi-transient and dynamic response experiments, using a Bendix DP-F2 based electronic control unit prototype, are performed to verify the feasibility of digital control and incremental actuation for the metering valve. Recommendations to improve the hardware are made.

In Chapter 6 and Chapter 7, the metering section of the proposed electronic fuel control unit is modelled and validated. The model is used (in later chapters) to develop an optimal control strategy.

In Chapter 8, the fuel control unit with electronically controlled metering valve is modelled and tested experimentally. First, a Proportional Derivative (PD) digital controller is linked to the model and simulation results are produced for fuel flow demands at a particular operating point. Then, more complex digital controller algorithms are proposed and tested experimentally.

In Chapter 9, on-line controller tuning, employing an optimization method, is proposed and tested. The tuning

technique can be used for test bench calibration of the electronic controller.

In Chapter 10, a two-actuator electronic fuel control unit is presented as an improvement over the one-actuator unit. The dynamic response of the unit is simulated for several control configurations. The mathematical model developed in Chapter 6 and Chapter 7 is used as a basis for simultaneous optimization of the two digital controllers employed to control the metered fuel flow.

CHAPTER 4

SYSTEM AND CONCEPT DESCRIPTION

4.1 Description of the Complete System Including Engine

The Bendix Avelex DP-F2 hydromechanical fuel control unit is primarily used on the PT6 Series of free turbine engines, manufactured by Pratt & Whitney Canada Limited. Fig. 4.1 shows a simplified information flow diagram of the complete system for a turboprop application.

The fuel control receives a signal from the pilot demanding a particular fuel supply rate to establish the required power level. Certain engine controlling parameters are sensed by the fuel control unit and the desired engine power is obtained by automatic fuel flow adjustment. In turboprops, additional input is received from the propeller speed governor. The propeller control unit adjusts the pitch angle of the blades to match the torque of the load with the torque of the engine thus keeping the speed close to constant.

At low air speeds or reverse thrust operation, the propeller blades are positioned manually by the power control lever. As the speed of the engine (gas generator) increases, the propeller blades pitch angle decreases in a pre-scheduled manner. This is known as the "Beta" control range.

PT6 ENGINE AND PROPELLER CONTROL SYSTEM

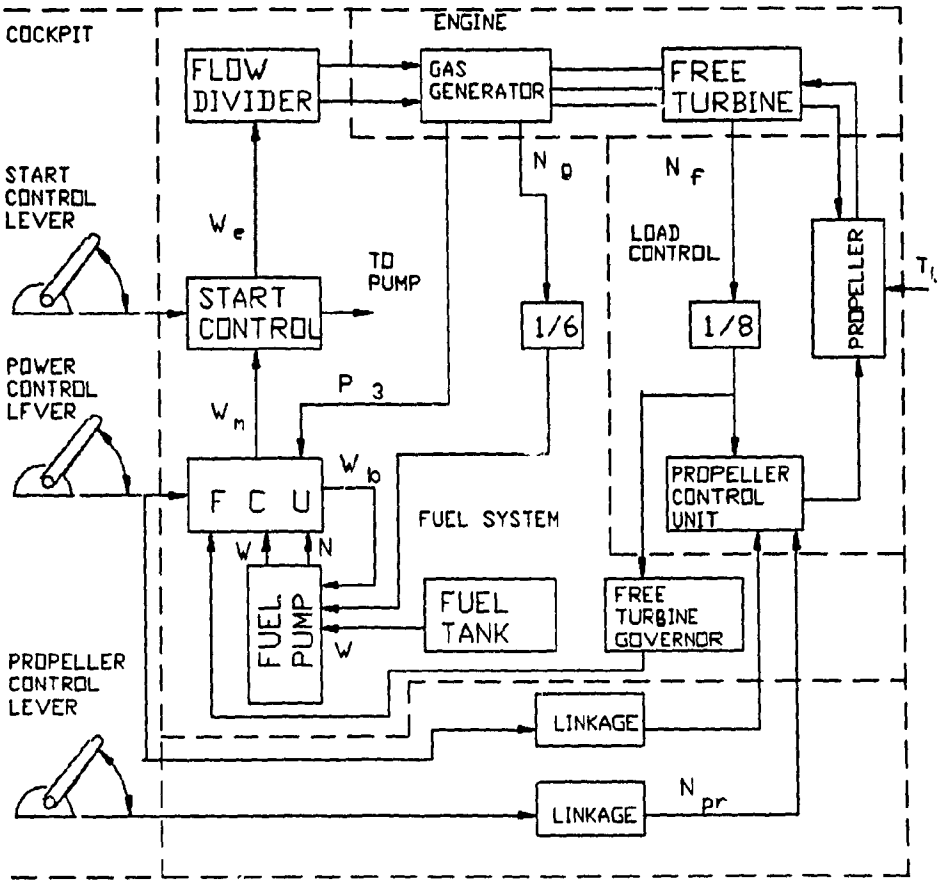

Fig. 4.1 Pratt and Whitney PT6 turboprop engine fuel controls

The start control lever has three positions; Cut-Off, Run and Hi-Idle. In "Cut-Off", the fuel is diverted from the two nozzle supply manifolds back to the pump inlet. Residual fuel in the manifolds is dumped overboard to prevent fuel coking by heat absorption from the nozzle system. In the "Run" position, as the engine accelerates, the fuel is progressively supplied to the two manifolds.

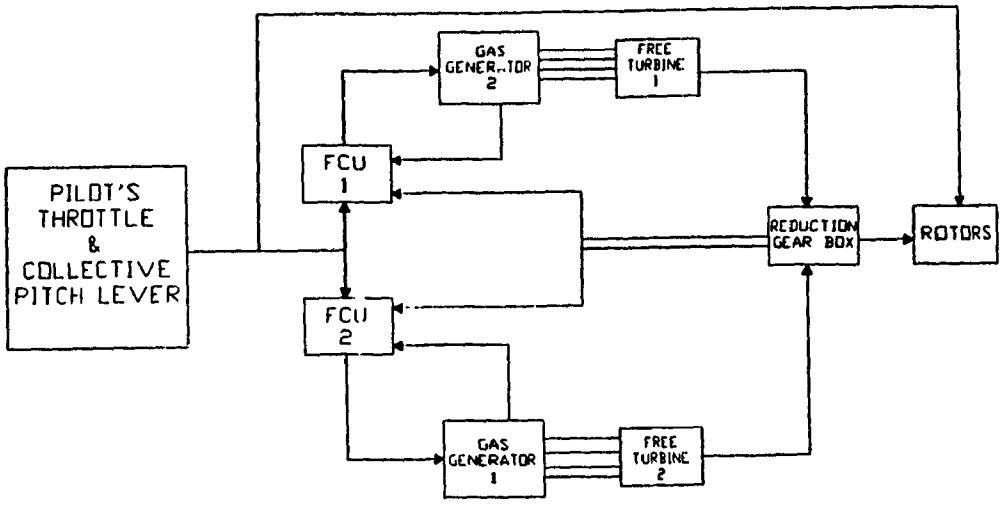

Fig. 4.2 Controls of twin engine installation

In a turboshaft application, driving the rotor of a helicopter for example, the output shaft speed is held essentially constant, Fig. 4.2. The engine power output is established by setting the gas generator speed. When the load is changing by varying the rotor collective pitch (CLP), the power turbine speed governor readjusts (resets) the gas generator speed selected by changing the fuel flow rate. Any variations in the gas generator speed occurring because of changes in the compressor load, are corrected by the gas generator speed governor.

The basic difference in the control philosophy between a turboprop and a turboshaft is that, in the former the

load speed is maintained by changing the load (propeller pitch angle) and in the latter by changing the fuel flow. The gas generator speed in a turboprop is maintained (as selected by the pilot's power lever) by the main fuel control unit speed governor, while on a turboshaft it is reset to a new value in order to meet a change in power demand.

4.2 Hydromechanical (Conventional) Fuel Control Unit

The schematic of the main hydromechanical fuel control unit is shown in Fig. 4.3. The fuel is supplied to the fuel control unit by a high pressure positive displacement (gear) pump driven at a fraction (1/6) of the gas generator (compressor) speed.

The fuel control unit consists of three main sections:

- Metering section (Hydraulic)
- Computing section (Pneumatic)
- Speed governor section (Mechanical)

The metering section of the fuel control unit employs a metering valve and a by-pass valve working in parallel. The by-pass valve maintains constant differential pressure across the metering valve by releasing back to the tank excess fuel delivered by the high pressure gear pump. A pressurizing valve is used to bias the system pressure, so

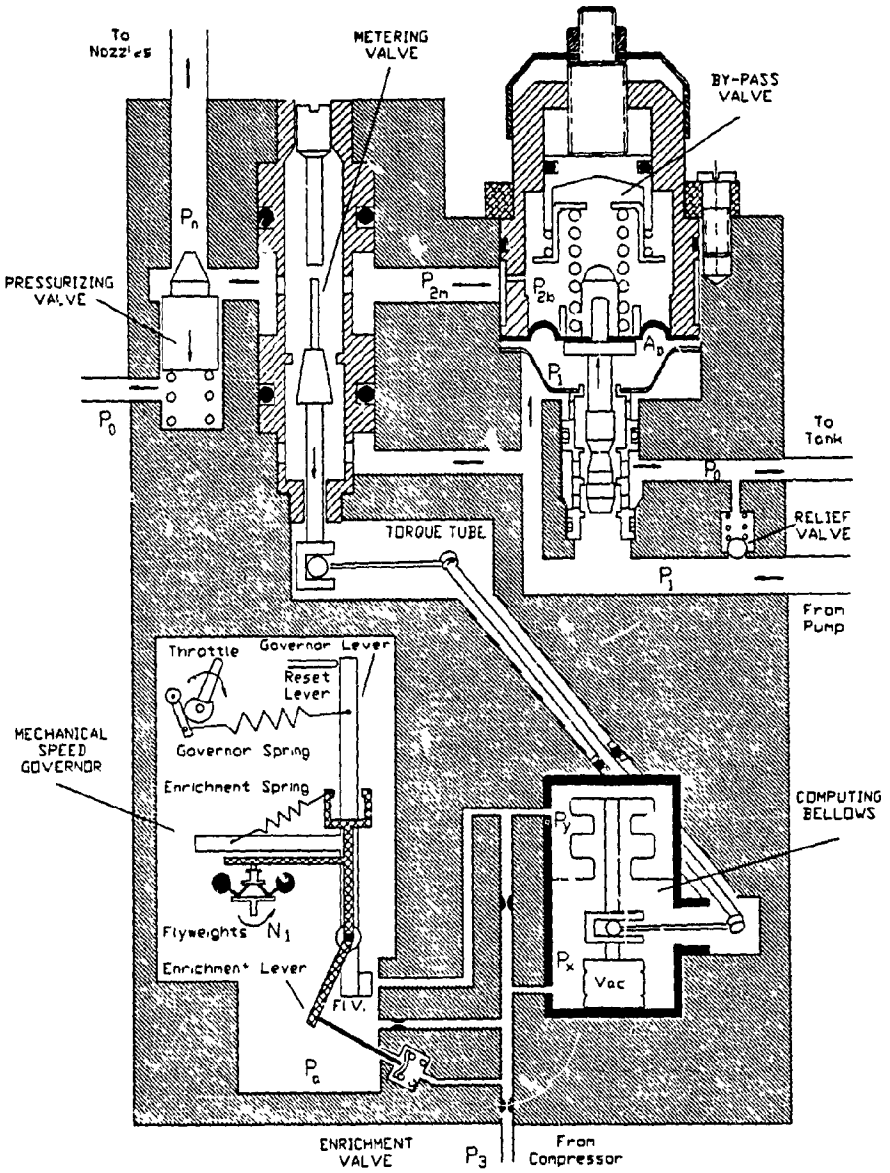

Fig. 4.3 Main components of the Bendix DP-F2 fuel control unit

that the pressure difference across the metering valve can be created by the by-pass valve even at low flows. The fuel flow to the nozzles is proportional to the metering valve position.

In the computing section, the compressor pressure and the governor flapper valve movement are used to position the metering valve. Cascaded orifices are used in the air flow lines to create a pressure difference P_x-P_y across the bellows. The pressure force in the bellows is used to actuate the metering valve via the torque tube assembly. The acceleration bellows is evacuated on one side. A pressure force is generated even when the pressure P_x and P_y are equal. This is the case during engine acceleration.

The mechanical governor is part of the computing mechanism. The governor spring is preloaded by a cam which has a direct link to the pilot's collective pitch lever. At a preset speed, the centrifugal force of the governor weights overcome the spring preload and displace the governor sleeve as they move apart. This actuates the governor lever and thus the flapper valve. As a result, a differential pressure is created across the bellows.

4.3 Fuel Control Unit Requirements

A typical fuel flow schedule, as required by the PT6A-27 engine, is shown in Fig. 4.4. The following events

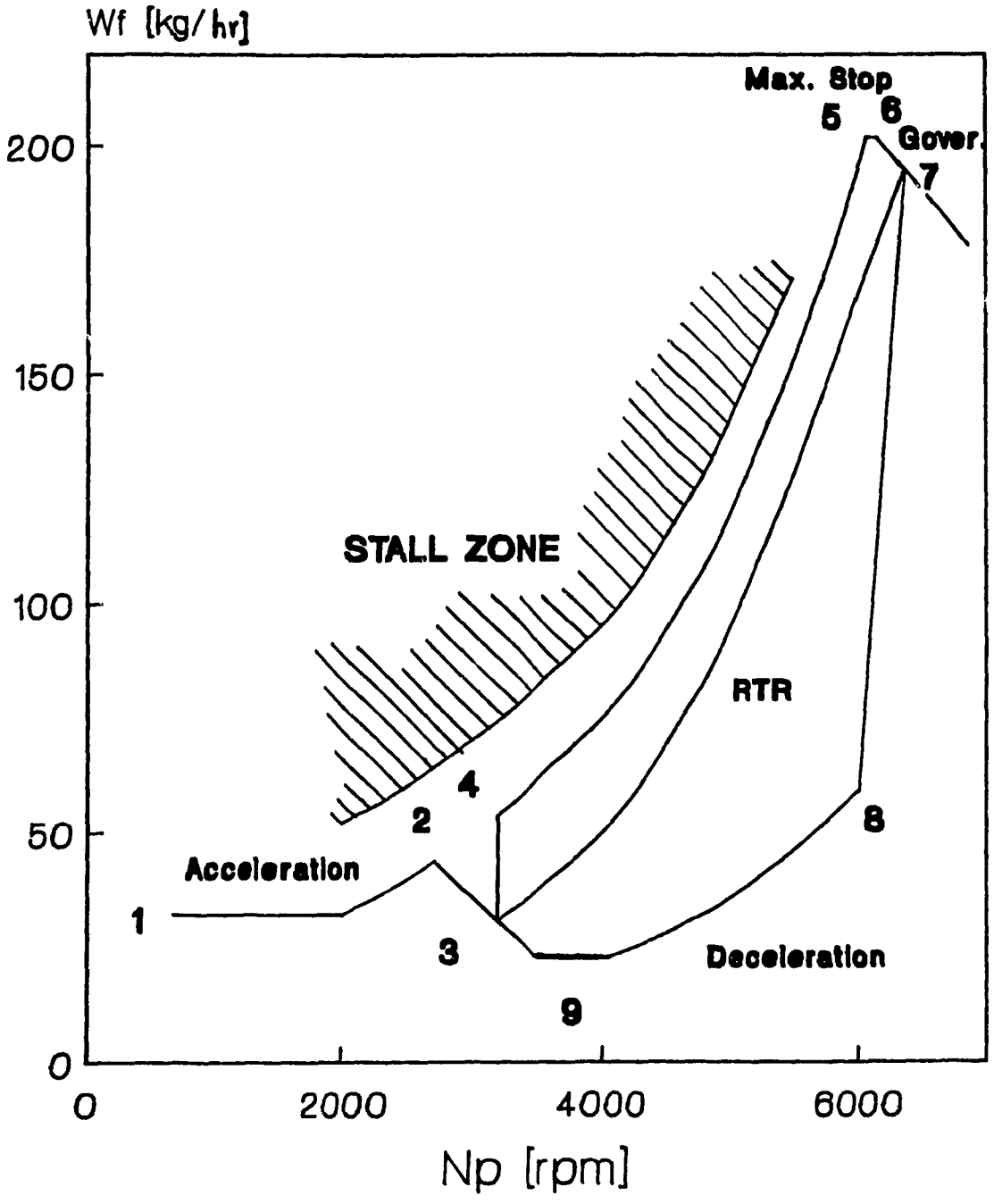

Fig. 4.4 Typical fuel delivery schedule for a PT6 engine

take place during a ground start up.

The throttle lever is in the "Cut Off" position while the gas generator is rotated (cranked) to approximately 15% of its maximum speed. Then, the pilot's power lever is moved to "Idle", corresponding to the 30 degree position of the fuel control unit throttle lever. The engine (gas generator) accelerates from point 1 to point 2 following the acceleration curve as shown in the Figure. The fuel is delivered in "open-loop" control, based on the compressor discharge pressure which actuates the bellows and thus the metering valve. At point 2, the mechanical governor centrifugal weight force overcomes the governor spring preload force and starts to open the governor flapper valve. This decreases the bellows differential pressure P_x - P_y and causes the metering valve to close until the total spring force (bellows spring plus torque tube spring) balances the bellows pressure force. Thus, point 3 is obtained which is located on the intersection of the Required-To-Run curve and the speed governing line at Idle. The engine speed is maintained at this point by the mechanical speed governor.

The power lever is then moved to its maximum position, corresponding to 90 degrees on the fuel control unit throttle lever. This increases the force on the governor spring and closes the flapper valve. The fuel flow "jumps" to point 4 on the acceleration curve because the metering

valve opens instantly by the increased bellows force. Then, the metering valve continues to open gradually, based on the compressor pressure signal. The flow is pre-scheduled to be the maximum allowable for rapid acceleration, while the stall zone is avoided. The acceleration curve is followed until the maximum flow stop is encountered; point 6. As compressor speed and thus compressor pressure, may still be increasing, some excess spring force will accumulate against the maximum flow stop. When the governor centrifugal force overcomes the governor spring preload, the flapper valve starts to open. The metering valve, however, starts closing only after the accumulated force against the maximum stop is released. Eventually, point 7 (100% speed) on the Required-To-Run curve is attained. At this level, however, the power turbine governor is already operative and it resets the gas generator governor to a new set point by adding or removing governor spring preload force. The fuel flow is established at a level required to maintain the selected load speed.

When the engine load is reduced, by changing the pitch angle of the rotor blades, the speed of the rotor and of the power turbine increase. As a result, the "reset" action of the power turbine governor reduces the gas generator speed and point 8 on the deceleration curve is obtained. To further decelerate the engine, the lever is positioned to "Idle". The governor spring preload is reduced and the

flapper valve opens more. This results in choked airflow in the governor orifice and the deceleration fuel flow is determined by the compressor pressure. At point 9, the metering valve contacts the minimum flow stop while the engine decelerates until the governor spring preload overcomes the centrifugal force and the governor flapper valve starts to close. This brings the fuel flow rate back to point 3.

4.4 Digital Electronic System: Concept Presentation

Two parameters are affecting the fuel flow rate metered to the nozzles of the gas turbine engine. These are, the pressure difference across the metering valve and the flow area of the metering valve. The differential pressure, however, is not kept exactly constant because of the effects of the by-pass valve spring force and the fuel flow forces acting on the conical surfaces of the valve.

The major part of this thesis deals with replacing the traditional hydromechanical control of these two parameters with electronic equivalents. The transition is performed in two phases. First, the metering valve actuation is performed electronically while the by-pass valve is kept in its original configuration. Second, both valves are controlled electronically using digital actuators. This procedure results in two distinct electronic fuel control

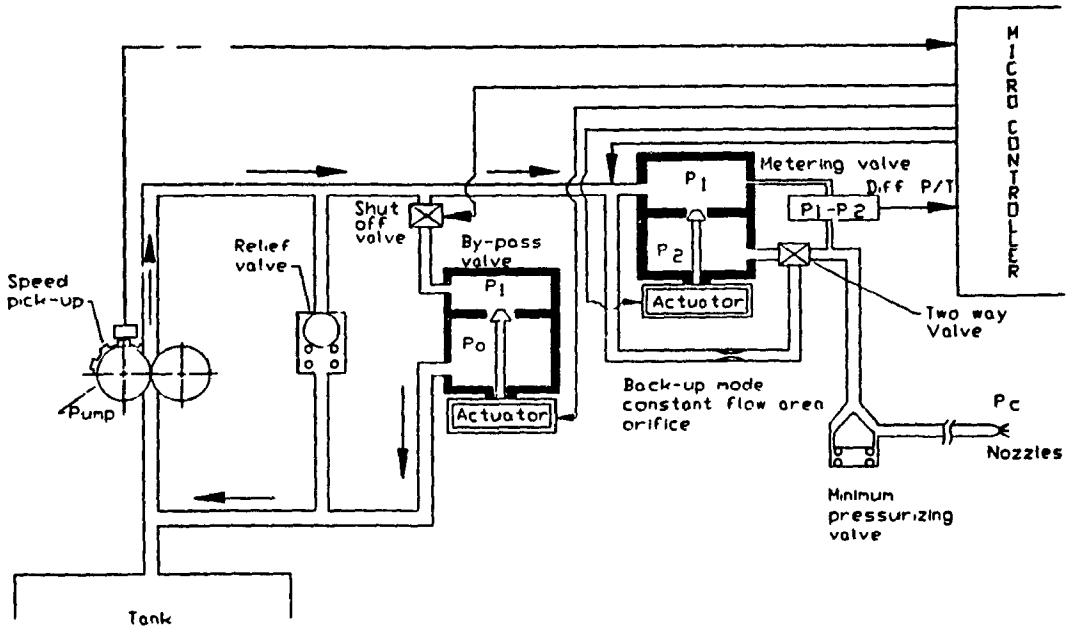

Fig. 4.5 Proposed concept of electronically controlled fuel metering system with two actuators

units.

The concept of the final configuration is shown schematically in Fig. 4.5. The operation is as follows: The by-pass valve maintains the differential pressure $P_1 - P_2$ across the metering valve by controlling the release of fuel from P_1 to P_0 area. The signal of the differential pressure transducer is brought to the microcontroller and is compared to the demanded differential pressure. The controller operates on the error and sends the control signal to the actuator driver in order to change the

position of the by-pass valve and to maintain the required differential pressure.

The metering valve opens to provide the flow area required by the engine fuel schedule. The fuel flows from P_1 to P_2 area under constant differential pressure, maintained by the by-pass valve. The metering valve is operated by a digital actuator. This control can be based either on the engine speed signal or the compressor pressure signal. An appropriate fuel delivery schedule (i.e. acceleration, speed governing, steady state or deceleration) has to be selected. The fuel flow rate can be measured by a turbine flowmeter or synthesized using the differential pressure and metering valve position signals. A cascaded fuel flow control strategy can be implemented using the speed as well as the fuel flow feedback signals.

The proposed electronic system, together with the shut-off valve and a motive flow valve (if required), should be equivalent, if not better, to the conventional DP-F2 FCU. The electronic unit has the advantage of flexibility and employs fewer mechanical components. Requirements such as change of the acceleration schedule or fuel enrichment can easily be implemented by reprogramming the EPROM of the microcontroller. Traditional components of the FCU, such as the mechanical speed governor, pneumatic computing unit (bellows) and air orifice system are eliminated.

In case of failure of one of the two electronically operated valves, either the by-pass valve or the metering valve, the full fuel flow management is assumed by the second valve. The function of the valves in the back-up mode is described below.

If the by-pass valve fails, the fuel flow to the by-pass valve will be cut-off automatically by a solenoid operated "on-off" valve. P_1 pressure will be set to a level of approximately 70 bar by the relief valve. Consequently, the metering valve will control the nozzle flow area with the differential pressure ranging from approximately 22 bars to 68 bars. This would require a pressure balanced metering valve to eliminate the pressure forces on the valve profile.

If the metering valve fails, the fuel flow through the metering valve will be cut-off by a solenoid operated "two way" valve. A parallel flow path will be opened to the nozzles through a constant flow area orifice. Then, the fuel flow rate to the nozzles will be controlled by the differential pressure created by the by-pass valve.

To reduce the hazard of malfunction due to possible electronics failure, each valve should be under separate microcontroller management. In both modes of failure, the fuel control unit is not expected to operate at optimum capability.

4.5 Electronic Fuel Control Unit Prototypes

The hydromechanical DP-F2 unit was modified to obtain two versions of the electronic unit. In the first, Fig. 4.6, the DP-F2 FCU was "stripped" from the computing bellows and was equipped with a digital linear actuator (AIRPAX, series 92200, model K92211-P2). Technical data of the actuator is given in Appendix A (Fig. A.1). The

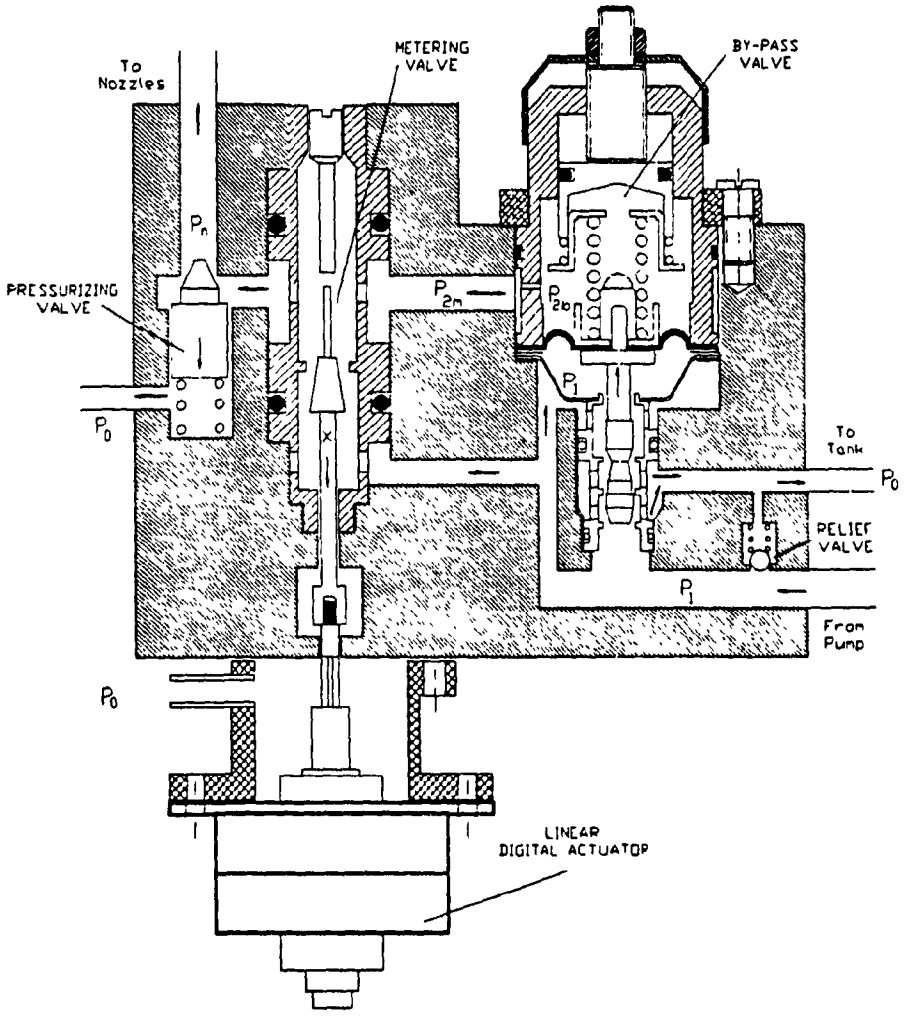

Fig. 4.6 Schematic of the first version of the electronic fuel control unit

movement of the actuator rod was transmitted to the metering valve using the ratio arm. In the second version, Fig. 4.7, the by-pass valve was also modified by removing the diaphragm and spring, and was brought under the control of a second digital actuator (AIRPAX, series 92200, model K92211-P2). Note that, the actuator operating the metering valve is shown attached directly to the valve. This would require some design modifications to overcome fuel leakage problems. The schematic is, nevertheless, used to demonstrate the concept of the electronically actuated metering valve.

4.6 Digital Electronic Controller

An electronic microcontroller is needed for the implementation of the digital control concepts. The controller should accept analog input signals from sensors mounted on the engine and the fuel control unit and should operate the linear digital actuator attached to the metering valve. The controller should be able to monitor the flow of the control signals and perform all necessary computing functions in real time. That is, all calculations and data acquisition should be performed at high enough speeds to keep-up with the physical processes of the fuel control unit and engine. Communication with the Air Borne Computer (ABC) should be established by an asynchronous

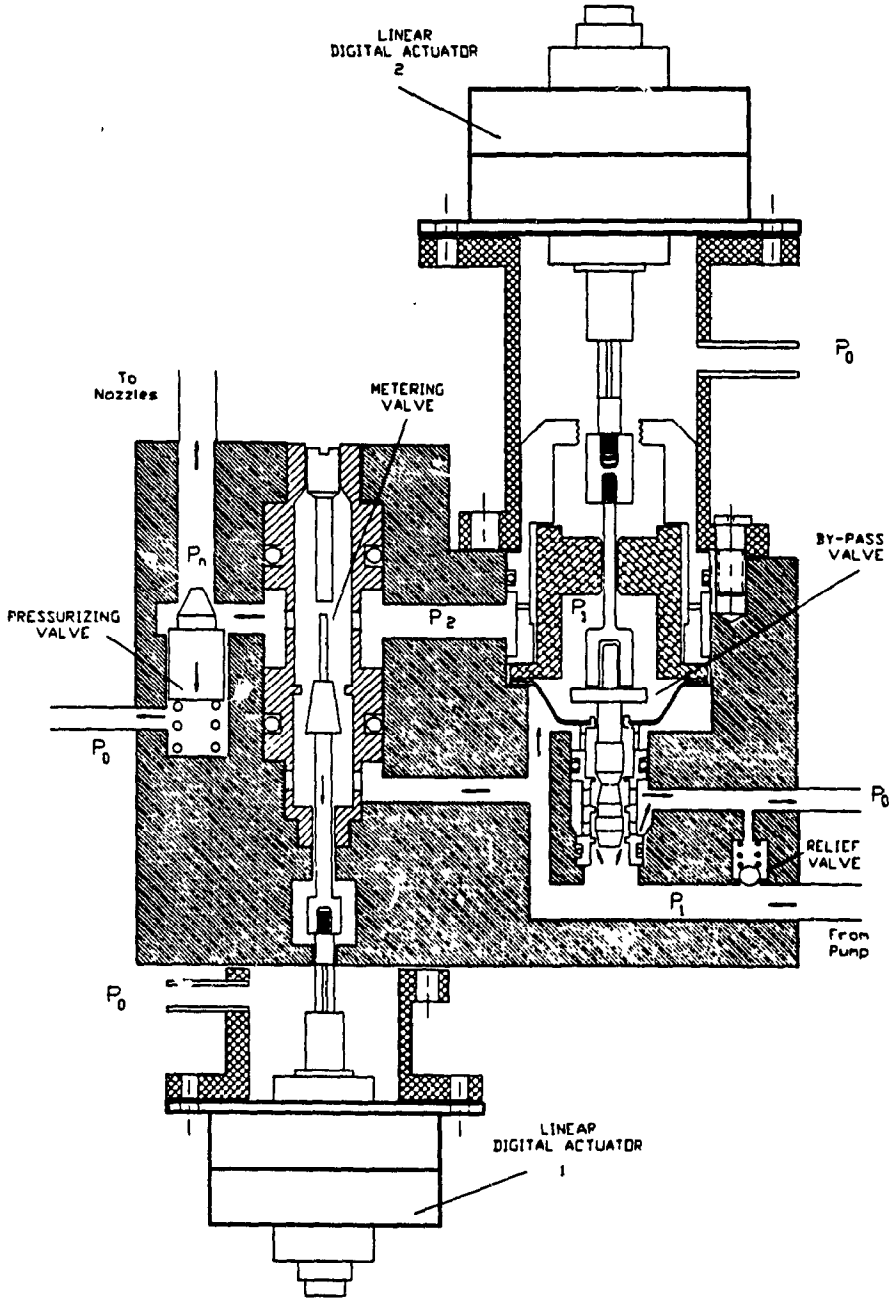

Fig. 4.7 Schematic of the second version of the electronic fuel control unit

serial Input/Output link.

An electronic controller design is proposed here. It is based on the Intel M80C196KB 16-bit Embedded Single Chip Microcontroller. The M80C196KB is a CHMOS version of the MCS-96 family of microcontrollers. It performs better than the earlier NMOS version and consumes less power. It can be placed in Idle and Power Down modes to further decrease electric power consumption. The reference frequency of the controller is 12 MHz. CPU operations are 16 bit wide and can be performed "from" or "to" any of the registers which constitute 232 bytes of on-chip RAM. This eliminates accumulator bottleneck and thus data throughput is increased. 8K of ROM memory which could be used to store the final control code is available on-chip as an option. More details about the microcontroller are included in Appendix D.

Figure 4.8 shows the layout of the proposed electronic controller. The microcontroller chip performs most of the required functions with minimum support from external devices. The control code resides in the EPROM, external to the microcontroller. This is a more practical approach than programming the ROM of the microcontroller since most of the FCU adjustments are implemented through software. Erasing and reprogramming the EPROM is preferred to replacing the microcontroller. The decoder (74LS138) is used to produce a Chip Select Pulse (CSP) whenever the

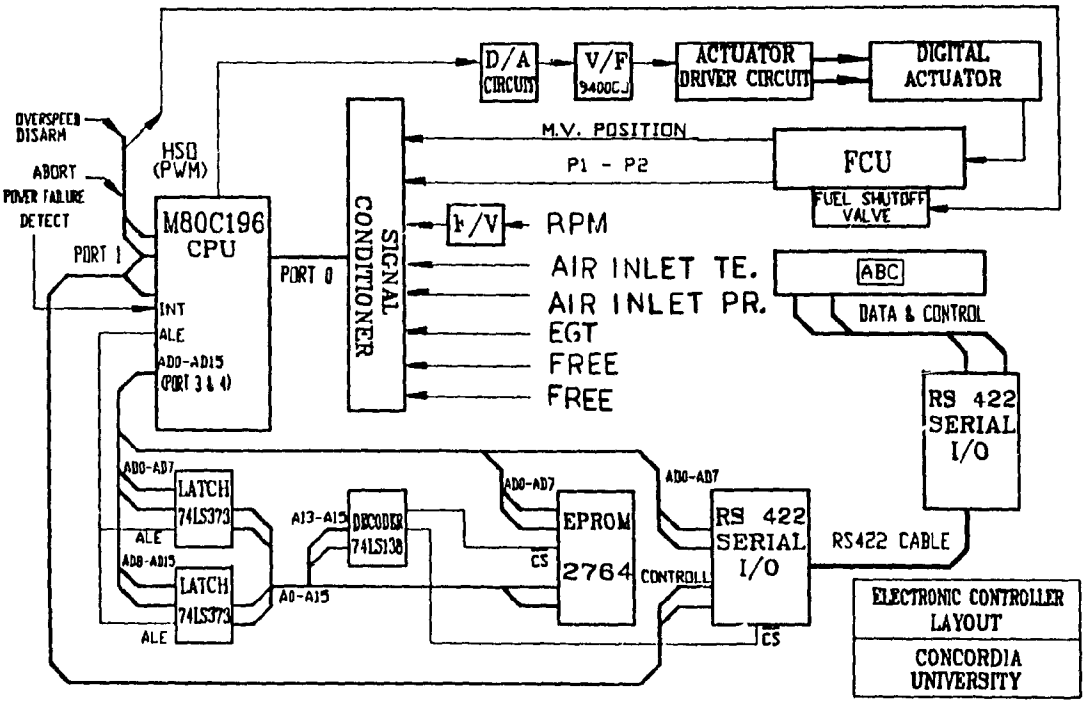

Fig. 4.8 Proposed digital electronic controller layout

memory or other peripherals are accessed.

Port 0 is used to read the analog input signals. All analog inputs are filtered to eliminate noise and are conditioned to a full scale voltage of 5 VDC. Details of the conditioning circuitry are shown in Fig. 4.9. The analog inputs are represented by a 10-bit resolution corresponding to 0.1% of F.S.. This is four times better than the 0.4% F.S. accuracy of the 8-bit representation.

Eight analog input signals can be sampled every 15 msec. These include, engine speed, metering valve position, differential pressure across the metering valve, inlet air temperature, inlet air pressure and exhaust gas

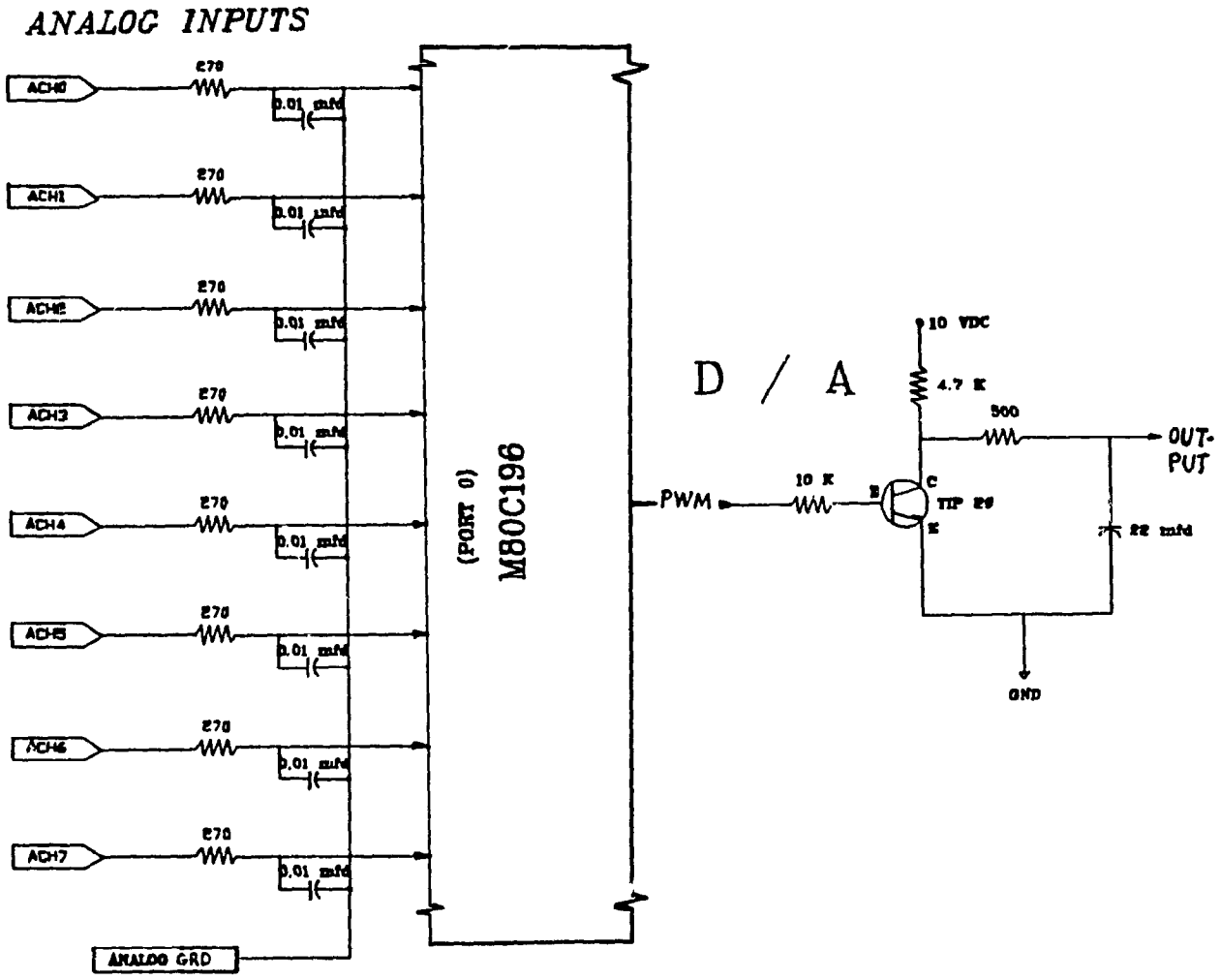

Fig. 4.9 Analog input/output signal conditioning circuit

temperature. Two channels are free in case other variables need to be sampled. The position of the metering valve and the differential pressure signals can be used to compute the fuel flow rate. Alternatively, the flow signal can be obtained using the nozzle injection pressure and the known flow area of the nozzle orifices. This approach, however, may produce erroneous results due to possible contamination

of the orifices with carbon deposits. It can, nevertheless, be used for test bench calibration of the unit. The fuel flow could also be measured directly using a turbine flow meter. A frequency to voltage converter is used to convert the frequency speed signal to a DC analog signal. This conversion is preferred to loading the CPU with frequency counting. The exhaust gas temperature signal can be used to avoid high inlet turbine temperatures, excessive power extraction or compressor stall.

A digital to analog converter is not needed if only one analog control output is used. In the present case, the actuator may be controlled using the Pulse Width Modulated (PWM) output available on-chip. This signal can be integrated, as shown in Fig. 4.9, to produce a DC voltage. The level of the voltage depends on the duty cycle of the PWM output.

The M8251A USART with the RS-422 receivers and drivers can be used to establish a serial communication with the Air Borne Computer (ABC). The ABC may request data (e.g. EGT, W_f, RPM, etc.), status information (e.g. diagnostic information about the state of the FCU) or issue a command to the FCU (e.g. to accelerate the gas generator to idle or to full speed, or to shut down the engine).

The engine starting procedure and communication between the ABC and the FCU can be as follows: The FCU is commanded by the ABC to start the engine. After the start

command, DC input is applied and the starter turns the gas generator (in case of a two shaft engine) which starts and accelerates to idle speed. The gas generator speed remains at idle while the load is at minimum. Then the ABC transmits a command to accelerate to full (rated) speed. When that speed is reached, the engine speed governing mode takes over. A speed change request should not overshoot or undershoot the final speed more than 1%. When the engine has to be shut down, a command is transmitted from the ABC to instruct the FCU to cut-off the fuel supply.

The FCU would detect a power failure by receiving an interrupt from pin 2 of port 1. Automatically it should shut-off the fuel flow and then reset. At that state the shut-off valve should be closed and the digital actuator should remain in its last position. Start up would be possible after a few seconds. At start up, the actuator should reset before the shut-off valve is opened. If the power is briefly interrupted the fuel FCU should not reset and the shut-off valve should remain open. This is possible by connecting a large capacitor in the power supply and power return line. An auxiliary power (battery) can be used as a standby.

Port 1 is used as a digital Input/Output. The status of pin 0 would indicate if the overspeed is disarmed or not. If the state is low and an overspeed (speed exceeding 110% of the rated speed) has occurred, the fuel flow to the

engine should shut-off. This is done by driving pin 2 low. This would switch off the power transistor thus closing the solenoid operated shut-off valve. If the state of pin 0 is high, the FCU will not shut off the engine. This may be important in certain cases such as during take-off. Pin 1 is used to interrupt the CPU when the abort switch is closed resulting in a low voltage level. If this is the case, an engine shut-off can occur.

CHAPTER 5

EXPERIMENTAL STUDY - CONCEPT FEASIBILITY

5.1 Test Facilities and Experimental Set-Up

Preliminary tests were performed using the first prototype of the electronic fuel control unit in which the metering valve was under electronic control. An AIRPAX linear digital actuator, model K92121-P2 with step size 0.05 mm, was used. In subsequent experiments (see Chapter 7 and Chapter 8), the actuator was replaced with another AIRPAX linear actuator, model K92211-P2, which has higher step resolution (0.025 mm) and can apply larger linear force. A test bench, BOSCH EFEP 515, originally made for testing and calibrating diesel fuel injection pumps was modified to accommodate the electronic fuel control unit. The schematic and a picture of the fuel control unit with fuel pump and measuring instruments are shown in Fig. 5.1.

The high pressure gear pump which supplied fuel to the fuel control unit was driven at selected speeds, in the range of 650 rpm to 6500 rpm, by an electric AC motor equipped with variable speed controller. The pump was made by SUNDSTRAND AVIATION, model 0255323-101-03, originally used in PT6-27 engines. Computer control was introduced to the electric motor to enable the programming of the pump

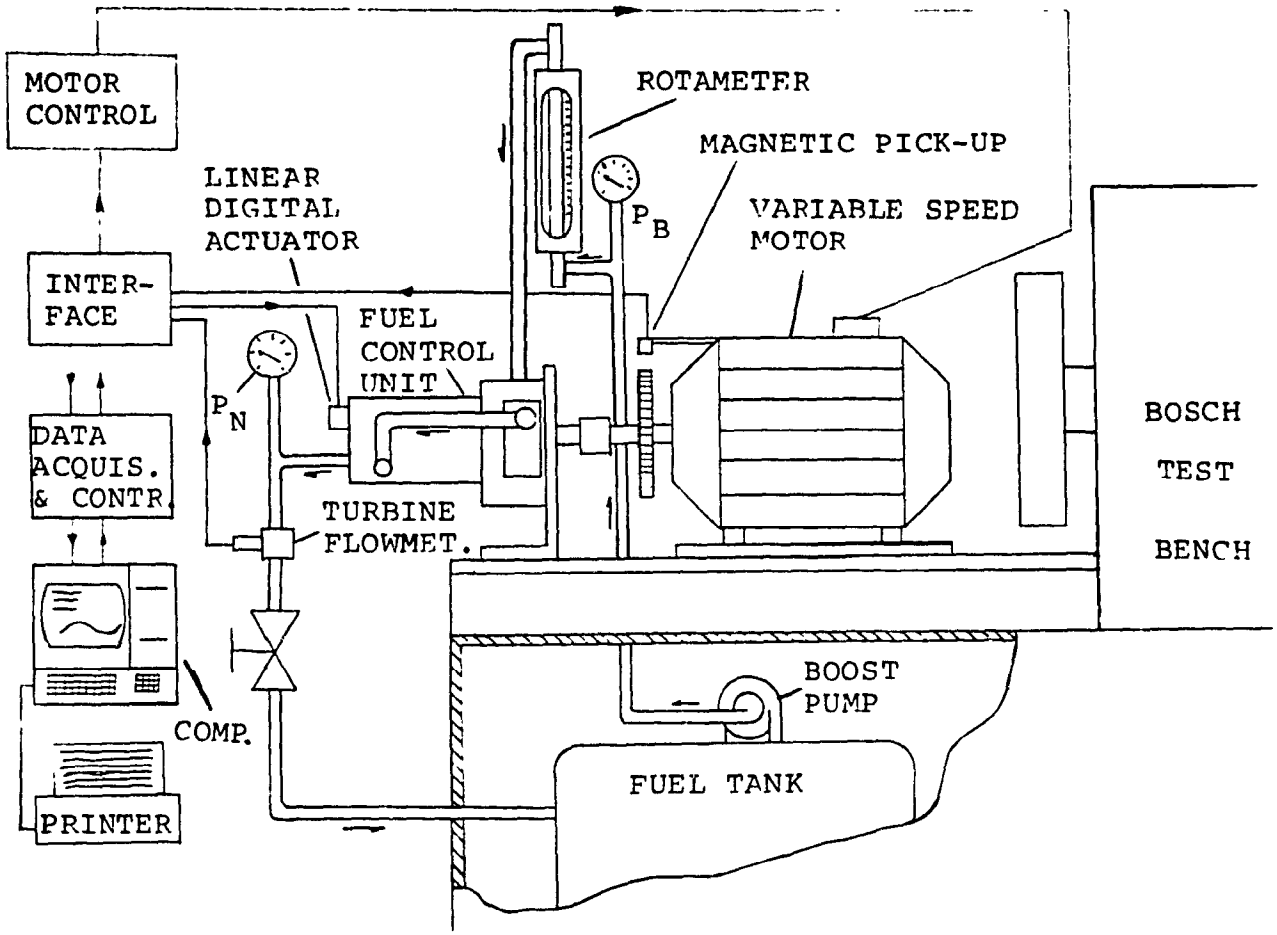

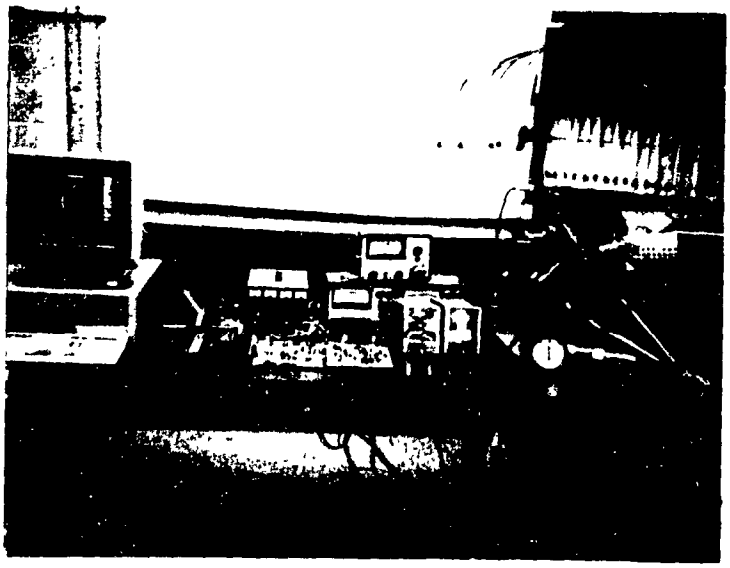

Fig. 5.1 Fuel control unit with monitoring system installed on the test bench and driven by the variable speed motor

speed. A DC voltage level was supplied to the variable speed motor driver/controller to impose a proportional motor speed. The speed control system was capable of accelerating or decelerating the fuel control unit through the full operating range, i.e. from idle to maximum speed, in less than one second. This is significantly faster than the time an engine would require to accelerate from idle to full power. The dynamic response of the electric motor driving the fuel pump is shown in Appendix A, Fig. A.6.

The test bench could boost the inlet pressure to the fuel control unit pump up to 4 bars, adjustable through a pressure regulator. Calibration Fluid SAE J965-150413, designated for calibration of diesel fuel injection pumps, was used. Small differences in the viscosity of the fluid with that designated for the calibration of fuel control units for gas turbine engines, was acceptable for the purpose of the present experiments.

For measuring the fuel pump speed, the pump drive shaft was fitted with a 60-tooth gear and a magnetic pick-up. The frequency signal generated by the rotation of the shaft was converted via a frequency to voltage converter to a DC voltage proportional to the pump speed. An LVDT travel transducer, made by AVL, Model 424, was used to measure the metering valve movement. A second LVDT travel transducer, Model 420, was used to measure the by-pass valve movement. Both LVDTs were equipped with a

carrier amplifier, AVL Model 3075-A02. Modifications made on the fuel control unit for the installation of the two travel transducers are shown in Fig. 5.2. Steel diaphragm pressure transducers were used to measure the pump discharge pressure, the differential pressure across the by-pass valve and the nozzle injection pressure. The transducers were made by VALIDYNE and were equipped with indicator amplifiers, Model CD12. A turbine flowmeter made by COX, Model AN 8-4, fitted with a magnetic pick-up, was used to measure the "metered" fuel flow. Some of the sensors are shown mounted on the fuel control unit in Fig. 5.3. Technical details and calibration curves are shown in Appendix A.

An IBM XT microcomputer equipped with IBM data acquisition peripherals was used for reading the measured variables and also for the implementation of the digital controller. A distribution panel was used for making Input/Output signal connections. Additional electrical circuits were built for conditioning of the input signals and for interfacing the control output signals with the digital actuator driving circuits. Also, demultiplexing circuits were built to increase the number of available A/D channels from four to eight.

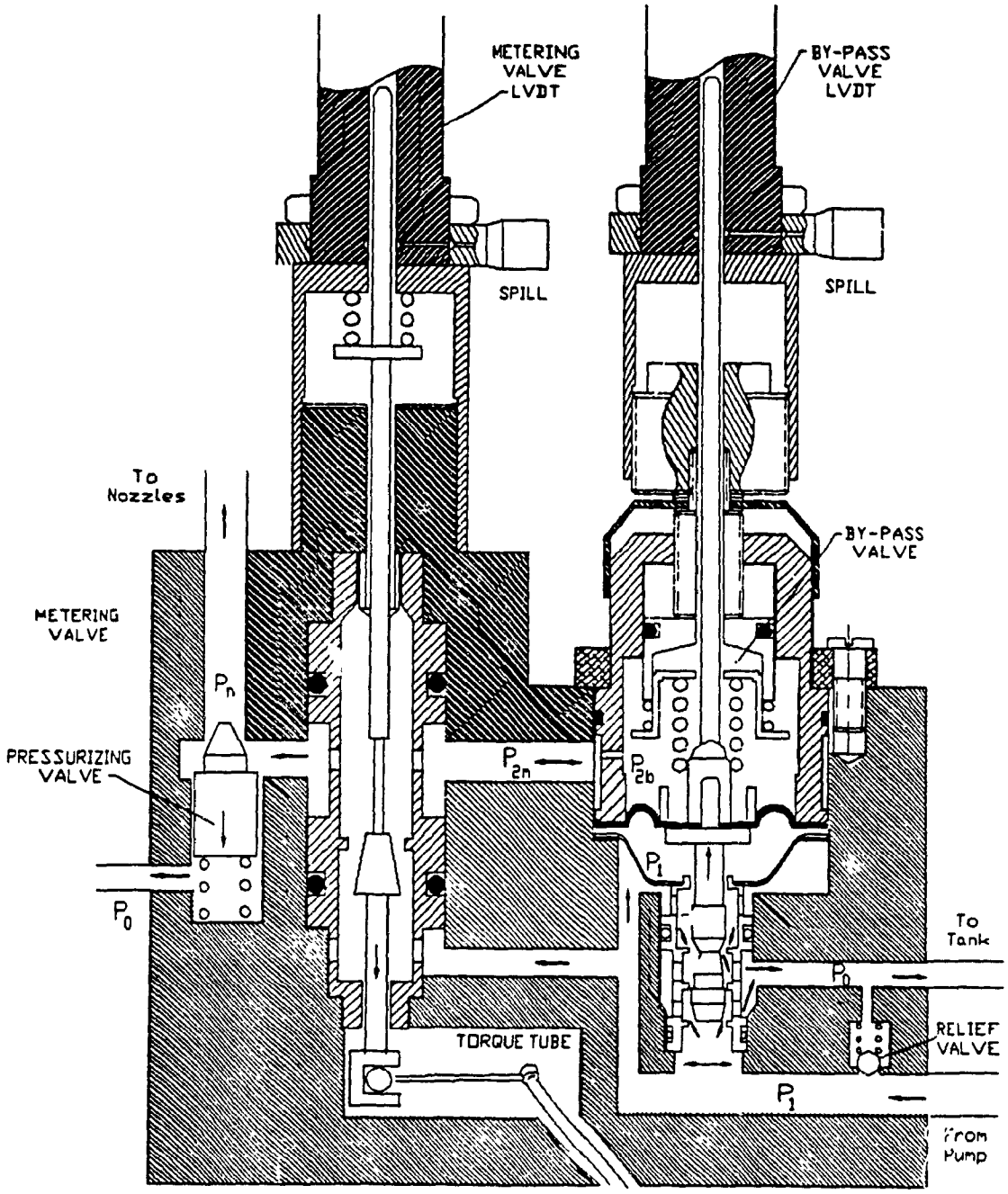

Fig. 5.2 LVDT travel transducers installed on the metering and by-pass valves

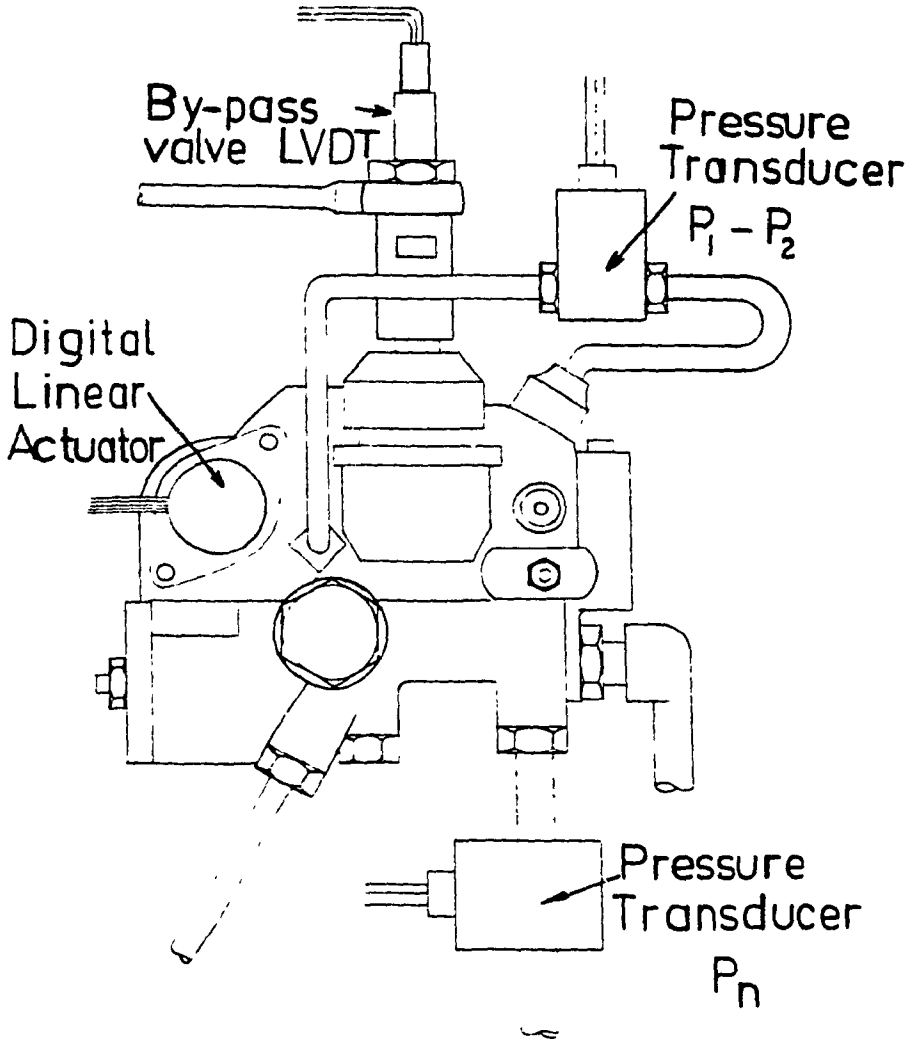

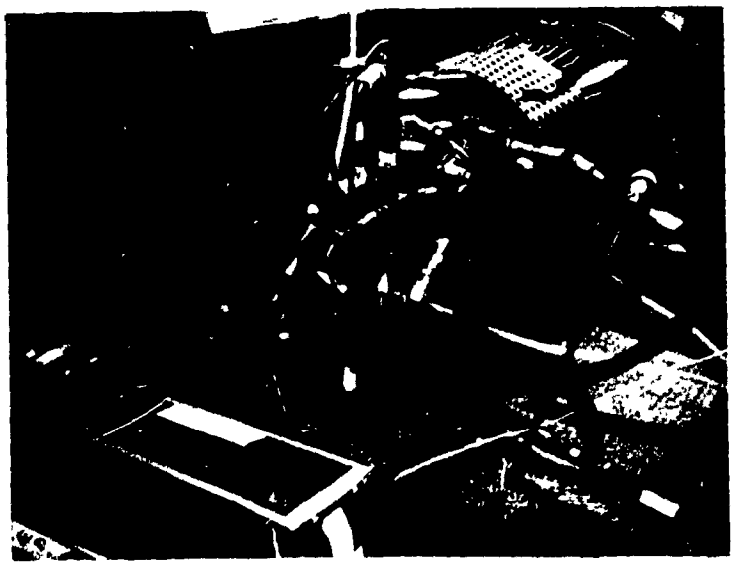

Fig. 5.3 Experimental electronic fuel control unit equipped with sensors

5.2 Test Procedure

Open loop tests were performed to evaluate the accuracy and the dynamic response of the electronic fuel control unit. Two basic types of tests were performed. First, the pump speed was cycled and the metering valve was controlled according to a particular fuel flow schedule. The dynamic response of the unit was tested for abrupt changes of the pump speed at maximum speed governing. Pump speed, fuel flow, differential pressure and the by-pass valve movement were recorded.

It is noted that, at the time when these tests were performed, the metering valve was not yet instrumented with the LVDT. Therefore, the position of the valve was obtained by counting the number of steps commanded to the digital actuator.

5.3 Results and Discussion

Figure 5.4 shows the total number of steps commanded to the digital actuator and the resulting fuel delivery rate at all operating modes of the engine. The differential pressure across the metering valve and the by-pass valve movement are shown in Fig. 5.5. Fuel scheduling was initiated at the engine starting speed, continued through acceleration, changed to maximum speed governing, then to deceleration and finally ended at the ground idle.

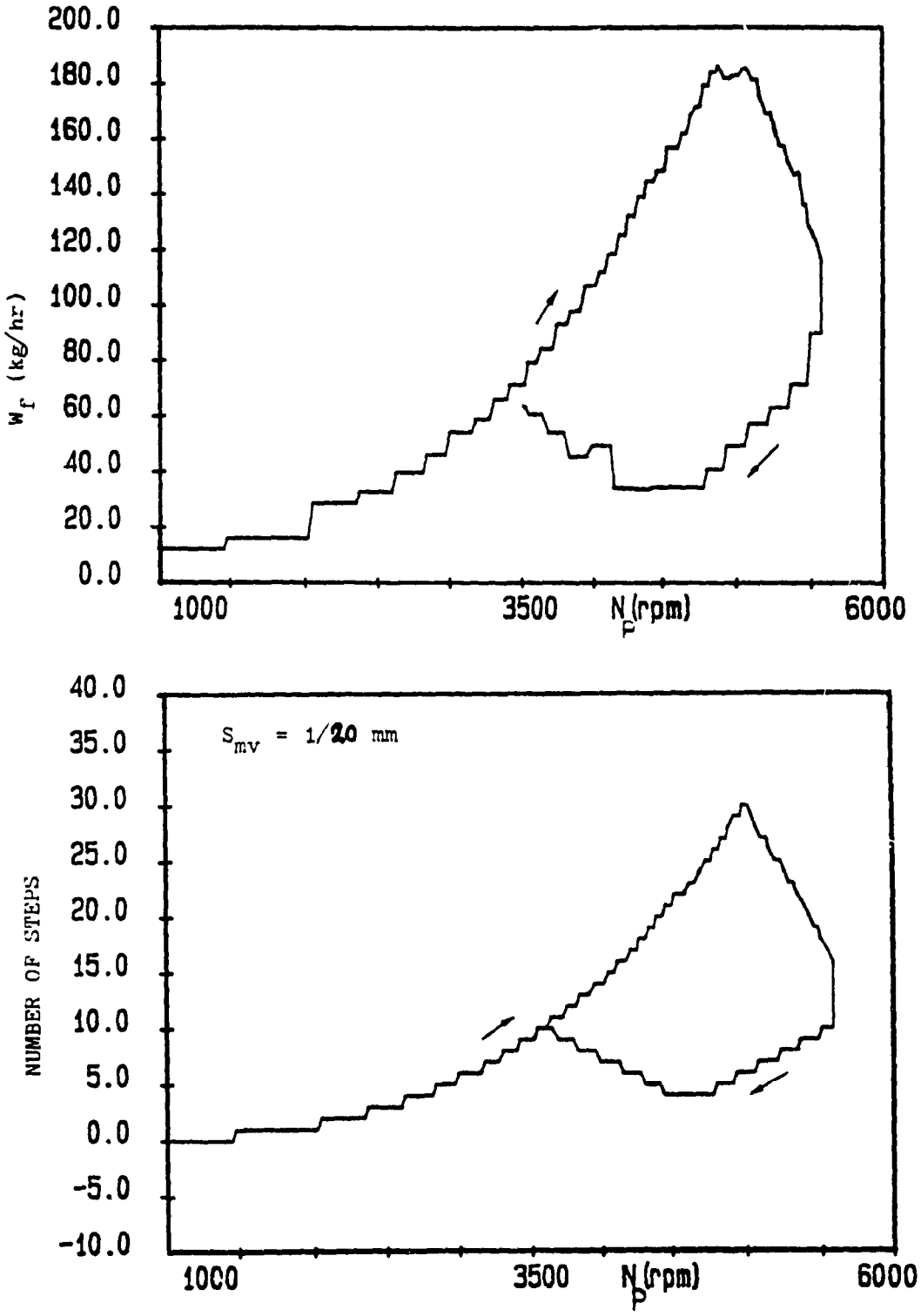

Fig. 5.4 Number of steps commanded to the actuator and fuel flow rate vs pump speed

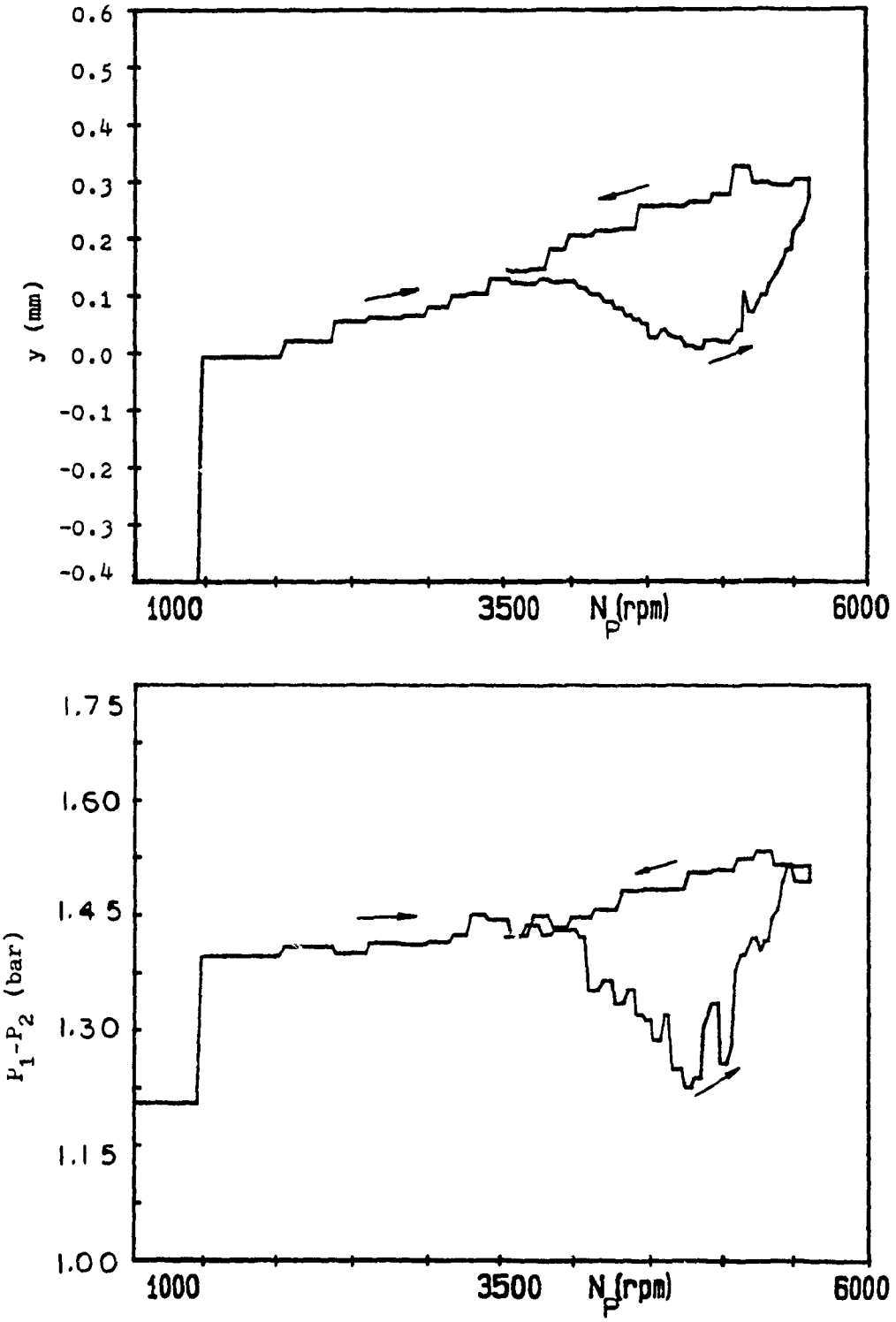

Fig. 5.5 Pressure difference across metering valve and by-pass valve position vs pump speed

It is obvious from these records that the step size of the actuator (0.05 mm) is too large and it should be reduced in order to improve the discrete character of the fuel flow. The transition from acceleration to maximum governing shows some irregularities at the peak of the curve which are not consistent with the metering valve movement. This suggests that the metering valve is restrained by the increased pressure at high speeds and as a result steps are lost. Also, the actuator cannot be stopped within a single step when it is moving at a high stepping rate (higher than what is known as the "slewing" rate). Change towards smaller steps should help the motor overcome the increased load. This would also improve the accuracy of the metered fuel; however, the transient process would be slower.

The plot of pressure difference across the by-pass valve reveals some fluctuations at high speeds. These fluctuations, however, are not followed by the by-pass valve movement. This suggests that the by-pass valve motion is damped and the valve is not acting fast enough to follow the differential pressure changes.

For the particular fuel schedule used in the present experiments, the differential pressure started to drop drastically at about 4000 rpm. This indicated that the metering valve position exceeded the maximum allowed at the particular pump speed. The differential pressure drop

resulted in a non-proportional relationship between fuel flow rate and metering valve opening. The differential pressure was restored when the valve opening was reduced to obtain the deceleration schedule, Fig. 5.5. The limits of metering valve movement as a function of pump speed were established in subsequent experiments (see Chapter 7).

Figure 5.6 shows results at the maximum speed governing mode, when the actuator movement was reversed. The shift in the fuel flow rate is related to the backlash of the lead screw* of the linear actuator and also to hysteresis caused by friction in the torque tube and seals. This latter phenomenon is typical of the conventional metering valve in Bendix units. Fig. 5.7 shows the effect of hysteresis on the pressure and the by-pass valve movement.

The dynamic response of the system at maximum speed governing, when the speed was abruptly† increased by approximately 10%, is shown in Fig. 5.8. The purpose of this test was, first, to determine if the stepper motor was

---

* A lead screw is used to convert the rotary motion of the digital actuator to linear motion.

---

† As seen from the dynamic response of the electric motor, Fig. A.6, it is not possible to impose a step change in the pump speed. However, the dynamic response of the electric motor is considerably faster than the response of a typical small gas turbine engine.

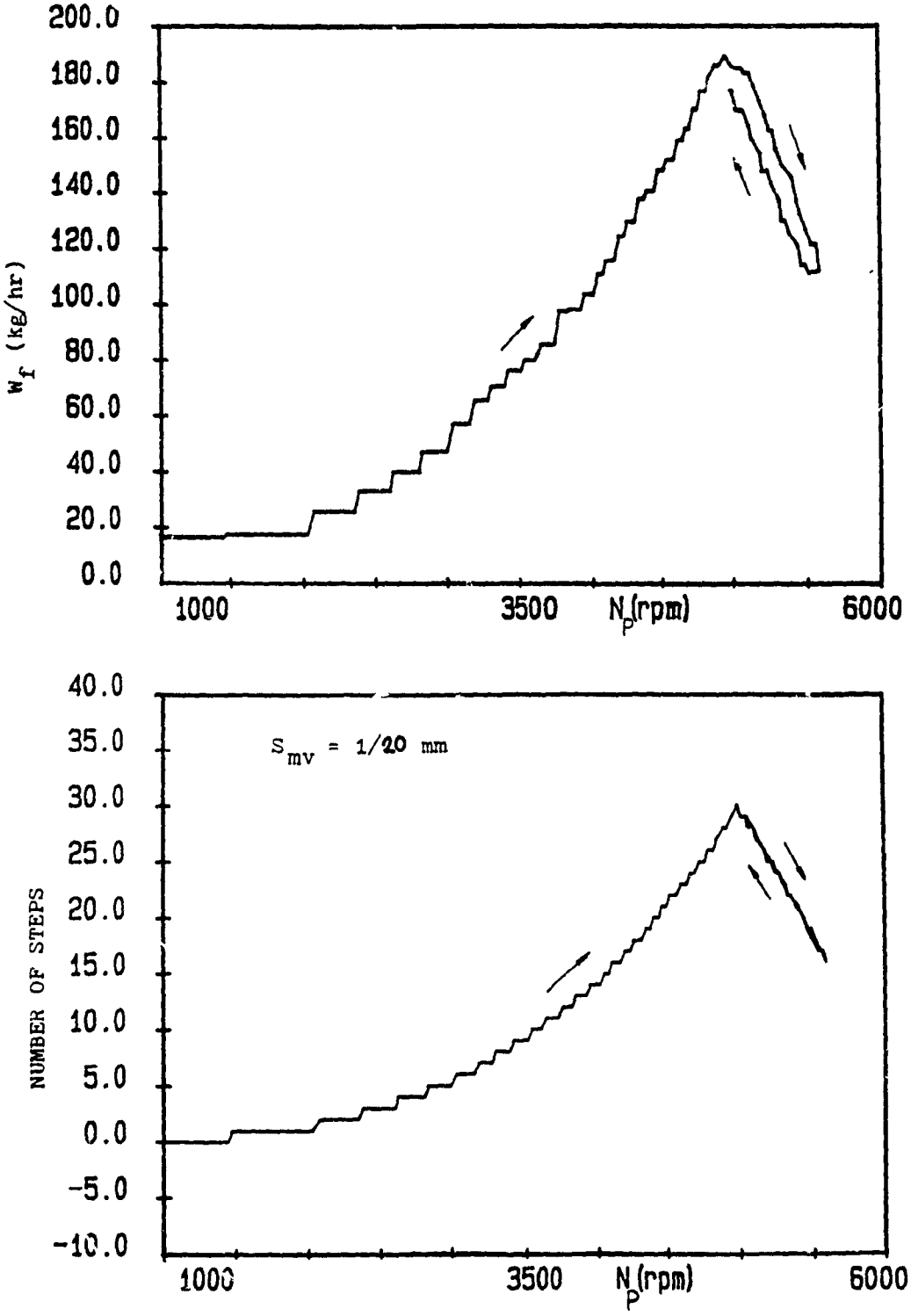

Fig. 5.6 Metering valve cycled at maximum speed governing; Recorded fuel flow rate

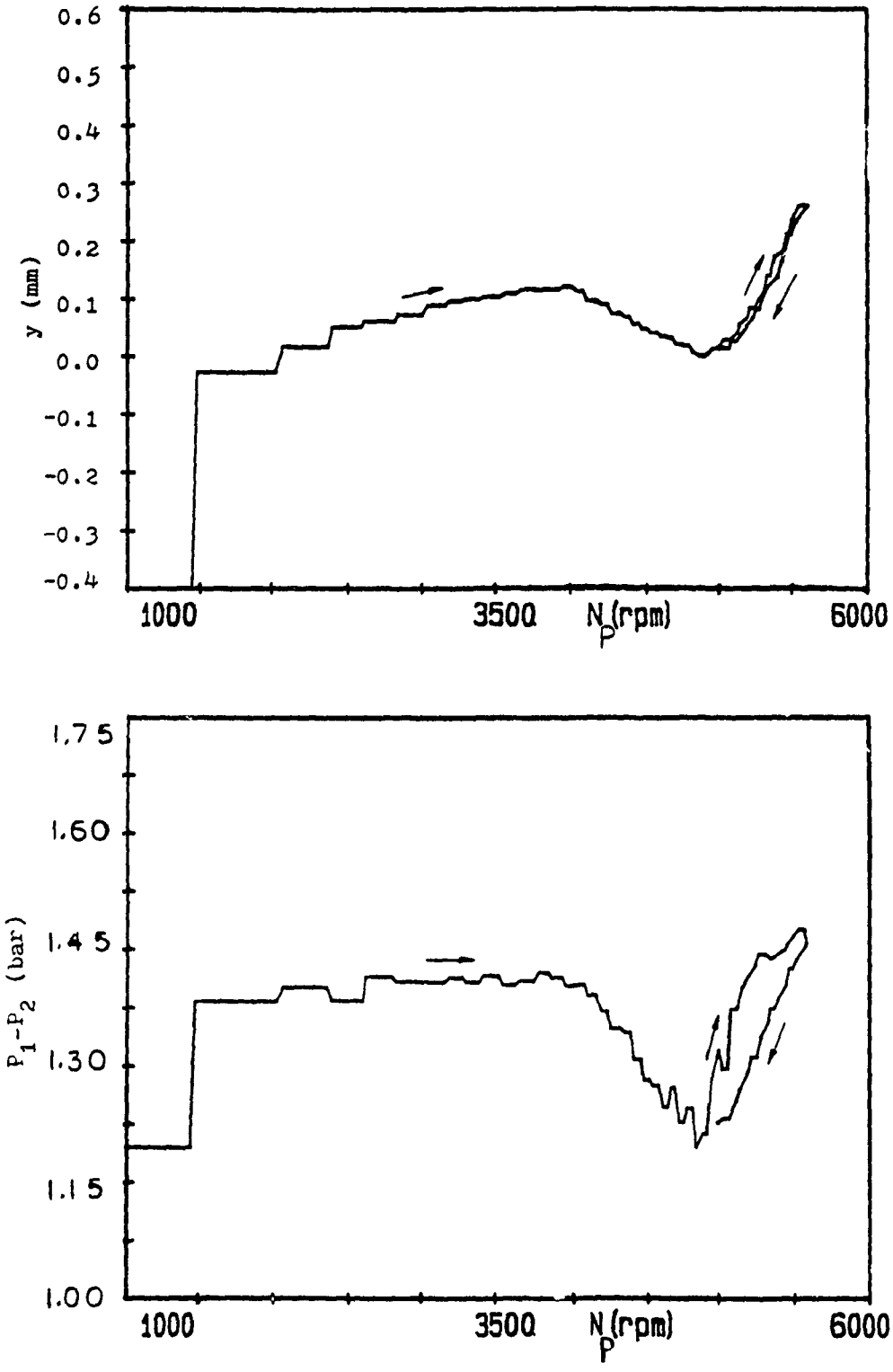

Fig. 5.7 Differential pressure and by-pass valve movement at maximum speed governing reversal

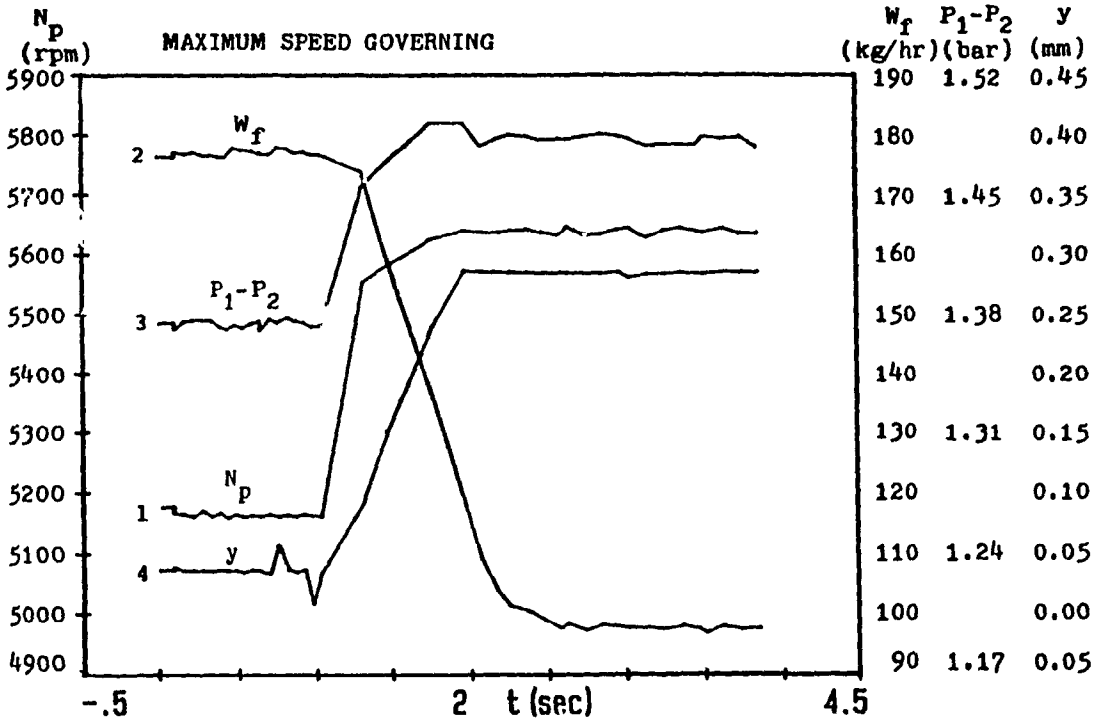

Fig. 5.8 Records of fuel flow rate, pressure difference across the metering valve and by-pass valve movement obtained during a rapid speed increase at maximum speed governing

fast enough to impose a rapid change in the position of the metering valve and second, to observe the response of the conventional by-pass valve, in order to determine whether a second digital actuator could operate the valve as fast as the conventional diaphragm actuator.

It takes almost one second to decrease the fuel flow rate to its final value, i.e. approximately twice the time taken for the speed increase. Small overshoot is observed in the dynamic response of the differential pressure. The overshoot is not, however, reflected in the by-pass valve dynamic response. This is due to the damping of the by-pass

valve movement which results from the fuel flow through the throttling orifice in the top chamber of the valve (see Chapter 6). As expected, the by-pass valve opening is increased in order to return the increased amount of excess fuel back to the pump inlet.

5.4 Summary

The use of electronic incremental control in the metering valve of a modified hydromechanical fuel control unit is possible. The transient response of the metering valve is not far from that required and it can be improved by selecting a more suitable digital actuator. The recorded dynamic response of the by-pass valve shows that the valve could be operated electronically using a second linear actuator. The electronically controlled by-pass valve would further increase the flexibility and capabilities of the system (see Chapter 10). The prototype of such a by-pass valve was made and tests verified the feasibility of such a controller.

Following the results of this preliminary investigation, it became apparent that a stronger actuator with smaller step size was needed to control the metering valve. Alternatively, a pressure balanced valve could be used to eliminate actuator loading.

CHAPTER 6

MATHEMATICAL MODEL OF FUEL METERING SECTION

6.1 General

The metering section of the proposed electronic system is the same as the one in the conventional fuel control unit. The only difference is the way the metering valve is actuated. Detailed analysis and model validation of the metering section is essential for the development of the electronic controller.

The model presented here is based on the work of MacIsaac et al (49) who derived the model of the metering section of a fuel controller. Their derivations, however, were not well documented. Steady state results did not include the effect of the minimum pressurizing valve and the validation of the dynamic model was not presented. Also, a detailed investigation of the flow forces in the by-pass valve was not performed.

To establish faith in that work and to further improve the model, the metering section is remodelled here and complex modules, such as the by-pass valve, are given special attention.

6.2 Modelling of the Metering Section

A simplified functional diagram of the hydromechanical fuel controller, attached to an engine for a turboshaft application, is shown in Fig. 6.1. The metering and computational sections are shown in dashed lines. During gas generator acceleration, the bellows (in the computing section) uses the ambient pressure and temperature information (P_a, T_a) and the compressor discharge pressure (P_3), to generate a force (F_{mv}) which actuates the metering valve. The mechanical governor flapper valve is closed ($X_f = 0$). During maximum speed governing, the mechanical speed governor uses the throttle lever input angle (α_1), the gas generator speed (N_1), and the power turbine speed governor force (F_g), to position the flapper valve. Based on the additional input from the flapper valve, the bellows actuates the metering valve in order to produce the required fuel flow rate and maintain constant load speed (N_2).

The mathematical model of the different modules of the unit can be linked together to obtain the response of the complete system. In this study, emphasis is focused on the modelling of the metering section. The schematic and the computational diagram of the metering section are shown in Fig. 6.2 and Fig. 6.3 respectively. The metering section consists of the metering valve, the by-pass valve, the

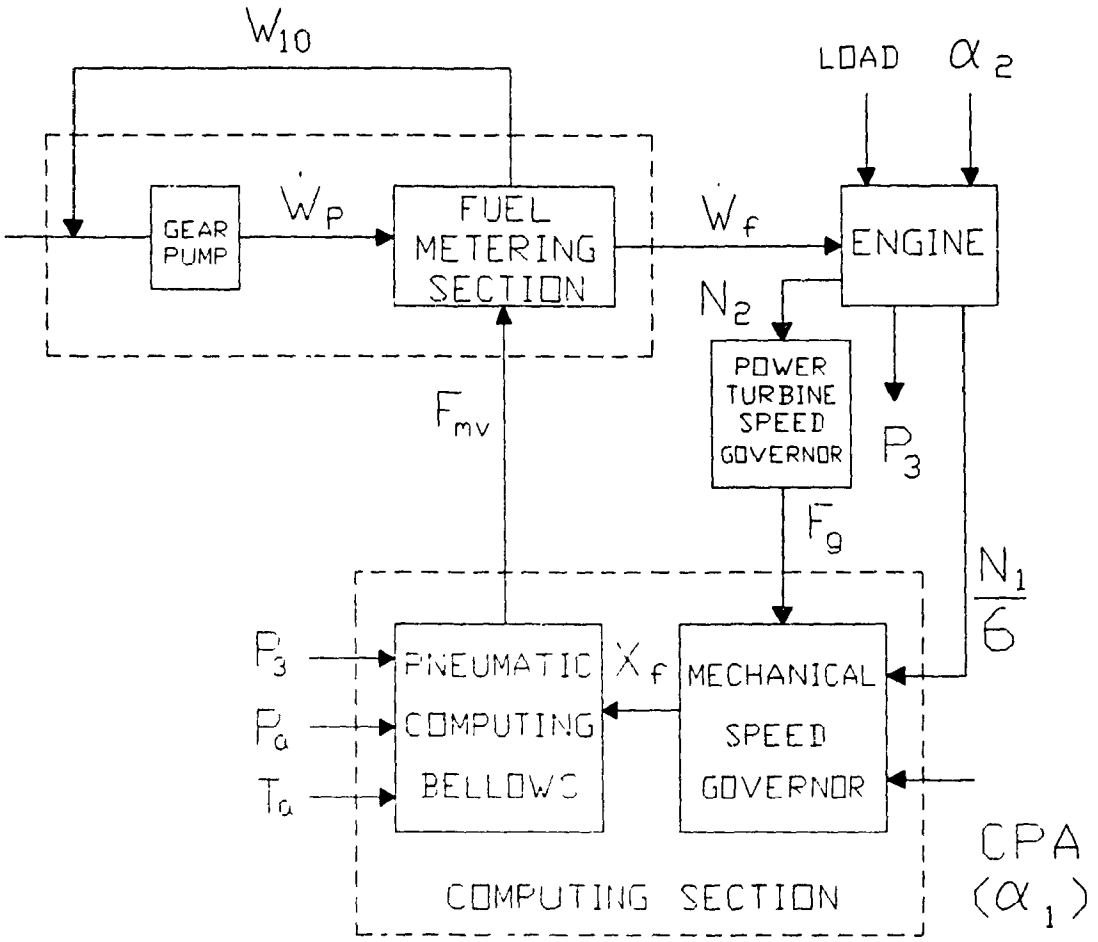

Fig. 6.1 Functional diagram for the Bendix DP-F2 fuel control unit

minimum pressurizing valve and the volumes formed between the valves and other flow restrictions. The high pressure gear pump is driven at a speed directly proportional to the gas generator speed. Excess fuel flow is returned, through the by-pass valve, back to the pump inlet.

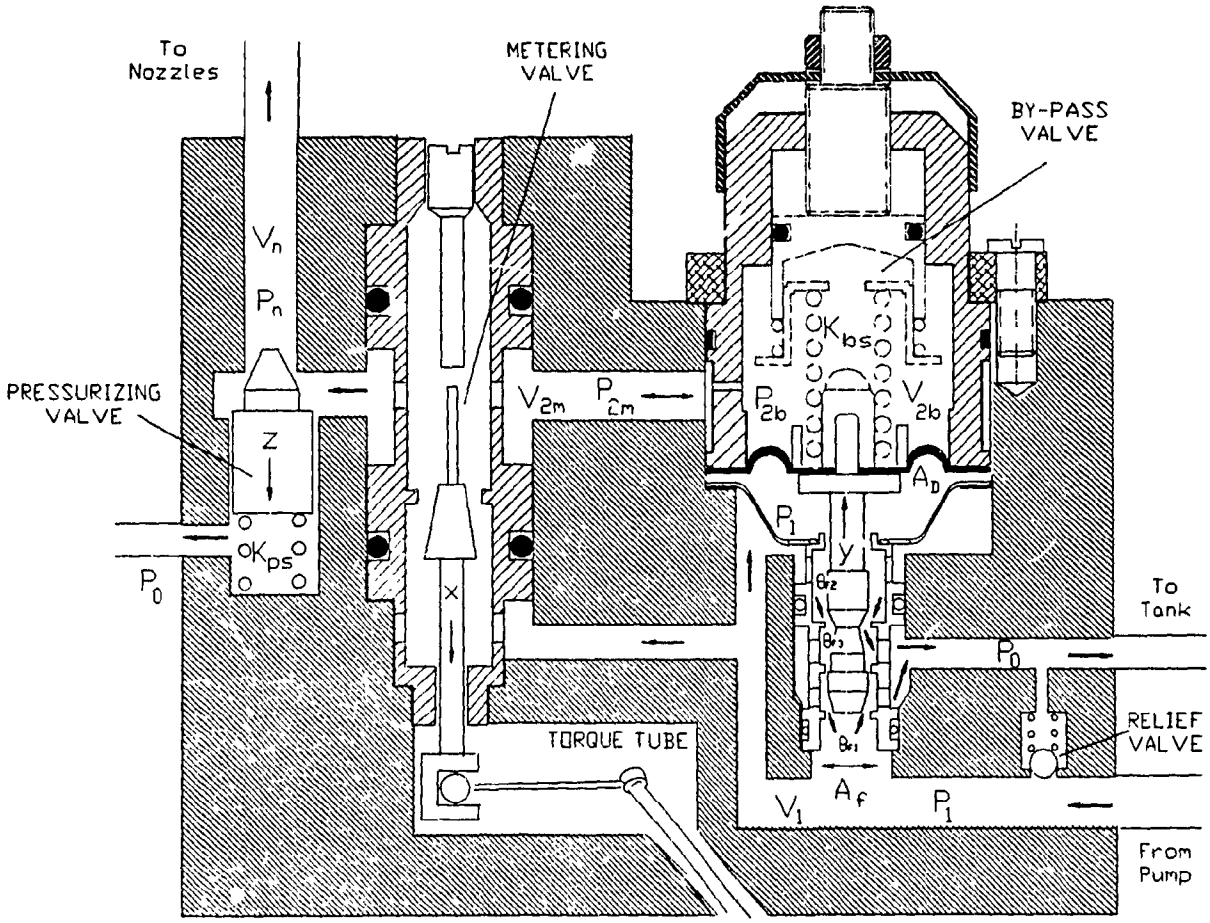

Fig. 6.2 Schematic of the metering section of the Bendix DP-F2 fuel control unit

6.2.1 Modelling of Fuel Flow

Pump delivery

The fuel flow delivered by the positive displacement (gear type) pump, used to supply fuel to the fuel control unit, is a function of the rotational speed and the pressure difference across the pump:

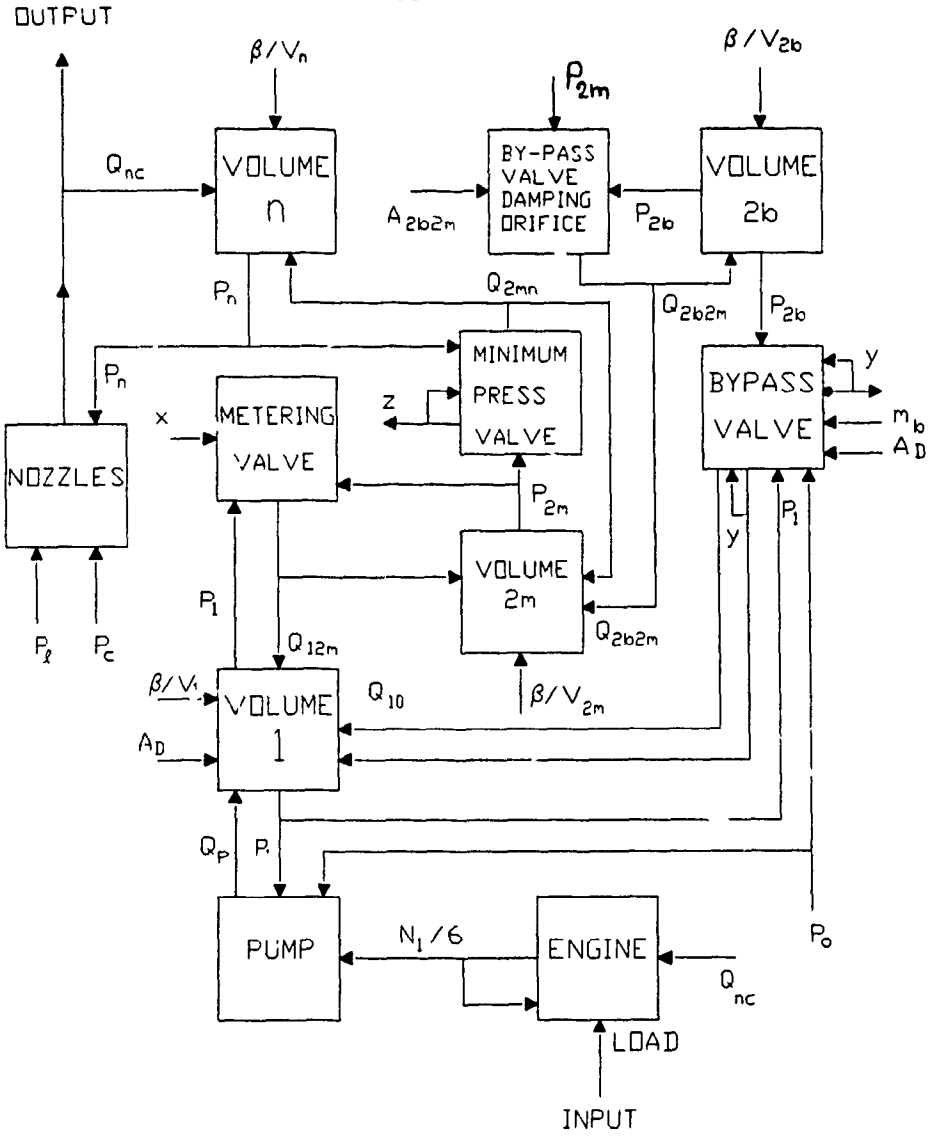

Fig. 6.3 Computational diagram of the metering section of the fuel control unit

$$Q_p = f(N_p,\ P_1 - P_0) \qquad (6.1)$$

For small perturbations about an operating point:

$$\Delta Q_p = C_1\ \Delta N + C_2\ \Delta(P_1 - P_0) \qquad (6.2)$$

where

$$C_1 = \frac{\partial Q_p}{\partial N_p} \qquad \text{and} \qquad C_2 = \frac{\partial Q_p}{\partial (P_1 - P_0)}$$

The value of C_1 is the pump displacement and C_2 is the coefficient of leakage across the pump due to the difference between intake and discharge pressures. The pump characteristic was examined experimentally (see Appendix B) and it was found that C_2 was close to constant at high differential pressures across the pump. At normal operating conditions of the fuel control unit, the differential pressure across the pump is high. Therefore, the value of C_2 is considered to be constant. In order to express Equation (6.1) in terms of total values instead of deviations, a constant is added which represents the intersection of the Q_p-axis and the fuel flow characteristic plane. Therefore, the pump delivery is described by:

$$Q_p = C_1 N + C_2 (P_1 - P_c) + C_3 \qquad (6.3)$$

Metering Valve Flow

The fuel metered is related to the flow area in the metering valve and the differential pressure across it:

$$Q_{12m} = (C_d)_{12m} K A_{12m} \sqrt{P_1 - P_{2m}} \qquad (6.4)$$

where $K = \sqrt{\frac{2}{\rho}}$

The effect of the pressure change on the density of the fuel is very small and the fuel flow can be assumed incompressible. This assumption is quite reasonable because the percentage of change in density is equal to the change in pressure divided by the bulk modulus of elasticity of the fuel. That is, $\Delta\rho/\rho=\Delta P/\beta$. In the present case, the maximum possible change in density is around 0.1%.

The metering valve has a truncated-cone-like profile. The flow area, A_{12m}, formed between the metering valve orifice and the valve profile is:

$$A_{12m} = a_1x^2 + a_2x + a_3 \qquad (6.5)$$

The evaluation of coefficients a_1, a_2, a_3 for different metering valve positions is shown in Appendix B. Experiments were performed to establish the flow coefficient $(C_d)_{12m}$. Results showed that its value did not deviate much from the expected value of 0.6, especially at high fuel flows (see Appendix B).

By-pass Valve Flow

The excess fuel flow, returned to the pump through the by-pass valve, is given by:

$$Q_{10} = (C_d)_{10} K A_{10} \sqrt{P_1 - P_0} \qquad (6.6)$$

where, A_{10}, is a function of valve position and geometry:

$$A_{10} = b_1 y^2 + b_2 y + b_3 \qquad (6.7)$$

where

$b_1 = -\pi (\sin^2\theta_{b1}\cos\theta_{b1} + \sin^2\theta_{b2}\cos\theta_{b2})$

$b_2 = \pi D_{bo}(\sin\theta_{b1} + \sin\theta_{b2})$

b_3 = area due to valve overlap

Detailed derivation of the flow area constants is shown in Appendix B.

It was observed, from initial experiments, that there was a substantial leakage in the by-pass valve when the valve was closed. This, however, did not affect normal operation because the pump always supplied fuel in excess of the fuel flow rate required by the engine. The by-pass fuel flow rate was always much greater than the maximum possible leakage through the valve. As a result, the by-pass valve was always open during normal operation. For the sake of completeness of the mathematical model, however, leakage flow was described by*:

---

* A simple technique to reduce leakage is to increase the overlap of the valve.

$$Q_{10} = (C_d)_{10} K (A_{10})_{\ell} \sqrt{P_1 - P_0} \qquad (6.8)$$

for $y = y_{min}$

Damping Orifice Flow

The damping orifice stabilizes the by-pass valve motion by restricting the fuel flow "from" and "to" the top chamber of the valve. This builds-up pressure which opposes the movement of the valve. The flow through the damping orifice is:

$$Q_{2b2m} = (C_d)_{2b2m} K A_{2b2m} \text{ sgn}(P_{2b}, P_{2m}) \sqrt{|P_{2b} - P_{2m}|} \qquad (6.9)$$

The term $\text{sgn}(P_{2b}, P_{2m})$ is included to account for the possibility of the fuel flowing in either direction.

Minimum Pressurizing Valve Flow

The minimum pressurizing valve builds up sufficient pressure inside the system to operate the by-pass valve servo control also at low flows. It also isolates the nozzle manifold in case of engine shut-down thus preventing post-shutdown flooding. The pressure in the fuel control unit is retained and the system is ready for faster restarts (50).

The flow through the pressurizing valve is given by:

$$Q_{2mn} = (C_d)_{2mn} K A_{2mn} \sqrt{P_{2m} - P_n} \qquad (6.10)$$

where, (see Appendix B):

$$A_{2mn} = c_1 z^2 + c_2 z \qquad (6.11)$$

and

$$c_1 = -\pi (\sin^2\theta_p \cos\theta_p)$$

$$c_2 = \pi D_{po} \sin\theta_p$$

At high flow rates, the pressurizing valve is forced against its maximum stop. When this occurs, the valve behaves as a fixed orifice.

Nozzle Flow

The fuel flow through the nozzles is:

$$Q_{nc} = (C_d)_{nc} K A_{nc} \sqrt{P_n - (P_c + P_\ell)} \qquad (6.12)$$

Where P_ℓ is included to account for line friction losses (49). The compressor delivery pressure, P_3, and the position of the metering valve are given as functions of the engine speed. The value of $(C_d)_{nc} A_{nc}$ was determined experimentally and is shown in Fig. B.9.

6.2.2 Modelling of Fuel Flow Accumulation

Metering Valve High Pressure Volume

The pressure build-up is a function of the enclosed fuel volume, the fuel flow influx and the effective fuel bulk modulus of elasticity. In the volume upstream of the metering valve, the pressure change is described by:

$$\frac{dP_1}{dt} = \frac{\beta}{V_1}\left(Q_p - A_D\frac{dy}{dt} - Q_{12m} - Q_{10}\right) \qquad (6.13)$$

The total change of the original volume due to the by-pass valve diaphragm movement is very small and can be neglected. The rate of change of the volume, however, is comparable to the other flow terms and is included in the above relationship.

Metering Valve Low Pressure Volume

The pressure in the volume downstream of the metering valve is described by:

$$\frac{dP_{2m}}{dt} = \frac{\beta}{V_{2m}}\left(Q_{12} + Q_{2b2m} - Q_{2mn}\right) \qquad (6.14)$$

By-pass Valve Volume

The pressure in the upper volume of the by-pass valve is given by:

$$\frac{dP_{2b}}{dt} = \frac{\beta}{V_{2b}} \left(A_D \frac{dy}{dt} - Q_{2m2b}\right) \qquad (6.15)$$

As in the case of Equation (6.13), the total change of the original volume is not affected significantly by the diaphragm movement.

Nozzle Manifold Volume

The pressure in the nozzle manifold is described by:

$$\frac{dP_n}{dt} = \frac{\beta}{V_n} \left(Q_{2mn} - Q_{nc}\right) \qquad (6.16)$$

6.2.3 Modelling of Valve Motion

Metering Valve

The motion of the metering valve is discrete. It is assumed to follow the steps as commanded by the electronic controller. Its motion is incremental and is described by:

$$x = S_{mv} \text{ INTEGER } (f\ t) \qquad (6.17)$$

By-pass Valve

Forces acting on the by-pass valve, during a transient process, are created by the pressure difference across the diaphragm, the diaphragm spring and the change of momentum of the fuel flowing against the valve conical profile. The pressure force is given by:

$$F_{bp} = (A_{De} - A_f)\ P_1 - A_{De}\ P_{2b} \qquad (6.18)$$

The derivation of the effective pressure area, A_{De}, is shown in Appendix B.

To evaluate the flow force, the change of momentum of the fuel is considered. The relative motion of the valve with respect to the fuel flow is also taken into account. The flow force is:

$$F_{bf} = A_f P_1 - 2C_d A_e (P_1 - P_0) - B_b \frac{dy}{dt} \qquad (6.19)$$

where

$$A_e = (A_{10})_1 \cos\theta_{f1} + (A_{10})_2 (\cos\theta_{f2} - \cos\theta_{f3})$$

$$B_b = \rho K (A_{10})_1 \sqrt{P_1 - P_0}$$

$(A_{10})_1$, $(A_{10})_2$ are the flow areas on each end of the by-pass valve:

$$(A_{10})_1 = (b_1)_1\ y^2 + (b_2)_1\ y + (b_3)_1$$
$$(A_{10})_2 = (b_1)_2\ y^2 + (b_2)_2\ y + (b_3)_2$$

where $(b_1)_1 = -\pi\ (\sin^2\theta_{b1}\cos\theta_{b1})$

$(b_1)_2 = -\pi\ (\sin^2\theta_{b2}\cos\theta_{b2})$

$(b_2)_1 = \pi\ D_{bo}\sin\theta_{b1}$

$(b_2)_2 = \pi\ D_{bo}\sin\theta_{b2}$

$(b_3)_1$ = area due to overlap of bottom valve port

$(b_3)_2$ = area due to overlap of top valve port

Derivation of the above flow area constants is shown in Appendix B.

The spring force is:

$$F_{bs} = k_{bs} y + F_{bso} \tag{6.20}$$

When the valve hits a stop, for example, at its minimum (closed) position, it can be assumed, for modelling purposes, that it comes into contact with a second spring of very large rate. Equation (6.20) can be rewritten as:

$$F_{bs} = k_{bs} y + k_{wbs}(y - y_{min}) + F_{bs0} \tag{6.21}$$

where $k_{wbs} = 0$ for $y > y_{min}$

$k_{wbs} = 10^6$ for $y < y_{min}$

The dynamic force balance of the by-pass valve is described by the following equation:

$$\frac{d^2y}{dt^2} = \frac{1}{M_b}\left[A_{De}(P_1 - P_{2b}) - 2C_d A_e (P_1 - P_0) - F_{bs} - B_b \frac{dy}{dt}\right] \tag{6.22}$$

Prediction of the flow angles, for a geometry such as that of the by-pass valve, is very difficult. Therefore, A_e was found experimentally and was expressed as a function of the metering valve position. The relationship is shown in

Appendix B, Fig. B.11. In the case of the double actuator system, the estimation of the flow forces is not necessary. The by-pass valve is assumed to follow the actuator motion. For proper operation, the triggering rate to the actuator driver is limited to ensure the actuator force (see Fig. A.1) is well above the unbalanced pressure force.

Minimum Pressurizing Valve

The forces acting on the minimum pressurizing valve depend on the valve displacement. The valve cone is subjected to the upstream, as well as to the downstream pressure. It can be assumed, without significant error, that the separation line of the two pressure areas is defined at the minimum flow area, Fig. B.7. The static force balance is described by the following equation:

$$\frac{d^2z}{dt^2} = \frac{1}{M_p}\left[A_1 P_{2m} + A_2 P_n - A_3 P_0 - k_{ps} z - k_{wps}(z - z_{max}) - B_p \frac{dy}{dt} - F_{ps0}\right] \tag{6.23}$$

where $A_1 = A_3 - A_2$

$$A_2 = \pi \left(\frac{D_{po}}{2} - \sin\theta_p \cos\theta_p \, z\right)^2$$

$$A_3 = \frac{\pi D_p}{4}$$

and $k_{wps} = 0$ for $z < z_{max}$

$k_{wps} = 10^6$ for $z > z_{max}$

CHAPTER 7

VALIDATION OF MATHEMATICAL MODEL

7.1 General

Steady state and transient response experiments were performed to establish the validity of the mathematical model. The data acquisition system was used to read the instruments. The experimental procedure was fully automated on a Personal Computer and tests were performed several times to check repeatability.

7.2 Experimental Procedure

The procedure for obtaining steady state results is shown in the flow chart in Fig. 7.1. The computer implementation of the procedure was done using Turbo-C code (see Appendix E). The metering valve position was fixed while the pump speed was incremented slowly. At each state, sufficient time was allowed for the system to attain equilibrium. Then, the variables were sampled and stored in the computer memory. After the complete range was covered, the pump was returned to its original speed, the metering valve opening was increased and the procedure repeated. The code execution was terminated when the full travel of the metering valve was completed.

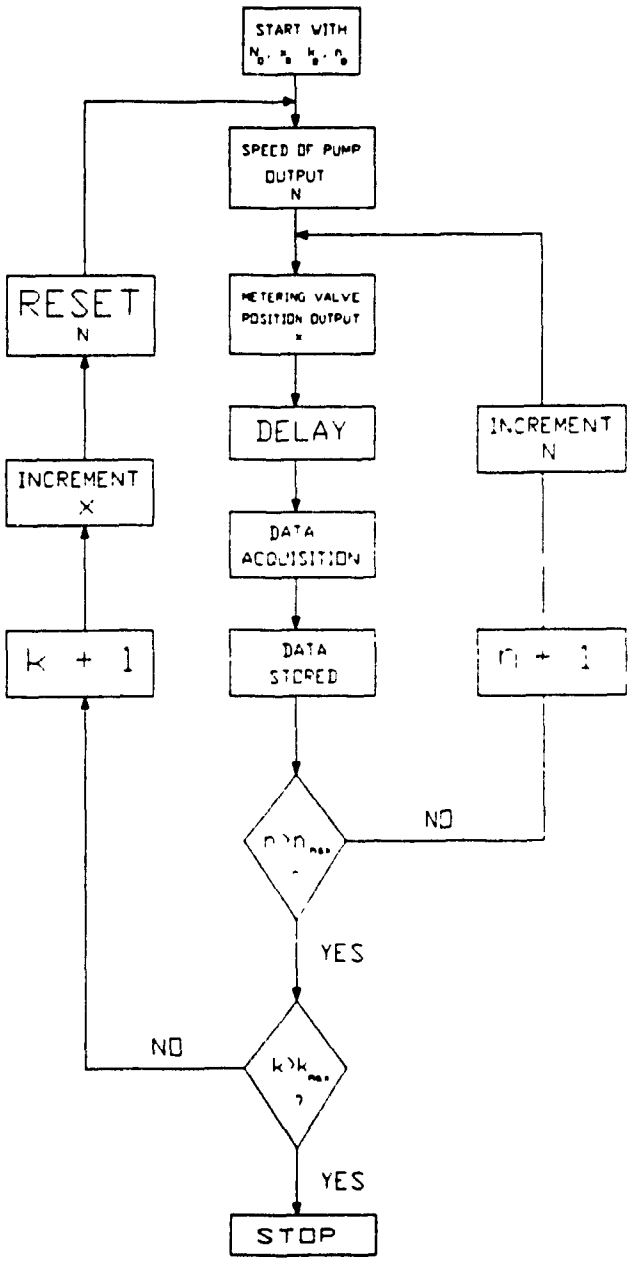

Fig. 7.1 Flow chart of procedure for steady state experiments

To investigate the dynamic response of the system, the metering valve opening was abruptly increased. After one second, it was returned to its original position. Step inputs were not possible since the triggering frequency input to the actuator driver was limited for proper operation. The actuator driver was set in "free running" mode to allocate more time for the computer to acquire data, while the valve was actuated. All variables were sampled at a frequency of 76 Hz. At the end of the transient, results were stored in the computer memory for further processing. The flow chart of the procedure is shown in Fig. 7.2. The Turbo-C code is given in Appendix E.

7.3 Experimental Results

The fuel control unit variables were plotted as functions of the pump speed and metering valve position. That created a "picture" of all possible operating conditions. Figure 7.3 shows metered fuel flow. At low metering valve openings, the differential pressure always attains the required value, Fig. 7.4. Therefore, the flow is a function of metering valve position only. Excess of fuel delivered by the pump is by-passed back to the pump inlet. This can be seen from Fig. 7.5 which shows the displacement of the by-pass valve. At low metering valve flows, the nozzle pressure and the pump delivery pressure

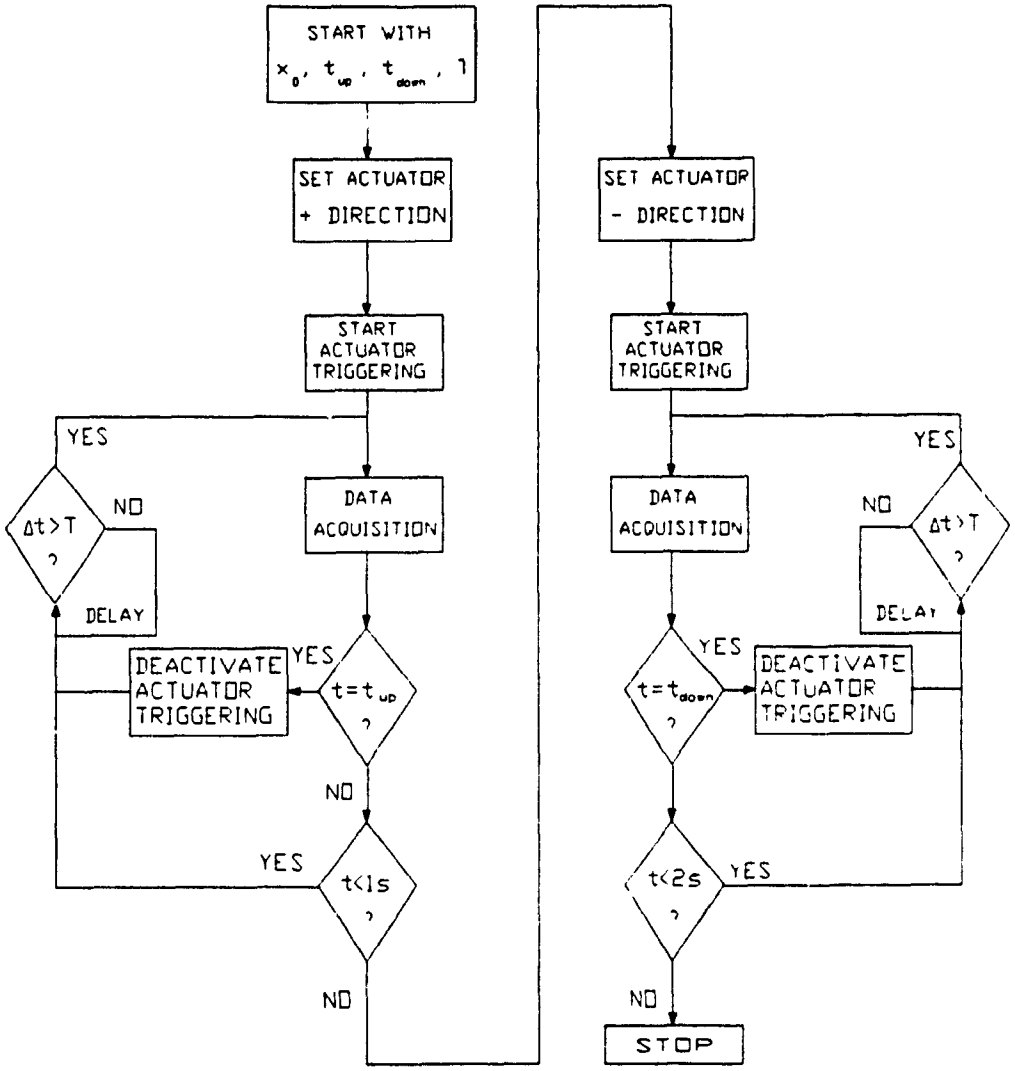

Fig. 7.2 Flow chart of procedure for dynamic response experiments

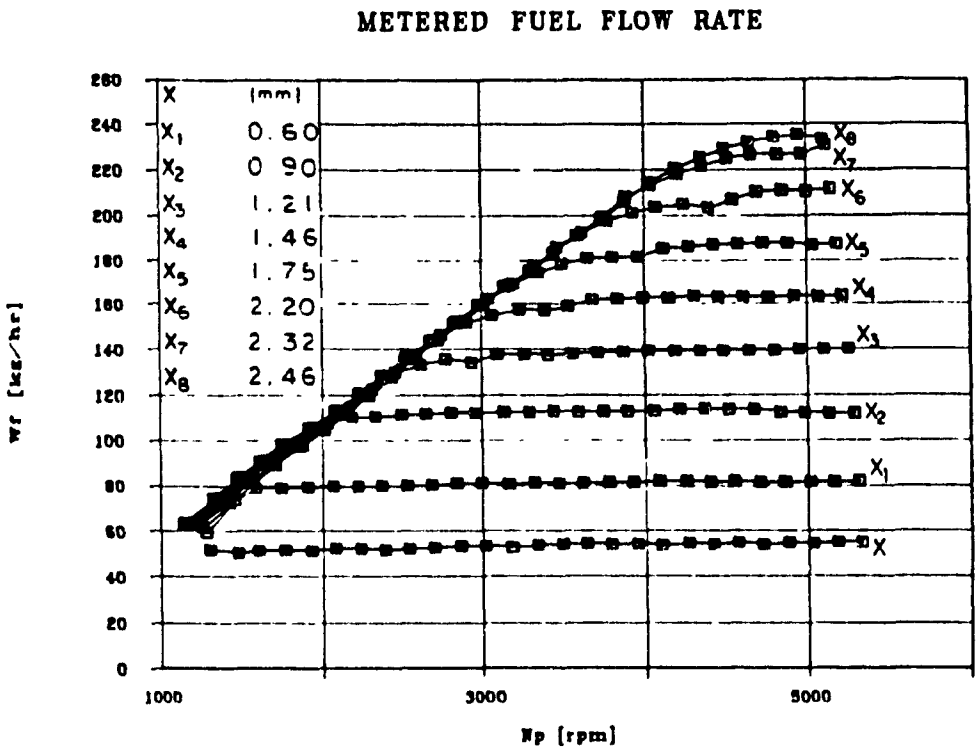

Fig. 7.3 Experimental steady state results for the metered fuel flow rate

are at their minimum value. This is essentially set by the minimum pressurizing valve preload (see Fig. 7.6 and Fig. 7.7).

As the metering valve opening is increased, the by-pass valve starts to close to prevent the differential pressure from decreasing. When the pump speed is very low, the by-pass valve is completely closed and all fuel delivered by the pump goes through the metering valve. In this case, the differential pressure is only a function of the fuel flow passing through the metering valve restriction which is the same as the fuel delivered by the

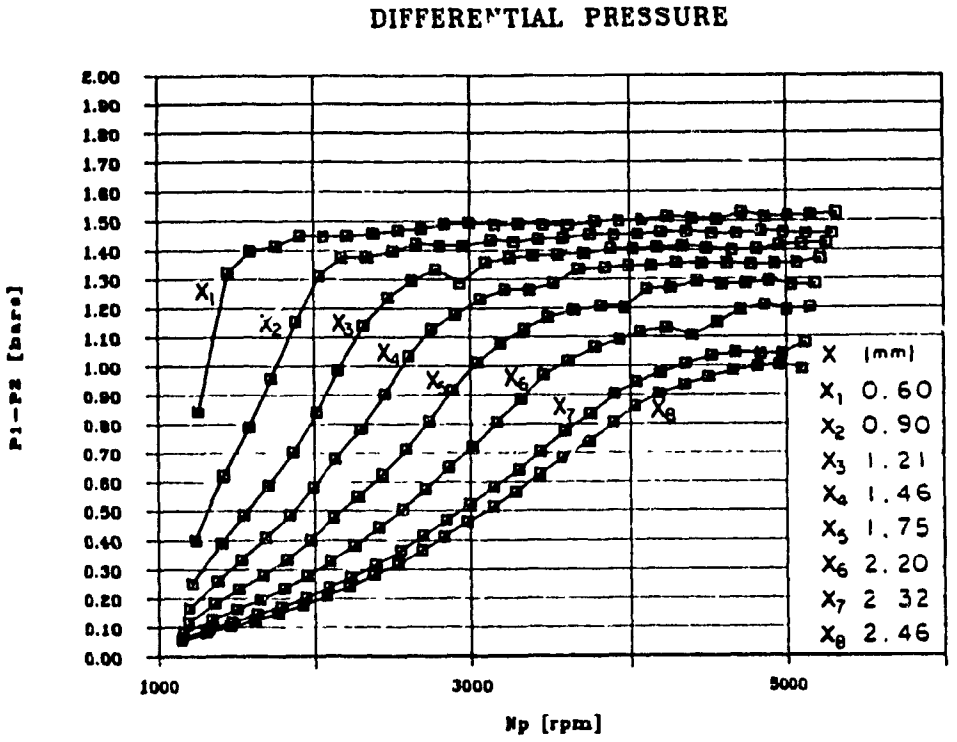

Fig. 7.4 Experimental steady state results for the differential pressure

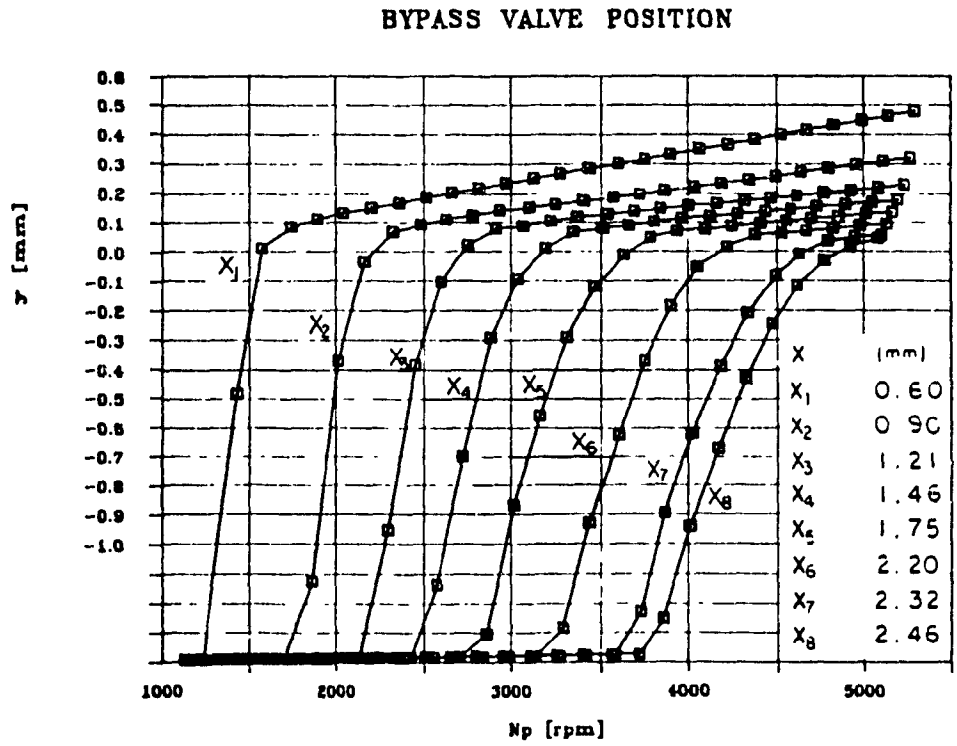

Fig. 7.5 Experimental steady state results for the by-pass valve travel

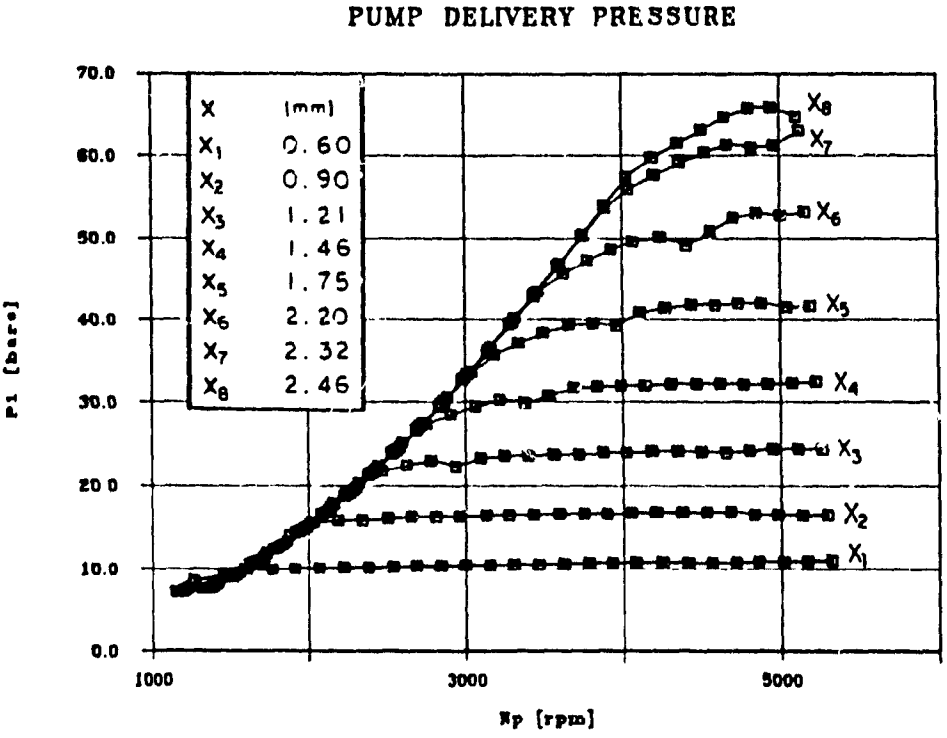

Fig. 7.6 Experimental steady state results for pump delivery pressure

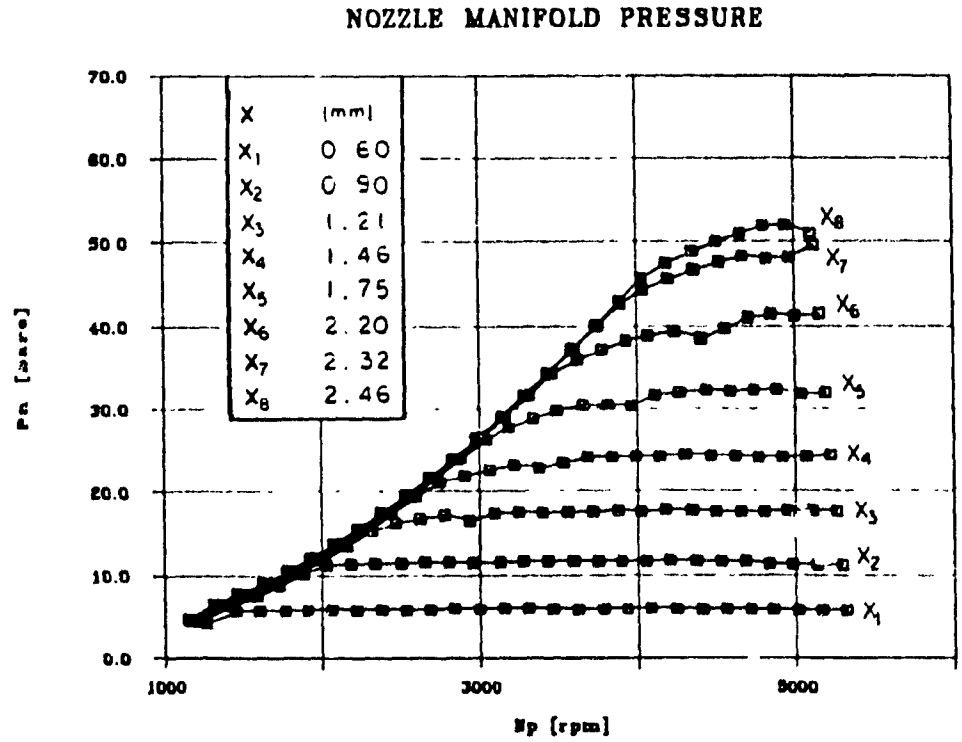

Fig. 7.7 Experimental steady state results for the nozzle manifold pressure

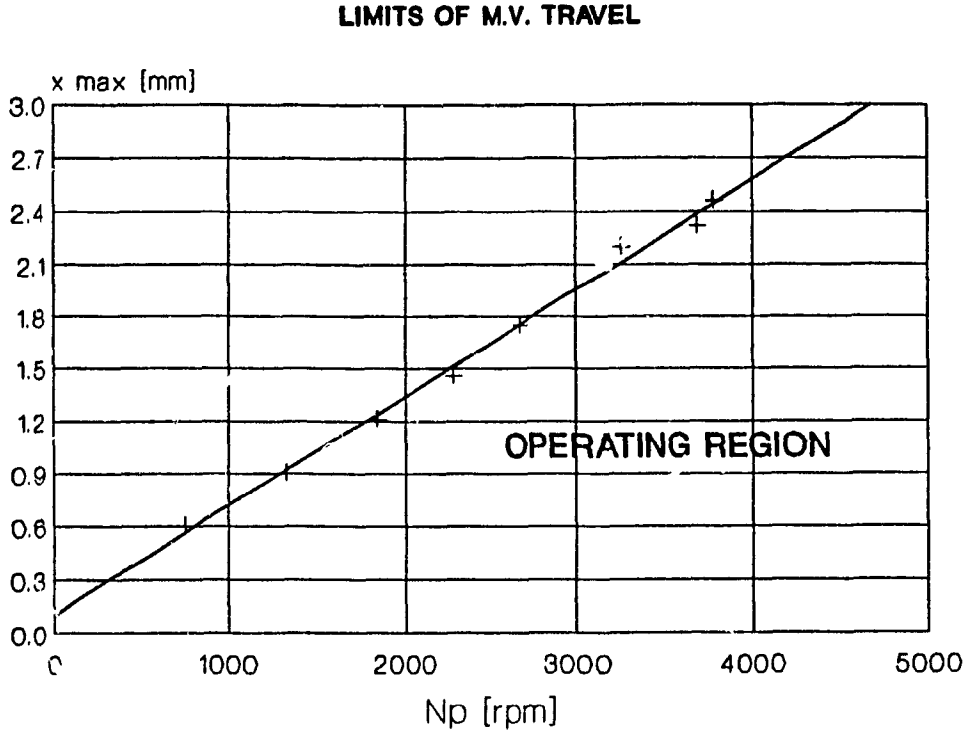

Fig. 7.8 Experimental steady state results for the maximum metering valve travel allowed as function of pump speed

pump. This condition is not permitted during normal operation of the fuel contol unit because the fuel flow to the engine cannot be controlled effectively by the metering valve. The maximum metering valve opening allowed as a function of pump speed is shown in Fig. 7.8.

When the by-pass valve is completely closed, all fuel delivered by the pump should flow through the metering valve. A quick inspection of Fig. 7.3 and Fig. B.1 (Appendix B) suggests that this is not the case. Substantial leakage occurs in the by-pass valve when the

valve is closed. This was confirmed experimentally. The leakage, however, can be tolerated since it is less than the minimum flow required to be by-passed during normal operating conditions.

7.4 Digital Computer Simulation

Two mathematical models, one for the steady state and the other for the dynamic response, were implemented on a digital computer. The steady state model was used to predict the behavior of the system for the complete travel of the metering valve at different pump speeds. It was also used to provide initial conditions for the dynamic model which, when validated, will be used for further study of the system.

7.4.1 Simulation of Steady State

The steady state model was obtained from the dynamic model (Chapter 6) by setting all the "dynamic" terms equal to zero (i.e. $d / d t = d^2 / dt^2 = 0$). The following set of equations was obtained:

Flow Equations

$$Q_p = C_1 N + C_2 (P_1 - P_0) + C_3 \qquad (7.1)$$

$$Q_{12m} = (C_d)_{12m} K A_{12m} \sqrt{P_1 - P_{2m}} \quad (7.2)$$

$$Q_{10} = (C_d)_{10} K A_{10} \sqrt{P_1 - P_0} \quad (7.3)$$

$$Q_{2mn} = (C_d)_{2mn} K A_{2mn} \sqrt{P_{2m} - P_n} \quad (7.4)$$

$$Q_{nc} = (C_d)_{nc} K A_{nc} \sqrt{P_n - (P_C + P_\ell)} \quad (7.5)$$

Flow Continuity

$$Q_p = Q_{12m} + Q_{10} \quad (7.6)$$

$$Q_{12m} = Q_{2mn} \quad (7.7)$$

$$Q_{2mn} = Q_{nc} \quad (7.8)$$

Force Balance

$$F_{bp} + F_{bf} - F_{bs} = 0 \quad (7.9)$$

$$A_1 P_{2m} + A_2 P_n - A_3 P_0 - k_{ps} z - k_{wps} (z - z_{max}) - F_{p0} = 0 \quad (7.10)$$

where

$$F_{bp} = A_{De} (P_1 - P_{2m}) - A_f P_1 \quad (7.11)$$

$$F_{bf} = A_f P_1 + F_{bf1} + F_{bf2} \quad (7.12)$$

$$F_{bs} = k_{bs} y + k_{wbs} (y - y_{min}) + F_{bs0} \quad (7.13)$$

$$A_2 = \pi \left(\frac{D_{po}}{2} - \sin\theta_p \cos\theta_p z \right)^2 \qquad (7.14)$$

$$A_1 = A_3 - A_2 \qquad (7.15)$$

$$k_{wbs} = 0 \quad \text{for } y > y_{min}$$
$$K_{wbs} = 10^6 \quad \text{for } y < y_{min}$$
$$k_{wps} = 0 \quad \text{for } z < z_{max}$$
$$K_{wps} = 10^6 \quad \text{for } z > z_{max}$$

and

$$F_{bf1} = -2C_d A_e P_1 = (K_1 y^2 + K_2 y + K_3) P_1 \qquad (7.16)$$

$$F_{bf2} = 2C_d A_e P_0 = -(K_1 y^2 + K_2 y + K_3) P_0 \qquad (7.17)$$

where

$$K_1 = -2C_d \left[(b_1)_1 \cos\theta_{f1} + (b_1)_2 (\cos\theta_{f2} - \cos\theta_{f3}) \right]$$

$$K_2 = -2C_d \left[(b_2)_1 \cos\theta_{f1} + (b_2)_2 (\cos\theta_{f2} - \cos\theta_{f3}) \right]$$

$$K_3 = -2C_d \left[(b_3)_1 \cos\theta_{f1} + (b_3)_2 (\cos\theta_{f2} - \cos\theta_{f3}) \right]$$

Note: A_e was determined experimentally (see Appendix B). Equation (7.16) and Equation (7.17) were replaced by:

$$F_{bf1} = (K_{f1} / 2)\, x - K_{f2} / 2 \qquad (7.16)'$$

$$F_{bf2} = (K_{f1} / 2)\ x - K_{f2} / 2 \qquad (7.17)'$$

Flow Areas

$$A_{12m} = a_1\ x^2 + a_2\ x + a_3 \qquad (7.18)$$

$$A_{10} = b_1\ y^2 + b_2\ y + b_3 \qquad \text{for } y>y_\ell \qquad (7.19)$$

$$A_{10} = b_2'\ y + b_3' \qquad \text{for } y<y_\ell \qquad (7.19)'$$

$$A_{2mn} = c_1\ z^2 + c_2\ z \qquad (7.20)$$

where, y_ℓ is the valve displacement that would produce a flow area equal to the maximum leakage area. Note, that the leakage decreases when the valve overlap increases. This occurs as the valve moves to its minimum stop (maximum overlap is about 1 mm). Leakage coefficients b_2' and b_3' were determined experimentally.

7.4.1.1 Numerical Method for Solving the Steady State Model

The resulting non-linear set of equations is rather difficult, if not impossible, to solve analytically. Different numerical methods were considered and some were tested in order to find the most suitable method for the computer available (an IBM AT). The Second Order Least Squares method was tried first. However the round-off error predominated, due to ill conditioning of the gradient

matrix. This resulted in divergence of the solution vector. Correction methods were not effective in alleviating the problem.

Consequently, the Newton's first order method was tried. Error correction proved to be effective in this case and the solution vector converged after few iterations. Typical computational time to produce the solution for one operating point, on an AT Personal Computer equipped with an 80287 coprocessor, was approximately 5 secs. The computational method is described briefly below.

The set of equations was represented by $F(\underline{x})$. An initial guess of the solution was represented by $\underline{x}_o$. $F(\underline{x})$ was linearized by taking Taylor series expansion about a point $\underline{x}_k$ near the solution $\underline{x}^*$.

$$F(\underline{x}^*) = F(\underline{x}_k) + J(\underline{x}_k)S \qquad (7.21)$$

where, J is the Jacobian of F and $S = \underline{x}^* - \underline{x}_k$

Since $F(\underline{x}^*) = 0$, Equation (7.21) reduced to:

$$\underline{x}^*_{k+1} = \underline{x}_k - J^{-1}(\underline{x}_k)\, F(\underline{x}_k) \qquad (7.22)$$

Equation (7.22) gave only an approximation of the solution and the computational process had to be repeated. In every iteration the linear system of equations,

$$J(\underline{X}_k)S = - F(\underline{X}_k) \qquad (7.23)$$

was solved for S, and then the solution vector was updated using: $\underline{X}_{k+1} = S + \underline{X}_k$.

In order to converge, S had to be corrected for the round-off error as follows. For S′ representing the solution of Equation 7.23, F′ was evaluated by,

$$JS' = - F' \qquad (7.24)$$

Subtracting Eq. 7.24 from Eq. 7.23,

$$J(S-S') = - (F-F') \qquad (7.25)$$

Solution of Eq. (7.25) produced the error E = S - S′. Then S was evaluated as S = S′ + E. The process was repeated until E was reduced to a very small number ($E \leq 10^{-6}$).

The above numerical scheme was implemented using Turbo-C code. The algorithm was tested with a set of non-linear equations of known solution. Then it was applied to produce the solution of $F(\underline{X}) = 0$, where $F(\underline{X})$ was the following set:

$$f_1 = x_1 - C_2 x_6 + C_2 P_0 - (C_1 N + C_3)$$

$$f_2 = x_2 - (C_d)_{12m} K x_{11} \sqrt{x_6 - x_7}$$

$$f_3 = x_3 - (C_d)_{10} K x_{12} \sqrt{x_6 - P_0}$$

$$f_4 = x_4 - (C_d)_{2mn} K x_{13} \sqrt{x_7 - x_8}$$

$$f_5 = x_5 - (C_d)_{nc} K A_{nc} \sqrt{x_8 - P_c}$$

$$f_6 = x_1 - x_2 - x_3$$

$$f_7 = x_2 - x_4$$

$$f_8 = x_4 - x_5$$

$$f_9 = x_{14} + x_{15} - x_{16}$$

$$f_{10} = x_{19}x_7 + x_{20}x_8 - k_{ps}x_{10} - k_{wps}(x_{10} - z_{max}) - A_3P_0 - F_{ps0}$$

$$f_{11} = x_{14} - A_{De}x_6 + A_{De}x_7$$

$$f_{12} = x_{15} - x_{17} - x_{18}$$

$$f_{13} = x_{16} - k_{bs}x_9 - k_{wbs}(x_9 - y_{min}) - F_{b0}$$

$$f_{14} = x_{20} - \pi \left(\frac{D_{p0}}{2} - \sin\theta_p \cos\theta_p x_{10} \right)^2$$

$$f_{15} = x_{19} + x_{20} - A_3$$

$$f_{16} = x_{17} - (K_{f1} / 2) x + K_{f2} / 2$$

$$f_{17} = x_{18} - (K_{f1} / 2) x + K_{f2} / 2$$

$$f_{18} = x_{11} - a_1x^2 - a_2x - a_3$$

$$f_{19} = x_{12} - b_1x_9^2 - b_2x_9 - b_3$$

$$f_{20} = x_{13} - c_1x_{10}^2 - c_2x_{10}$$

The vector of the system variables, $\underline{X}$, was:

$x_1 = Q_p$ $\quad x_8 = P_n$ $\quad x_{15} = F_{bf} - A_f P_1$

$x_2 = Q_{12m}$ $\quad x_9 = y$ $\quad x_{16} = F_{bs}$

$x_3 = Q_{10}$ $\quad x_{10} = z$ $\quad x_{17} = F_{bf1}$

$x_4 = Q_{2mn}$ $\quad x_{11} = A_{12m}$ $\quad x_{18} = F_{bf2}$

$x_5 = Q_{nc}$ $\quad x_{12} = A_{10}$ $\quad x_{19} = A_1$

$x_6 = P_1$ $\quad x_{13} = A_{2mn}$ $\quad x_{20} = A_2$

$x_7 = P_{2m}$ $\quad x_{14} = F_{bp} + A_f P_1$

The position of the metering valve, x and the pump speed were the inputs to the code. The numerical solution required the evaluation of the Jacobian of $F(\underline{X})$ which was a 20x20 sparse ill-conditioned matrix. The numerical instability was overcome as explained earlier.

7.4.1.2 Simulation Results and Validation of Steady State Model

Simulation results were produced for the full travel of the metering valve at pump speeds of 1800 rpm, 2600 rpm, 3400 rpm and 5000 rpm. Experimental and theoretical results are shown in Fig. 7.9 through Fig. 7.14. Fig. 7.9 shows simulation and experimental results for the metered flow. The simulated metered flow, at low metering valve openings, is lower than the experimental one. This occurred because the flow coefficient was assumed constant. As can be seen from Fig. B.8, the flow coefficient is higher at low

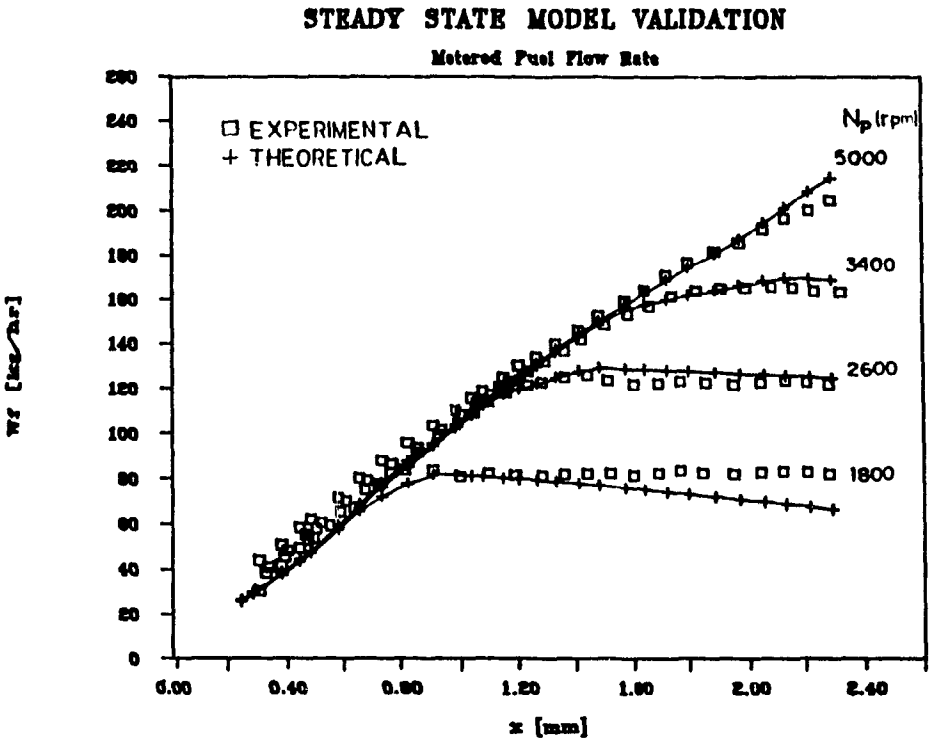

Fig. 7.9 Experimental and simulation steady state results for the metered fuel flow rate

metering valve openings. There is also a small discrepancy in the flow at high metering valve opening at pump speed 5000 rpm. This may be due to inaccuracies stemming from errors in the flow coefficient, the fuel flow delivered by the pump, the differential pressure and also from manufacturing imperfections in the metering valve profile. Errors can also be attributed to drift and sensitivity changes in the instruments.

Figure 7.10 compares the calculated and measured differential pressure. Differences between the simulation and the experimental results of up to 10% exist. These

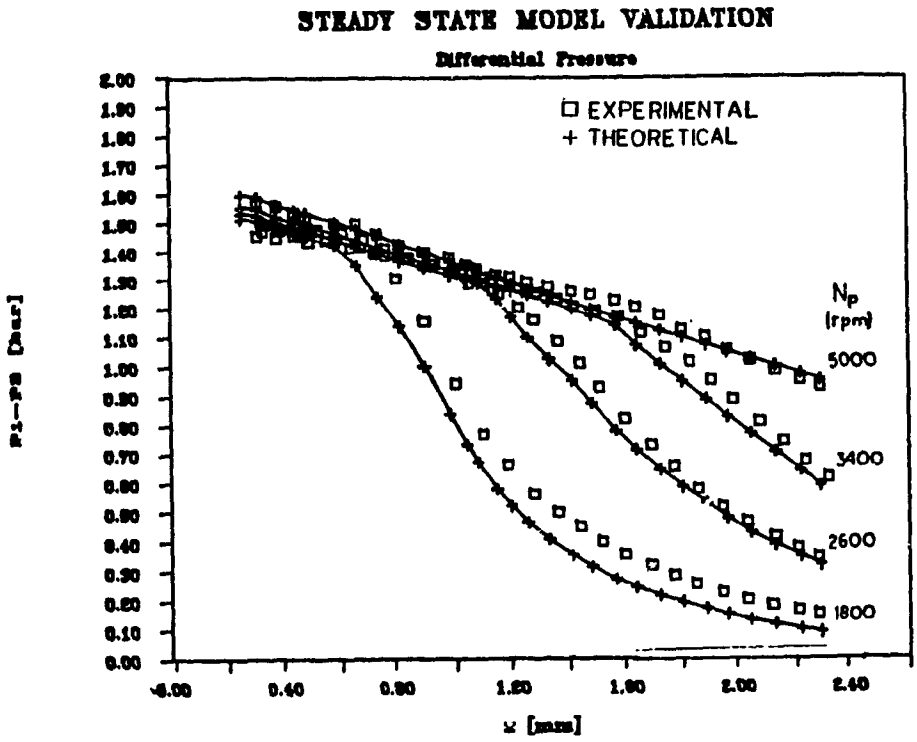

Fig. 7.10 Experimental and simulation steady state results for the differential pressure

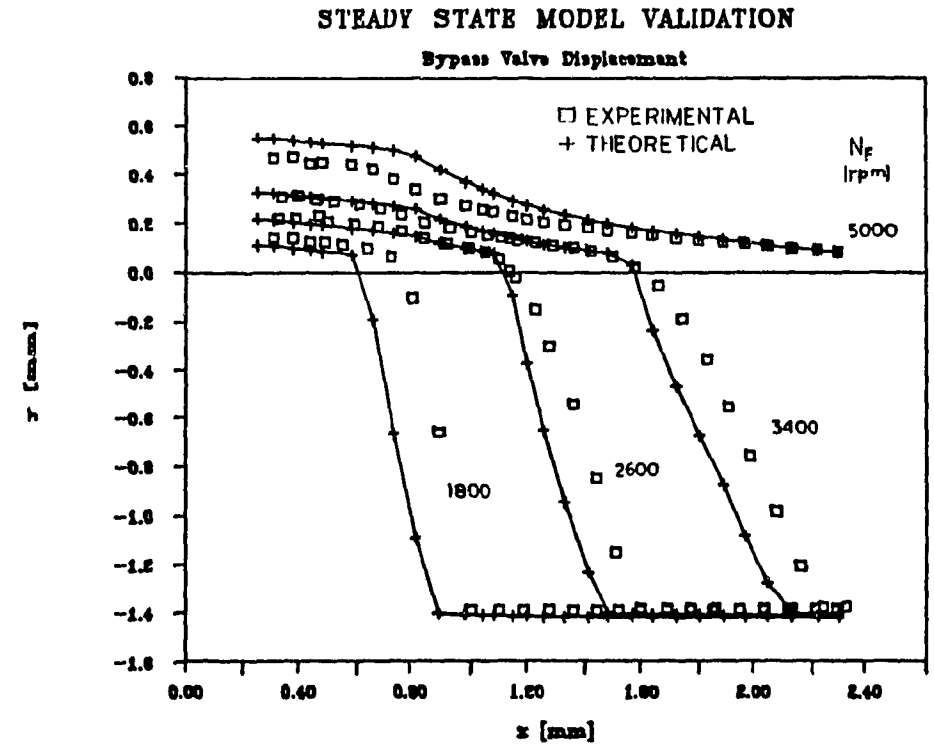

Fig. 7.11 Experimental and simulation steady state results for the by-pass valve travel

discrepancies are acceptable for the purpose of the present analysis. Greater differences exist in the region where the the by-pass valve starts to close, Fig. 7.11. The region where the by-pass valve overlaps is not of great concern since it represents an "out of range" operation and the model does not need to be very accurate. The case when the valve hits the stop is well predicted by the model. Numerical instabilities occurred, however, when a very high spring rate for the stop was used. The problem was eliminated by reducing the value of the spring rate. Errors in the by-pass valve movement are closely related to errors in the fuel flow delivered by the pump.

Fig. 7.12 shows the pump discharge pressure. At low metering valve openings, the pressure is biased to 10 bars and is kept constant as long as the minimum pressurizing valve is operational. At higher metering valve openings, the minimum pressurizing valve hits the maximum stop and the delivery pressure of the pump starts to increase further as the speed is increased. The displacement of the minimum pressurizing valve is shown in Fig. 7.13. The small discrepancy between the experimentally deduced value (using the flow equation) and the valve travel predicted by the simulation is most probably due to the leakage of fuel back to the pump inlet.

Fig. 7.14 shows results for the nozzle injection pressure. During experiments the nozzles were "simulated"

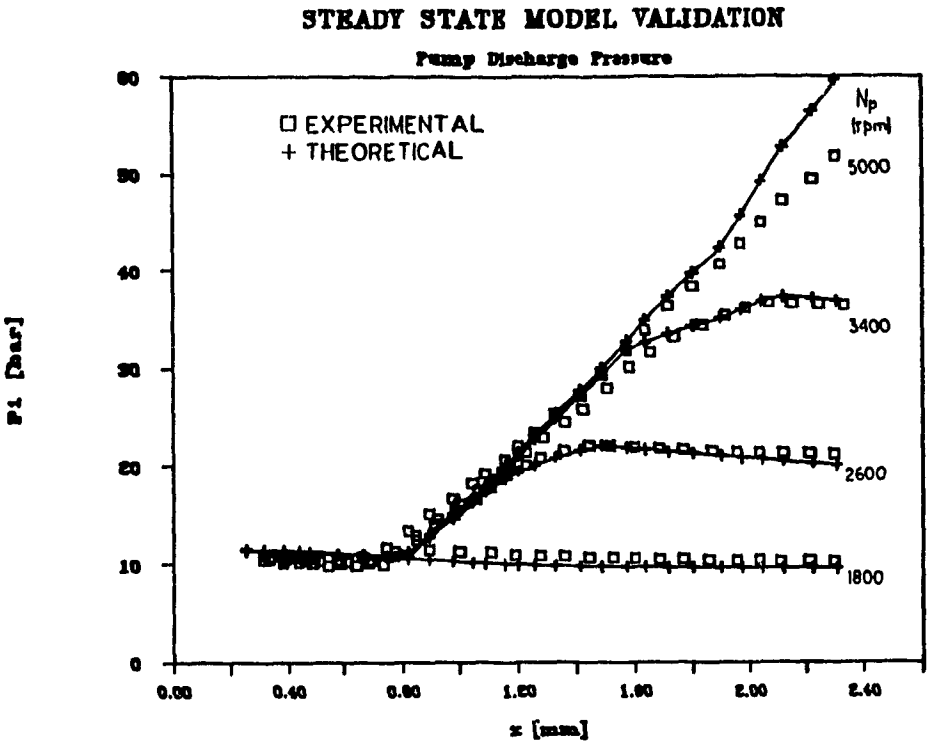

Fig. 7.12 Experimental and simulation steady state results for pump delivery pressure

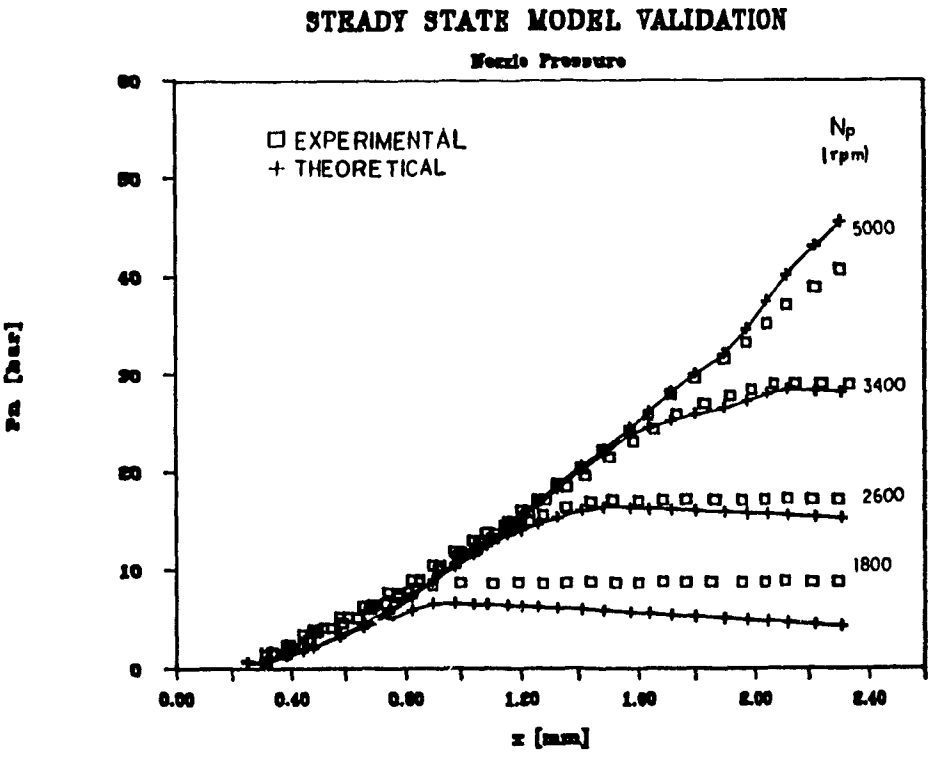

Fig. 7.13 Experimental and simulation steady state results for nozzle manifold pressure

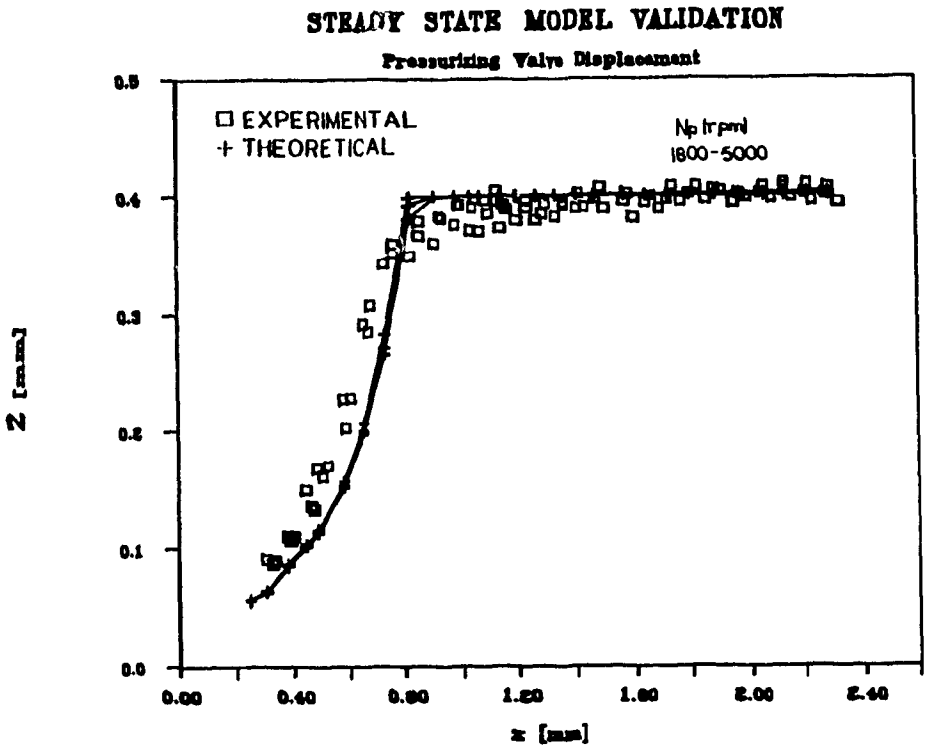

Fig. 7.14 Experimental and simulation steady state results pressurizing valve travel

by a fixed orifice. The fuel discharged to the ambient pressure. For the real case when fuel is discharged to a combustion chamber, the pressures within the fuel control unit will increase by the same amount as the combustion chamber back pressure. The system model can be used to predict this case or any other case with different end conditions (pressures).

In general, the developed model described the system very well. Discrepancies occurred mainly because of friction between valves and their sleeves. Small errors in the system parameters such as rate of springs, flow areas

and in the fluid properties, contributed also to the differences between simulation and test results.

7.4.2. Simulation of Transient Response

The dynamic model was implemented on a digital computer using the TUTSIM dynamic system simulation language. The package employed the Euler and Adams Bashforth rules of integration. Discrete time blocks for sampled data processing were also available. Model parameters were changed interactively to assist examination of their effect faster.

TUTSIM block formulation resembles modelling on an analog computer. The block structures for the different modules of the metering section, as shown in Fig. 7.3, are presented in Appendix C.

7.4.2.1 Simulation Results and Validation of Dynamic Model

The dynamic mathematical model described the system quite well. Experimental and simulation results of the dynamic response of the fuel control unit for an approximated pulse actuation of the metering valve are shown in Fig. 7.15. Small discrepancies are attributed to errors in the estimation of the volumes of the various chambers within the fuel control unit and piping system and also to the estimation of the effective bulk modulus of

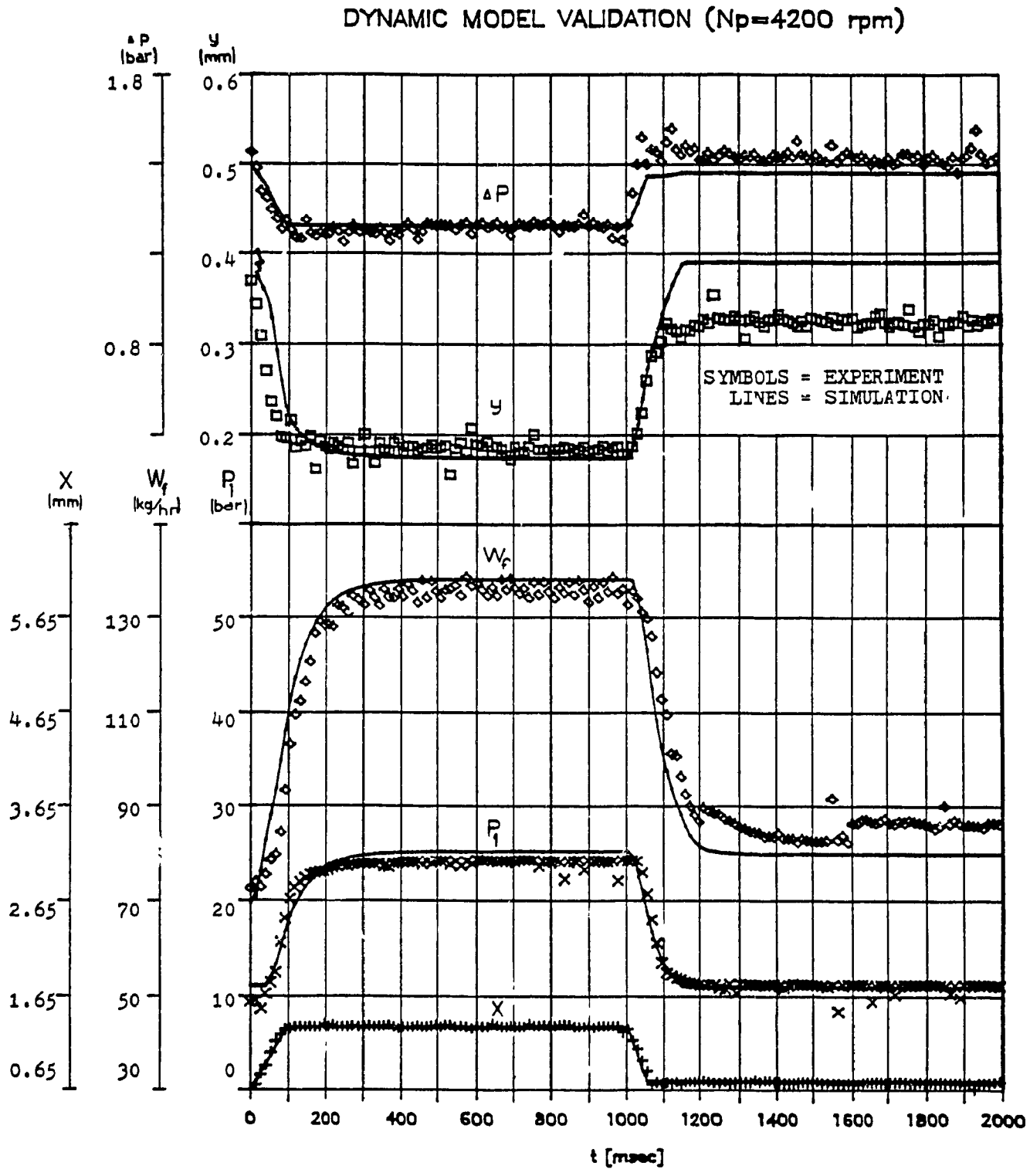

Fig. 7.15 Experimental and simulation dynamic response results

elasticity of the fuel.

The dynamic model developed here is a good representation of the system and can confidently be used for the design of the electronic controller. An alternate approach would be to consider the metering section of the fuel as a "black box" and perform process identification using the experimental results presented above. This, however, would mask the effect of important system parameters and therefore, prevent the designer from making useful suggestions about possible improvements in the system design.

CHAPTER 8

DESIGN OF A DIGITAL CONTROLLER

8.1 General

To overcome problems encountered in the design of electronic fuel control units due to process transport delays and other non-linearities, some appropriate digital controllers were analyzed and tested. First, a Proportional Derivative (PD) digital controller algorithm was linked to the model of the electronic fuel control unit and simulation results were obtained. This controller and some other more effective controller algorithms were analyzed and then realized on the test bench using the prototype of the electronic fuel control unit.

8.2 Proposed Control Strategy for the Complete System - Including Engine

In the following, an electronic fuel controller for a free turbine engine is proposed, Fig. 8.1. This control scheme is an electronic equivalent of the hydromechanical control used in a twin PT6 engine installation for helicopters. To achieve this control, very accurate transducers (sensors) and actuators must be employed. The number of signals required depend on the sophistication of the control strategy.

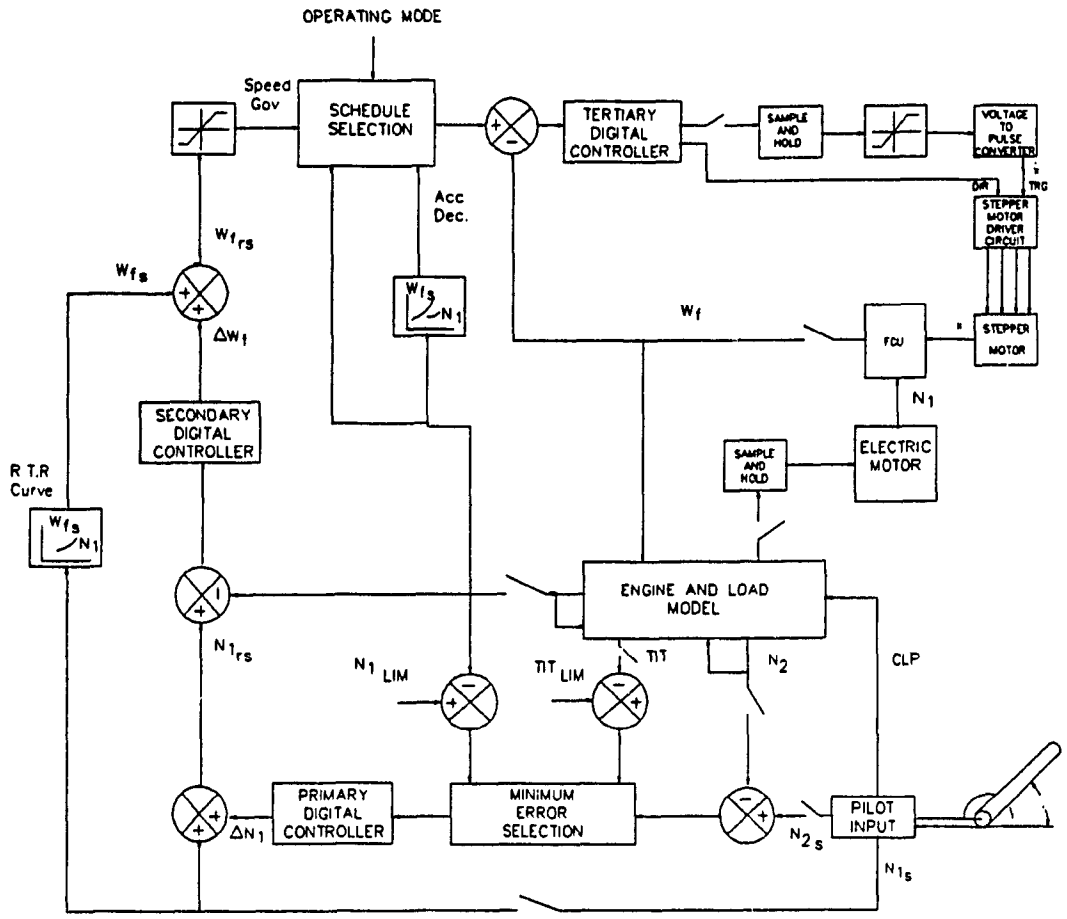

Fig. 8.1 Block diagram of control strategy for the complete system

The controller is composed of three control loops in cascade. The primary loop controls the power turbine speed by readjusting the gas generator set speed. The secondary loop regulates the gas generator speed at the new set point by varying the fuel flow demands. The tertiary loop achieves the fuel flow as set by the two other loops. This

control loop acts directly on the actuating mechanism of the metering valve(s) of the fuel control unit and it should respond as fast as possible to a fuel flow change demand from the two external control loops. The design of this tertiary controller is of main interest here. A typical operating procedure describing the function of the electronic controller is discussed below.

The pilot selects the load by setting the rotor blades and the desired gas generator and rotor speeds, N_{1s} and N_{2s} respectively. The engine accelerates and the fuel flow is modulated according to the acceleration schedule. At about 70% to 75% of N_1 (51), depending on the load, the rotor speed governing control mode takes over and the power turbine speed governor readjusts (resets) the gas generator speed set point as required to achieve the selected rotor speed. The required to run (RTR) engine characteristic is used to determine the fuel flow demand in advance. The control anticipates the fuel needed and can avoid excessive speed deviations during transients.

The tertiary controller acts on the error (the difference between the demanded and actual fuel flow) to produce a voltage signal. This signal enters a voltage to frequency converter and a rectangular waveform is produced to trigger the actuator driver which sends a sequence of pulses to drive the actuator in the proper direction and thus increase or decrease the fuel flow. The controller

output voltage and, therefore, the actuator triggering rate, is limited to a maximum value of 200 steps/sec. This ensures that the actuator produces a linear force high enough to drive the valve when the controller output is very high. The nozzle pressure provides a measure of the fuel flow and, for experimental purposes, it can be used as a direct feedback signal. This control strategy achieves isochronous speed control and there is no need for load speed set point adjustment, as in hydromechanical fuel control units, in order to avoid speed droop.

8.3 Controller Structures

The fuel flow control loop (tertiary controller) is analyzed below without engine speed interaction (constant engine speed), Fig. 8.2. Three digital controller structures are studied; the classical proportional derivative (PD), the proportional derivative with Smith predictor and the Dahlin controller. An integral term was not included in the controller since the stepper motor is of low inertia and it integrates (sums-up) the executed steps. For the two latter control structures, a linearized process model is needed.

From experimental results (see Chapter 7) it was found that a first order model with dead time could describe the flow processes very accurately. The transfer function

CONVENTIONAL PD CONTROLLER

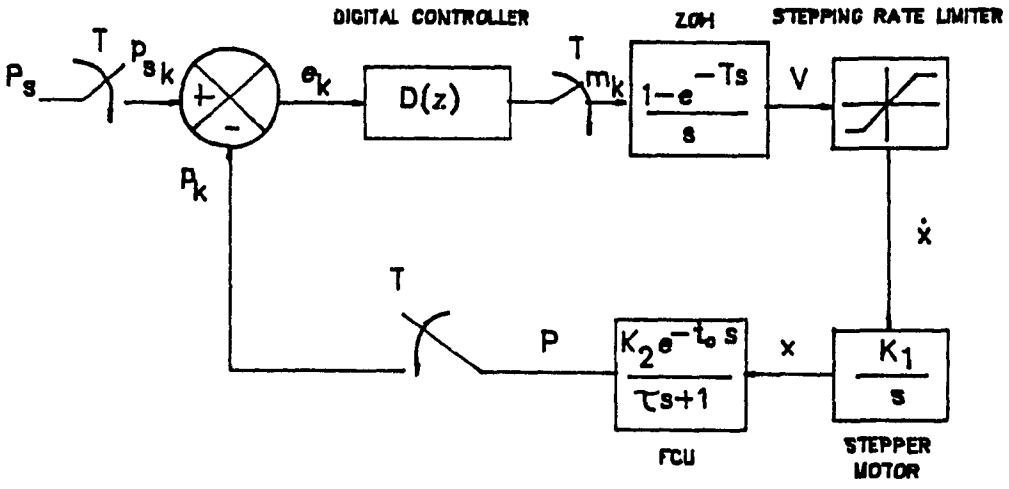

Fig. 8.2 Fuel flow control loop

relating the nozzle pressure to the metering valve movement was:

$$\frac{P_n}{x} = \frac{290\ e^{-t_o s}}{0.05\ s + 1} \qquad (8.1)$$

Including the stepper motor and the voltage to frequency converter transfer functions (see Appendix A), the overall plant transfer function G(s) was:

$$\frac{P_n}{V} = \frac{202\ e^{-t_0 s}}{s(0.05s + 1)} \qquad (8.2)$$

A simple digital PD controller, without filtering of the derivative term, was used:

$$m_k = k_1 e_k + k_2(e_k - e_{k-1}) \qquad (8.3)$$

This type of controller algorithm presents some problems because of the dead time inherent to the process transfer function. The proportional integral with Smith predictor, on the other hand, anticipates this delay and acts accordingly (52), (53), (54), (55), Fig. 8.3. To implement this scheme, the model of the flow process must get updated when operating at different conditions. This can be done by performing on-line model identification or by using stored model parameter information obtained during unit calibration. The performance of the controller depends on the accuracy of the model. Small inaccuracies in the model are tolerated since their effect is only transitory and do not appear at steady state.

To derive the controller algorithm, the Pulse Transfer Function (transfer function that takes into account the zero order hold) of the process transfer function G(s) without the time delay t_0, was obtained. That is:

CONVENTIONAL PD WITH SMITH PREDICTOR

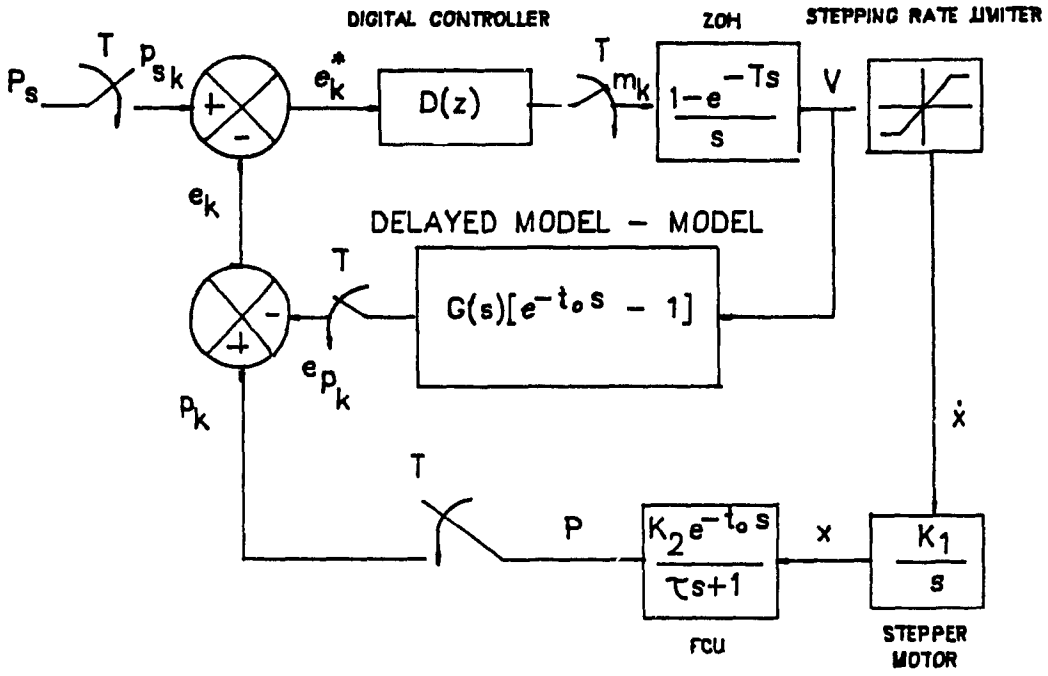

Fig. 8.3 Smith predictor control scheme

$$GH(s)=\left(\frac{1-e^{-Ts}}{s}\right)\left(\frac{K}{s(\tau s+1)}\right) \qquad (8.4)$$

Taking z-transforms:

$$GH(z) = (1-z^{-1})\ Z\left(\frac{K}{s^2(\tau s+1)}\right) \qquad (8.5)$$

Using partial fractions:

$$GH(z) = \frac{az^{-2} + bz^{-1}}{1 - cz^{-1} + dz^{-2}} \qquad (8.6)$$

where:

$$a = K\tau \left(1 - e^{-T/\tau} - T/\tau \, e^{-T/\tau} \right)$$

$$b = K\tau \left(T/\tau + e^{-T/\tau} - 1 \right)$$

$$c = 1 + e^{-T/\tau} \qquad (8.7)$$

$$d = e^{-T/\tau}$$

The error correction due to the predictor term is:

$$Z\left[GH(s)\left(e^{-t_o s} - 1\right)\right] = - \frac{a\left(z^{-2} - z^{-N-2}\right) + b\left(z^{-1} - z^{-N-1}\right)}{1 - cz^{-1} + dz^{-2}} \qquad (8.8)$$

The resulting finite difference recursive formula is:

$$e_{p_k} = a\left(m_{k-N-2} - m_{k-2}\right) + b\left(m_{k-N-1} - m_{k-1}\right) + ce_{p_{k-1}} - de_{p_{k-2}} \qquad (8.9)$$

Then, the corrected error,

$$e_k^* = e_k + e_{p_k} \qquad (8.10)$$

can be used in Eq.(8.3).

The Dahlin controller (56), (57), (58), can also eliminate problems due to system transport delays. The controller is synthesized in such a way as to obtain a specified response of the closed loop. The resulting controller structure should not contain predictor elements or other unrealizable terms. From the specified closed loop response and the process transfer function, the controller transfer function can be obtained:

$$D(s) = \frac{1}{G(s)} \left(\frac{K(s)}{1 - K(s)} \right) \qquad (8.11)$$

If a first order plus dead time closed loop transfer function is desired:

$$K(s) = \frac{e^{-t_o s}}{\lambda s + 1} \qquad (8.12)$$

which has the Pulse Transfer Function:

$$KH(z) = \frac{(1 - e^{-T/\lambda}) z^{-N-1}}{1 - e^{-T/\lambda} z^{-1}} \qquad (8.13)$$

The transfer function of the digital controller is:

$$D(z) = \frac{1}{GH(z)} \left(\frac{KH(z)}{1 - KH(z)} \right) \qquad (8.14)$$

The process inversion, 1/GH, cancels the dynamics of the process in the closed loop transfer function. The term in parenthesis accounts for the way the dynamics of the controller affect the closed loop response.

The transfer function of the process is similar as found in Eq. (8.6) with the only difference being the term z^{-N} which is introduced in the numerator to account for the flow transport delay. Substituting the transfer function of the process and Eq. (8.13) in Eq. (8.14), the controller transfer function becomes:

$$D(z) = \frac{(1-e^{-T/\lambda}) - (1+e^{-T/\tau})\ (1-e^{-T/\lambda})z^{-1} + (1-e^{-T/\lambda})e^{-T/\tau}z^{-2}}{b+(a-be^{-T/\lambda})z^{-1} - ae^{-T/\lambda}z^{-2} - b(1-e^{-T/\lambda})z^{-N-1} - a(1-e^{-T/\lambda})z^{-N-2}} \qquad (8.15)$$

The recursive controller formula is then obtained:

$$m_k = Ae_k - Be_{k-1} + Ce_{k-2} - Dm_{k-1} + Em_{k-2} + Fm_{k-5} + Gm_{k-6} \qquad (8.16)$$

where

$$A = (1 - e^{-T/\lambda})/b$$

$$B = (1+e^{-T/\tau})(1-e^{-T/\lambda})/b$$

$$C = e^{-T/\tau}(1-e^{-T/\lambda})/b$$

$$D = (a - be^{-T/\lambda})/b \qquad (8.17)$$

$$E = ae^{-T/\lambda}/b$$

$$F = 1-e^{-T/\lambda}$$

$$G = a(1-e^{-T/\lambda})/b$$

This controller has the advantage of using only one tuning parameter, λ. The inversion of the process, however, can cause ringing of the controller output with very harmful effects on equipment. To correct the problem, poles close to -1 must be removed from the controller transfer function and the controller gain must be adjusted to balance the effect of such removal (56).

8.4 Simulation Results and Discussion

Simulation results were first produced for the PD digital controller in order to verify the feasibility of such controller and also to observe the effect of the discrete valve movement on the response. Simulation time on an IBM AT with an 80386, 25 MHz, microprocessor and 80387,

20 MHz math co-processor, was 12 minutes for a 1 second transient. Figure 8.4 shows the dynamic response of the system to a fuel flow change demand.

The discrete movement of the metering valve is reflected in all important variables of the fuel control unit; that is, on the fuel flow rate, the differential pressure and the movement of the by-pass valve. Also, big pulsations result in the pump delivery pressure, Fig. 8.5.

The minimum pressurizing valve opens fully when the fuel flow has increased approximately 30% of its total change. In the period when the valve is active, the pump delivery pressure is kept constant. This, however, does not seem to affect the response of the fuel flow rate. It is, though, somehow visible in the response of the by-pass valve. The differential pressure is, on the other hand, maintained essentially constant by the hydromechanical servo-control.

The step size of the actuator used in this simulation was quite large (0.05 mm) and consequently the final fuel flow rate could not be achieved accurately; the actuator was "hunting" about the final position trying to reach the scheduled fuel flow. The "hunting" frequency depended on the controller gains. If the engine were included in the control loop, equilibrium between the fuel flow and the engine load might not be reached and the system would have remained in a continuous transient.

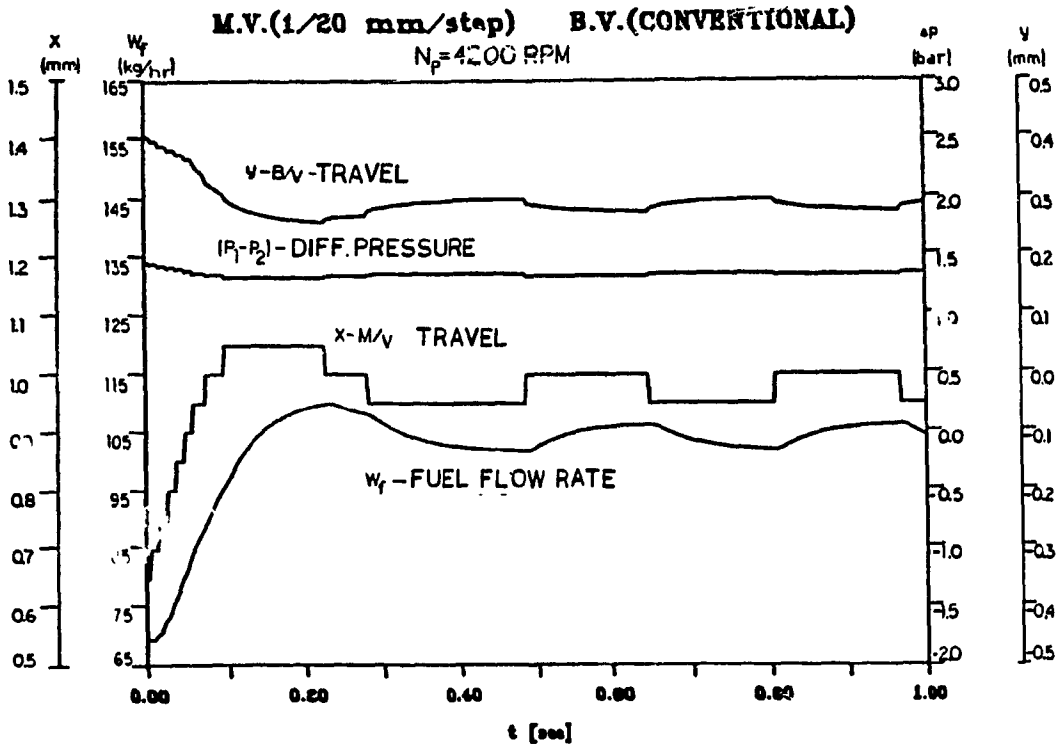

Fig. 8.4 Simulation of dynamic response of electronic fuel control unit to a step fuel flow demand

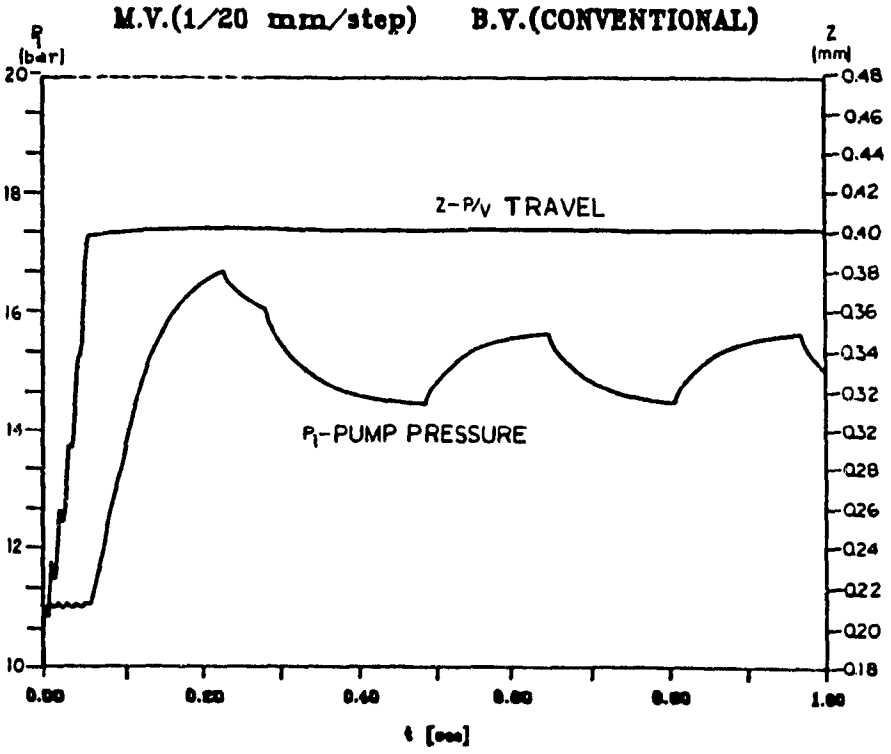

Fig. 8.5 Simulation results for minimum pressurizing valve travel and pump discharge pressure

The "hunting" problem can be eliminated electronically by using a monostable multivibrator after the voltage/frequency converter. The pulse train of the feedback signal should be used to trigger the multivibrator. The delay time should be adjusted slightly shorter than the period of the "hunting" pulses (59). This assumes that the "hunting" period is known "a priori". A simpler solution is to use an actuator with smaller step size. Results with a step size of 0.0125 mm are shown in Fig. 8.6 and Fig. 8.7.

It is observed that this actuator step size could achieve a fuel flow change as fast as the larger actuator step size, but without the big fluctuations of the fuel flow. This was possible because with the smaller step size, the controller gains could be increased further without causing instability or excessive overshoots. A very small step size, on the other hand, might not have produced a fast response, even if the gains were large enough to drive the controller output to saturation. The best actuator step size could be found by optimizing the system response.

8.5 Experimental Results

Some typical responses to pulse fuel flow demands were obtained experimentally using an actuator of 0.0125 mm step size. In Fig. 8.8, the response of the nozzle pressure is

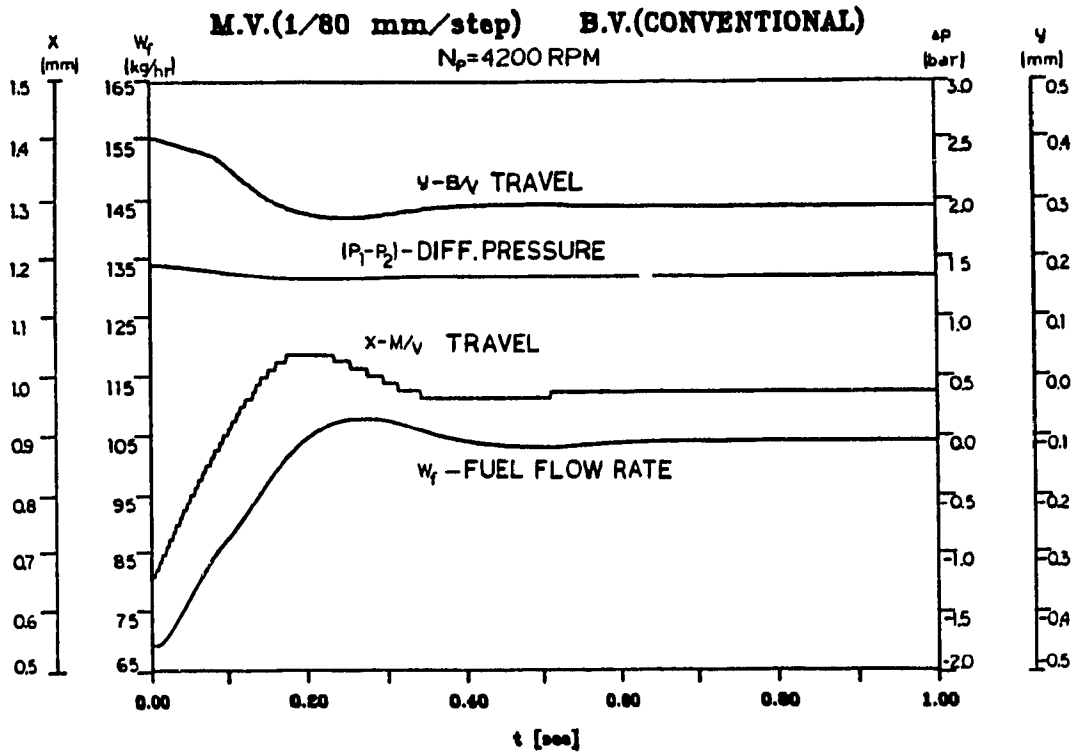

Fig. 8.6 Simulation of dynamic response of electronic fuel control unit with the metering valve actuator step size reduced

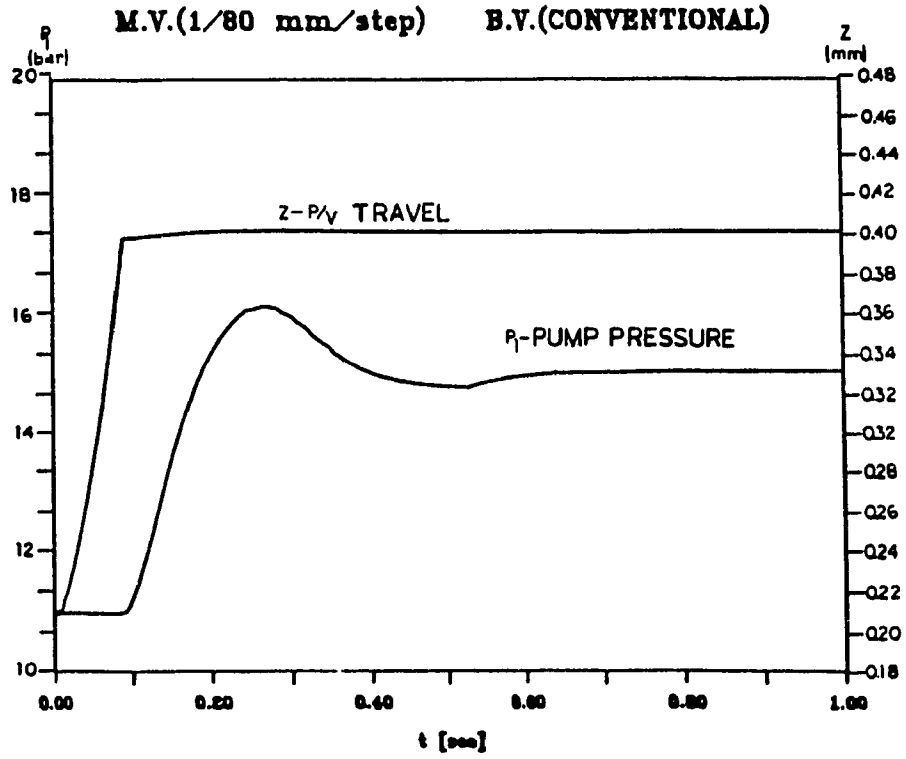

Fig. 8.7 Simulation results for minimum pressurizing valve travel and pump discharge pressure with the metering valve actuator step size reduced

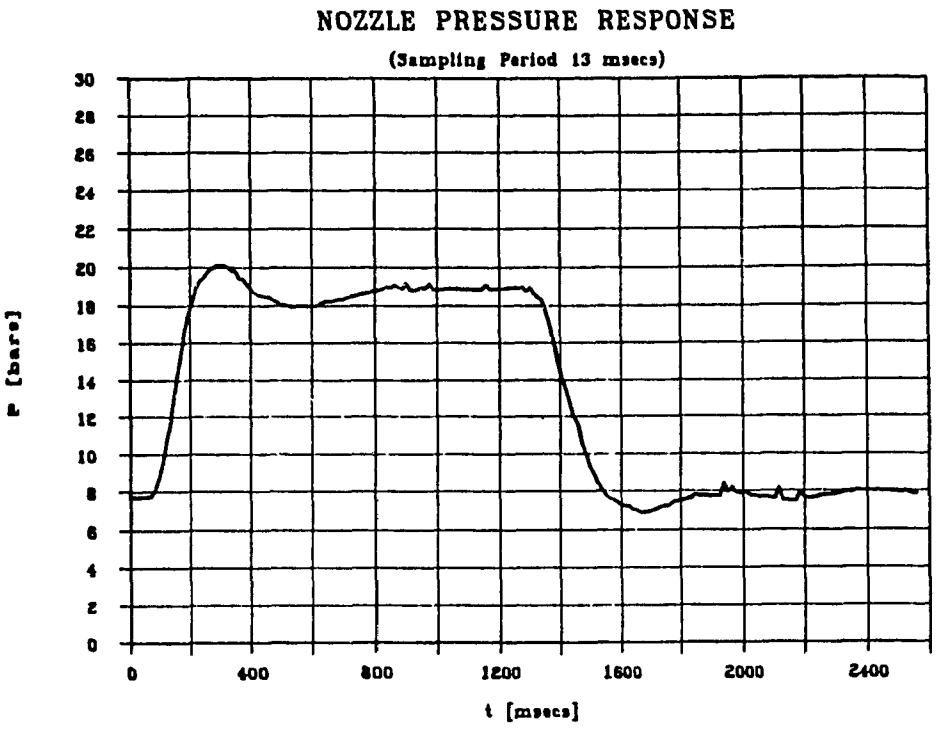

Fig. 8.8 System response with PD controller

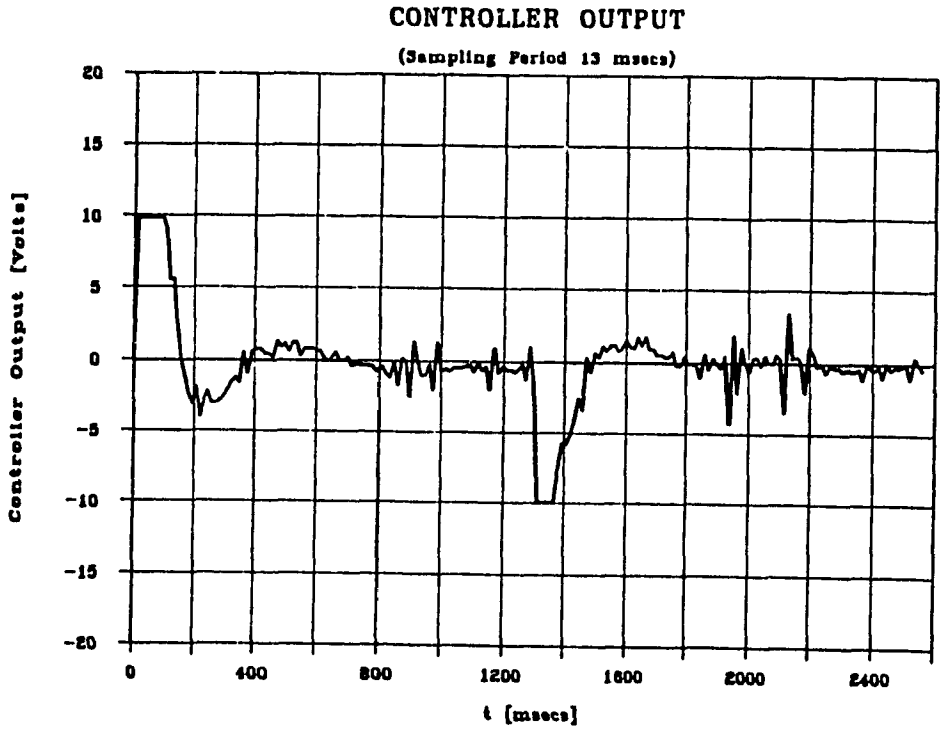

Fig. 8.9 Controller output (after step rate limiter)

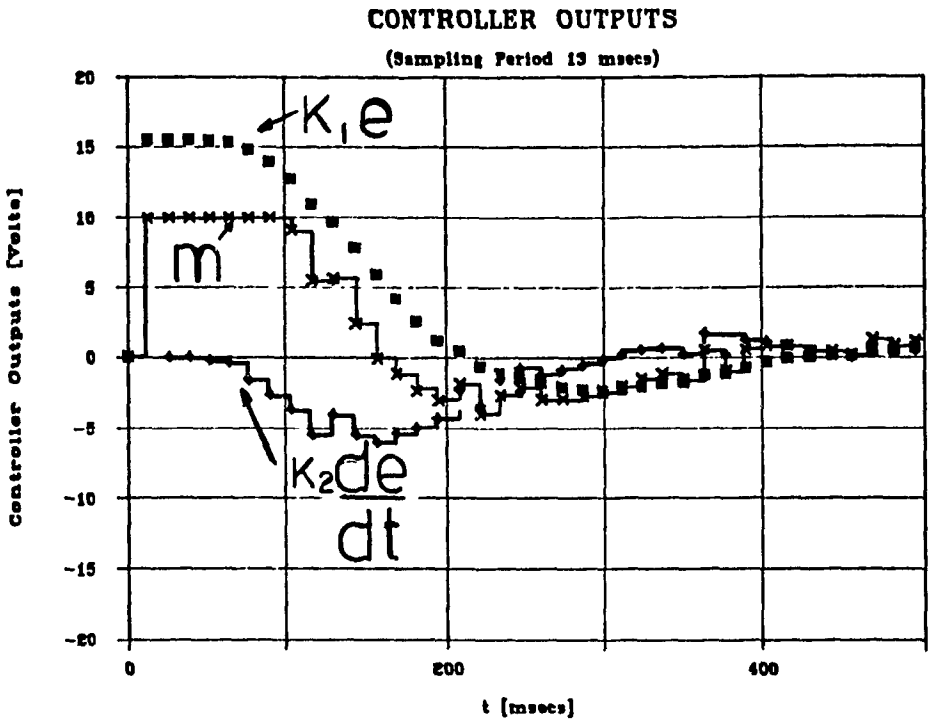

Fig. 8.10 Proportional Derivative and total (limited) controller output for the first 500 msecs

shown when the conventional proportional derivative controller was used. Fluctuations are present in the output flow. These can be associated with the noise in the feedback signal which is further intensified by the derivative action of the controller. The controller output, after the actuator step rate limiter, is shown in Fig. 8.9. The proportional and derivative parts of the controller together with the total controller output, are shown in Fig. 8.10 on an expanded time scale. At the beginning of the transient, when the fuel flow error is large, the controller output is saturated and the system responds at

maximum speed. The derivative component, however, is not active at the biginning of the transient due to the dead time present in the system response. This inactivity of the derivative part, eventually, results in system overshoot. Of course, a smaller proportional gain could be used, but this would not result in the fastest response possible.

The problem seems to be corrected when the Smith predictor is introduced in the control, Fig. 8.11. The derivative part is active during the dead time period (see Fig. 8.12 and Fig. 8.13), even though the actual output is not responding right away to the set point change. The modelling of the flow process is quite accurate, as seen in Fig. 8.11. This eventually results in a more effective action of the Smith Predictor algorithm.

Figure 8.14 shows a typical response of the unit when the Dahlin controller was used. In the controller algorithm derived, Eq. (8.15), a pole equal to -0.86 resulted from the "zero" of the process transfer function. This pole caused excessive ringing of the controller output (see Fig. 8.15). The ringing, however, was not reflected on the controlled output which was relatively smooth. The problem was corrected by replacing the term, containing the pole causing the problem, by its $K_{p1} = (1+ 0.86)$. The dynamic response of the system and the modified controller output are shown in Fig. 8.16 and Fig. 8.17 respectively.

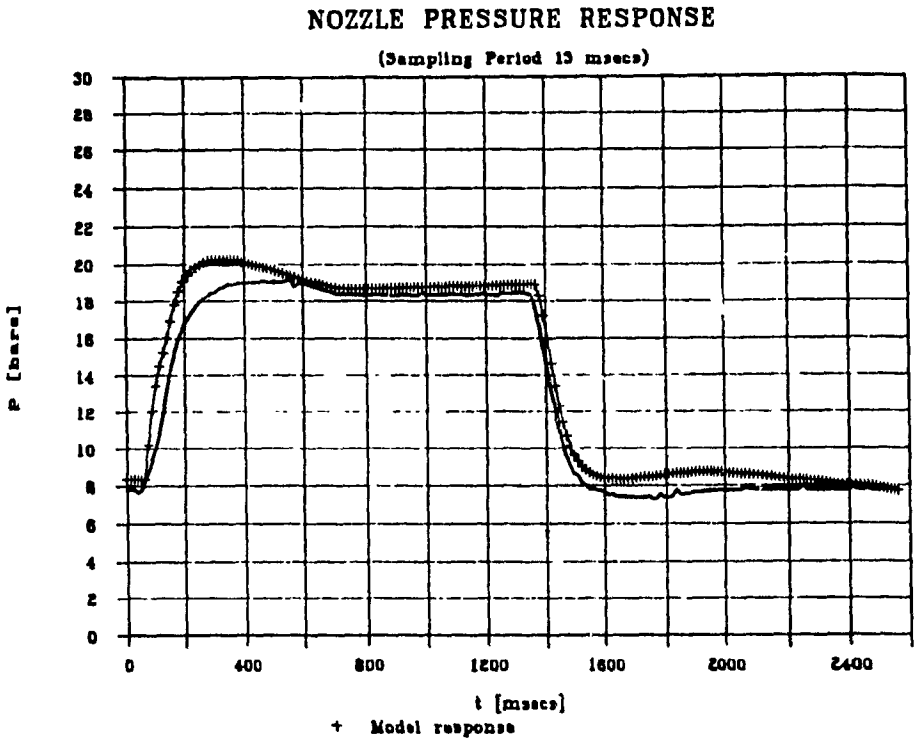

Fig. 8.11 System response and predicted response using Smith Predictor control algorithm

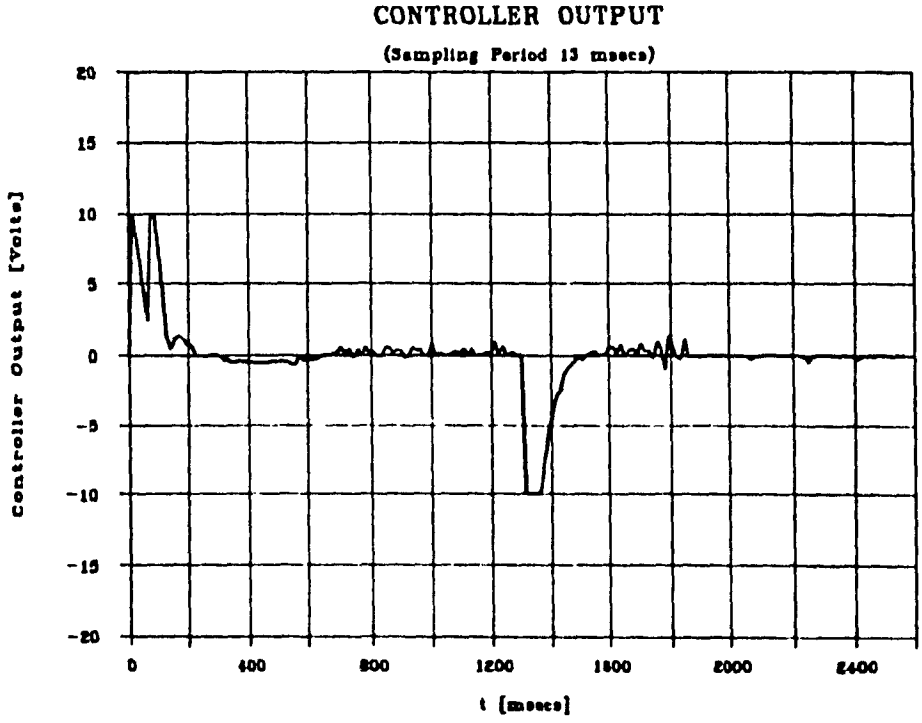

Fig. 8.12 Controller output after step rate limiter

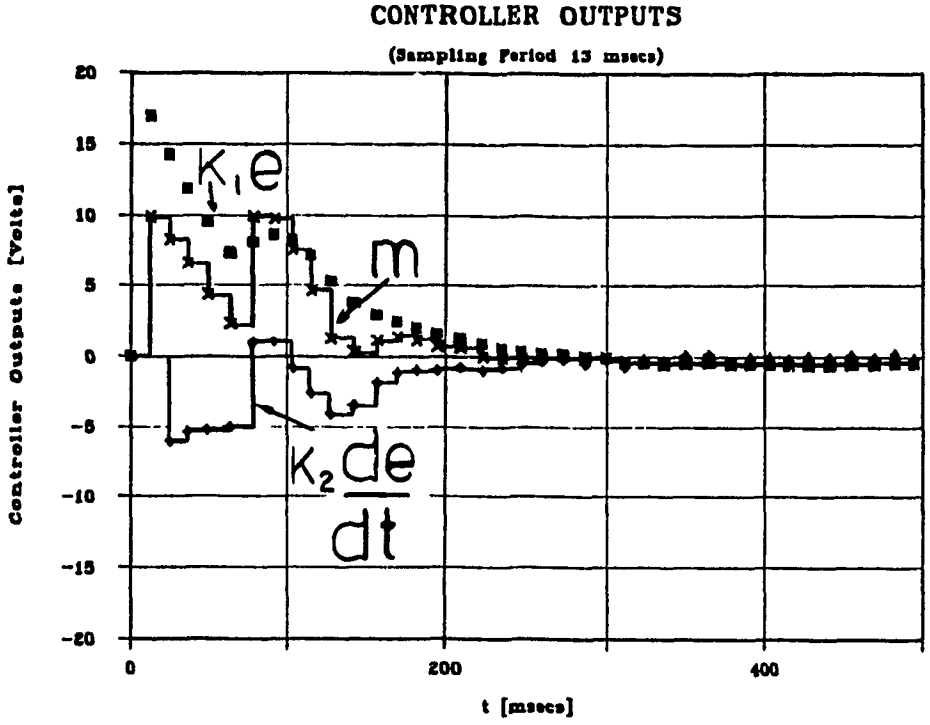

Fig. 8.13 Proportional Derivative and total (limited) controller output for the first 500 msecs

8.6 Summary

Some distinct features of the system under incremental metering valve control were observed, using the developed fuel control unit model. Three types of digital controllers, for the tertiary control loop of the proposed engine electronic controller, were implemented experimentally. The Smith predictor and the Dahlin algorithms were found to perform better than the conventional PD controller especially in the the presence of system transport delays.

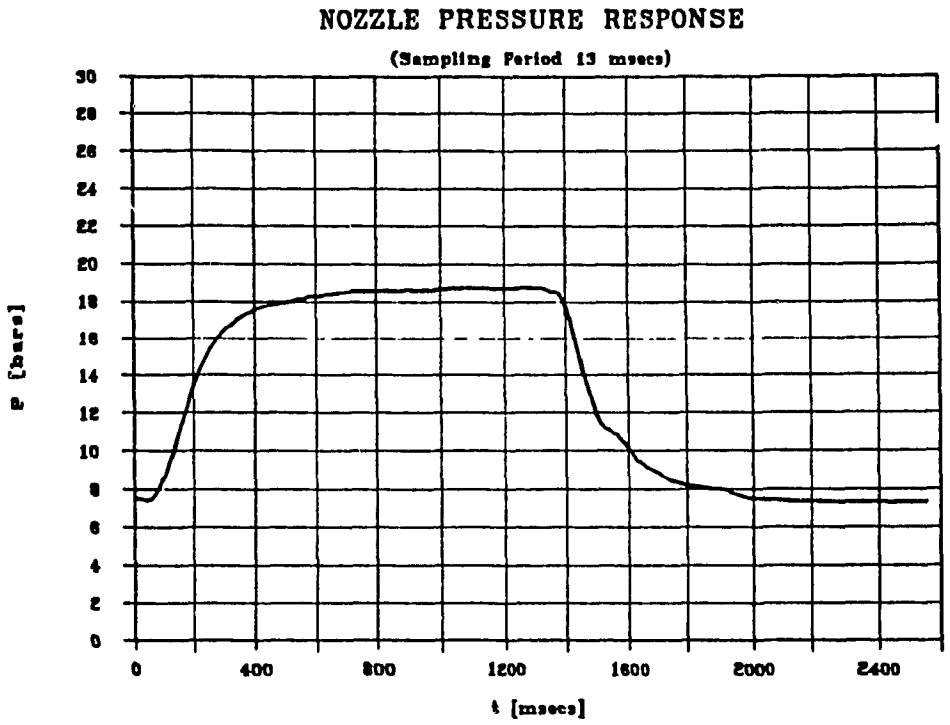

Fig. 8.14 System response with the Dahlin controller

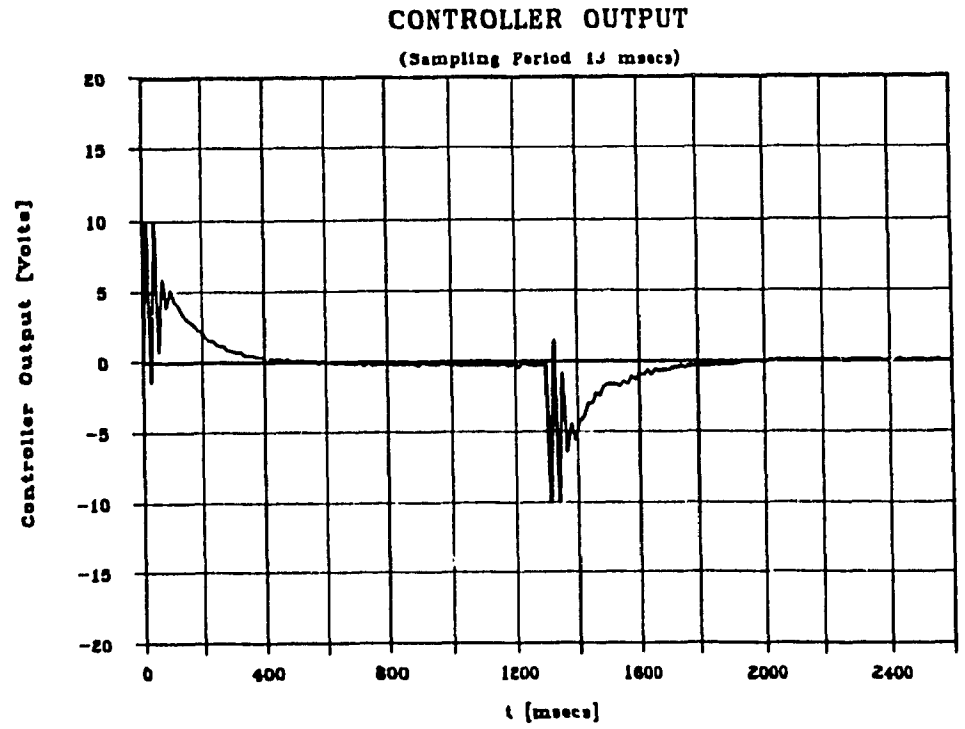

Fig. 8.15 Output of the Dahlin Controller

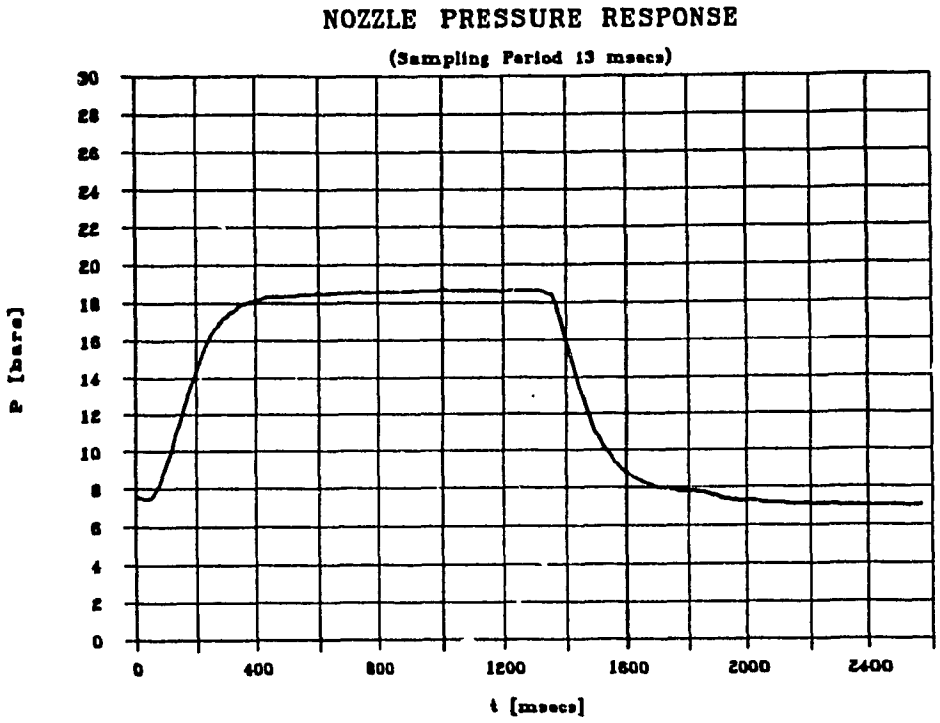

Fig. 8.16 System response with pole causing ringing removed

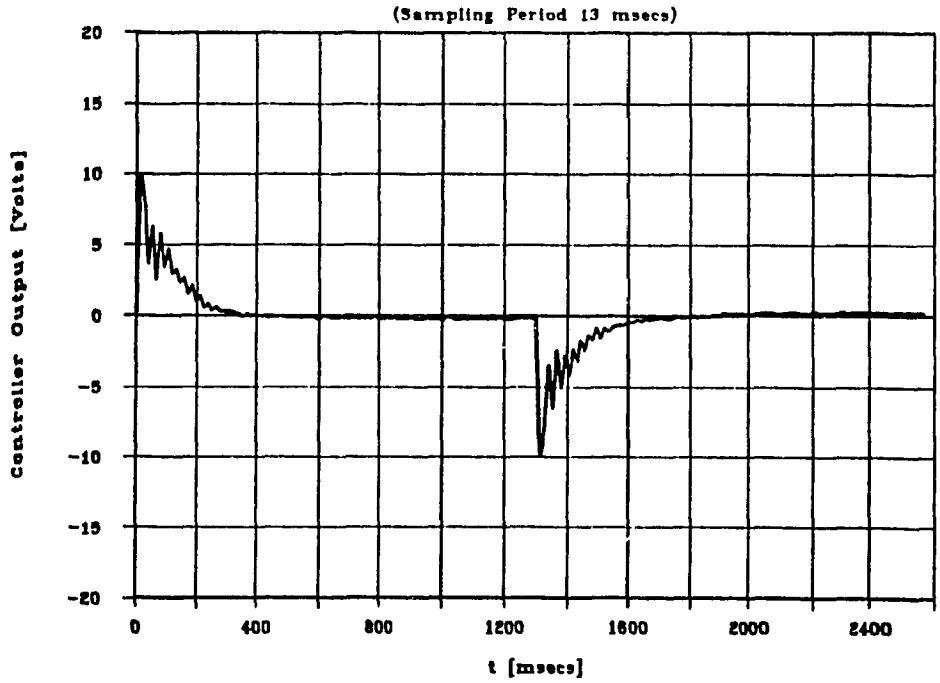

Fig. 8.17 Controller output with pole causing ringing removed

CHAPTER 9

EXPERIMENTAL TUNING OF THE DIGITAL CONTROLLER

9.1 General

An experimental tuning method for the digital controller operating the metering valve was formulated using a multivariable optimization technique. The method was verified using the prototype of the electronic fuel control unit.

9.2 Tuning Method

A reference fuel flow step demand followed by an opposite step is used as an input to the system, Fig. 9.1. A pulse input is used to account for the different system response to flow increase and flow decrease demands. The sampled response is used to calculate a digital performance index such as Integral Square Error (ISE), Integral Time Absolute Error (ITAE) or Integral Absolute Error (IAE). A penalty for excessive overshoot is added to form a penalized objective function. The tuning procedure starts with a set of nominal controller parameters. Each controller parameter is perturbed by a small amount and the run repeated. The calculated values of the objective function from the regular and perturbation runs are passed

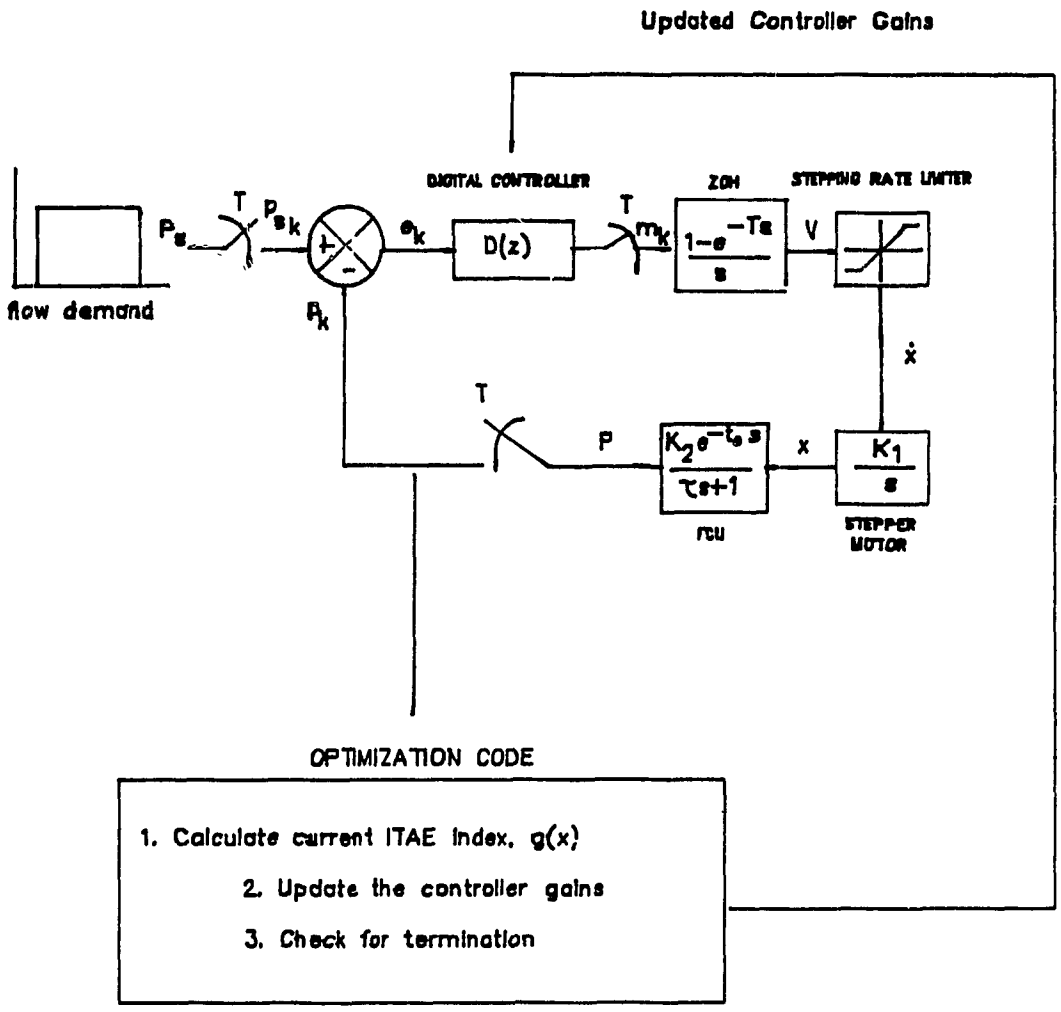

Fig. 9.1 On-line controller optimization method

to the optimization code which updates the controller gains. The procedure is repeated until no further reduction in the objective function is observed.

With the overshoot (or undershoot), P_r, of the first peak above (or below) the set point, P_s, not exceeding 10 per cent, the constrained nonlinear programming problem was formulated as:

$$\text{minimize } [f(\underline{X}) = \text{INDEX}(\underline{X})] \tag{9.1}$$

subject to

$$G(\underline{X}) = (P_r - 0.1\, P_s) \leq 0 \tag{9.2}$$

where, INDEX represents a transient performance index and $\underline{X} = (k_1, k_2, k_3)^T$ is the design vector. The constraint is dealt with by imposing an exterior penalty function term (60), (61), to the objective function when the constraint is violated. This converts the problem to an unconstrained one:

$$\min f(\underline{X}) = \text{INDEX}(\underline{X}) + K \max[G(\underline{X}), 0] \tag{9.3}$$

where K is a number which is sequentially increased to drive the solution to the constraint boundary when the constraint is active. The minimum of the penalized objective function is identical to the minimum of the constrained problem stated by Eq. (9.1) and Eq. (9.2).

The gradient descent updating formula is used to obtain the controller parameters for the next trial. The search direction is taken opposite to the gradient direction. The updating formula is given by:

$$\underline{X}_{k+1} = \underline{X}_k - \lambda_k^* \, g(\underline{X}_k) \tag{9.4}$$

where

$$\underline{g}(\underline{X}) = \nabla f(\underline{X}_k)$$

The parameter λ_k^* is the optimum magnitude of the step size in the search direction. It is chosen to minimize:

$$f[\underline{X}_k - \lambda_k \underline{g}(\underline{X}_k)] \qquad (9.5)$$

Gradient information is obtained by using a finite difference approximation from the small perturbation experimental runs. For example, the first element of the gradient vector is found by perturbing parameter k_1 by a small amount Δk_1, while keeping k_2 and k_3 constant. The partial derivative is calculated as:

$$\underline{g}_1(\underline{X}) = [f(\underline{X} + \Delta k_1 \underline{u}_1) - f(\underline{X})] / \Delta k_1 \qquad (9.6)$$

where

$$\underline{u}_1 = (1,0,0)$$

Problems did arise because of the magnetic field disturbance from the electric motor driving the fuel pump. High noise levels caused errors in the calculation of the partial derivatives, especially when small perturbations were used. With larger perturbations, however, the partial derivatives were not accurately approximated. A solution to

this problem was found by assuming the partial derivatives to be analytic functions of the perturbation size. Three successive perturbations of equal size were performed and the corresponding gradients evaluated. A linear function was fit through the points and extrapolated to zero perturbation size. Using the least squares approximation, the partial derivative of the index with respect to k_i was given by:

$$g_i = (4/3)g_{i1} + (1/3)g_{i2} - (2/3)g_{i3} \qquad (9.7)$$

where, g_{i1}, g_{i2} and g_{i3} denote the partial derivatives calculated from the first, second and third small perturbation runs. To ensure accuracy, this process was repeated several times and an average was taken.

9.3 Experimental Results

A conventional PID controller was used to test the feasibility of the tuning method. Several experimental runs were performed in order to observe the system behavior at different controller gain settings. A nominal set of gains ($\underline{X} = [6,0.5,4.5]^T$) was found to produce an acceptable response (i.e. no large overshoots or excessive delays). The effect of each controller gain on the indices was

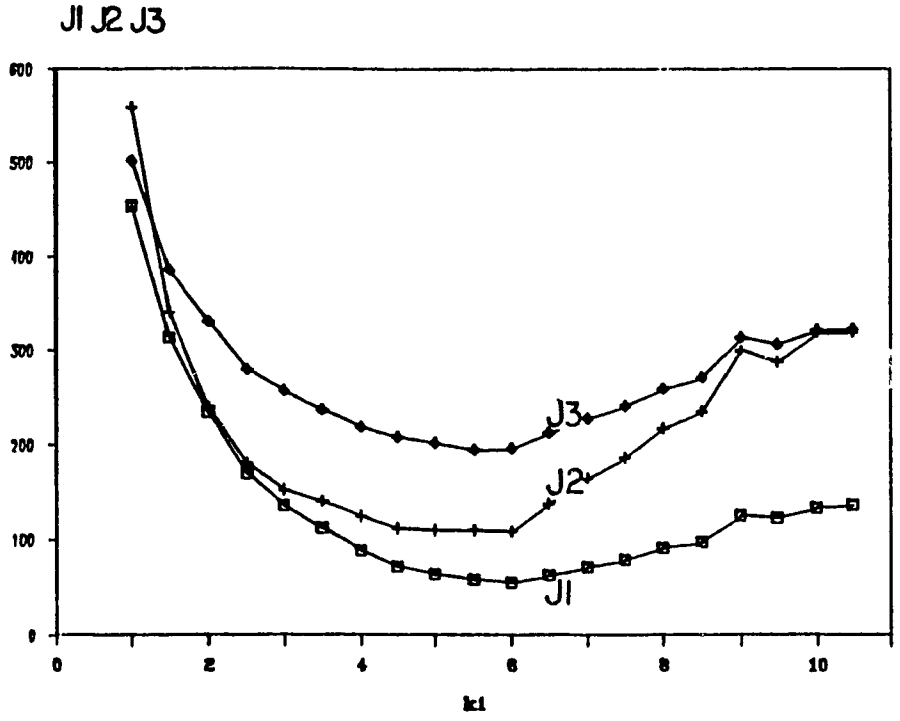

Fig. 9.2 Partial minimization with respect to k_1

observed by varying it about its nominal value while fixing the other two gains.

The proportional gain had the largest effect clearly displaying an optimum, Fig. 9.2. Since the penalized ITAE index showed best selectivity, it was chosen for further investigation. Figure 9.3 shows the effect of k_2. The system performed better at low k_2 values*. Figure 9.4 shows the variation of the objective function due to K_3. The gradient was small at high values of K_3 and a "flat"

* The optimization procedure should eventually eliminate this gain

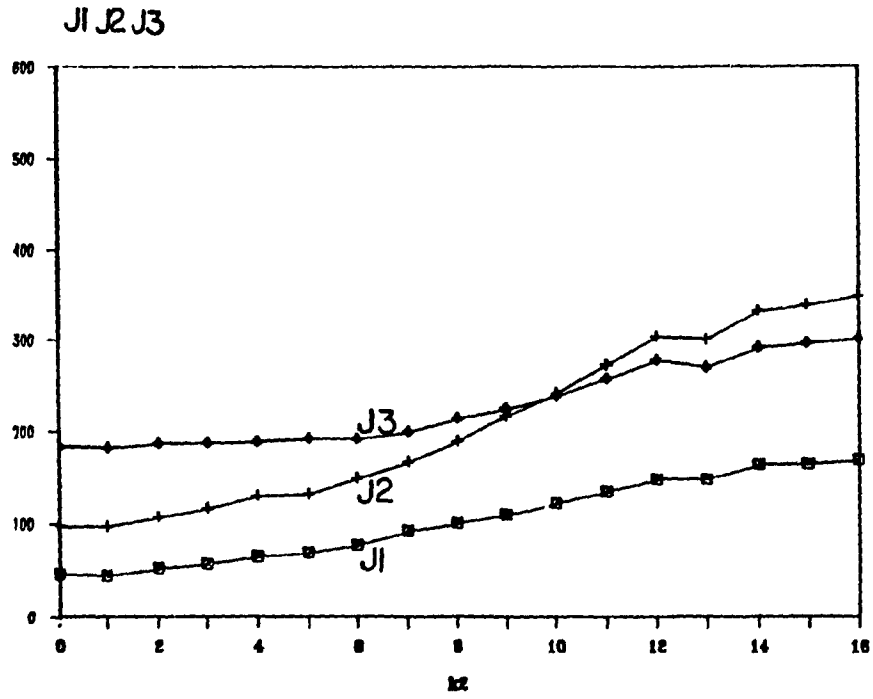

Fig. 9.3 Partial minimization with respect to k_2

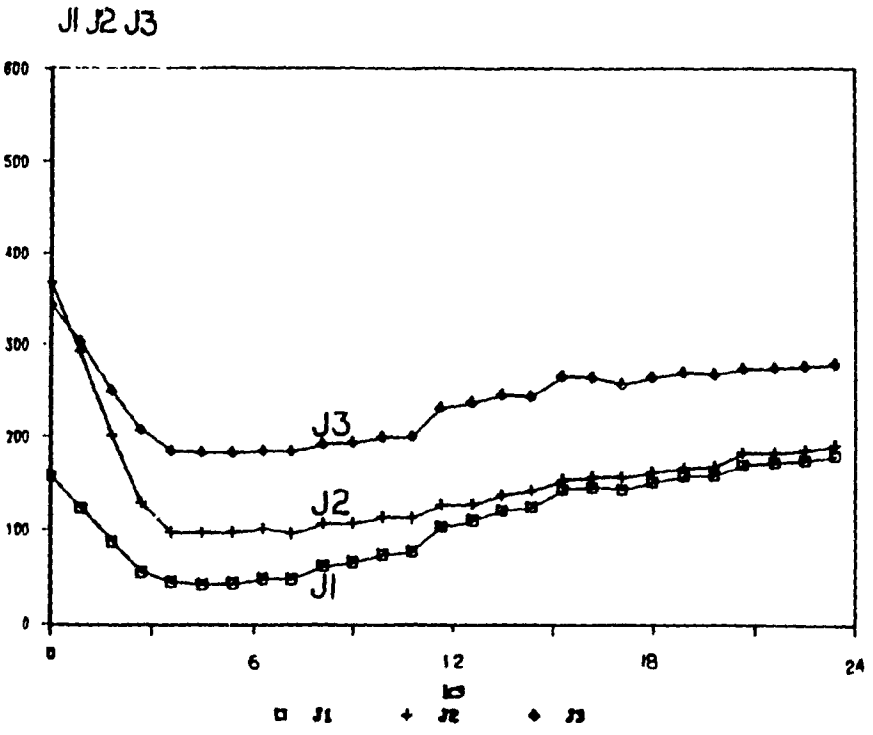

Fig. 9.4 Partial minimization with respect to k_3

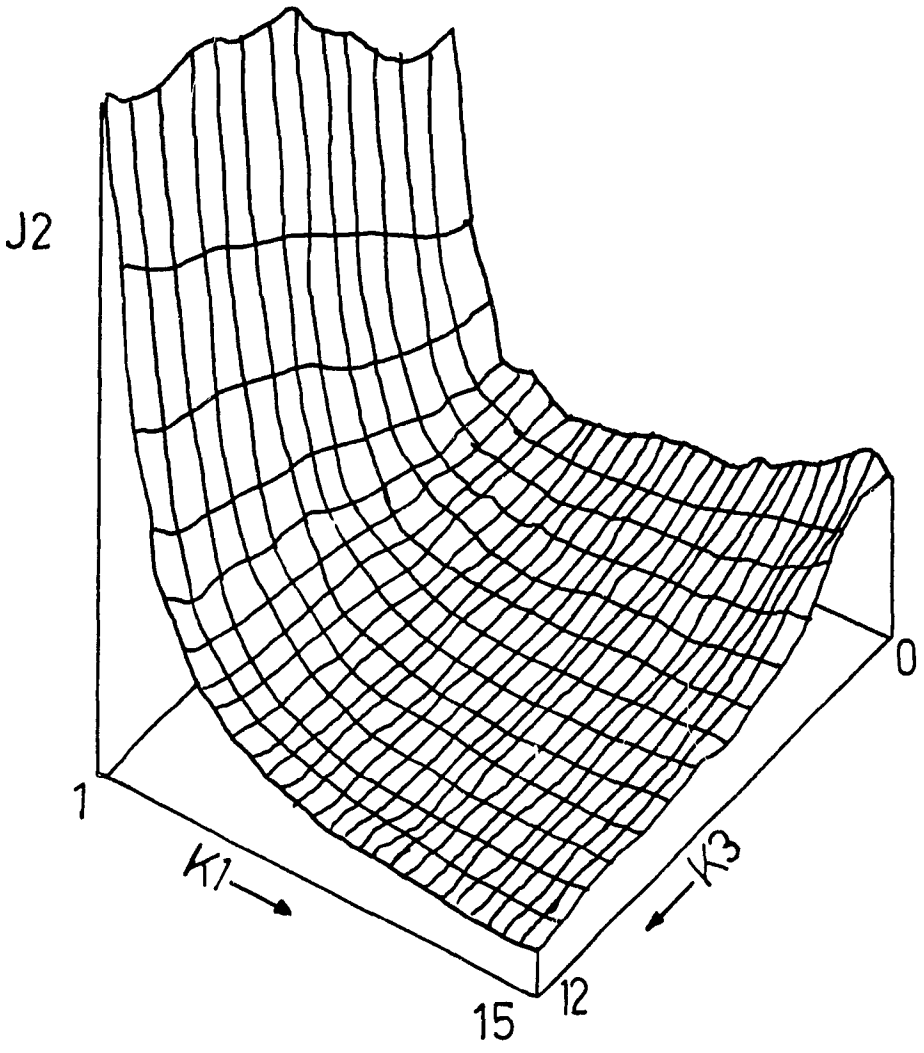

Fig. 9.5 Objective function surface without overshoot/ undershoot penalty

existed at the minimum.

The topography of the ITAE index is shown in Figure 9.5, with k_1 and k_3 as independent variables and k_2 fixed at 0.5. Figure 9.6 shows the change in the surface when the overshoot constraint was applied. The selectivity improved

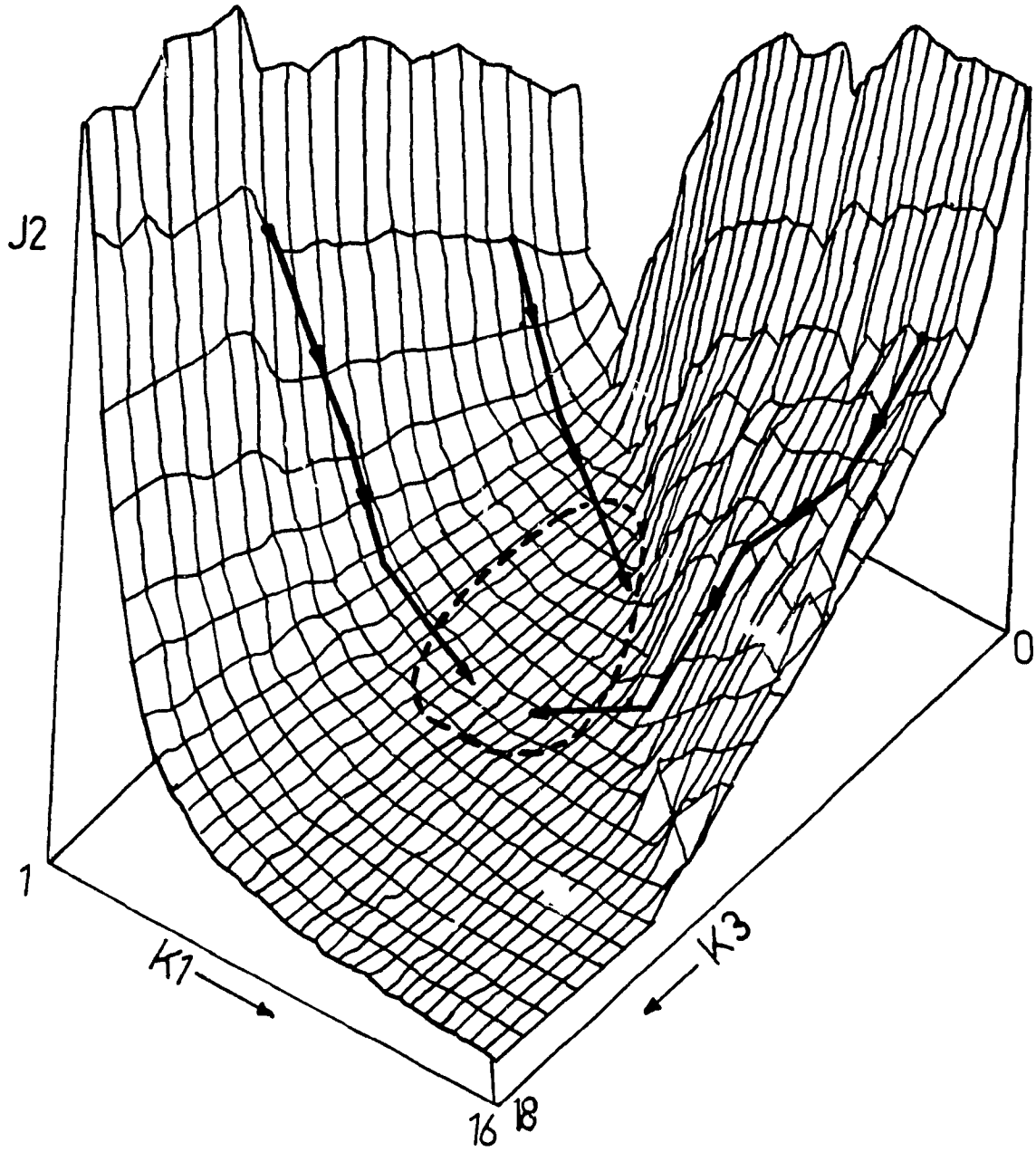

Fig. 9.6 Objective function surface with overshoot/undershoot constraints

and the tuning method performed better. The penalized surface region was somewhat more irregular due to the variability of the overshoot.

Paths to the minimum from different initial points are shown on the surface, Fig. 9.6. The convergence points differed due to the presence of multiple small "valleys" near the minimum. The noise intensified the problem, and thus prevented convergence to a unique solution. The system, however, performed close to optimum with any of these final gain settings. The marked area in the graph shows the domain that gives objective function values within 5 per cent of the minimum.

Figures 9.7 to 9.10 show the history of the controller gain updates and the corresponding improvement in the ITAE index when all three gains were included in the optimization. Curves for two different starting points, one corresponding to overdamped and the other to underdamped system response, are shown. The code produced the optimum settings within 7 to 30 iterations. The system response, however, did not change substantially after the fifth iteration, even if gain K_2 continued to change. This was due to the small effect that k_2 had on the system response. As expected, K_2 was eventually eliminated. Converging time was approximately 5 minutes. Substantial time was spent averaging the value of the objective function through multiple runs.

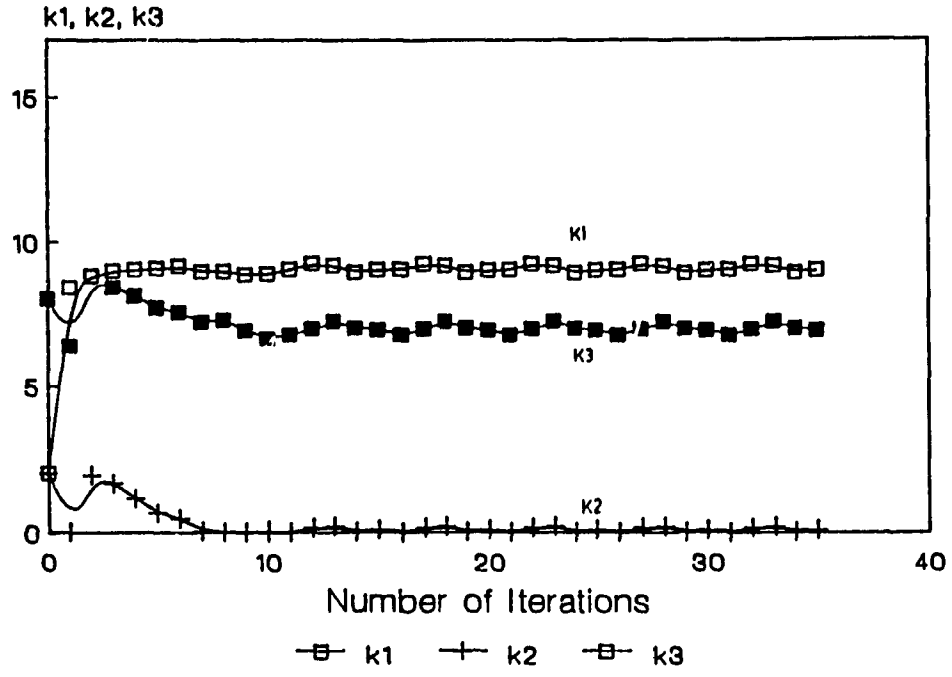

Fig. 9.7 Convergence to optimum gains

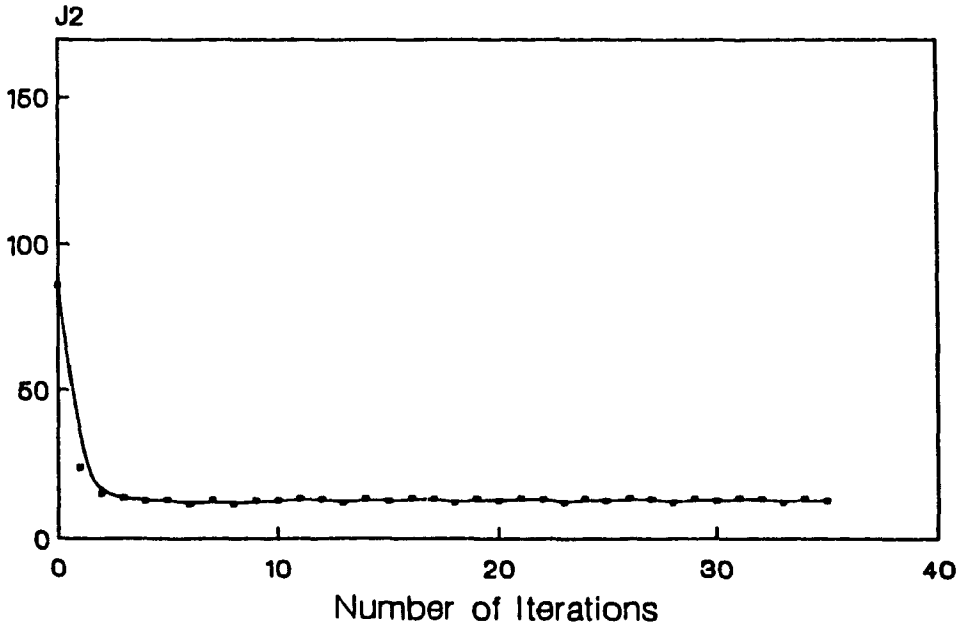

Fig. 9.8 Number of iterations to optimum

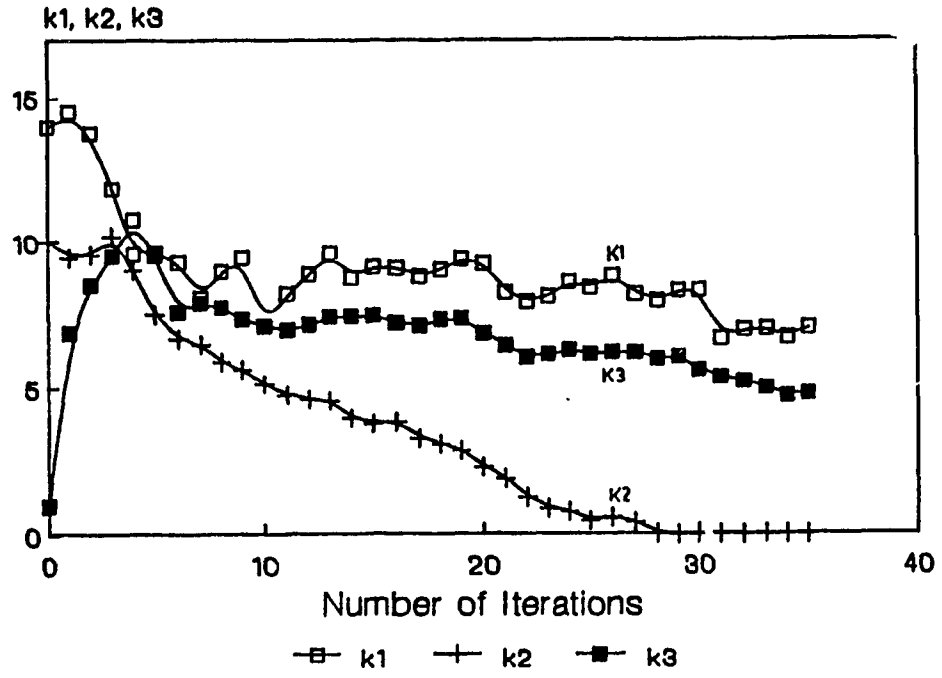

Fig. 9.9 Convergence to optimum gains

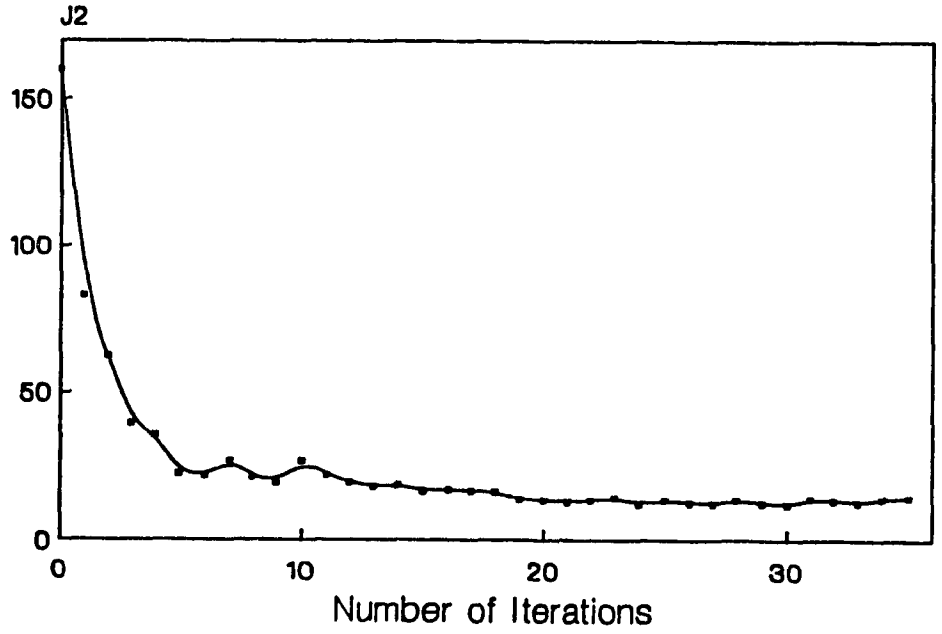

Fig. 9.10 Number of iterations to optimum

Figure 9.11 and Figure 9.12 show typical tuning responses starting from underdamped and overdamped systems respectively. Curves corresponding to original, second and fourth (sixth for the underdamped case) iterations of the tuning progression are shown. The ability of the method to bring the response close to the optimum very quickly, is clearly illustrated.

9.4 Summary

In this chapter the use of a "smart" (computer operated) test bench for tuning the controller of the electronic fuel control unit was demonstrated. The advantage of the method was that an analytical model of the fuel control unit or controller was not needed. The nature of the objective function was not known exactly and its character was deduced from experimental runs.

This method can be used to tune simultaneously multiple controllers and could be particularly useful for the tuning of the three controllers of the complete engine electronic system described in Chapter 8. The tuning procedure can be repeated throughout the operating region and results can be stored and used by the digital controllers as a "look-up" chart.

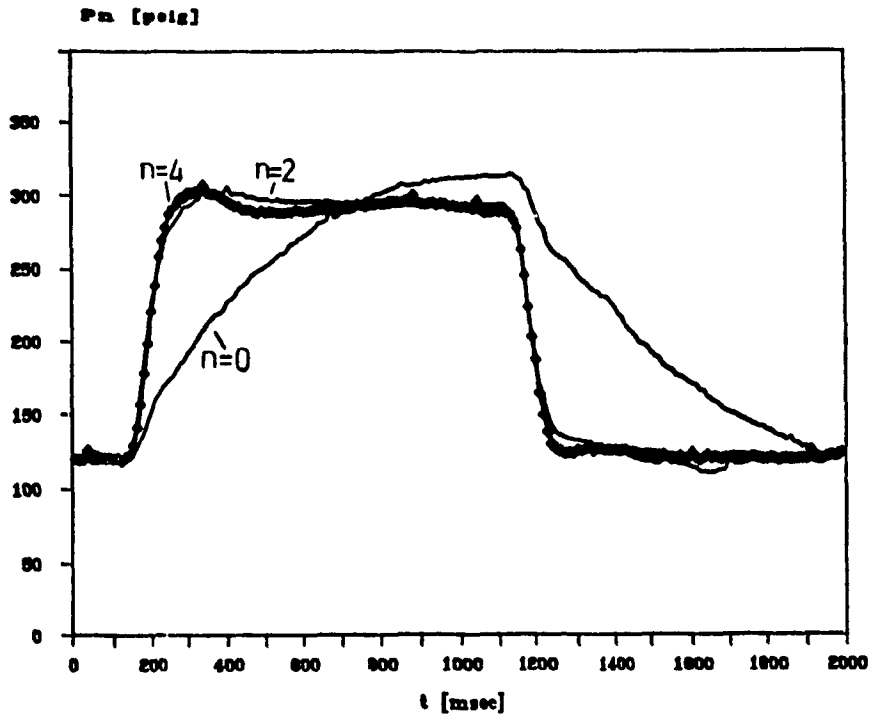

Fig. 9.11 Controller tuning: overdamped case

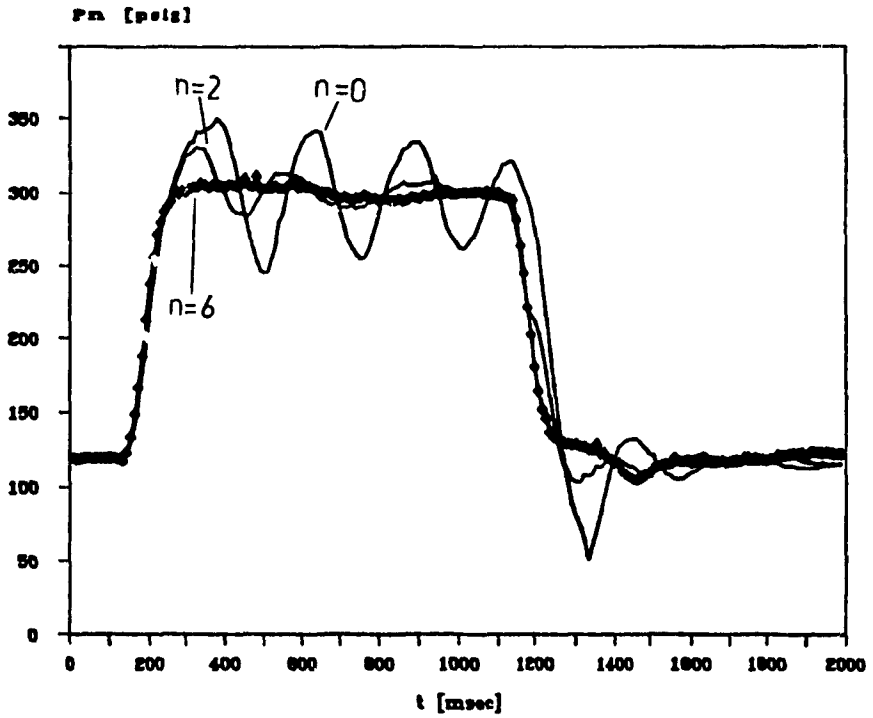

Fig. 9.12 Controller tuning: underdamped case

CHAPTER 10

ELECTRONIC FUEL CONTROL UNIT WITH TWO DIGITAL ACTUATORS

10.1 General

The feasibility of electronic control employing two valves operated by linear digital actuators is investigated in this chapter. The analysis is a direct follow-up of the electronic control unit in which only the metering valve was under microprocessor control. The validated mathematical model of the metering section is used to predict the behavior of the system.

The system is equipped with two digital electronic actuators which operate the metering valve and the by-pass valve (see Fig. 4.7). The flexibility of this configuration offers the possibility to perform functions not possible by conventional fuel control units or by the single actuator electronic unit already discussed. A unique back-up capability is also possible (see Chapter 4). In case of failure of one valve, the other valve can perform the fuel scheduling.

Some control strategies are proposed, investigated and discussed. The system performance is optimized by selecting best controller parameters. The univariate direct search optimization method with exterior penalty for overshoots is used.

10.2 Control Strategies

Three control strategies were investigated. The block diagram of the first is shown in Fig. 10.1. The actuator operating the by-pass valve is under separate control and maintains a constant pressure across the metering valve. The controller of the metering valve produces its output signal based on the fuel flow error and drives the actuator according to the changes in the fuel flow demand. This control is similar to the single actuator electronic unit where the by-pass valve is under hydromechanical control.

The second control strategy, shown in Fig. 10.2, employs two digital controllers operating simultaneously on the fuel flow error. The two valves assist each other to achieve faster fuel flow rate response. To avoid severe "hunting" of the by-pass valve, its control is deactivated when the flow error is small. This technique improves the system transient response significantly.

The problem with the second strategy is that, there is no unique position of the valves to achieve the demanded fuel flow. Many different combinations can produce the same fuel flow. This may result in undesirable valve positioning, if after long operation one actuator would occasionally "lose" steps. To avoid this problem, the third control strategy, shown in Fig. 10.3, was applied. The metering valve would perform the control by trying to

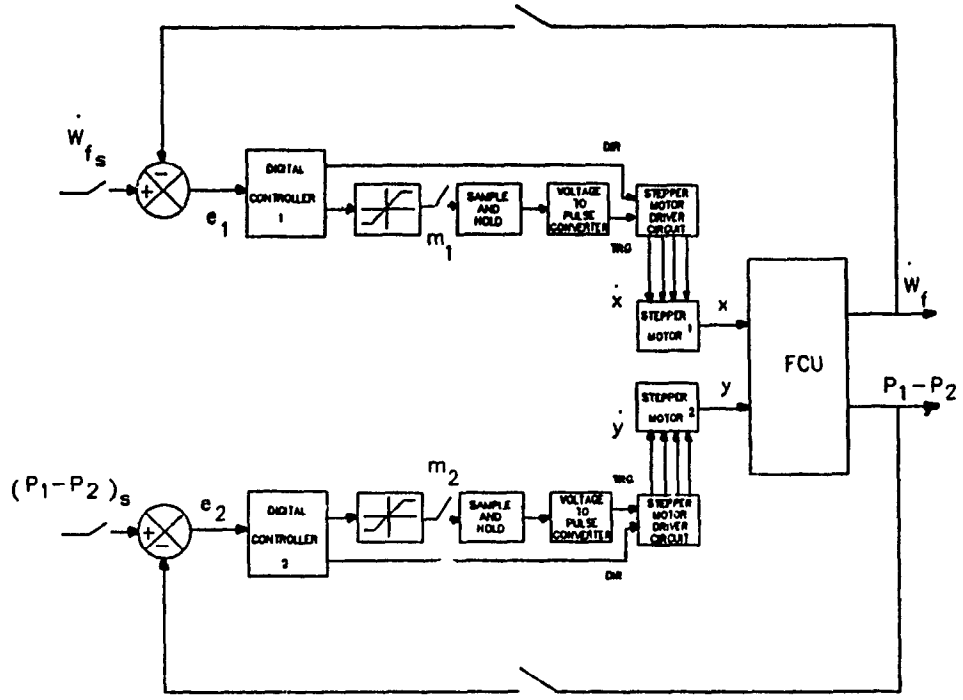

Fig. 10.1 First control strategy of the two-actuator electronic fuel control unit

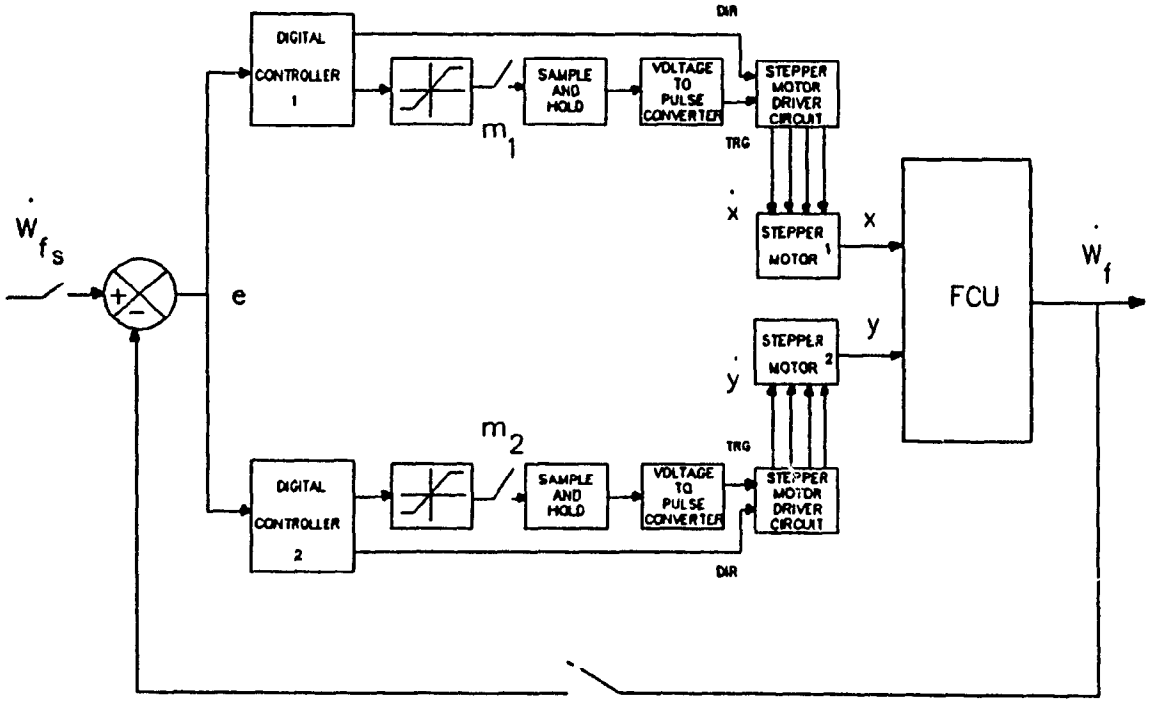

Fig. 10.2 Second control strategy of the two-actuator electronic fuel control unit

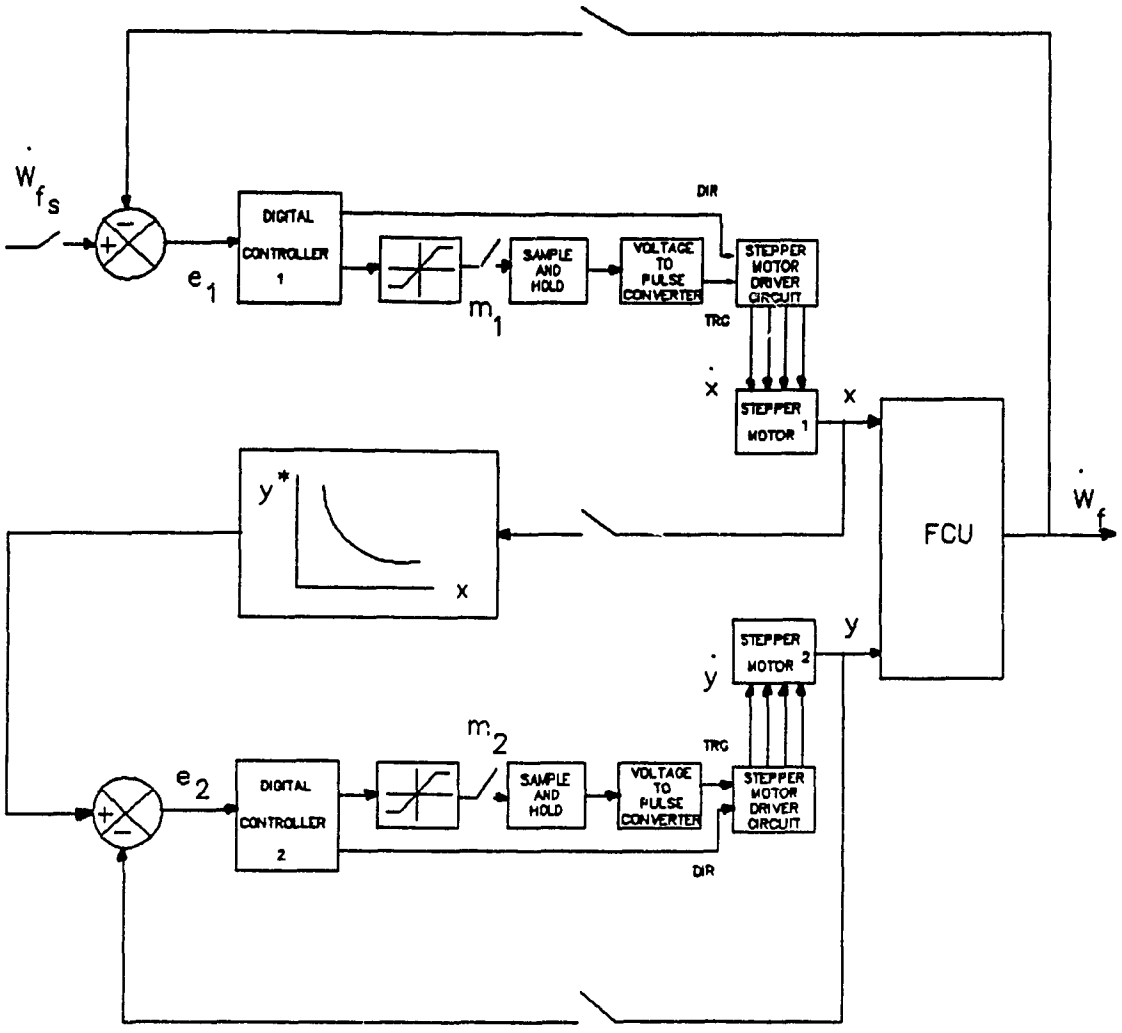

Fig. 10.3 Third control strategy of the two-actuator electronic fuel control unit

establish the desired fuel flow while the by-pass valve would "follow" the motion of the metering valve. The relative position of the two valves at steady state has to be established "a priori" and stored in a "look-up" chart. For the implementation of this type of control, the position signals of both valves are needed for feedback.

10.3 Simulation Results and Discussion

Simulation results were obtained for an abrupt change in the fuel flow demand. Fig. 10.4 shows results obtained when constant differential pressure was maintained across the metering valve (first control strategy). The step size of the actuator operating the metering valve was 0.0125 mm

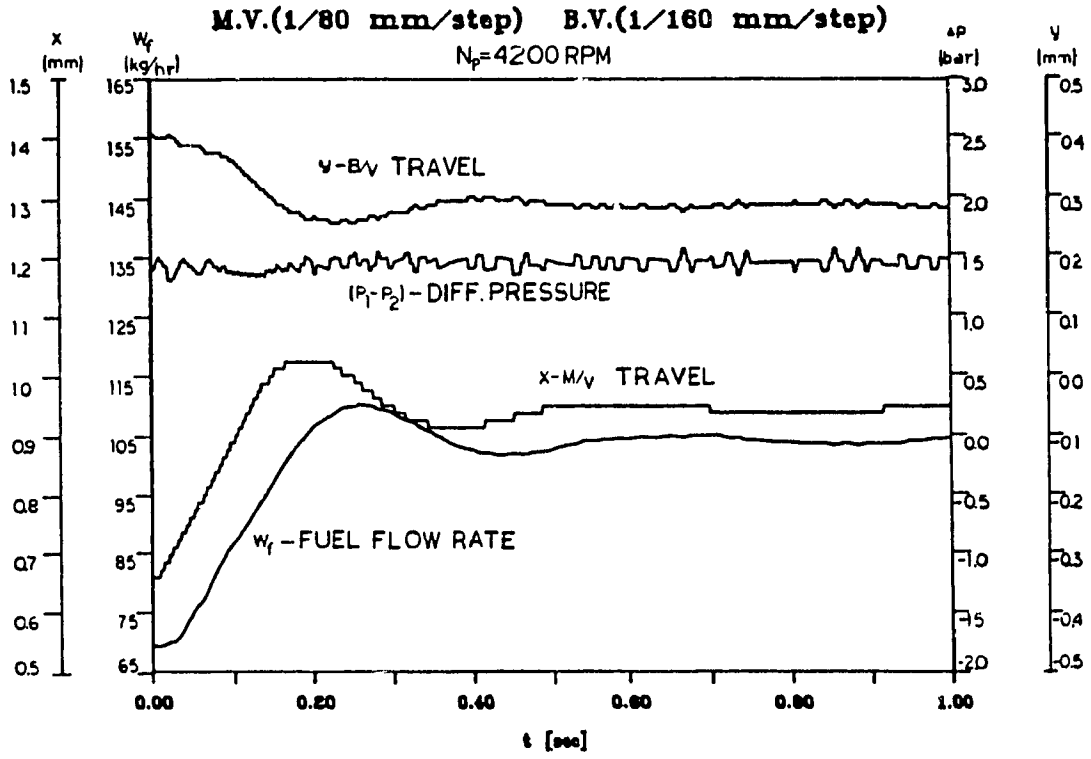

Fig. 10.4 System response (first control strategy)

and of the actuator operating the by-pass valve was 0.00625 mm. A smaller step size was used in the by-pass valve because of its higher flow area gain. The by-pass valve responded to the metering valve movement in similar way as in the conventional system, see Fig. 8.6. The obvious

disadvantage of the system was "hunting", this time, also about the desired differential pressure. Due to the high by-pass valve flow area gain, every step of the actuator corresponded to a substantial differential pressure change. To avoid this, either the size of the actuator step or the valve flow area gain should be reduced. The latter solution is preferable because the step size is already quite small and further reduction might involve special actuator design. A big reduction in the by-pass valve gain, on the other hand, may slow down the response of the system considerably. A trade-off between the valve flow gain and the actuator step size is necessary.

Figure 10.5 shows simulation results obtained when both actuators responded to the fuel flow demand. The response was significantly faster as compared to the single actuator unit or the double actuator unit with the differential pressure kept constant. At the beginning of the transient, the controller output was at its maximum due to the big error in the fuel flow. Therefore, both valves were moving at their highest speed. The by-pass valve had higher flow area gain and caused rapid increase in the differential pressure. This provided an initial "boost" in the fuel flow rate change. When the error was reduced below the value causing controller saturation, the metering valve was moving more rapidly than the by-pass valve due to its higher controller gain. By making the metering valve more

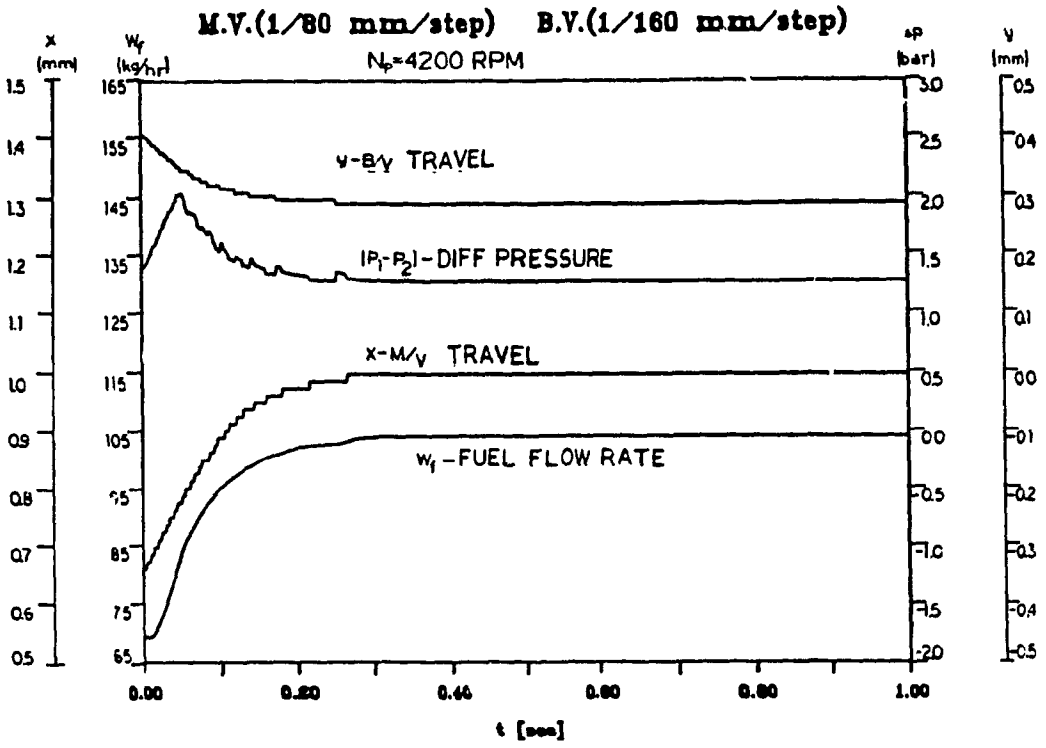

Fig. 10.5 System response (second control strategy)

sensitive to the fuel flow error, its control prevailed near steady state and the final fuel flow adjustment was performed only by the metering valve. As a result, the amplitude and the frequency of "hunting" were greatly reduced. In some applications where the "hunting" problem can be tolerated, the speed of response can be further improved by increasing the proportional gain of the by-pass valve controller.

Figure 10.6 shows results when the third control strategy was used. The controller responded similarly as in the second control strategy; however, with the by-pass

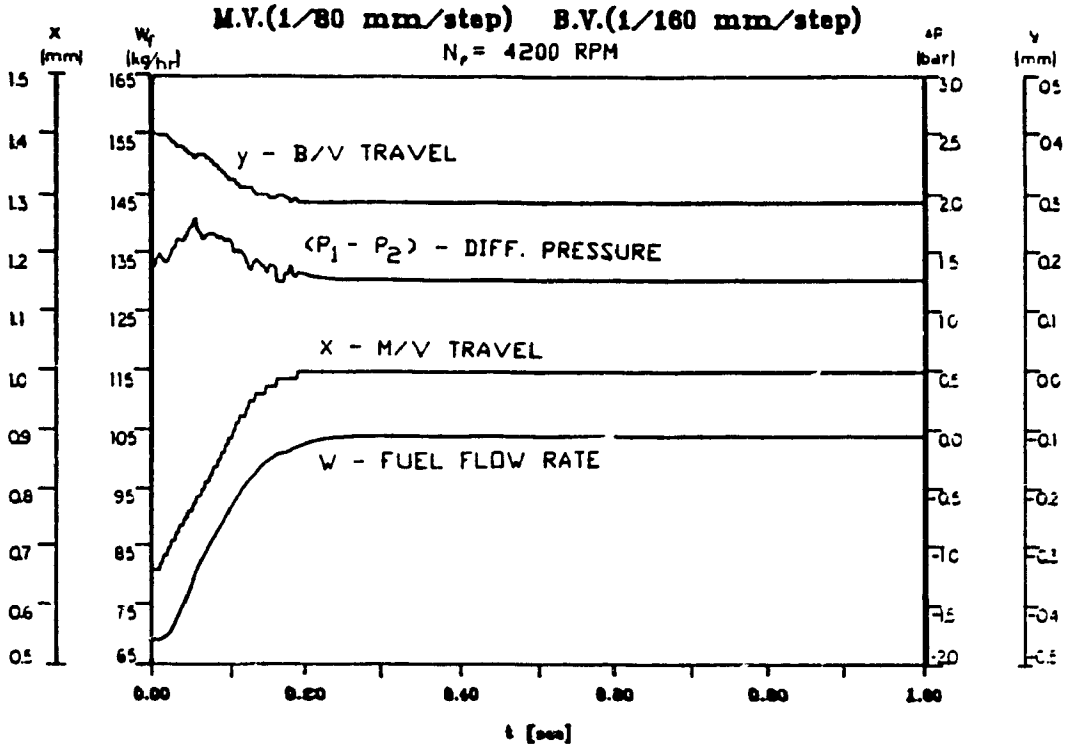

Fig. 10.6 System response (third control strategy)

valve "following" the movement of the metering valve. As a result, the response of the system was somehow delayed. An optimal path which "ties" the movement of the two valves could be prescheduled throughout the operating region.

Figure 10.7 compares the fuel flow rates achieved with the two electronic control units, to the fastest flow rate response possible, which corresponds to the case of instantaneous actuation of the metering valve. The response obtained with the two-actuator system, using the second control strategy, was closer to the fastest response possible. Proper choice of the actuators step size, the

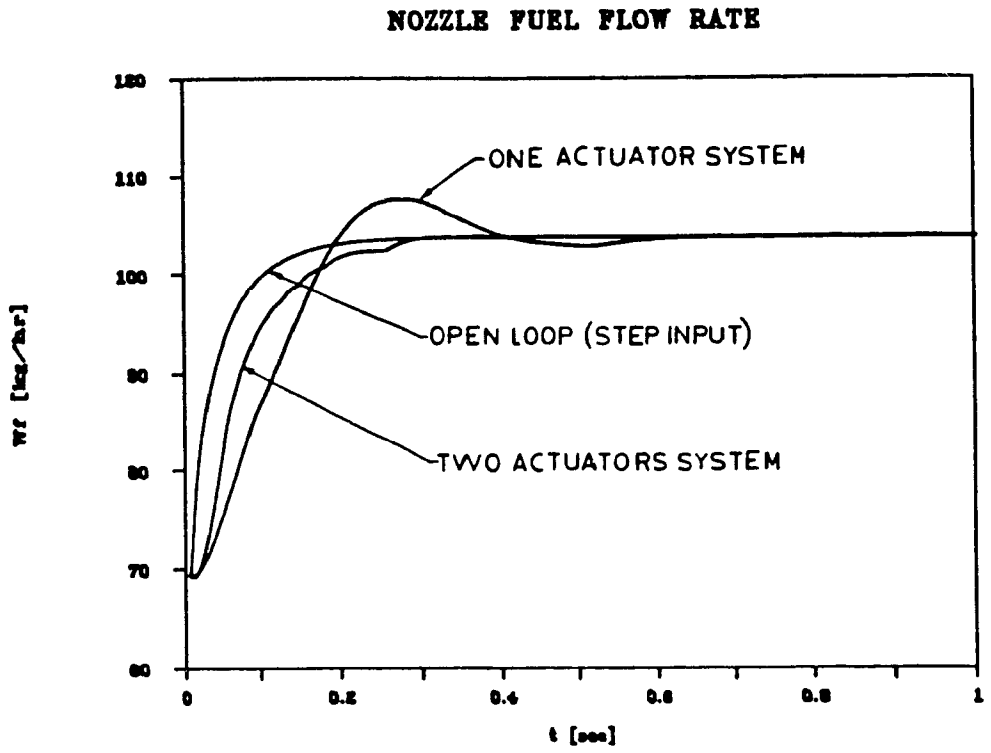

Fig. 10.7 Metered fuel flow response

flow area gains of the two valves and the gains of the controllers, can further improve the system response. This requires the solution of the optimization problem involving all the above parameters simultaneously.

10.4 Optimization of Interaction of the Two Valves

The optimization of the controller parameters for the two valves, was performed using the univariate direct search optimization method. The exterior penalty method was applied to penalize excessive overshoots. The parameters of both controllers were optimized simultaneously for

particular step sizes of the two actuators. The procedure was repeated in a systematic way to cover a wide range of step sizes. Then, the best step size combination was selected.

The constrained nonlinear programming problem was formulated as follows:

$$\text{minimize } [\text{ITAE}(\underline{X})] \tag{10.1}$$

$$\text{subject to } G(\underline{X}) = \int_{t_0}^{t_f} \max\,[0,\ (W_f)_r - 0.05(W_f)_s]\ dt = 0 \tag{10.2}$$

where, ITAE is the Integral of Time multiplied Absolute Error, and

$$\underline{X} = (P_{mv}, D_{mv}, P_{bv}, D_{bv})$$

s the design vector. The structure of the two controllers was:

$$m_1 = P_{mv}\ e_k - D_{mv}\ e_{k-1} \tag{10.3}$$

$$m_2 = P_{pv}\ e_k - D_{pv}\ e_{k-1} \tag{10.4}$$

The ITAE index was selected because it penalized more the steady state error and therefore, the "hunting". The constraint was imposed to prevent overshoots greater than 5%. An exterior penalty function term was added to the

objective function when the constraint was violated. The unconstrained optimization problem was then reformulated as:

$$\text{minimize } f(\underline{X}) = \text{ITAE} + K \max[G(\underline{X}),0] \qquad (10.5)$$

where, K was an appropriately chosen large number which would drive the solution to the boundary if the constraint would be active without, however, causing numerical instabilities.

The univariate multivariable optimization method used is a direct search (non-gradient) method that requires only the evaluation of the objective function in every iteration. Optimization starts with an arbitrary selection of the $\underline{X}$. The region containing the minimum with respect to the first parameter is bracketed and the objective function is evaluated at three suitable points. A quadratic function is used to approximate the objective function in the region. The quadratic is refitted until the error between the approximated and the evaluated objective function is very small. That is:

$$\left| \frac{h(\hat{\lambda}^*)-f(\hat{\lambda}^*)}{f(\hat{\lambda}^*)} \right| \leq \varepsilon \qquad (10.6)$$

where, $h(\lambda)$ is the quadratic interpolation of the objective

function, $\hat{\lambda}^*$ is an approximation of the controller "optimum" parameters and ε is a suitably chosen small number. The process is repeated sequentially with all parameters. The first cycle of the optimization is completed when all directions are searched. The procedure is terminated when no further improvement of the objective function is noted.

10.5 Optimization Results and Discussion

Optimization was performed only for the second control strategy of the two-actuator electronic unit. Figure 10.8 shows the update of the parameters of the two controllers when the actuator step size for the metering valve and the by-pass valve were 0.00625 mm and 0.025 mm respectively.

The proportional gain of the by-pass valve was optimized first, while the other parameters were kept constant. The quadratic approximation of the objective function was refitted until the error, as calculated by Eq. (10.4), was less than 10^{-5}. As seen in Fig. 10.9, the objective function was reduced significantly as compared to the initial value. This was due to the dominating effect of the by-pass valve proportional gain.

The proportional gain of the metering valve controller was "optimized" next. The optimum, with respect to this parameter was obtained in two iterations. The optimization

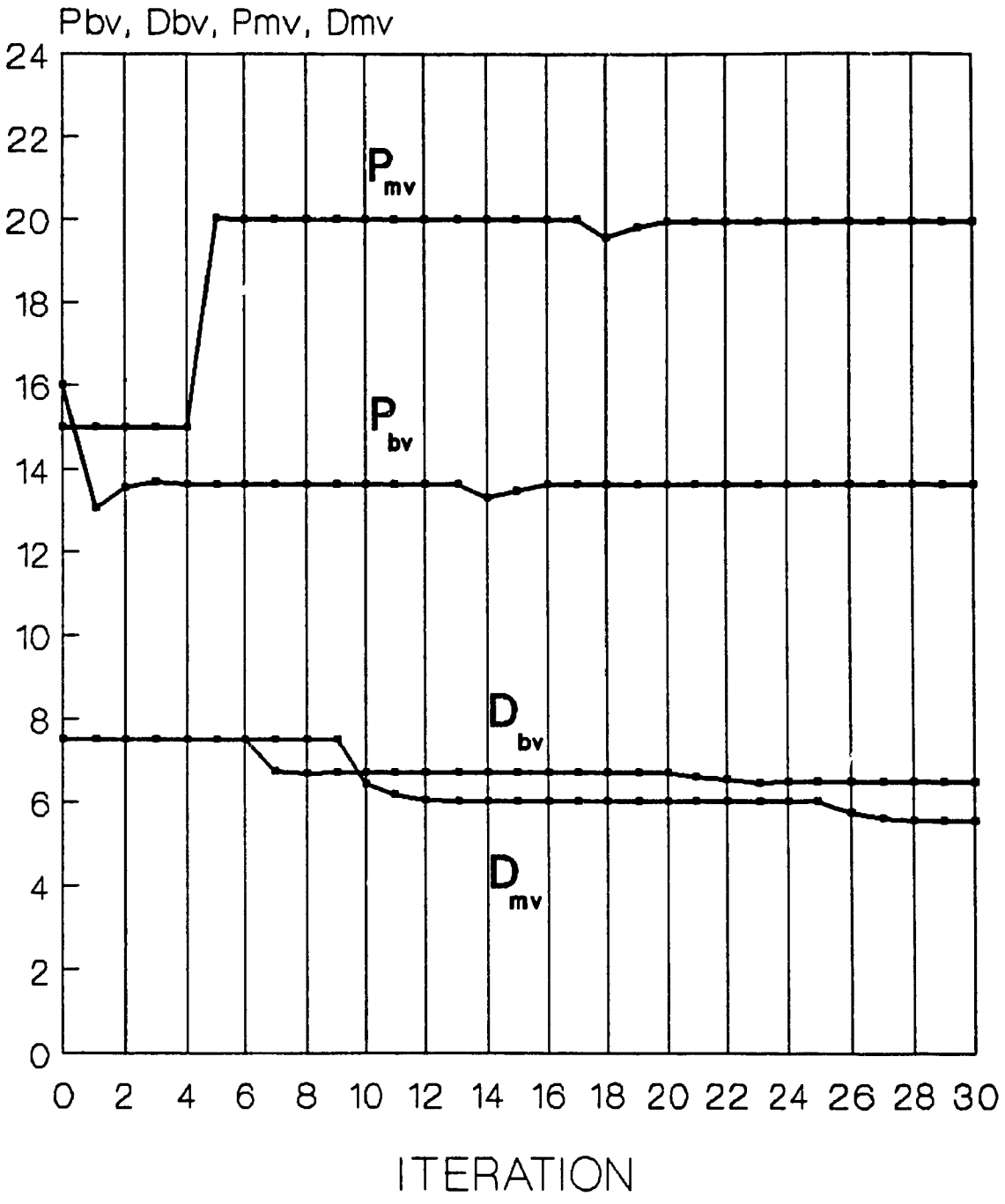

Fig. 10.8 Univariate optimization of controller parameters

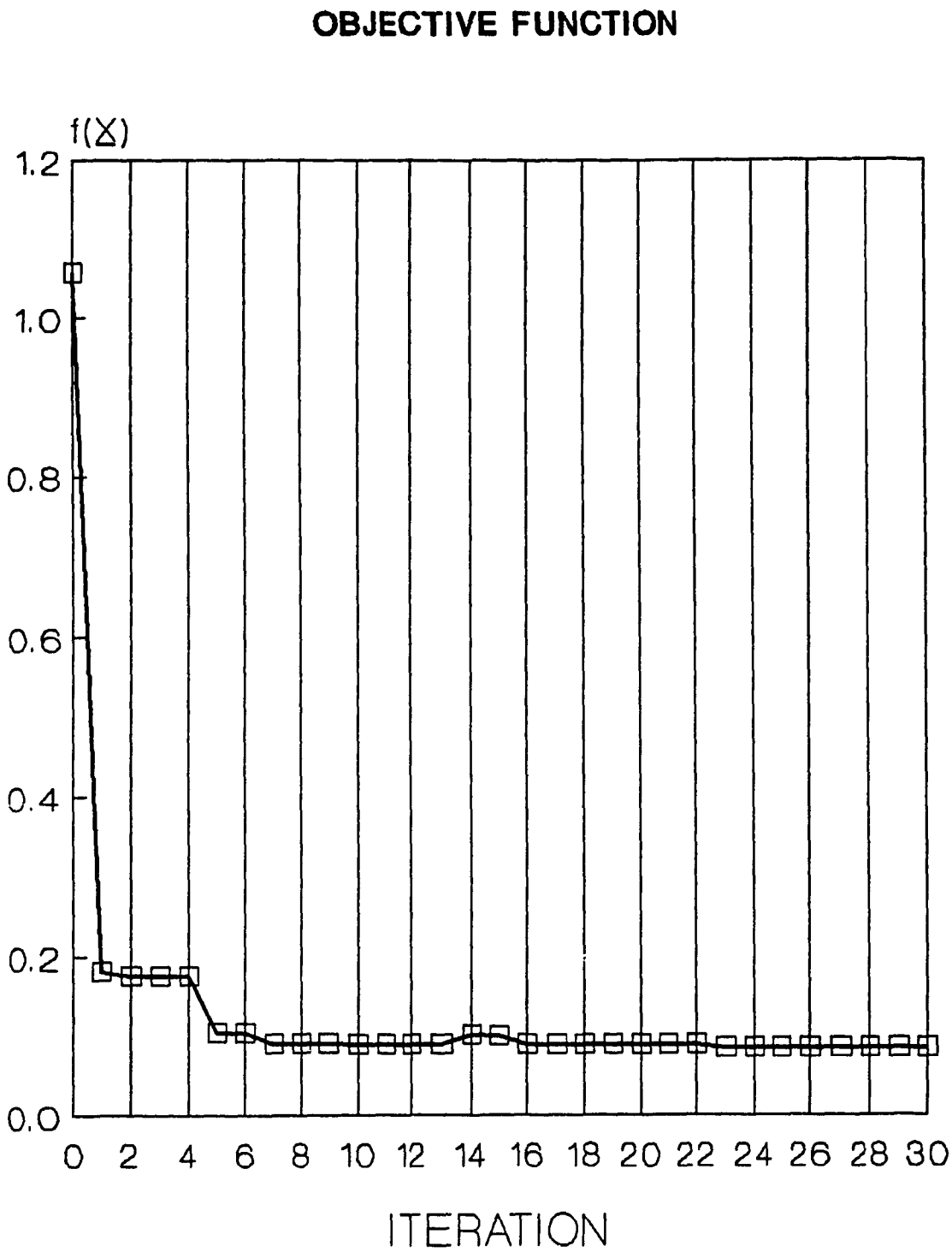

Fig. 10.9 Objective function vs number of iterations

was carried out in a similar way for the remaining two parameters. The effect of these parameters on the objective function was not as strong. This was due to the close relation of these parameters to their respective proportional gains which had already been optimized.

To complete the first optimization cycle, in all, the quadratic interpolation of the objective function was performed 13 times. In the second cycle, the parameters did not change much and no significant improvement of the objective function was noted. Thus, the optimization procedure terminated with the completion of the second cycle. The total computing time was 3 hrs, corresponding to 30 objective function evaluations (simulation runs).

The effect of each parameter about the optimum point is shown in Fig. 10.10 and Fig. 10.11. The objective function is increased abruptly when the constraint is violated. For the particular step size combination used, the proportional and derivative gains of the by-pass valve controller displayed higher selectivity as compared to the metering valve gains. However, the increased sensitivity to these parameters may not always be desired and ways to lower it, such as reducing the flow area gain of the valve or the actuator step size, could be used. A comparison of the optimum response to that of the open loop, with instant actuation of the metering valve, Fig. 10.12, clearly demonstrates the advantage of the two-actuator electronic

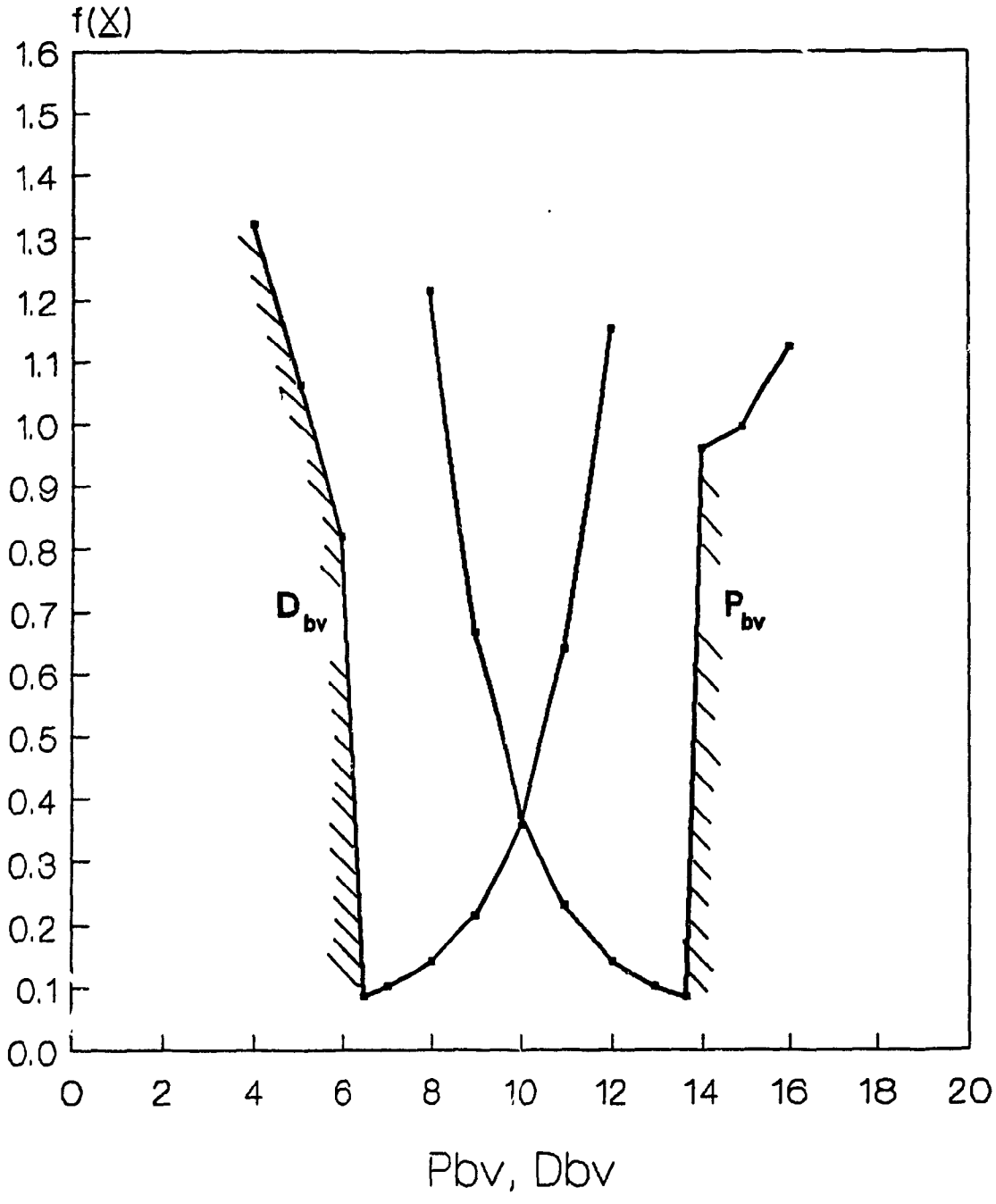

Fig. 10.10 Objective function vs by-pass valve controller parameters

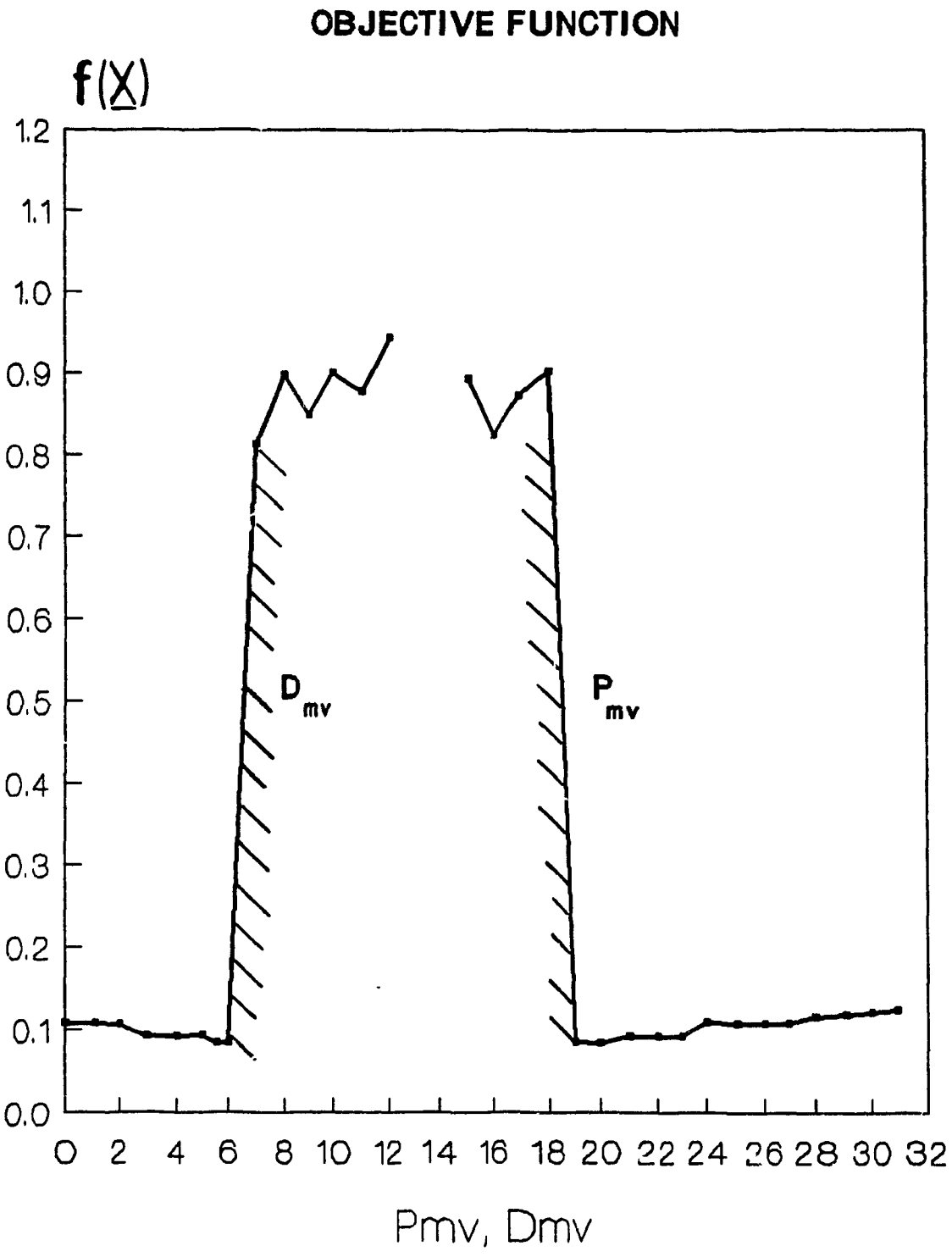

Fig. 10.11 Objective function vs metering valve controller parameters

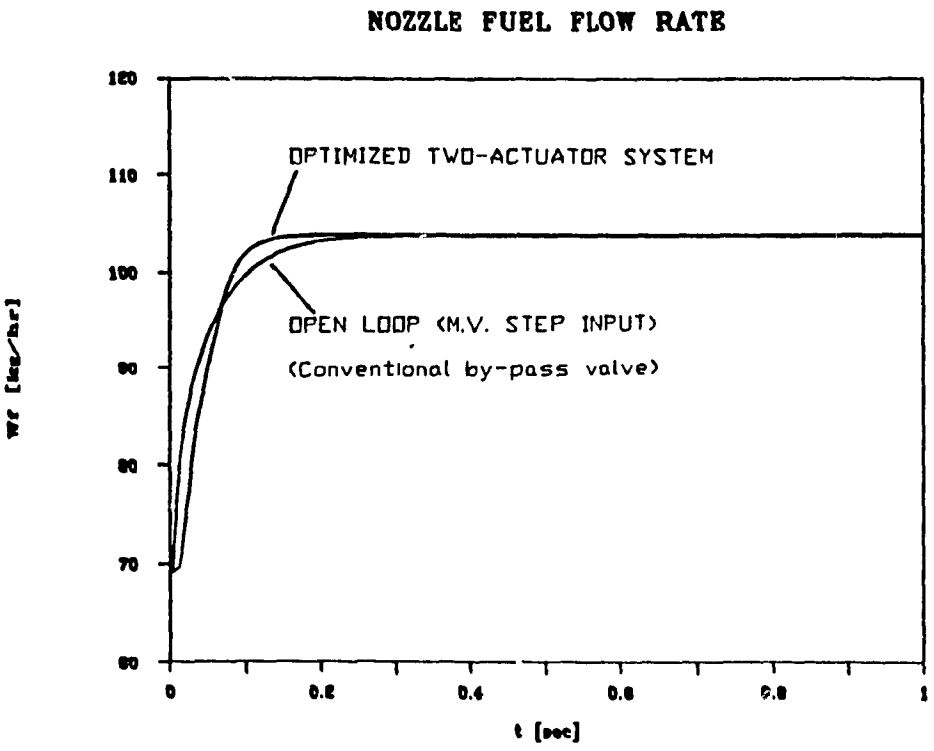

Fig. 10.12 Metered fuel flow response of optimized unit

fuel control unit.

The optimization process was repeated for various step sizes of the two actuators. To speed-up convergence, the initial guess of the controller parameters was based on intuition and proper interpretation of the results from the previous optimization. Basically, the controller proportional gain was adjusted to account for the change in actuator step size. The optimum objective function versus the step size of the two actuators is shown in Fig. 10.13.

When the actuator step size of the metering valve was very small, 0.00625 mm, and the by-pass valve step size was

large, 0.0375 mm, the gain of the by-pass valve controller had to be low to avoid overshoots and severe "hunting". The metering valve, on the other hand, because of its small step size, was unable to speed-up the response. As a result, the optimum objective function was quite high. When the by-pass valve step size was reduced, the performance of the system improved significantly. However, when the by-pass valve step size was reduced further, the valve was unable to react fast and the performance dropped slightly. But, when the step size of the metering valve was increased, the performance was improved again. The best operation occurred with a by-pass step size between 0.0125 mm and 0.025 mm and a metering valve step size equal to 0.00625. However, some additional criteria should be established before selecting the optimum.

The system response is very sensitive when large step size of the by-pass valve actuator is used, (see Fig. 10.10). A small deviation in the valve controller gains would result in poor performance. Also, for fuel flow demands other than the one used in the optimization, the system response would not be the best. To correct this, sensitivity constraints were applied. This eliminated from consideration all by-pass valve actuator step sizes greater than 0.02 mm. The choice of the optimum from what was left became easier when the best off-design performance was considered. The objective function was evaluated at three

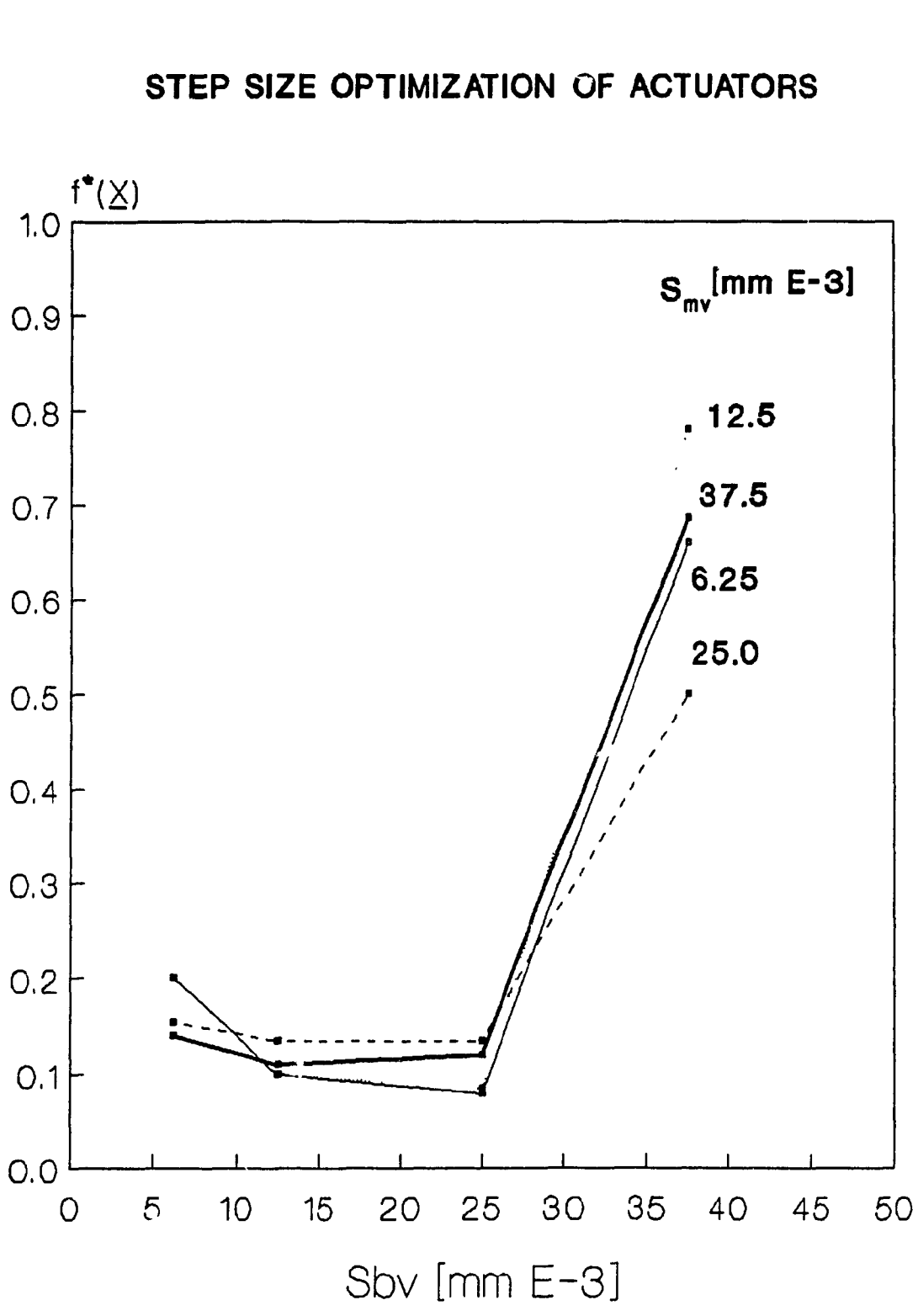

Fig. 10.13 Optimization of step size

different fuel flow demands; at optimum, at a higher and then at a lower than optimum. The controller gains were kept constant and the cumulative objective function was evaluated from the three runs. Results are shown in Fig. 10.14. The best performance was obtained when the step size of the by-pass valve actuator was 0.00625 mm. This implied that manufacturing limitations of the digital actuator (62), (63) determine the lower limit for the step size. It is possible to "step" the actuator at fractions of the full step (64), (65), (66). This, however, would involve more complex actuator driver design, the size and cost of which would make its use for this application unacceptable.

For the by-pass valve actuator size selected above, the cumulative objective function was plotted as a function of metering valve step size, Fig. 10.15. The best performance was obtained for a step size equal to 0.0375 mm. At lower step size, the metering valve was too slow to react to the fuel flow demand and at higher step size, the steady state fuel flow accuracy dropped.

Figure 10.16 and Fig. 10.17 show the response of the fuel control unit for the three different fuel flow demands with the optimum actuator step sizes as suggested by Fig. 10.12 and Fig.10.15 respectively. When the sensitivity limitation was not applied, Fig 10.16, severe hunting resulted at low fuel flow demands and excessive overshoots at high fuel flow demands. Also, at high flows, the

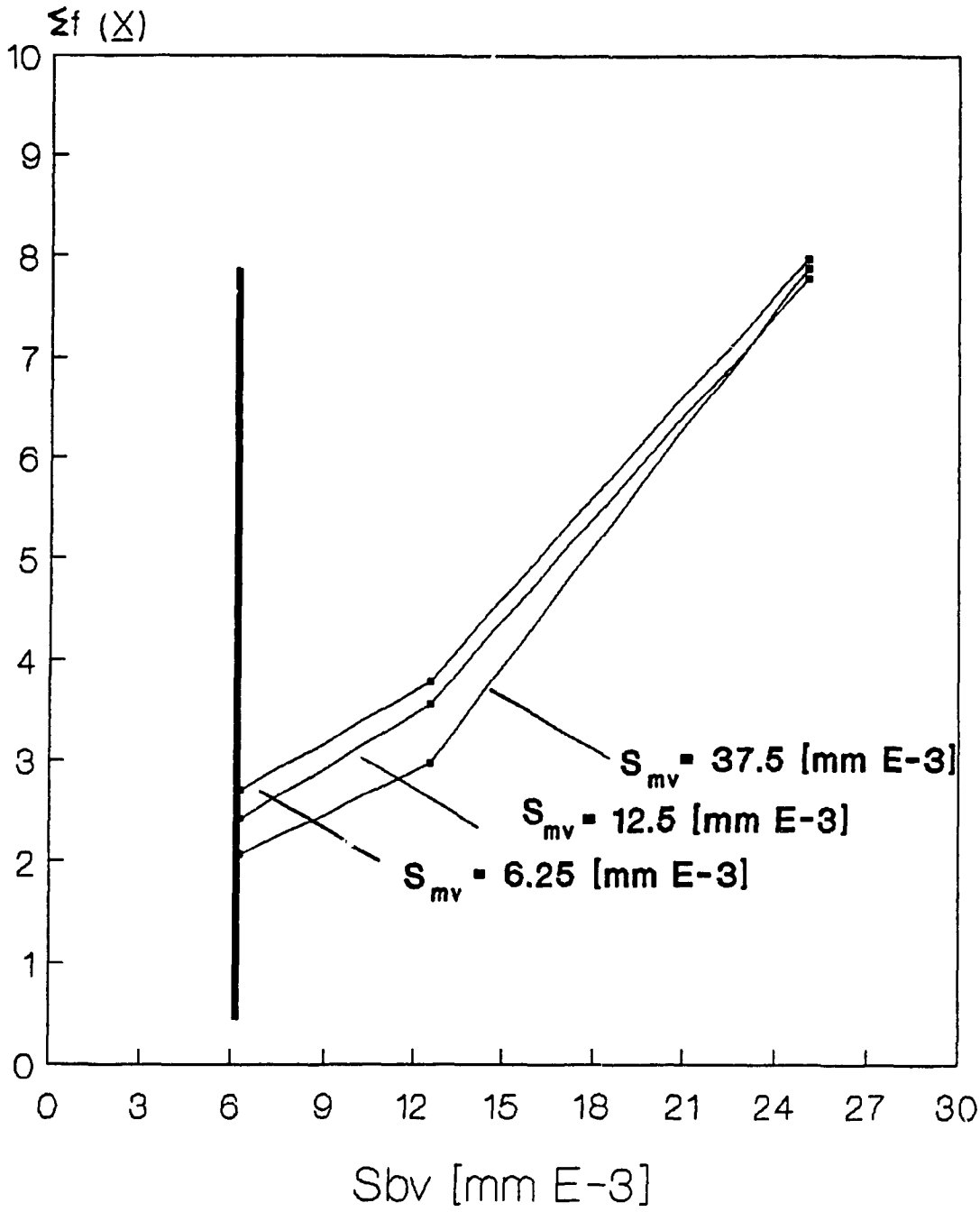

Fig. 10.14 Cumulative objective function vs step size of actuators

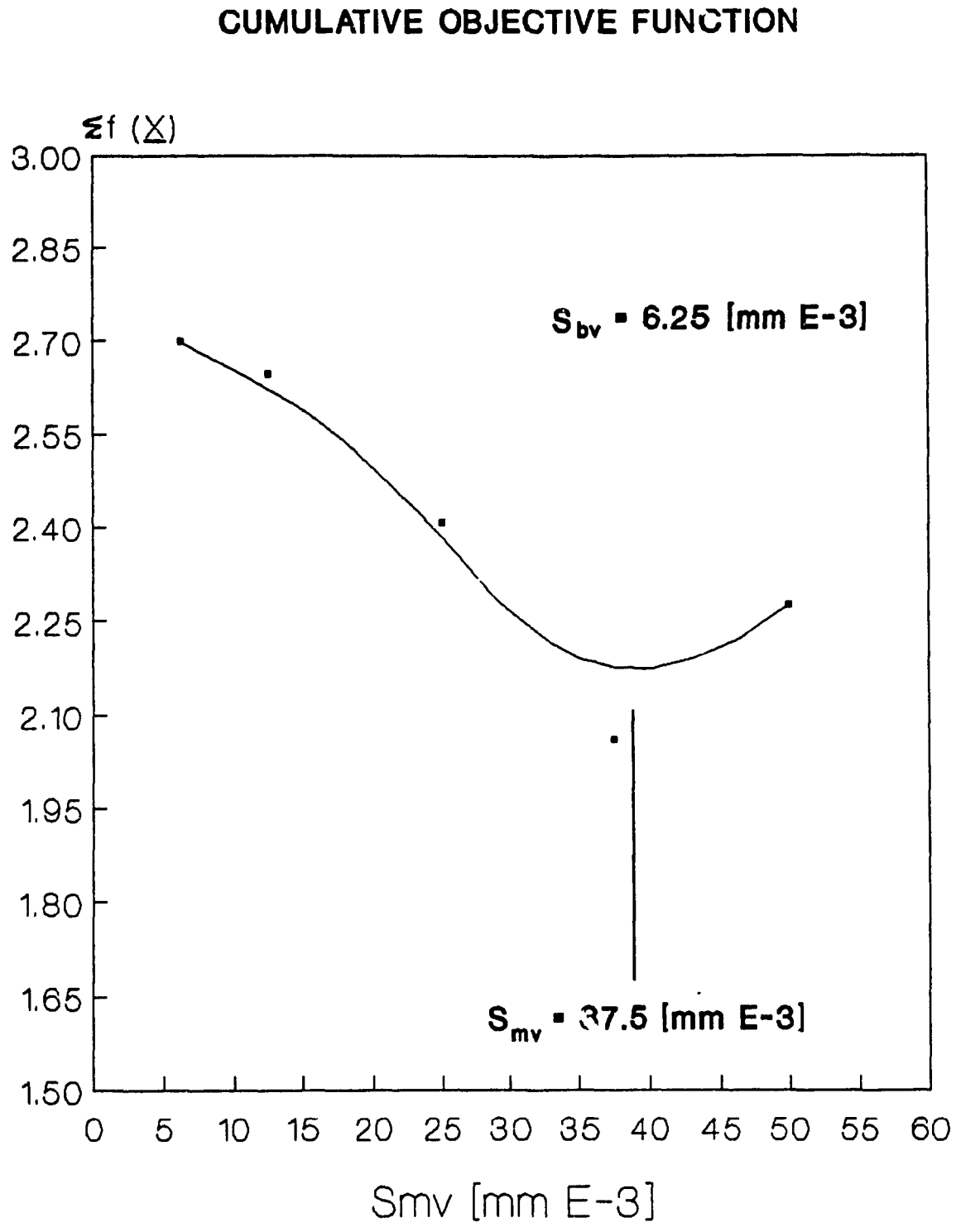

Fig. 10.15 Cumulative objective function vs step size of metering valve actuator

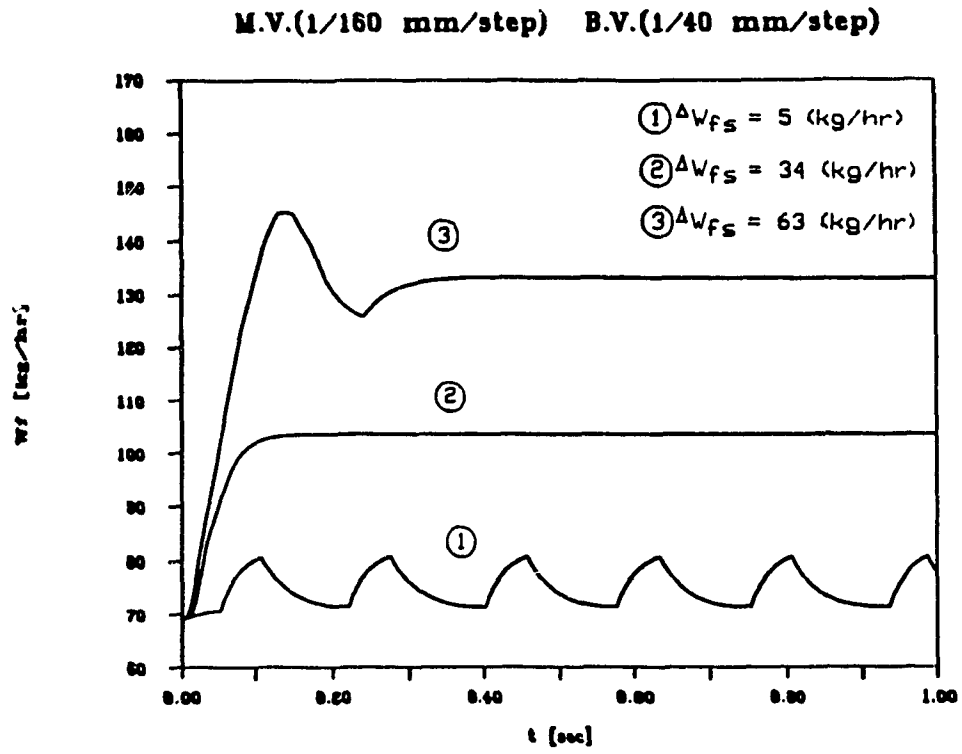

Fig. 10.16 Metered fuel flow response

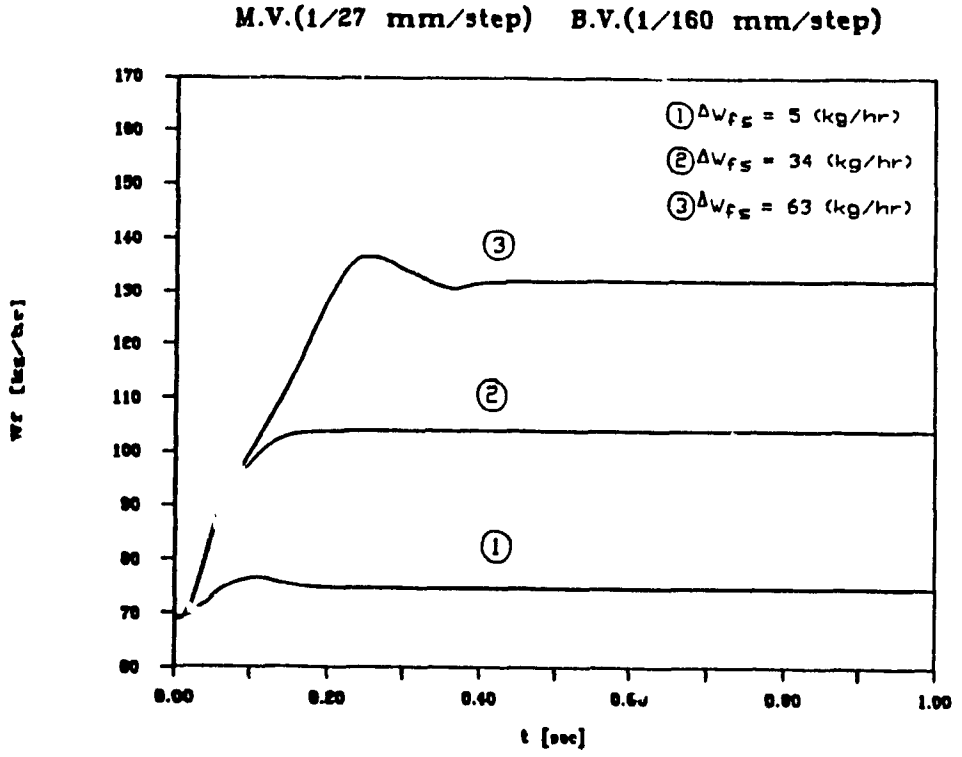

Fig. 10.17 Metered fuel flow with optimum actuator step sizes

differential pressure was quite large, Fig. 10.18. This would require higher linear force from the actuator in order to balance the pressure forces on the valve and ensure proper operation. As a result, a larger actuator would be needed.

When the optimum actuator step sizes, as shown in Fig. 10.15, were used, the rise time of the response was somehow longer, Fig. 10.17. However, there was no "hunting" and the system performed better at low and also at high fuel flows. Figure 10.19 shows results of the motion of the two valves and of the differential pressure response. The metering valve stroke was larger as compared with that in Fig. 10.18, but still within the limits (x_{max}= 3 mm). The differential pressure was kept close to its nominal value and as a result, the potential problem with excessive valve unbalanced pressure forces was avoided. The movement of the by-pass valve was smoother and the excessive fuel flow pulsations were eliminated.

10.6 Summary

A new concept of a fuel control unit involving the interaction of two digital actuators, was introduced and investigated. The mathematical model of the electronic fuel control unit was used to simulate the dynamic response of three different control schemes for abrupt fuel flow

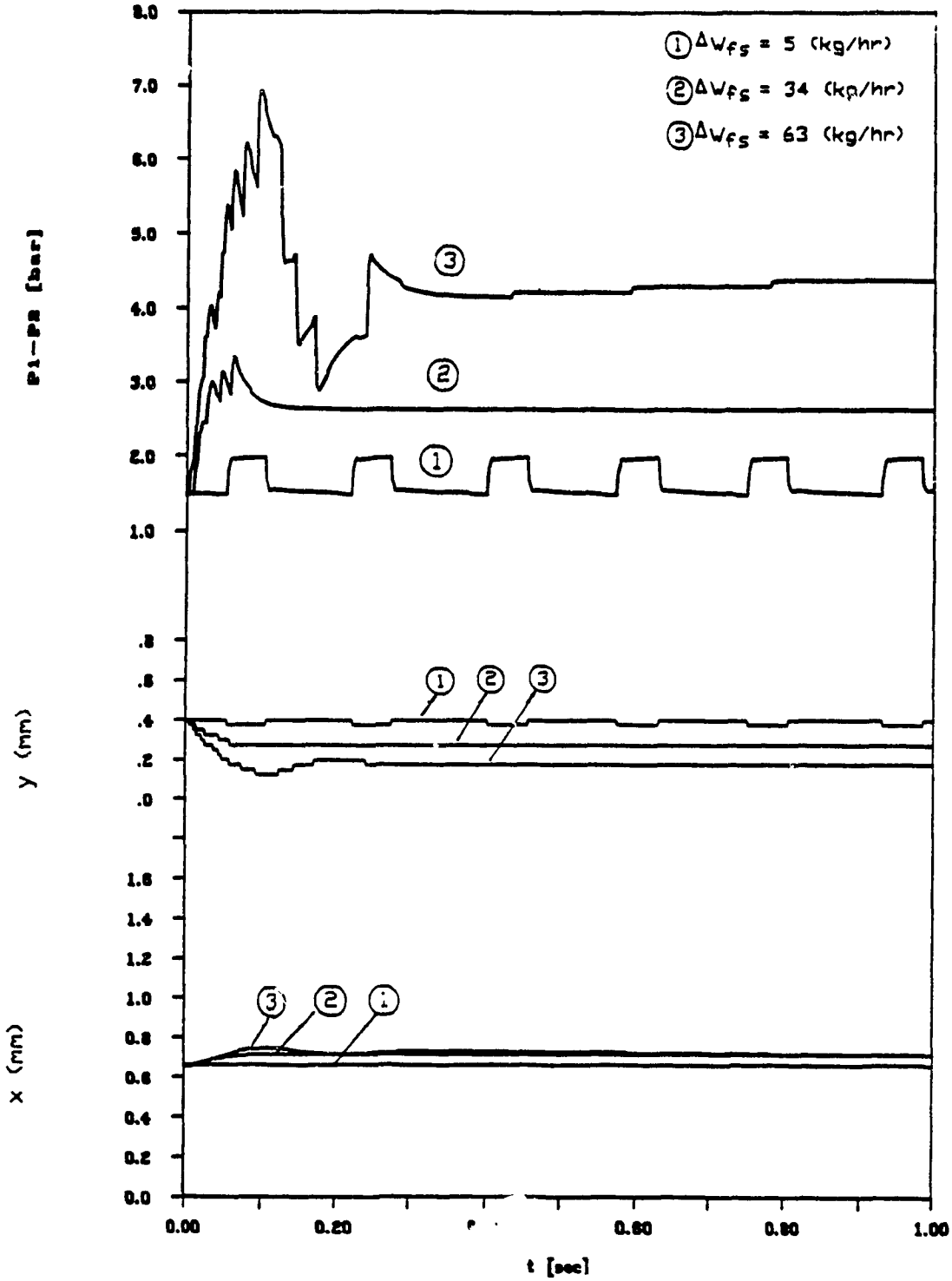

Fig. 10.18 Transient response of differential pressure, by-pass valve and metering valve

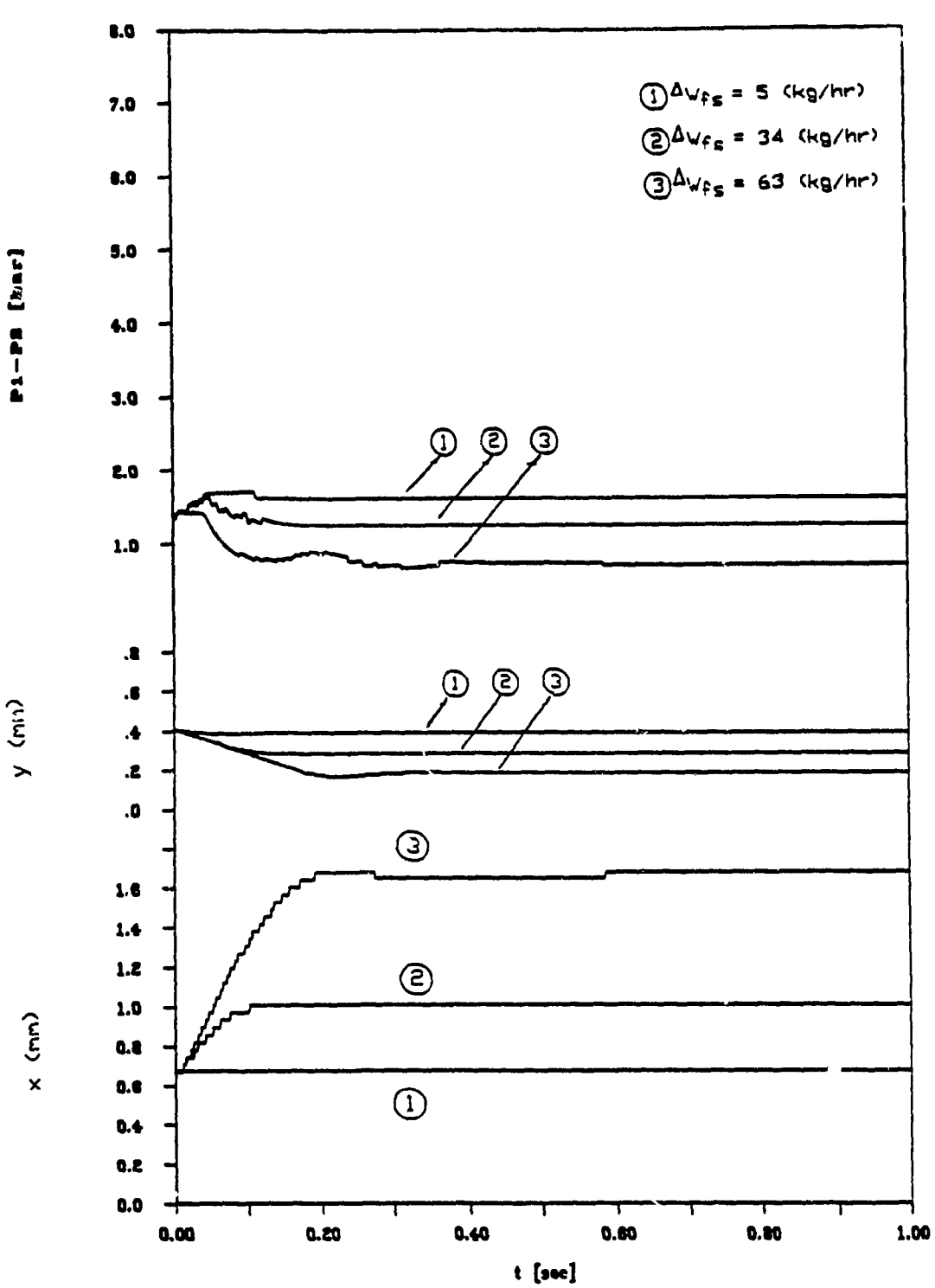

Fig. 10.19 Transient response of differential pressure, by-pass valve and metering valve for optimum settings

demands. Advantages, disadvantages and some unique features of these control schemes were noted. An optimization method was applied to find the optimum controller gains and to select the best step size combination for the two actuators operating the valves of the unit.

CHAPTER 11

CONCLUSIONS AND RECOMMENDATIONS

In traditional hydromechanical fuel control units, either the differential pressure across a metering valve or the flow area of the metering valve are used to meter fuel to the gas turbine engine. In most applications, the flow area is the principal control variable while the differential pressure is kept constant. This simplifies the control and reduces the computational requirements.

In this thesis, an electronic fuel control unit employing linear digital actuators was proposed and investigated. Two configurations of the unit, which was based on the conventional Bendix DP-F2 fuel metering system, were studied. In the first, one actuator was used to change the metering flow area while the differential pressure was kept constant using a by-pass valve. In the second, another actuator was added to provide electronic control for the differential pressure. Mathematical models of the electronic units were developed and used to predict the dynamic and steady state response under different control strategies. Both units demonstrated the ability to meter the fuel flow throughout the operating region.

Non-conventional controllers, such as Proportional Derivative with Smith Predictor and the Dahlin controller,

were derived and tested. These controllers offered compensation for the dead time in the flow processes and improved the dynamic response by making the control of the derivative term more effective. An experimental self-tuning method for the digital controller was formulated and tested. The method used the steepest descent optimization technique and found the optimum controller gains in a few iterations. This method could be used to tune experimentally a wide range of digital controllers, without the need of developing a mathematical model for the controlled process. The method could be used further to optimize the control when an engine is added to the loop.

Problems were encountered because of the discrete motion of the valves, when a large actuator step size was used. Large increments of the fuel flow resulted during acceleration. Also, severe "hunting" occurred at steady state. The step size of the actuator had to be optimized to improve the flow accuracy problem without unduly retarding the transient response.

The two-actuator electronic configuration showed greater flexibility and accuracy. The unit achieved fuel flow demands significantly faster than the conventional fuel control unit and the one-actuator electronic unit. The faster response was made possible by changing the differential pressure and the metering flow area simultaneously. The best interaction of the two actuators,

to achieve the fastest response possible without excessive overshoots or undershoots, was achieved by optimizing a "penalized" ITAE transient response performance index.

The two actuator electronic unit offerred also fuel flow metering redundancy. In the event one actuator or its electronic control would fail, the other actuator would be able to perform the fuel metering and provide the aircraft with the capability to "get-home".

To evaluate the performance of the electronic fuel control unit when mounted on an engine, a real time dynamic engine simulator, using a simplified engine model, could be introduced using a faster microcomputer or an analog computer. A full evaluation and optimization of the electronic fuel control unit would then be possible on the test bench. This would reduce the time and cost involved for engine testing. For more detailed engine models, which would not allow real time interaction, the model of the electronic fuel control unit could be linked to the engine model and the complete system could be studied on a digital computer.

In summary, this thesis has introduced new possibilities in the electronic fuel control for small gas turbine engines. New control schemes were developed. A controller tuning method for automated test bench calibration for electronic fuel control units, was formulated and tested. Finally, a two-actuator system was

proposed and optimized. This unit improved the fuel scheduling and provided fuel control redundancy. This last item requires further investigation to solve problems related to practical implementation. Also, the possibility of performing similar control with different types of actuators, such as torque motors or proportional solenoids, should be studied.

CHAPTER 12

FUTURE WORK

In this thesis the feasibility of digital control using an incremental actuator to operate the metering valve of an existing hydromechanical fuel control unit was established. Also, the potential of a unit employing two actuators was demonstrated. This is a first step towards the development of a certifiable full authority electronic fuel control unit.

A variety of problems arise when the fuel control unit unit is linked to a gas turbine engine. These problems are mainly due to the coupling which exists between the engine and the fuel controller. Stability of the complete system is related to the dynamics of the fuel control unit and should be thoroughly investigated. This is especially important in the case of small gas turbine engines, used in Remotely Piloted Vehicles or Auxiliary Power Units, which have small time constants.

To carry on such an investigation, an engine model is needed. To facilitate the analysis, a quasi-linear model can be derived (8), (67). This basically involves the derivation of the transfer function of the engine speed to the excess of fuel supplied. Engine parameters such as gain and time constant should be treated as functions of the

operating point and should be scheduled throughout the operating region. Stability should be investigated with regard to the fuel control unit controller parameters and the sampling time interval of the signals used for control. It is not likely that such a study would be possible in a closed form fashion. A computer would have to be used in order to graphically establish the limits of stability on the z-plane. Techniques such as the "describing function" or "phase plots", used in the analysis of nonlinear systems could also be employed to establish stability limits.

With regard to the structure of the digital control used in this thesis it should be pointed out that there are other possibilities which employ concepts from the modern control theory field. The usefulness of adaptive control (68) in improving the system response should be investigated. Reliability concerns and physical constraints arising from the implementation of such concepts should be carefully considered.

REFERENCES

1. Kuhlberg, J. F., Newirth, M. J., Kniat, J., and Zimmerman, W., H.,"Integration of the PW2037 Engine Electronic Control System in the Boeing 757 Airplane," SAE paper, Nr. 841554.

2. Frew, J. S. and Keck, C. F., "Electronic Control System for a Modern Turboprop Engine", SAE Paper 810620, 1981.

3. Glockler, O., Knapp, H. and Manger, H., "Present Status and Future Development of Gasoline Fuel Injection Systems for Passenger Cars", SAE Paper 800467.

4. Briggs, R. W. and Opdenbrouw, W. F., "Introduction Into Commercial Service for Electronic Controls Used on Large Turbofan Engines", SAE Paper, Nr. 841507, 1984.

5. Hawes, D. J., "Electronic Fuel Controls - Who Needs Them?", SAE Paper, Nr. 810619, 1981.

6. Peck, W. C., "Microelectronics in Fuel Controls", SAE Paper 650529, May, 1965.

7. Ronald, F., "Digital Techniques Applied to the Control of Gas Turbine Engines", SAE Paper 650528, 1965.

8. Ferre, G. E., and Lenkaitis, D. C., "Gas Turbine Engine Analog Simulation for Acceleration Sensing Fuel Control Studies", Gas Turbine Fuel Controls Analysis and Design, SAE Progress in Technology, Volume 9, PP. 26-34, 1965.

9. Keck, M. F., Fredlake, J. J. and Schwent G. V., "A Control Concept Combining the Best of the Current Hydromechanical and Electronic Technologies", SAE Paper 740380, April, 1974.

10. Fredlake, J. J., and Adams, M. R., "Electronic Fuel Controls for Executive Jet Aircraft", SAE Paper 831478, 1983.

11. Porter, R. D., "The Influence of Microcomputer Technology on Propulsion Management System Design", SAE SP, 1975.

12. Kniat, J., Bluish, J. A., "An Application of Redundancy in Digital Electronic Engine Control", SAE Paper 801200, 1980.

13. Evans, R. M., and Cusson, C., "Development of a Full Authority Digital Fuel Control for a Gas Turbine Engine Using a Hybrid Computer System as a Design Aid", Summer Computer Simulation Conference, Newport Beach, July 1978.

14. Janik, S., "Full Authority Digital Control for a Small Turbine Helicopter Engine", SAE Paper 831476, 1983.

15. Hawes, D., and Evans, R., "NDEC - A Control Concept for Helicopter Gas Turbines", 36th Annual Forum of the American Helicopter Society, Washington D.C,, May, 1980.

16. Evans, R. M., "Hybrid Computer Simulation in Digital Fuel Control Design", SAE Paper 821373, Aerospace Congress & Exposition, Anaheim, California, October 25-28, 1982.

17. Caine, D. C., and Rumford, K. J., "Electronic Control for Helicopter Engines", Proceedings of the American Helicopter Society, 34th Annual Forum, May, 1978.

18. Caine, D.A., and Janik, S., "Digital Control for Helicopter Powerplants", Journal of the American Helicopter Society, October, 1980.

19. Vizzini, R. W., Lenox, T. G. and Miller, R. J., "Full Authority Electronic Control Turbofan Engine Demonstration", SAE Paper 801199, October, 1980.

20. Vizzini, R. W., and Toot, P. D., "Full Authority Digital Electronic Control Application to a Variable Cycle Engine", SAE Paper 801203, 1980.

21. Linebrink, K. L., and Vizzini, R. W., "Full Authority Digital Electronic Control (FADEC) - Augmented Fighter Engine Demonstration", SAE Paper 821371, Aerospace Congress & Exposition, Anaheim, California, October, 1982.

22. McGlone, M. E., Miller, R. J., Davies, W. J. and Adams, P. T., "Full Authority Fault Tolerant Electronic Engine Control Systems for Advanced High Performance Engines (FAFTEEC)", SAE Paper 821398, October, 1982.

23. Newirth, D. M., and Bosco, C. J., "Flight Test Reliability Demonstration of Electronic Engine Controls", SAE Paper 801201, Aerospace Congress & Exposition, Los Angeles Convention Center, October, 1980.

24. Kast, H. B., "Backup Control for Variable Cycle Engine", SAE Paper 831475, 1983.

25. Mosca, V. G., "Extraordinary Benefits of Combined Environmental Reliability Testing (CERT) On Digital Electronic Engine Controls" SAE Paper 831480, 1983.

26. Zuliani, F. C. and Kline, G. N., "Microcomputer Brings Digital Power to the Small Gas Turbine", SAE Paper 821402, October, 1982.

27. Myers L. P., and Surcham, F. W, Jr., "Propulsion Control Experience Used in the Highly Integrated Digital Electronic Control (HIDEC) Program", SAE Paper 841553, 1984.

28. Digital Electronic Engine Controls Examined, Aerospace Engineering, pp.35-38, February, 1985.

29. Bayati, J. E., "The HiMAT RPRV Propulsion Control System", SAE Paper 760887, Aerospace Engineering and Manufacturing Meeting, San Diego, November 29 - December 2, 1976.

30. Georgantas, A.I., Krepec, T., and Cheng, R.M.H., "Investigations on Electronically Actuated Metering

Valve in a Fuel Control Unit for Small Gas Turbine Engines," Proceedings of the 1987 ASME International Computers in Engineering Conference and Exhibition, ASME, New York, August 9-13, 1987.

31. Georgantas, A.I., Krepec, T., and Cheng, R.M.H., "Interaction of Two Electronic Actuators Employed in a Fuel Control Unit for Small Gas Turbine Engines," Proceedings of the 1988 ASME International Computers in Engineering Conference and Exhibition, ASME, San Francisco, August 1-4, 1988.

32. Carrese, G., Georgantas A. I., and Krepec, T., "Multivariable Optimization Scheme for Tuning the Controller of an Electronic Fuel Control Unit for Small Gas Turbine Engines", Proceedings of the 1989 ASME International Computers in Engineering Conference and Exhibition, ASME, Anaheim, July 30 - August 3, 1989.

33. Georgantas, A. I., Carrese, G., and Krepec, T., "Designing and Tuning the Digital Controller of an Electronic Fuel Control Unit for Small Gas Turbine Engines", SAE Paper 892255, presented in the Aerospace Technology Conference and Exposition, Anaheim, California, September 25-28, 1989. Accepted for

publication in the 1989 SAE Tansactions.

34. Cropper, G. D., "Electronic Fuel Controls for Missile and RPV Gas Turbines", SAE Paper 751061, National Aerospace Engineering and Manufacturing Meeting, Culver City, Los Angeles, November 17-20, 1975.

35. Georgantas, A. I., Krepec, M. and Krepec, K., "Diesel Injection Pump Conversion for Alternate Applications", Paper presented at the Tenth Canadian Congress of Applied Mechanics in London, Ontario on June 2-7, 1985.

36. Georgantas, A. I., Krepec, M., and Krepec, T., "New Possibilities of Fuel Flow Modulation in Small Gas Turbine Engines", Paper presented at the Tenth Canadian Congress of Applied Mechanics in London Ontario on June 2-7, 1985.

37. Krepec, T., Krepec, M. and Georgantas, A. I., "Low Cost Electronic Fuel Control Concept for Small Gas Turbine Engines", Paper presented at the 7-th World Congress of IFToMM in Seville on September 17-22, 1987.

38. Georgantas, A.I., Krepec, T., and Cheng, R.M.H., "Low Cost Electronic Fuel Control Unit for Small Gas

Turbine Engines of Remotely Piloted Vehicles," Progress Report N° 1, CIC-0014, December 1987, Centre for Industrial Control, Concordia University, Montreal, Canada.

39. Georgantas, A.I., Krepec, T., and Cheng, R.M.H., "Low Cost Electronic Fuel Control Unit for Small Gas Turbine Engines of Remotely Piloted Vehicles," Progress Report N° 2, CIC-0015, May 1988, Centre for Industrial Control, Concordia University, Montreal, Canada.

40. Georgantas, A.I., Carrese, G., Krepec, T., and Cheng, R.M.H., "Low Cost Electronic Fuel Control Unit for Small Gas Turbine Engines of Remotely Piloted Vehicles," Progress Report N° 3, CIC-0016, December 1988, Centre for Industrial Control, Concordia University, Montreal, Canada.

41. Georgantas, A.I., Carrese, G., Krepec, T., Cheng, R.M.H., Spanoudakis, P., and Labbate, A., "Low Cost Electronic Fuel Control Unit for Small Gas Turbine Engines of Remotely Piloted Vehicles," Progress Report N°1, CIC-0014, July 1989, Centre for Industrial Control, Concordia University, Montreal, Canada.

42. Krepec. T., Georgantas, A. I., Taylor, M., and To, C. H., "New Family of Low Cost Electronic Fuel Control Units for Small Gas Turbine Engines", SAE Paper, Aerospace Technology Conference and Exposition, Dayton, Ohio, April, 1990.

43. Carrese, G., Krepec. T., and To, C. H., "Simulation, Testing and Optimization of a New Low Cost Electronic Fuel Control Unit for Small Gas Turbine Engines", SAE Paper, Aerospace Technology Conference and Exposition, Dayton, Ohio, April, 1990.

44. Georgantas, A. I., Krepec, T., Carrese, "Computer Aided Development of a Simple Electronic Fuel Control Unit for Remotely Piloted Flying Vehicles", International Computers in Engineering Conference and Exhibition, ASME, Boston, August 1990.

45. Carrese, G., Krepec, T., Georgantas, A. I., "Throttle Body Fuel Injection - A Different Approach", ISAATA, Florence, Italy, May 1990.

46. Swonger, K. B., Huffman, M. F., "Low Cost Control System for Expendable Turbine Engines", AIAA/ASME/SAE/ASEE 25th Joint Propulsion Conference, AIAA-89-2586, Monterey, CA, July 10-12, 1989.

47. Fuel Metering Valve, TECH DATA, South Bend Controls Inc., Bulletin PV-217, 1988.

48. Bi-Directional Driver, TECH DATA, South Bend Controls Inc., Bulletin PS-106, 1988.

49. MacIsaac, B.D., Gagne, R.E., and Inrig, C., "Analog and Digital Computer Models of the Metering Section of a Gas Turbine Fuel Controller," LTR-AN-22, May 1975, National Research Council Canada, Ottawa, Canada.

50. Treager, I. E., Aircraft Gas Turbine Engine Technology, Mc Graw-Hill Book Company, New York, pp.331, 1970.

51. Fuel Control System for PT6T-3 Twin Engine Installation, Operation and Service Manual, Bendix Aviation Electric Ltd.

52. McGregor, J. F., Taylor, P. A., and Wright, J. D., Advanced Process Control, McMaster University, Hamilton Ontario, May 1986.

53. Meyer, C. B. G., Wood, R. K., and Seborg, D. E., "Experimental Evaluation of Analytical and Smith Predictors for Distillation Column Control", AIChE

Journal, Vol. 25, No. 1, PP 24-32, January, 1979.

54. Doss, J. E., and Moore, C. F., "The Discrete Analytical Predictor - A Generalized Dead Time Compensation Technique", ISA Transactions, Vol. 20, No 4, 1982.

55. Corripio, A. B., Smith, C. L., and Murrill, P. W., "Evaluating Digital PI and PID Controller Performance", Instruments and Control Systems, pp. 55-57, July, 1973.

56. Dahlin, E.B., "Designing and Tuning Digital Controllers", Instrum. Control Systems, Vol. 4, p. 77, 1968.

57. Krivoshein, K. D., and Corripio, A. B., "A Study of Ringing and Dead Time Compensation in Dahlin's Digital Control Algorithm", ISA Transactions, Vol. 20, No. 4, 1982.

58. Mollenkamp, R. A., Smith, C. L., and Corripio, A. B., "Designing Digital Controllers for Fast Processes", Instruments and Control Systems, pp. 47-49, August 1973.

59. Cadzow, J.A., and Martens, H.R., "The Stepper Motor in Control Applications," Discrete-Time and Computer Control Systems, Prentice-Hall, Englewood Cliffs, New Jersey, 1970, pp. 365-367.

60. Rao, S. S., Optimization / Theory and Applications, Second Edition, Wiley Eastern Limited, New Delhi, India, 1984.

61. Fiacco, A. V., and McCormik, G. P., Nonlinear programming: Sequential unconstrained minimization techniques, Wiley, New York, 1968.

62. Digital Linear Actuators, Airpax Catalog, 1983.

63. Takashi, K., Stepping Motors and Their Microprocessor Controls, Clarendon Press, Oxford 1984.

64. Programmable Motion Control Seminar, Compumotor, Bulleting 8040-B1, Octomber, 1988.

65. Kuo, B. C., (Editor), Incremental Motion Control Systems and Devices: Proceedings: Fifteenth Annual Symposium, June, 1986.

66. Kompass, E. J., (Program Chairman), Proceedings of The

First Annual Motion Control Conference, Held as part of the Motion Control Conference & Expositionm, Boston, Massachusetts, April 11-13, 1989.

67. Saravanamuttoo, H.I.H. et al, Gas Turbine Performance and Design - Supplementary Course Notes, Carleton University, Ottawa, Canada, 1989.

68. Aström, K.J. and Wittenmark, Adaptive Control, Addison - Wesley, 1989.

69. Intel, "Military Products Handbook", Volume 1, 1989.

70. Intel, "EV80c196KB Microcontroller Evaluation Board", User's Manual, Release 001, February 20, 1989.

APPENDIX A

TECHNICAL DETAILS

AND

CALIBRATION CURVES

APPENDIX A

TECHNICAL DETAILS AND CALIBRATION CURVES

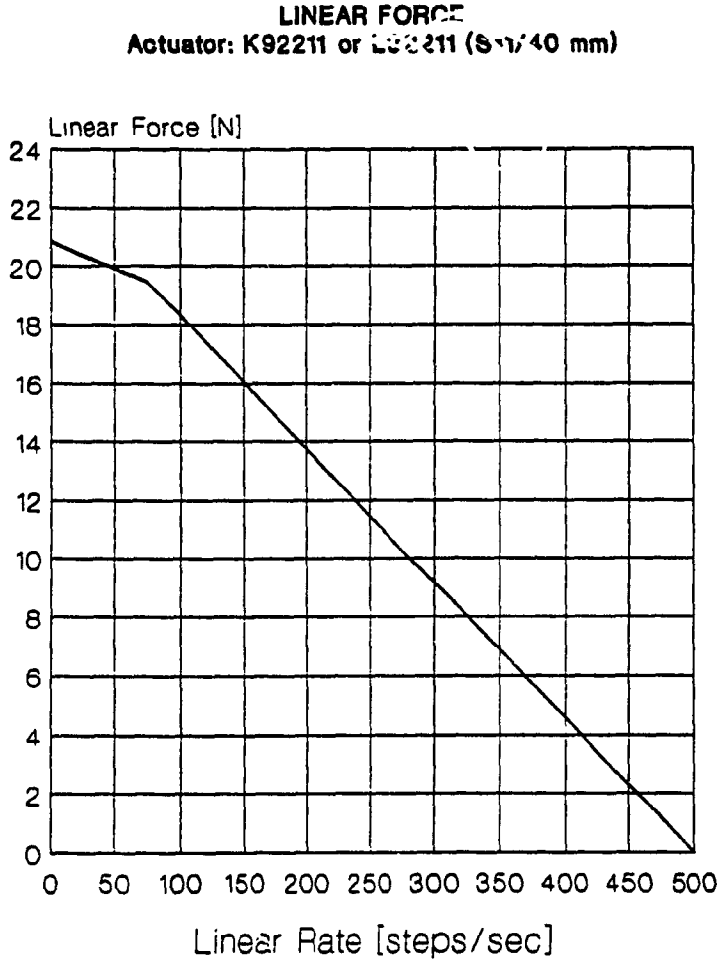

Fig. A.1 Linear force of the digital actuator as a function of stepping rate

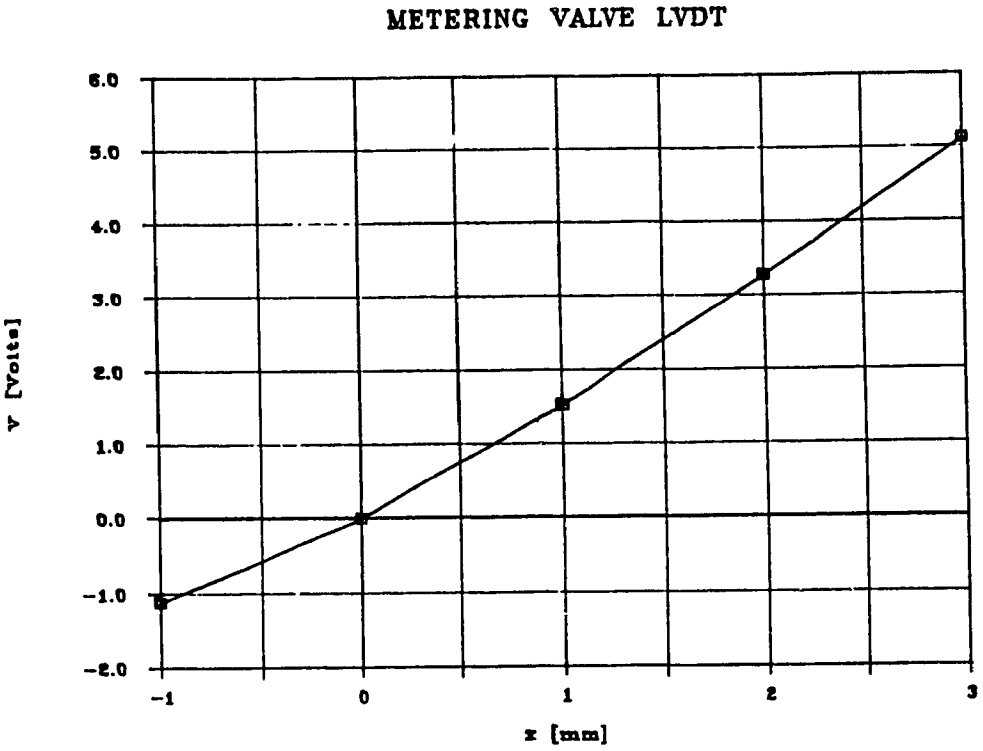

Fig. A.2 Calibration of metering valve LVDT

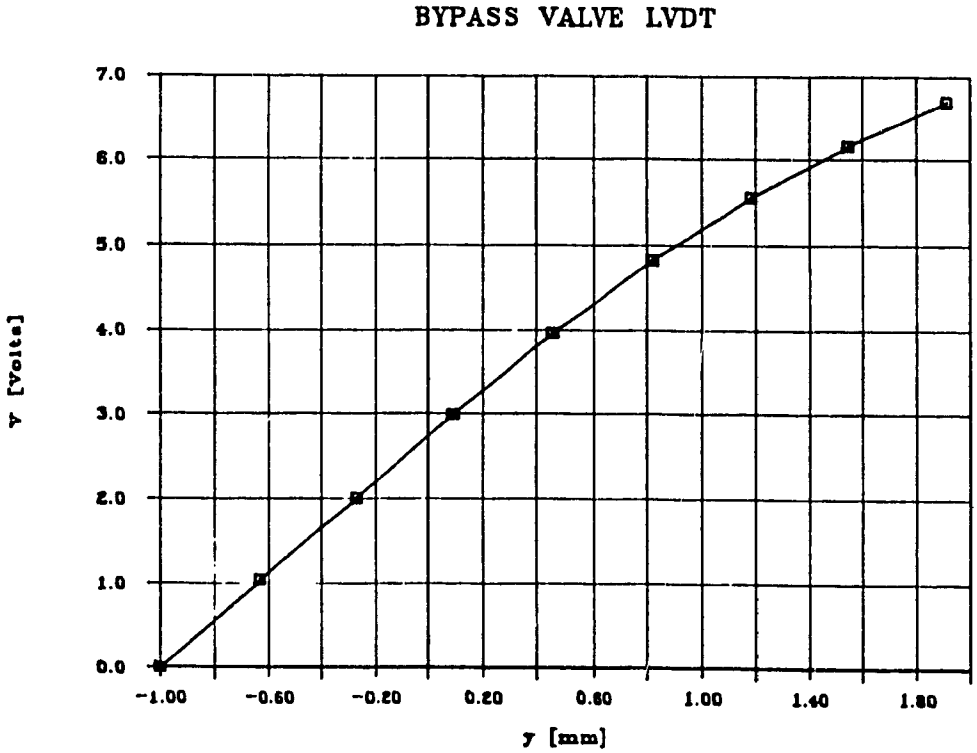

Fig. A.3 Calibration of by-pass valve LVDT

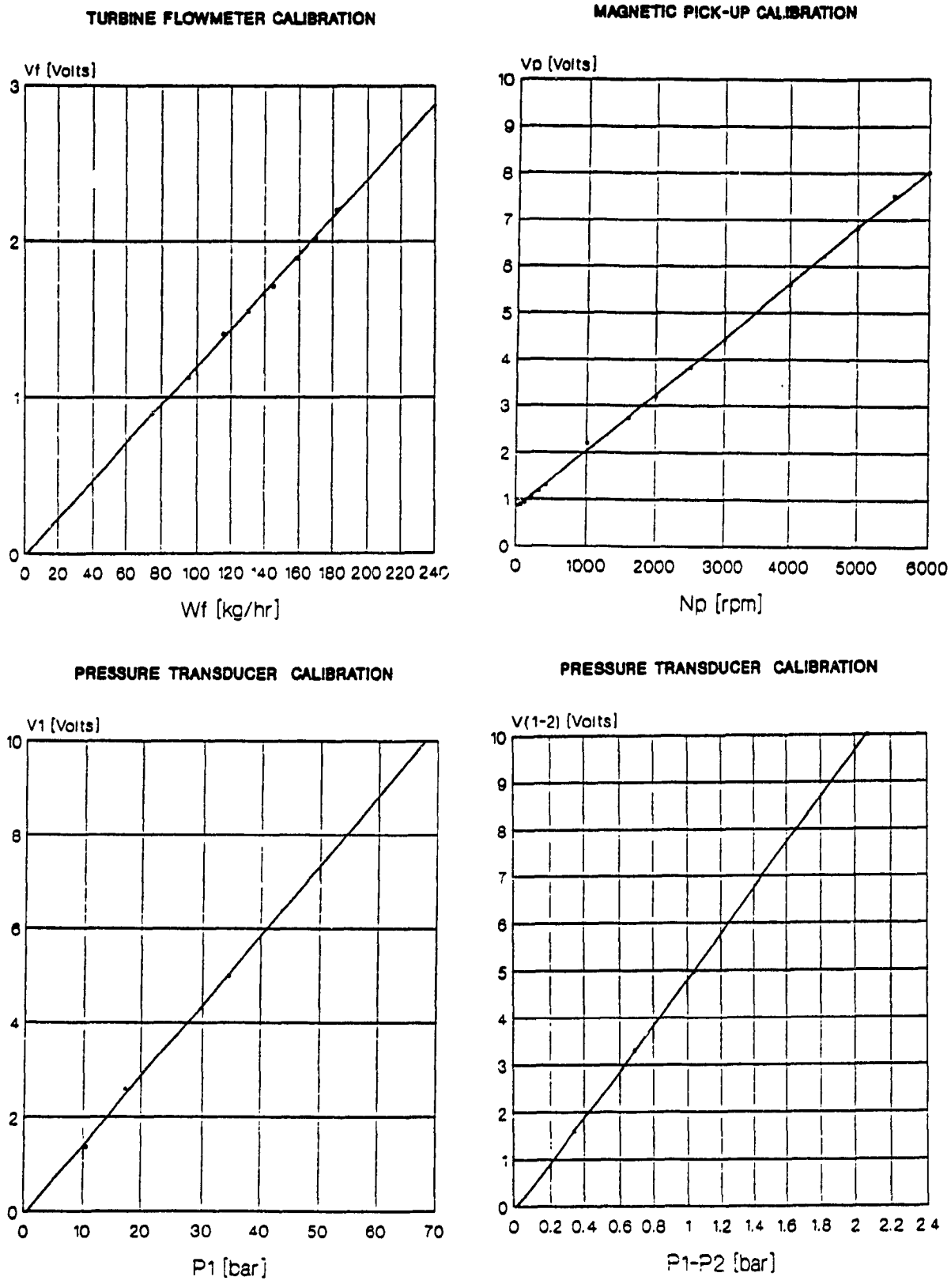

Fig. A.4 Calibration of turbine flowmeter, magnetic pick-up and pressure transducers

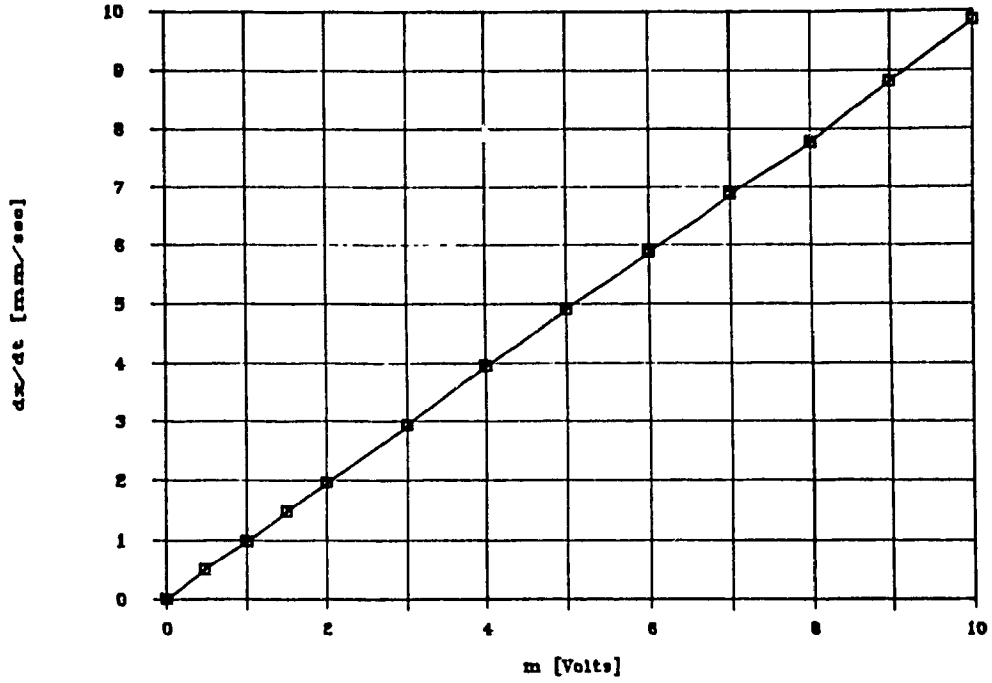

Fig. A.5 Metering valve velocity vs Controller output

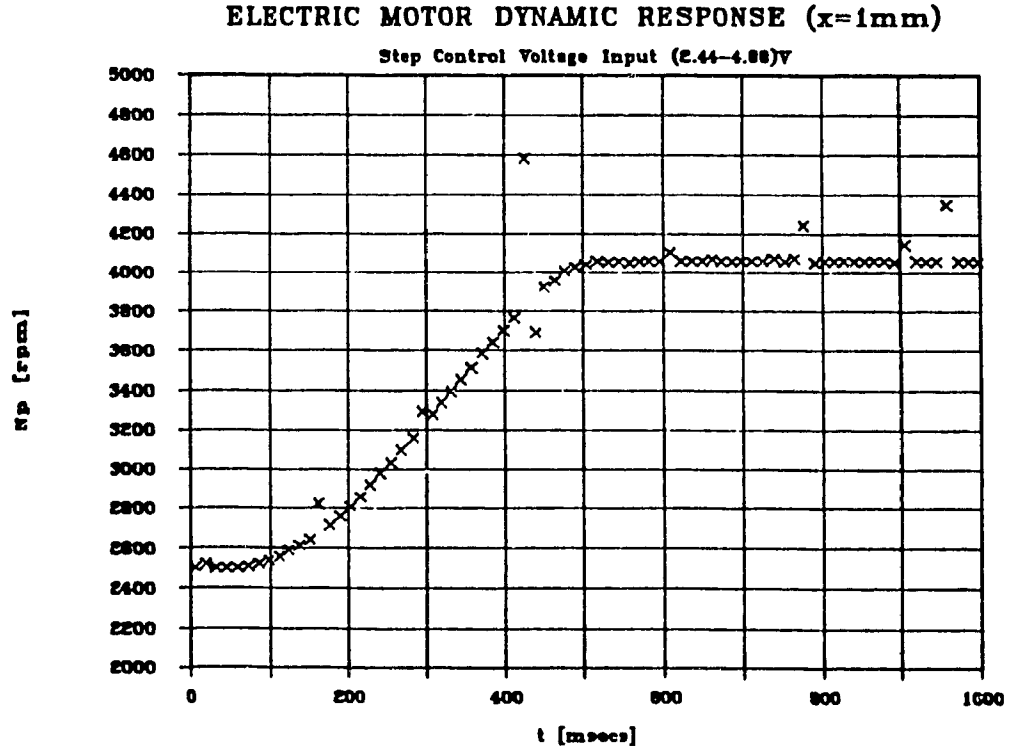

Fig. A.6 Dynamic response of electric motor driving the fuel control unit pump

APPENDIX B

DERIVATIONS RELATED TO SYSTEM MODELLING

APPENDIX B

DERIVATIONS RELATED TO SYSTEM MODELLING

B.1 Pump Fuel Flow Delivery

The pump delivery is a function of pump speed and the pressure difference across it. The pump characteristic is non-linear at low differential pressures. However, at higher pressures (>8.3 bar) the characteristic is fairly linear, Fig. B.1, and can be described by:

$$Q_p = C_1 N - C_2 \left(p_1 - p_0 \right) + C_3 \qquad (B.1)$$

where,

$$C_1 = 4.14 \times 10^{-8} \left(\frac{m^3}{sec.rpm} \right)$$

$$C_2 = 6.23 \times 10^{-12} \left(\frac{m^3}{N.sec} \right)$$

$$C_3 = - 2.38 \times 10^{-5} \frac{m^3}{sec}$$

Note that C_3 represents the intersection of Q_p-axis by the flow delivery characteristic surface.

B.2 Evaluation of Metering Valve Flow Area

The flow area of a conical valve, Fig. B.2, with constant angle is given by:

$$A = \pi \ell (r + R) \qquad (B.2)$$

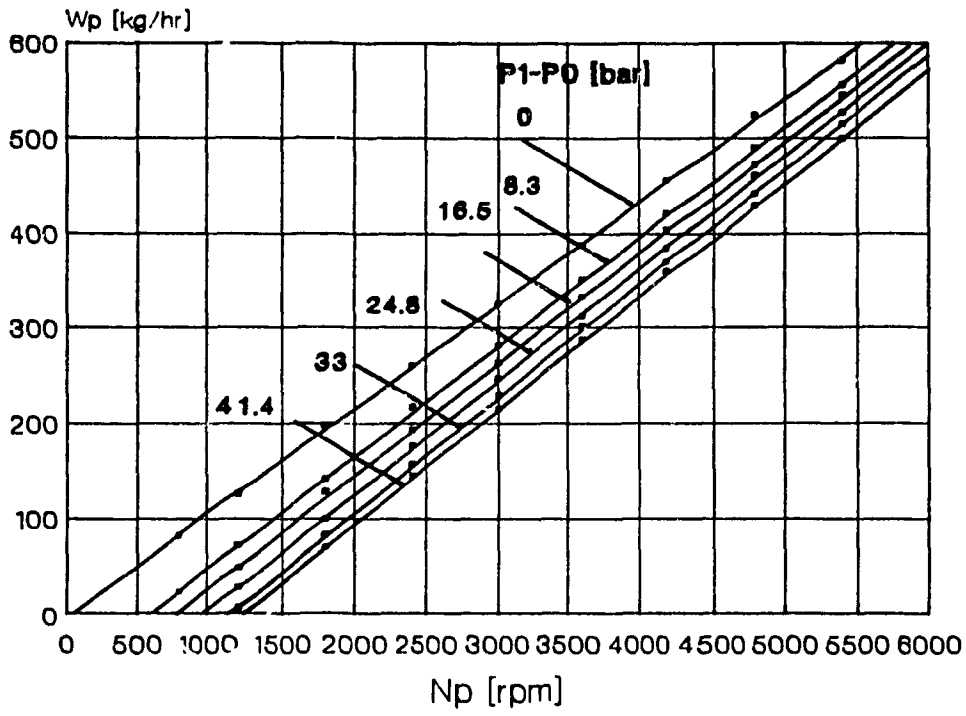

Fig. B.1 Experimental pump characteristic

The metering valve profile consists of three truncated cones, Fig. B.3, and the flow area can be expressed as follows:

$$A_{12m} = a_1 x^2 + a_2 x + a_3 \qquad (B.3)$$

The coefficients a_1, a_2, a_3 are evaluated as follows:

For $0 < x \leq x_1$-

$$A_{12m} = d_1 x^2 + d_2 x \qquad (B.4)$$

where,

$$d_1 = -\pi \sin^2\theta \cos\theta_1$$

$$d_2 = \pi D_{mo} \sin\theta$$

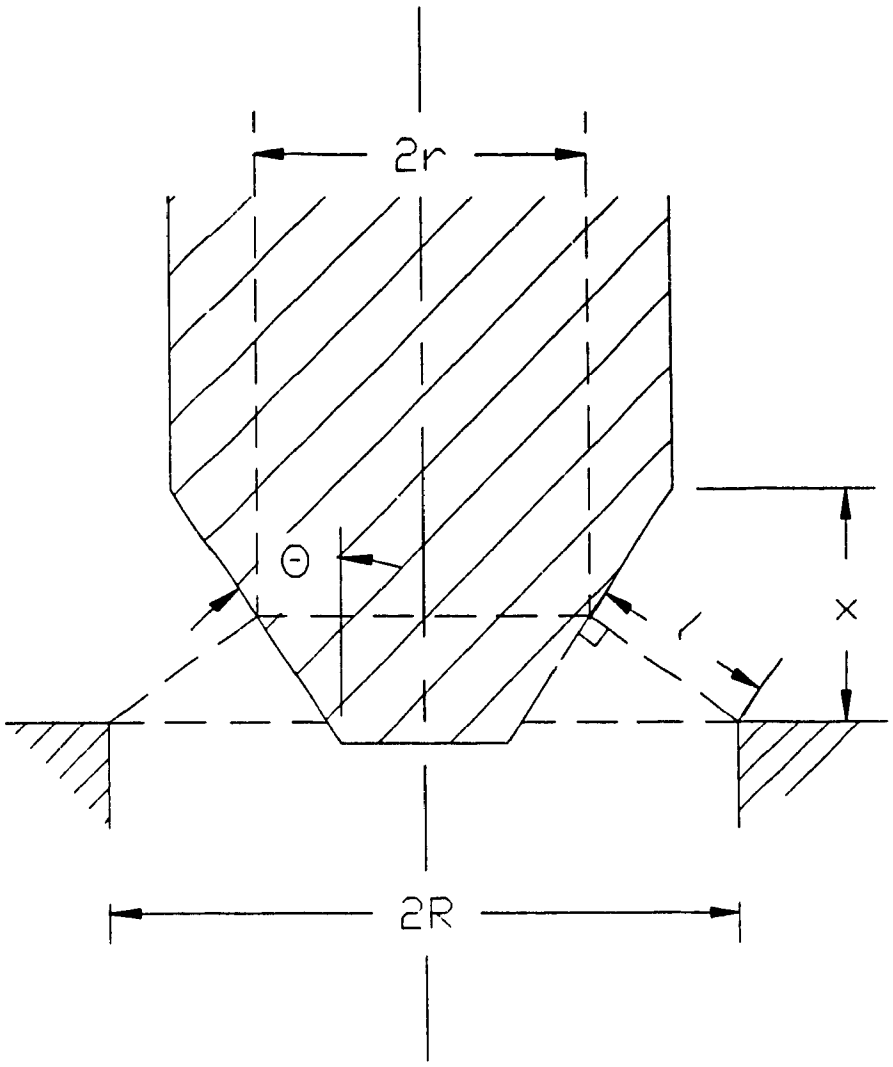

Fig. B.2 Flow area of a conical valve

Therefore

$$a_1 = d_1 \qquad a_2 = d_2 \qquad a_3 = 0$$

For $x_1 \leq x \leq x_2$

If the valve first cone were of angle θ_2 it would generate the same area as cone θ_1 but at smaller

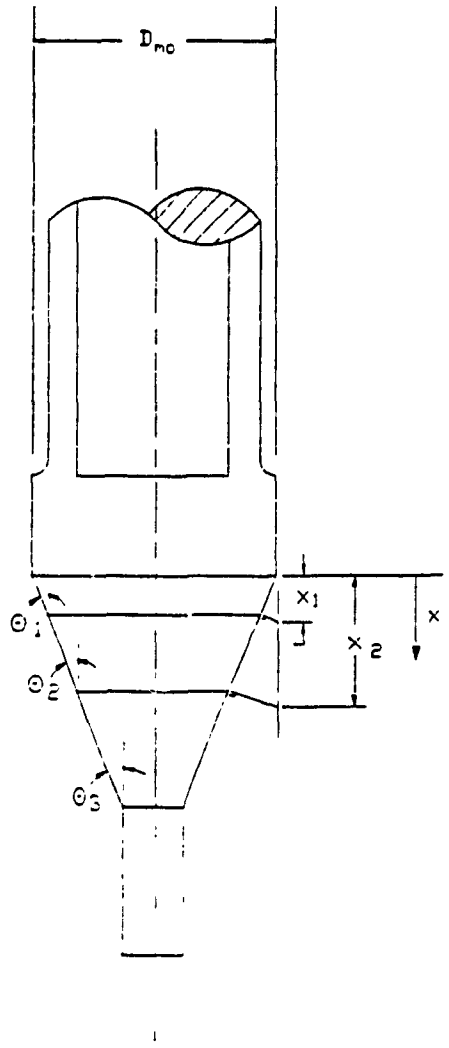

Fig. B.3 Metering valve

displacement, x_1^*. Setting:

$$e_1 x_1^{*2} + e_2 x_1^* = \left(A_{12m} \right)_{x=x_1} \qquad (B.5)$$

where,

$$\left(A_{12m} \right)_{x=x_1} = d_1 x_1^2 + d_2 x_1$$

$$e_1 = -\pi \sin^2\theta_2 \cos\theta_2$$

$$e_2 = \pi D_{mo} \sin\theta_2$$

x_1^* is obtained:

$$x_1^* = \frac{-e_2}{2e_1} - \left[\frac{1}{4} \left(\frac{e_2}{e_1} \right)^2 + \frac{1}{e_1} \left(A_{12m} \right)_{x=x_1} \right]^{1/2} \quad (B.6)$$

Then,

$$A_{12m} = e_1 \left(x + x_1^* - x_1 \right)^2 + e_2 \left(x + x_1^* - x_1 \right) \quad (B.7)$$

Therefore:

$$a_1 = e_1$$

$$a_2 = 2 e_1 \left(x_1^* - x_1 \right) + e_2$$

$$a_3 = \left[e_1 \left(x_1^* - x_1 \right) + e_2 \right] \left(x_1^* - x_1 \right)$$

For $x > x_2$

Similarly setting:

$$f_1 x_2^{*2} + f_2 x_2^* = \left(A_{12m} \right)_{x=x_2} \quad (B.8)$$

where,

$$\left(A_{12m} \right)_{x=x_2} = e_1 x_2 + 2 \left[e_1 \left(x_1^* - x_1 \right) + e_2 \right] x_2 + \left[e_1 \left(x_1^* - x_1 \right) + e_2 \right] \left(x_1^* - x_1 \right) \quad (B.9)$$

$$f_1 = -\pi \sin^2\theta_3 \cos\theta_3$$

$$f_2 = \pi D_{mo} \sin\theta_3$$

x_2^* is obtained:

$$x_2^* = \frac{-f_2}{2f_1} - \left[\frac{1}{4}\left(\frac{f_2}{f_1}\right)^2 + \frac{1}{f_1}\left(A_{12m}\right)_{x=x_2}\right]^{1/2} \qquad (B.10)$$

Then

$$A_{12m} = f_1\left(x + x_2^* - x_2\right)^2 + f_2\left(x + x_2^* - x_2\right) \qquad (B.11)$$

Therefore:

$$a_1 = f_1$$

$$a_2 = 2f_1\left(x_2^* - x_2\right) + f_2$$

$$a_3 = \left[f_1\left(x_2^* - x_2\right) + f_2\right]\left(x_2^* - x_2\right)$$

for $x_1 = 0.533$ mm $\quad x_2 = 1.905$ mm

$\theta_1 = 13°$ $\quad \theta_2 = 17.17°$ $\quad \theta_3 = 23.33°$

the flow area coefficients are shown in the Table below:

TABLE B.1

Metering Valve Flow Area Coefficients

	$0 \leqslant x \leqslant x_1$	$x_1 < x \leqslant x_2$	$x > x_2$
a_1	- 0.155	- 0.262	- 0.452
a_2	3.285	4.376	6.314
a_3	0	- 0.549	- 3.457

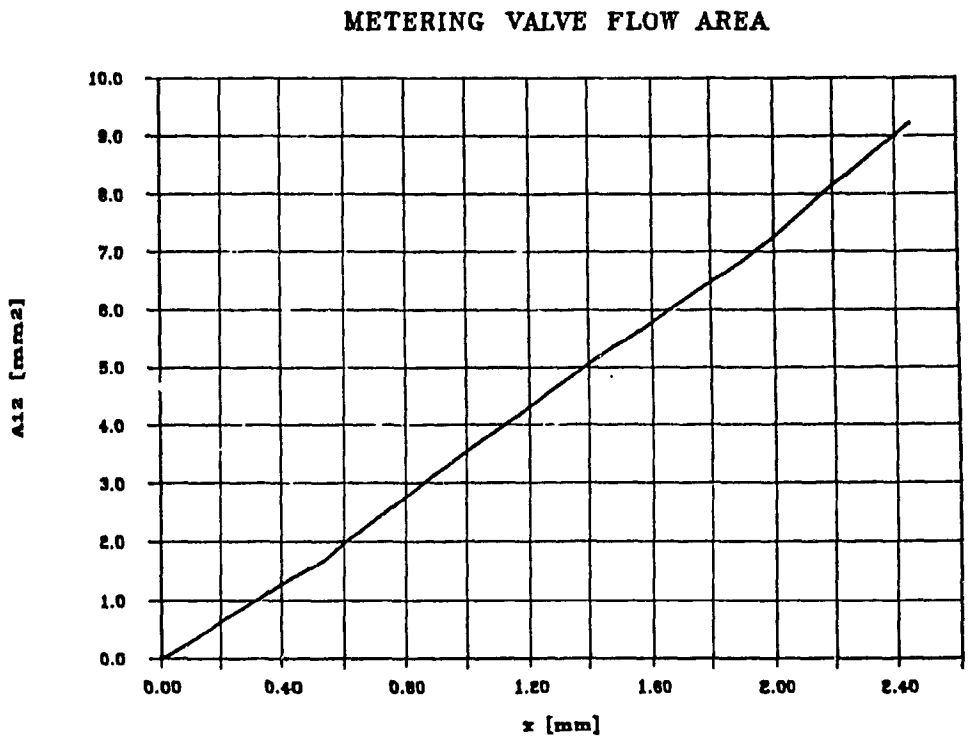

Fig. B.4 Metering valve flow area vs valve displacement

Figure B.4 shows the flow area of the metering valve flow as a function of valve displacement.

B.3 Evaluation of By-pass Valve Flow Area

The by-pass total flow area is evaluated as the sum of the two flow areas, (A_{10}), and $(A_{10})_2$, (see Fig. B.5). $(A_{10})_1$, $(A_{10})_2$ are the flow areas on each end of the by-pass valve:

$$(A_{10})_1 = (b_1)_1 \, y^2 + (b_2)_1 \, y + (b_3)_1$$

$$(A_{10})_2 = (b_1)_2 \, y^2 + (b_2)_2 \, y + (b_3)_2$$

where

$(b_1)_1 = -\pi\ (\sin^2\theta_{b1}\cos\theta_{b1})$

$(b_1)_2 = -\pi\ (\sin^2\theta_{b2}\cos\theta_{b2})$

$(b_2)_1 = \pi\ D_{bo}\sin\theta_{b1}$

$(b_2)_2 = \pi\ D_{bo}\sin\theta_{b2}$

$(b_3)_1$ = area due to overlap of bottom valve port

$(b_3)_2$ = area due to overlap of top valve port

The total flow area in the by-pass valve is:

$$A_{10} = b_1y^2+b_2y+ b_3 \qquad (B.12)$$

where

$b_1 = -\pi\ (\sin^2\theta_{b1}\cos\theta_{b1} + \sin^2\theta_{b2}\cos\theta_{b2})$

$b_2 = \pi\ D_{bo}(\sin\theta_{b1}+ \sin\theta_{b2})$

b_3 = area due to valve overlap

Fig. B.6 shows the flow area of the by-pass valve as a function of valve displacement.

B.4 Evaluation of Pressurizing Valve Flow Area

The pressurizing valve, Fig. B.7, consists of a single cone profile. The flow area is :

$$A_{2mn} = c_1\ z^2 + c_2\ z \qquad (B.13)$$

where,

$c_1 = -\pi \left(\sin^2\theta_p\ \cos\theta_p \right)$

$c_2 = \pi\ D_{po}\ \sin\ \theta_p$

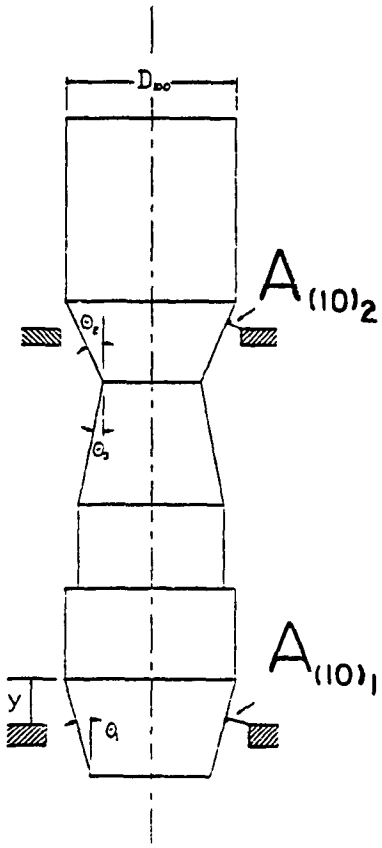

Fig. B.5 By-pass valve

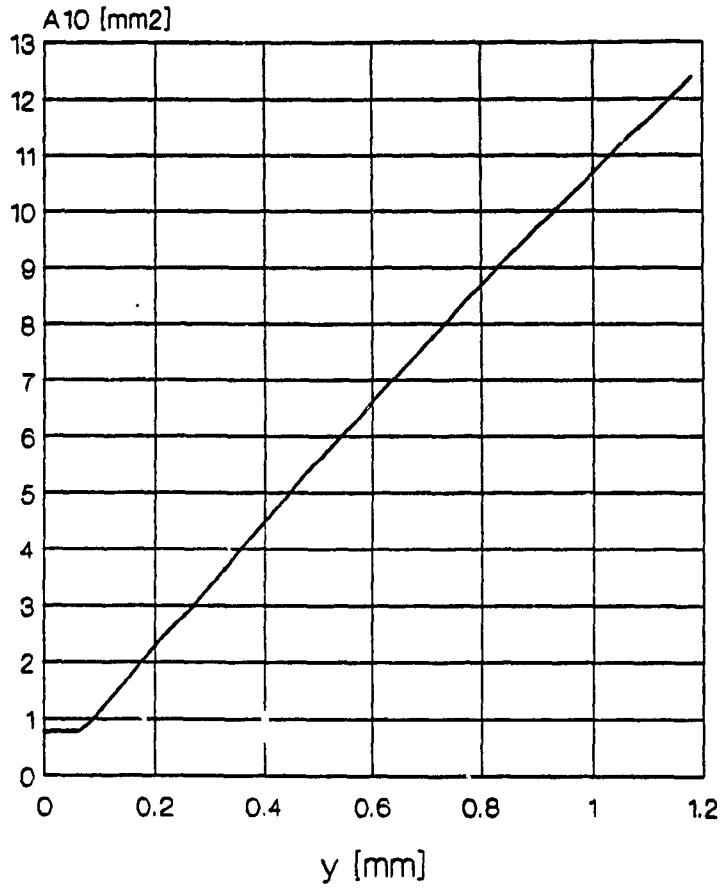

Fig. B.6 By-pass valve flow area vs valve displacement

B.5 Metering Valve Flow Coefficient

The metering valve flow coefficient was obtained experimentally as a function of valve position and pump speed. At metering valve openings greater than 1 mm, the flow coefficient is equal to approximately 0.6, Fig. B.8.

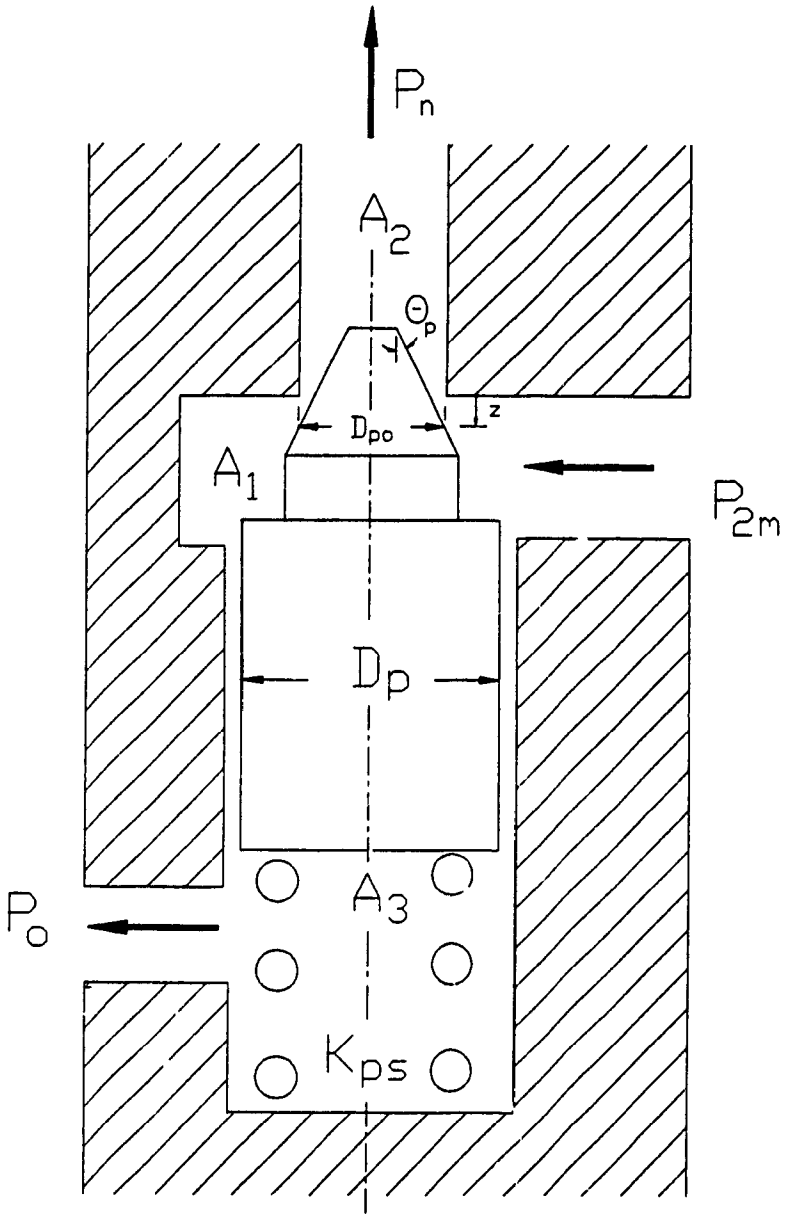

Fig. B.7 Minimum pressurizing valve

B.6 Nozzle Discharge Characteristic

An orifice of fixed flow area was used to represent the nozzles. The discharge coefficient was determined experimentally as a function of injection pressure, Fig. B.9.

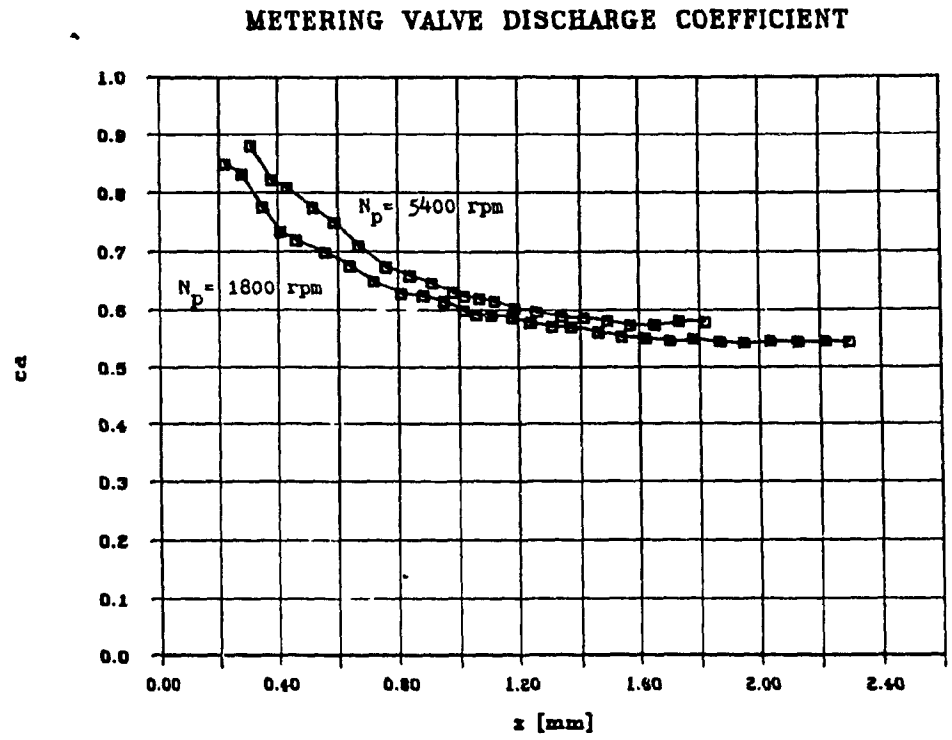

Fig. B.8 Flow coefficient of the metering valve as a function of valve position and pump speed

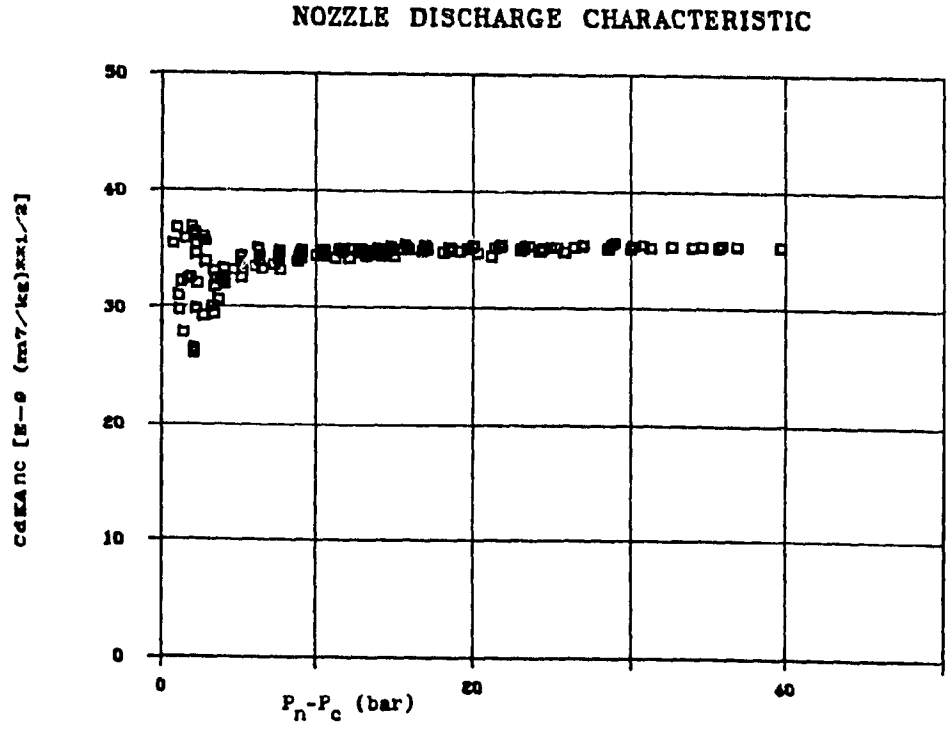

Fig. B.9 Nozzle discharge characteristic

B.7 By-Pass Valve Diaphragm Forces

Forces acting on the diaphragm and on the by-pass valve are shown in Fig. B.10b. To find the location of the effective force due to the fuel pressure on the diaphragm, the moment of an elemental force with respect to the diaphragm center is integrated over the total area, Fig. B.10a.

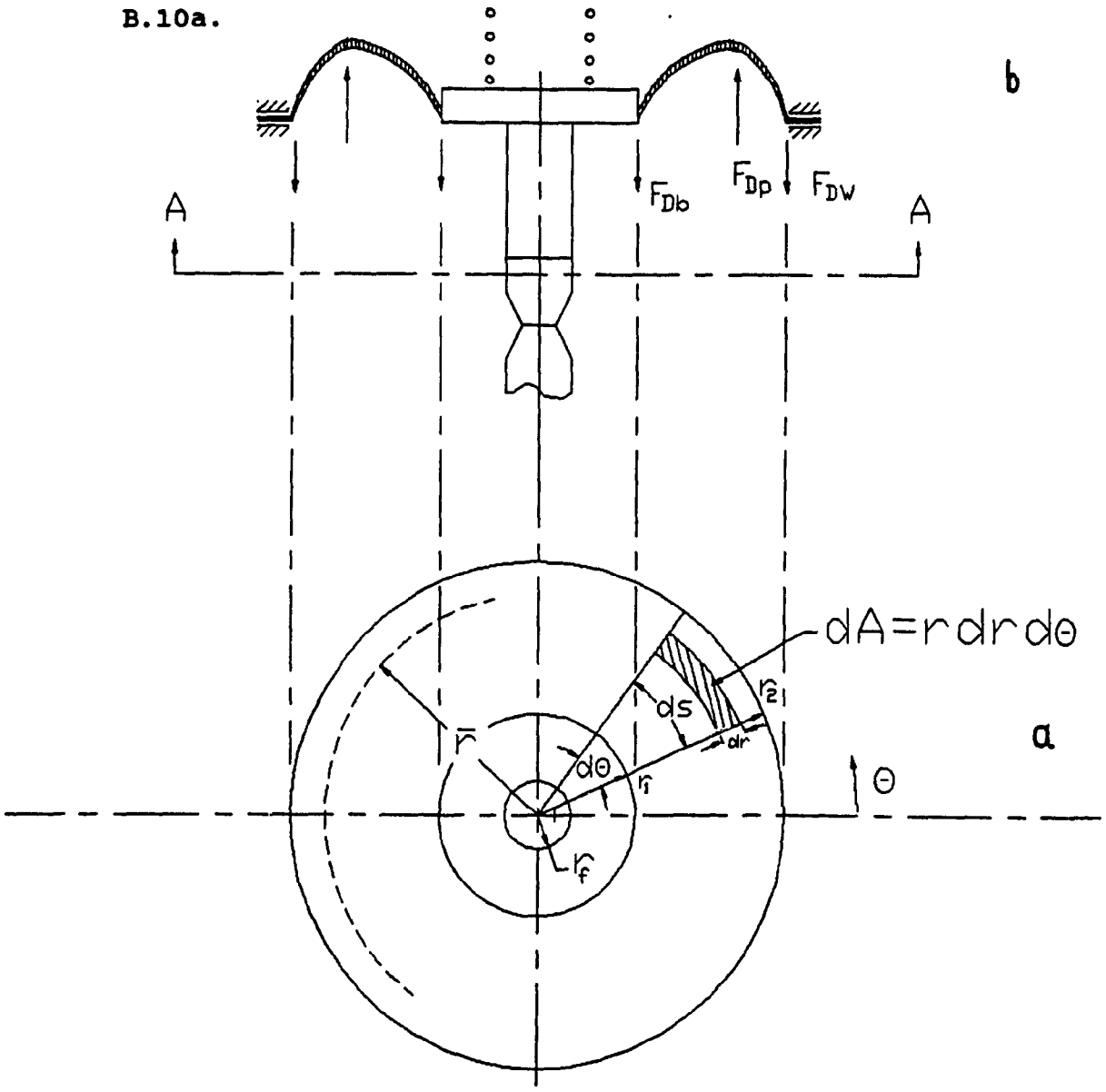

Fig. B.10 By-pass valve diaphragm forces

$$\left(P_1-P_{2b}\right) \int_0^{2\pi}\int_{r_1}^{r_2} r(rdr)d\theta = 2\pi \left(P_1-P_{2b}\right)\left(\frac{r_2^3- r_1^3}{3}\right) \qquad (B.14)$$

The effective force acts on a radius $\bar{r}$. Its force moment is:

$$\left(P_1-P_{2b}\right) \bar{r} \int_0^{2\pi} \int_{r_1}^{r_2}(rdr)d\theta = \pi\left(P_1-P_{2b}\right)\bar{r}\left(r_2^2-r_1^2 \right) \qquad (B.15)$$

From Eq. (B.14) and Eq. (B.15), $\bar{r}$ is obtained:

$$\bar{r} = \frac{2}{3}\left[\frac{r_2^3 - r_1^3}{r_2^2 - r_1^2}\right] \qquad (B.16)$$

The static force balance for the diaphragm gives the force that the by-pass valve exerts on the diaphragm:

$$F_{vD} = \pi\left[\frac{r_2 - \bar{r}}{r_2 - r_1}\right]\left(r_2^2 - r_1^2 \right)\left(p_1 - p_{2b}\right) \qquad (B.17)$$

The force that the diaphragm exerts on the valve is equal to F_{vD} but of opposite sign. The total force on the by-pass valve due to the differential pressure is:

$$F_{bp}= P_1\left[\pi(r_2-\bar{r})(r_2+r_1)+\pi(r_1^2-r_f^2)\right] - P_{2b}\left[\pi(r_2-\bar{r})(r_2+r_1)+\pi r_1^2\right] \qquad (B.18)$$

Therefore:

$$F_{bp} = \left(A_{De} - A_f\right)P_1 - A_{De}\, P_{2b} \qquad (B.19)$$

where, $$A_{De} = \pi\left[\left(r_2 - \bar{r}\right)\left(r_2 + r_1\right) + r_1^2 \right]$$

B.8 By-pass Valve Flow Forces

The flow angles needed to evaluate the flow forces in the by-pass valve cannot be easily derived theoretically. Therefore, for the fuel control unit under consideration, the flow forces were obtained experimentally.

$$F_{bf} = -2C_d A_e \left(P_1 - P_0\right) + A_f\, P_1 \qquad (B.20)$$

The area A_e can be obtained from the static force balance of the by-pass valve.

$$A_e = \frac{A_{De}\left(P_1 - P_{2b}\right) + F_{bs}}{2\, C_d \left(P_1 - P_0\right)} \qquad (B.20)$$

A_e is shown as a function of the metering valve position at different pump speeds in Fig. B.11.

The first term of equation (B.20) (RHS) is shown in Fig. B.12. A straight line was used to describe the relationship.

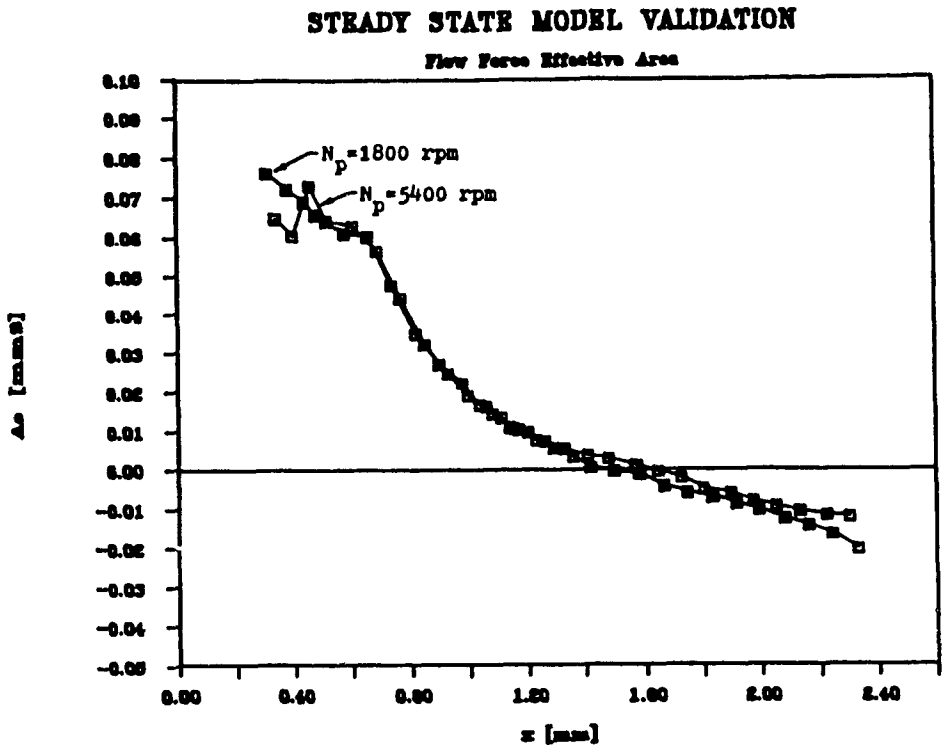

Fig. B.11 Flow force effective area

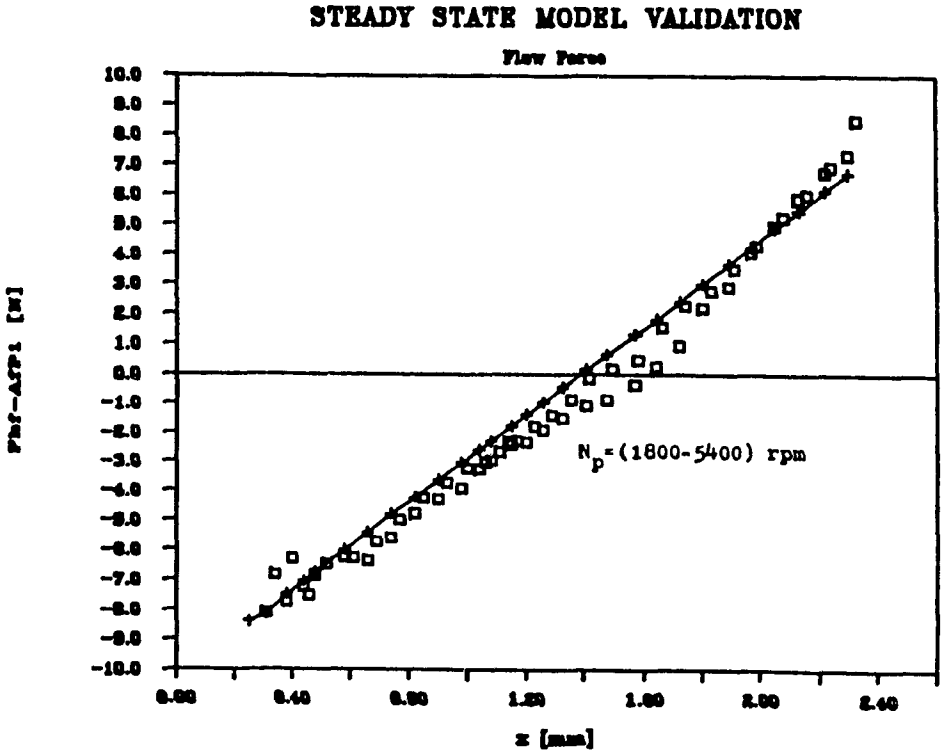

Fig. B.12 Flow force as a function of metering valve position

APPENDIX C

TUTSIM BLOCK DIAGRAMS FOR THE MODEL OF THE FUEL CONTROL UNIT AND DIGITAL CONTROLLER

APPENDIX C

TUTSIM BLOCK DIAGRAMS FOR THE MODEL OF THE FUEL CONTROL UNIT AND DIGITAL CONTROLLER

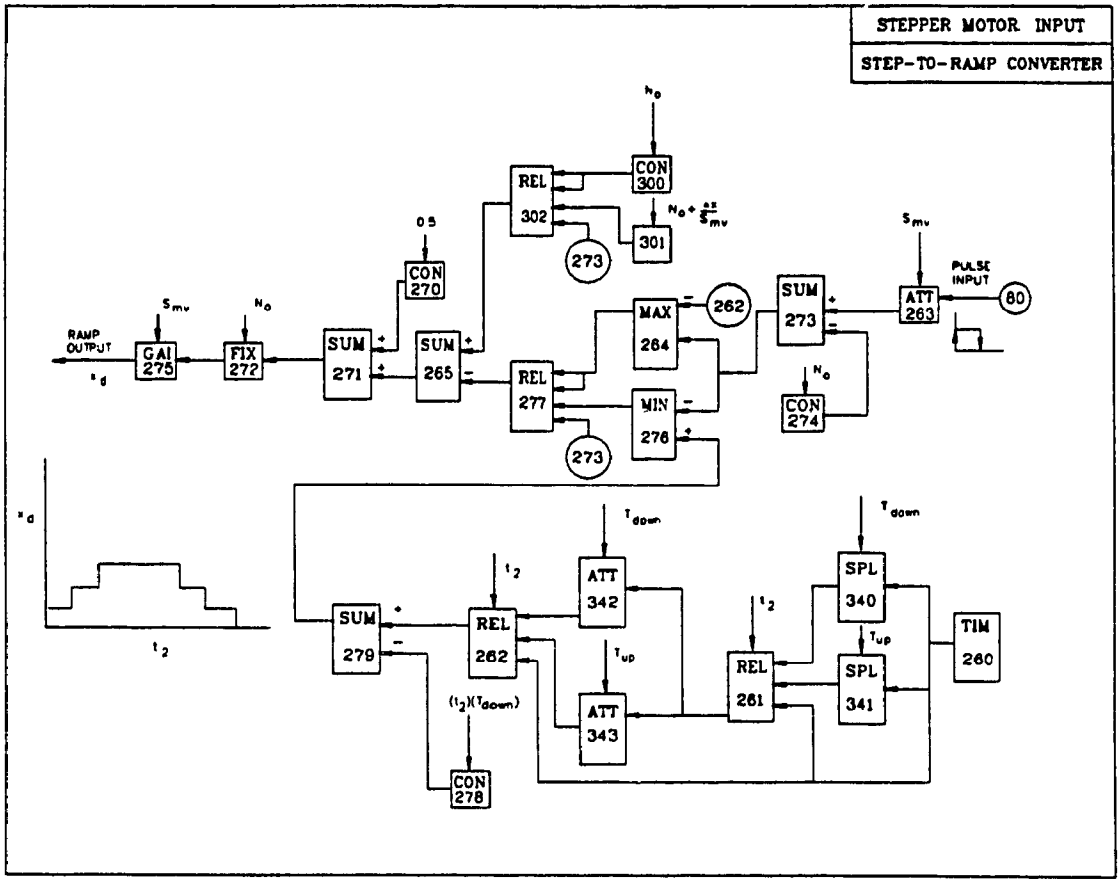

Fig. C.1 Block diagram of TUTSIM subprogram which simulates the incremental actuation of the metering valve during open loop tests

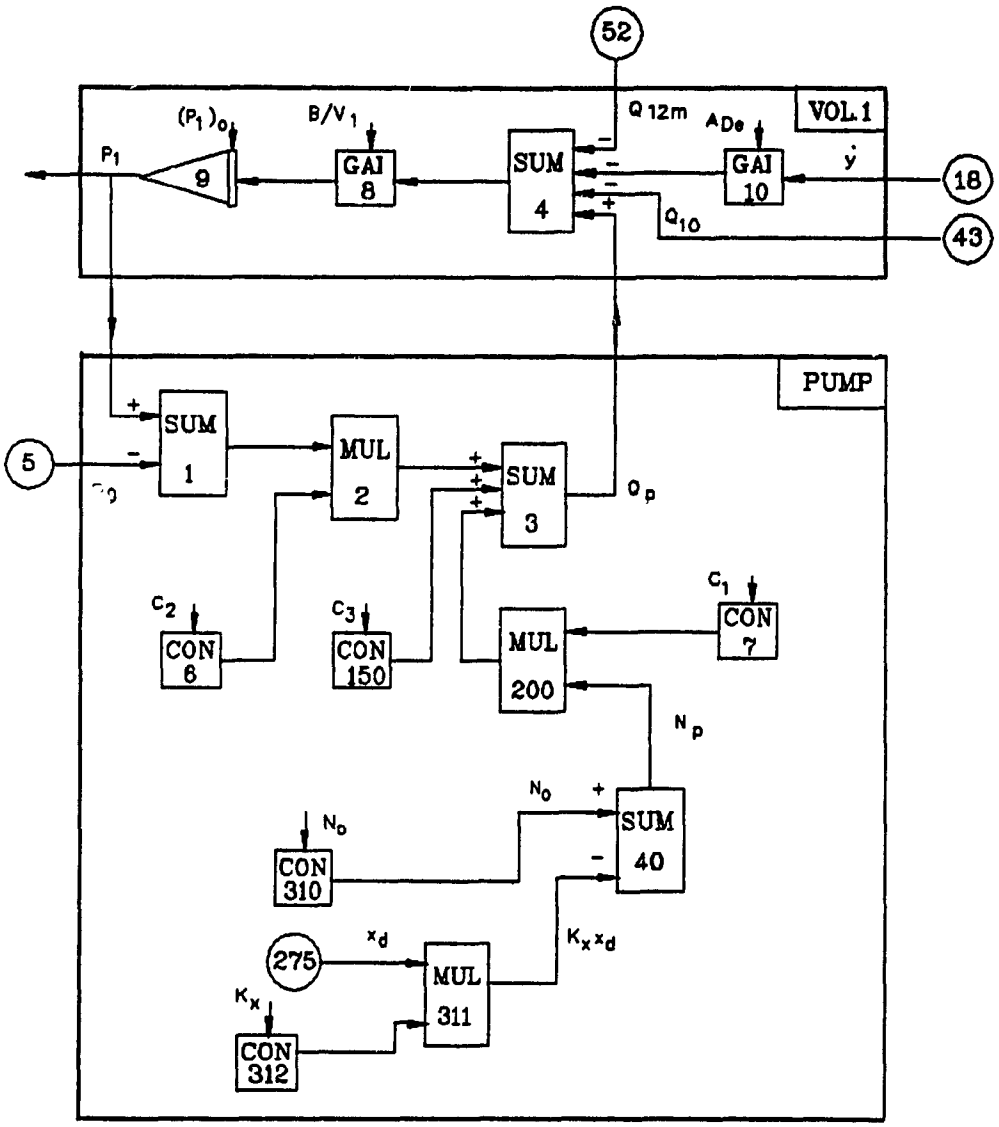

Fig. C.2 TUTSIM blocks for high pressure pump and pump discharge volume

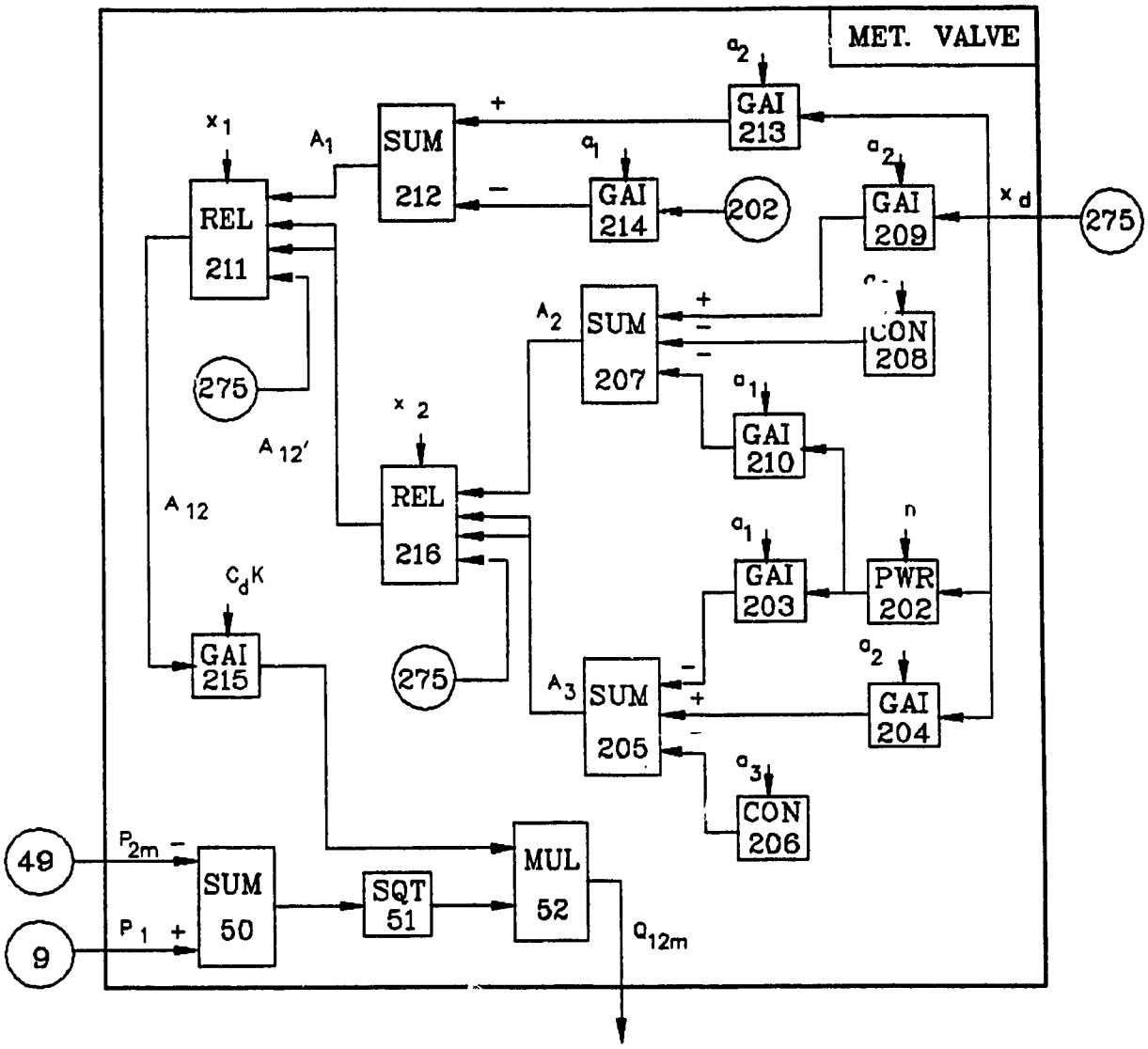

Fig. C.3 TUTSIM blocks for metering valve

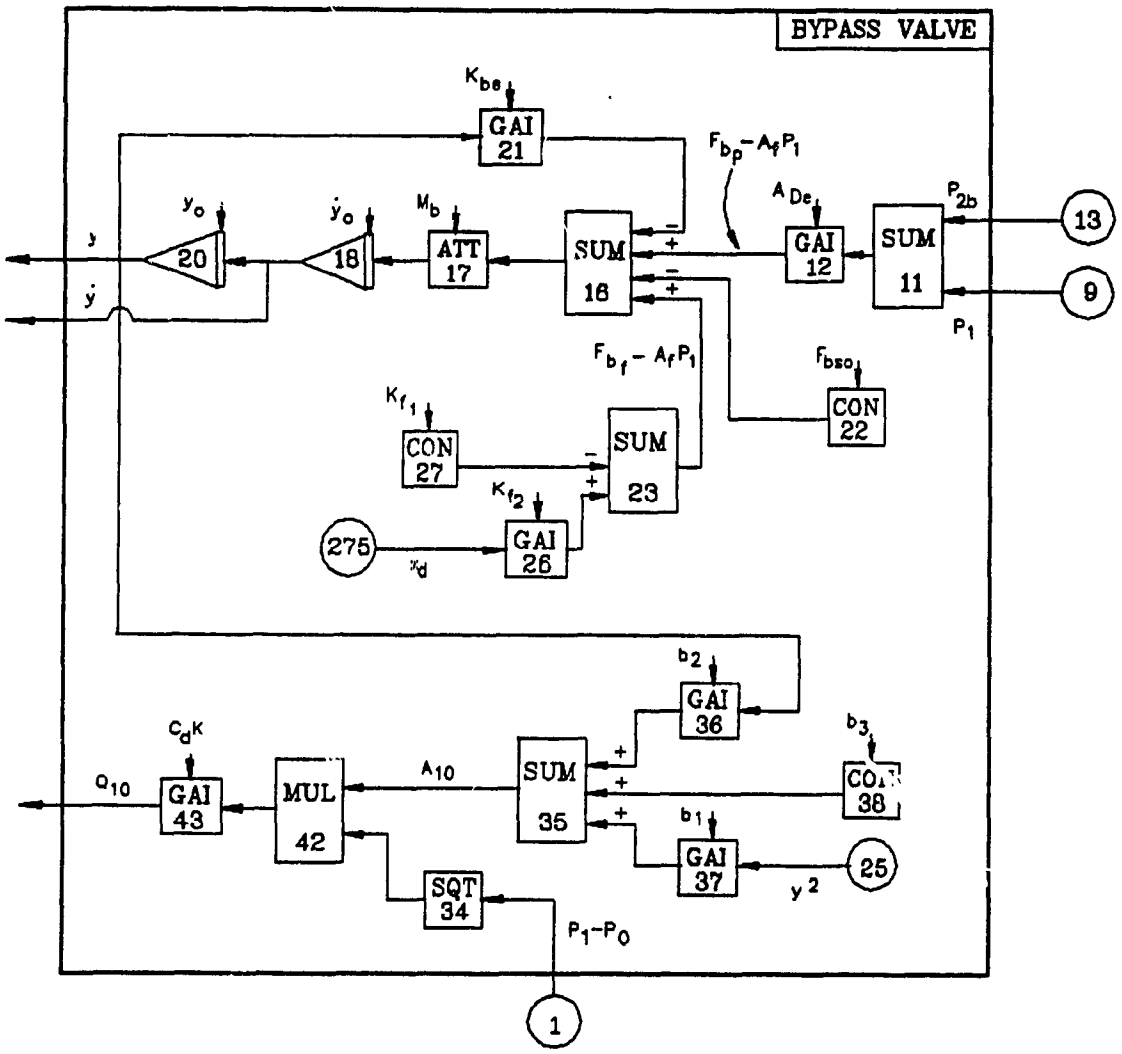

Fig. C.4 TUTSIM blocks for by-pass valve

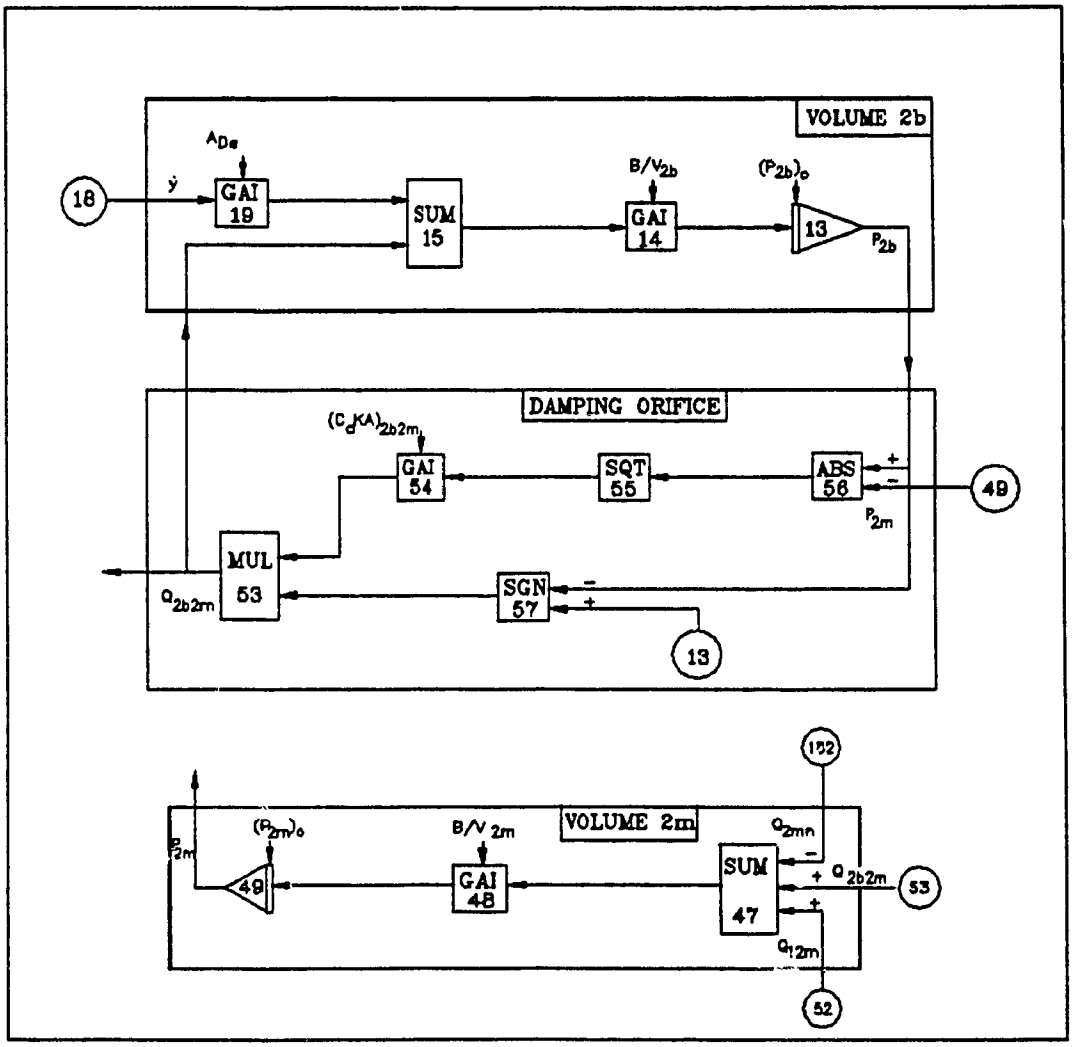

Fig. C.5 TUTSIM blocks for damping orifice with upstream and downstream volumes

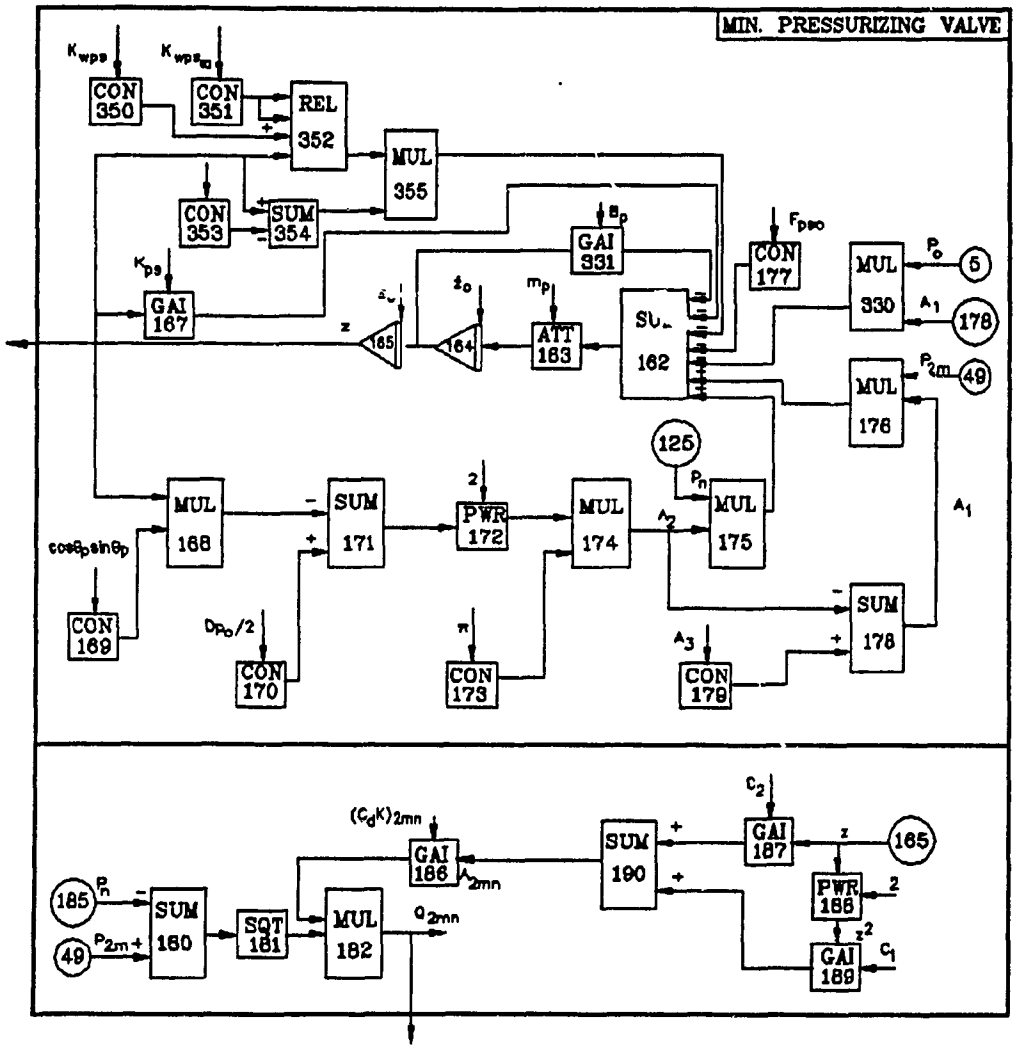

Fig. C.6 TUTSIM blocks for minimum pressurizing valve

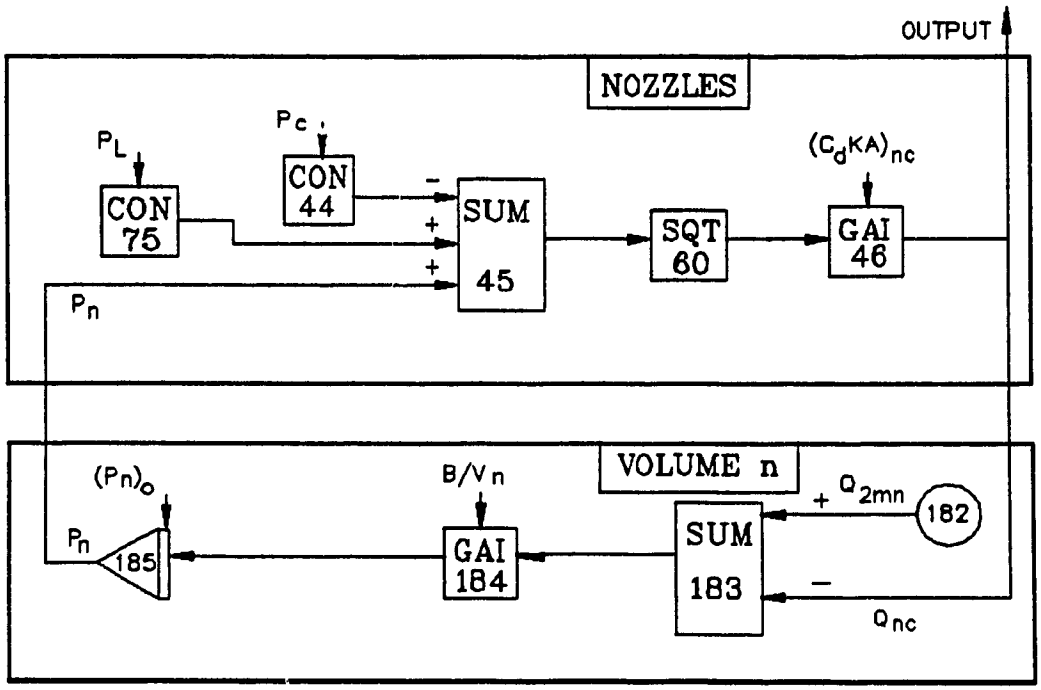

Fig. C.7 TUTSIM blocks for nozzle and nozzle manifold volume

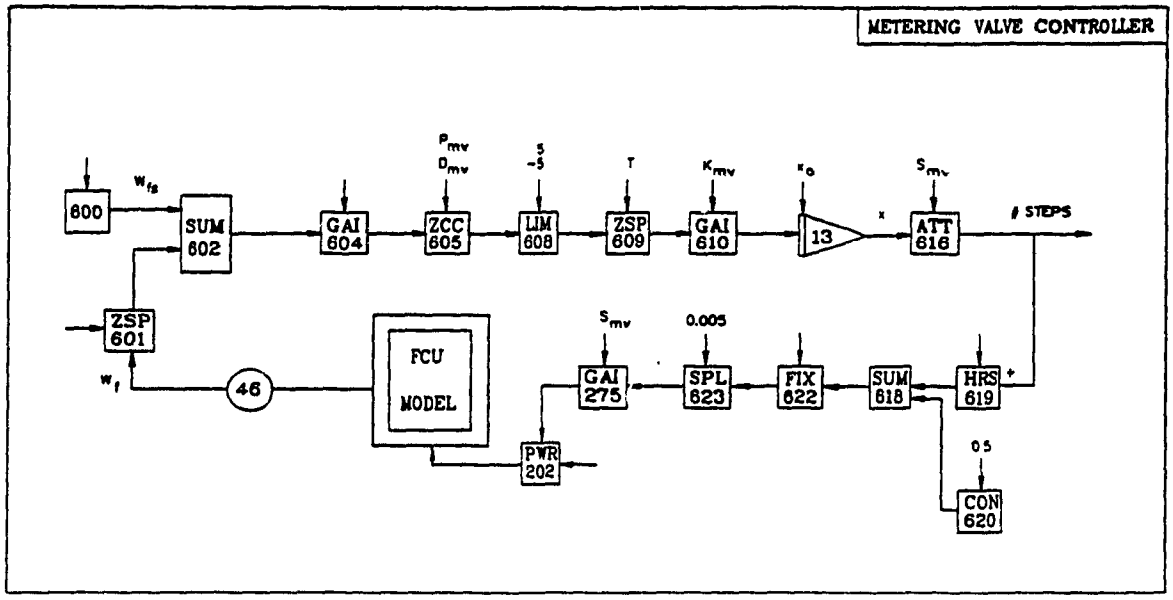

Fig. C.8 TUTSIM blocks for metering valve digital controller

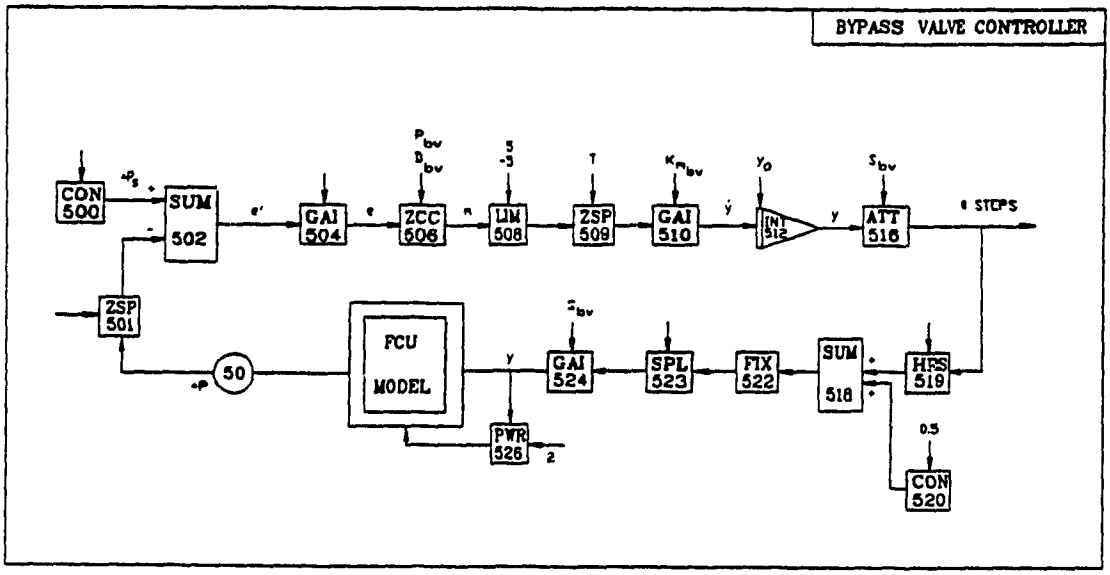

Fig. C.9 TUTSIM blocks for by-pass valve digital controller

APPENDIX D

DESCRIPTION OF THE Intel M80C196KB 16-BIT EMBEDDED MICROCONTROLLER AND EVALUATION BOARD

APPENDIX D

DESCRIPTION OF THE Intel M80C196KB 16-BIT EMBEDDED MICROCONTROLLER AND EVALUATION BOARD

D.1 Microcontroller

The schematic of the microcontroller Pin Package and Functional Block diagram are shown in Fig. D.1. Many peripherals are available on-chip. These are: a serial port, A/D converter (10 bit), PWM output, up to 48 I/O lines and a High-speed I/O subsystem which has two 16-bit timers/counters. 8K ROM memory is available as an option. Each peripheral is briefly discussed in the following.

The serial port can operate in full duplex asynchronous mode. That is, it can transmit and receive data simultaneously. The data frame used consists of 10 bits: 8 data bits (with LSB transmitted first), one start bit, one stop bit and even parity.

The analog to digital circuitry consists of a 10-bit Analog-to-Digital converter (A/D), Sample and Hold (S/H) circuitry and an 8-channel multiplexer. Conversion time is 18.2 μs. The digital output is equal to the ratio of the input voltage to the analog supply voltage (reference voltage).

The PWM output can be used as an 8-bit D/A output. The ON/OFF time of the PWM output is determined by comparing a number stored in a special register called the "PWM

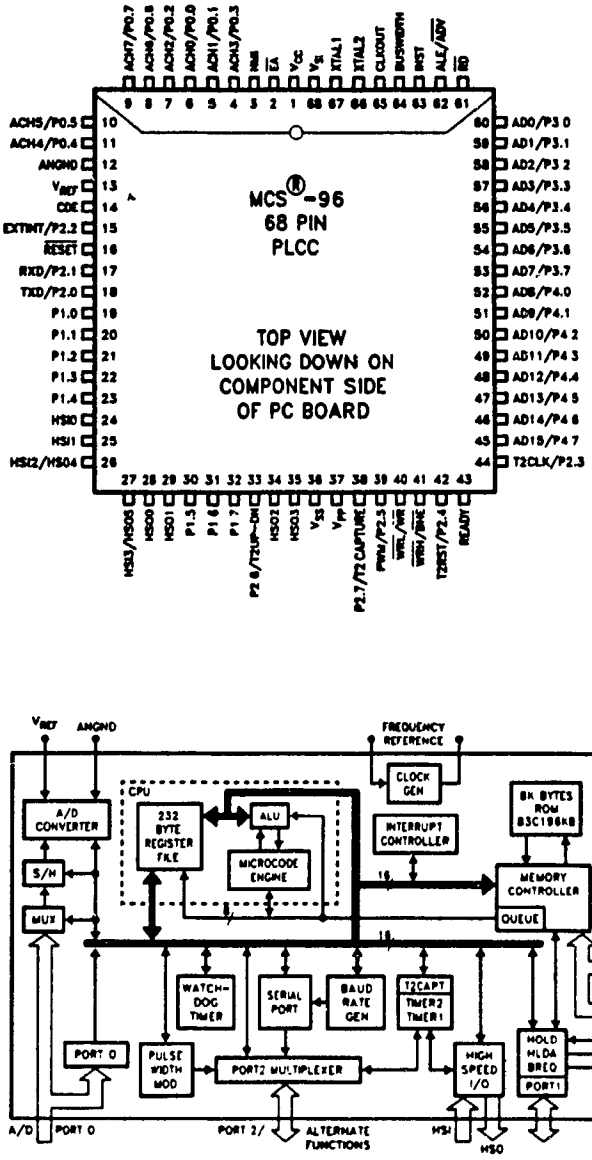

Fig. D.1 Microcontroller Pin Package and Functional Block Diagram (69)

register" to the count of an 8-bit counter. The output is high when the count is lower than the value stored in the PWM register and low when the count is higher. The duty

cycle is changed by storing a different number in the PWM register. The output waveform can be integrated to produce a DC level of 256 steps resolution. The HSO port can also generate a PWM output with very little CPU overhead. A duty cycle variable to 65536 steps (16-bit resolution) is possible.

The microcontroller has 8-bit I/O ports. Some of these ports are bidirectional while others perform more than one function. These ports are:

Port 0 : input for A/D converter
Port 1 : quasi-bidirectional
Port 2 : quasi-bidirectional, input output
Port 3 : open drain bidirectional (address/data)
Port 4 : open drain bidirectional (address/data)

The High Speed Input (HSI) unit can be used to count and measure events. It has four input lines. Every time an event occurs to any of these lines, it is marked by storing the value of a timer. High Speed Output (HSO) can generate events with minimum CPU overhead. Two interrupt vectors are associated with the HSO. These vectors can initiate an A/D conversion, set a maximum of four software timers or control the output of the 6 HSO output lines.

The 16-bit counters are used as time bases for the High Speed Input/Output units. Timer1 synchronizes events to real

time while Timer2 synchronizes events to external occurrences. Timer1 is clocked at a fraction (1/8) of the state clock while Timer2 is clocked externally.

Another important feature of the M80C196KB microcontroller is the Watchdog Timer (WDT) which provides a means to recover from a software upset. If the timer fails to be cleared every 64K state times, the RESET line is pulled low and the I/O lines are driven to a known state.

D.2 Microcontroller Evaluation Board

This board, shown in Fig. D.2, provides a hardware environment for software evaluation for the ROMless version of the microcontroller. The board is hosted on an IBM PC (or compatible) microcomputer. Communication is established through an on board Intel 82510 UART. This type of configuration frees the on-chip UART for user's applications. The board consists of six sections: Processor, Memory, Host Interface, Digital I/O, Analog Inputs and Decoding.

Most of the functions of the microcontroller are available on the evaluation board. Some functions are reserved for the host interface. The board includes a symbolic single line assembler / disassembler, single program execution, and up to 16 software break points. A complete code development environment using assembler (ASM-96) or high level languages such as Intel's iC-96 or

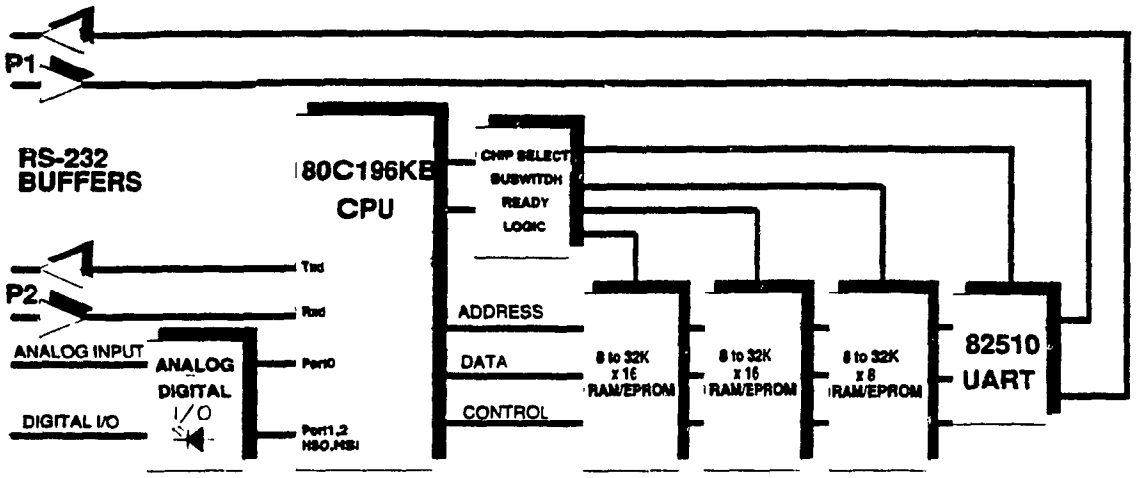

Block Diagram of the 80C196KB Board

Fig. D.2 Block Diagram of Evaluation Board (70)

PL/M is also supported. The board includes 24K bytes of SRAM used as ROMsim to store user's data and code. A Programmable Logic Device (PLD) controls the bandwidth of the microcontroller and the Chip-Select inputs. By changing the PLD, the memory on the board can be made to look like the memory system planned for the user's hardware application. Analog input conditioning and precision reference voltage are also available.

The evaluation board uses an Embedded Controller Monitor (ECM) written specifically for the MCS-96 family of 16-bit microcontrollers. The monitor program is broken into

two parts: one residing and executing on the evaluation board (iRISM-96 : Reduced Instruction Set Monitor) and the other on the host (iECM-96). Communication between these two programs is via the asynchronous serial channel. Using this monitor it is possible to load object code into the system RAM, examine and modify variables, execute code and step through code. All these features are very useful in the evaluation of the proposed controller design.

APPENDIX E

COMPUTER CODE FOR SIMULATION AND CONTROL

APPENDIX E
COMPUTER CODE FOR SIMULATION AND CONTROL

```
/*================================================================*/
/*  EFCU:  CODE FOR STEADY STATE EXPERIMENTS                      */
/*================================================================*/

#include <alloc.h>
#include <stdio.h>
#include <math.h>
#include <float.h>

#define absl(I) ((I)<0 ? -(I):(I))

_main()

{

/*----------------------------------------------------------------*/
/*      VARIABLES DECLARATION                                     */
/*----------------------------------------------------------------*/

        int rawdata[4];
        signed int tim[3000],tim1[3000];
        int xx[100],pn[100],flow[100],p1p2[100],speed[100],y[100],p1[100];
        int lo,adapt,device,chanlo,chanhi,ctrl,mode,stor,stat;
        int dev,chan,setup,rawval,kt,kk,raw,ikk,ks,kud,value,kav,hndshk;
        int ddevice,chann,chan1,bit,bbit,hi,de,bit2,low,high,step,dem,ave;
        long int count,counttt,counttttt,countt,rate,ke,sum,km,sum0,sum1,sum2,
        sum3,countttttt;

        FILE *fp, *_fopen();
        fp = _fopen("trs0.dat","w");

/*----------------------------------------------------------------*/
/*      INITIALIZATION OF DATA ACQUISITION ADAPTER                */
/*----------------------------------------------------------------*/

        adapt = 0 ;
        device = 9 ;
        chanlo = 0 ;
        chanhi = 3 ;
        ctrl = 0 ;
        mode = 0 ;
        stor = 0 ;
        count = 1 ;
        rate = 2000 ;
        stat = 0 ;
        bbit = 0 ;
        bit = 1 ;
        bit2 = 2 ;
        low = 0 ;
        high = 1 ;
        lo = 0 ;
```

```
        ddevice = 8 ;
        chann = 0 ;
        chan1 = 1 ;
        dev = 10 ;
        chan=0;
        setup=0;
        hndshk=0;
        rawval=-1;
        countt = 2000;
        counttttt=400;
        count'.t=20;
        countttttt=4000;
        ke=4090;
        kt = 0 ;
        hi = 1 ;
        value = 58 ;
        km=200;
        kk=0;

/*-------------------------------------------------------------------*/
/*      DEACTIVATE STEPPER MOTOR DRIVER - SET TRIGGER LOW            */
/*-------------------------------------------------------------------*/

        bitous(adapt,ddevice,bit2,&low,&stat);
        bitous(adapt,ddevice,bbit,&low,&stat);

/*-------------------------------------------------------------------*/
/*      SET DIRECTION OF STEPPER MOTOR                               */
/*-------------------------------------------------------------------*/

        bitous(adapt,ddevice,bit,&lo,&stat);

/*-------------------------------------------------------------------*/
/*      ACTIVATE STEPPER MOTOR DRIVER SET PIN                        */
/*-------------------------------------------------------------------*/

        bitous(adapt,ddevice,bit2,&high,&stat);

/*-------------------------------------------------------------------*/
/*      CLOSE METERING VALVE COMPLETELY                              */
/*-------------------------------------------------------------------*/

        for (step=0; step<300; step=step+1) {

        bitous(adapt,ddevice,bbit,&high,&stat);
        delay(adapt,counttt,&stat);
        high = 0 ;
        bitous(adapt,ddevice,bbit,&high,&stat);
        delay(adapt,counttt,&stat);
        high = 1 ;

        }
```

```
/*-------------------------------------------------------------------*/
/*      SET DIRECTION OF STEPPER MOTOR                               */
/*-------------------------------------------------------------------*/

        bitous(adapt,ddevice,bit,&hi,&stat);

/*-------------------------------------------------------------------*/
/*      INCREASE METERING VALVE FLOW AREA                            */
/*-------------------------------------------------------------------*/

        AREA:

        kk=0;
        kt=0;

/*-------------------------------------------------------------------*/
/*      ACTIVATE STEPPER MOTOR DRIVER SET PIN                        */
/*-------------------------------------------------------------------*/

        bitous(adapt,ddevice,bit2,&high,&stat);

/*-------------------------------------------------------------------*/
/*      TRIGGER 10 STEPS IN STEPPER MOTOR DRIVER                     */
/*-------------------------------------------------------------------*/

        for (step=0; step<10; step=step+1) {

        bitous(adapt,ddevice,bbit,&high,&stat);
        delay(adapt,counttt,&stat);
        high = 0 ;
        bitous(adapt,ddevice,bbit,&high,&stat);
        delay(adapt,counttt,&stat);
        high = 1 ;

        }

        delay(adapt,countttttt,&stat);

/*-------------------------------------------------------------------*/
/*      DEACTIVATE STEPPER MOTOR DRIVER                              */
/*-------------------------------------------------------------------*/

                bitous(adapt,ddevice,bit2,&low,&stat);

/*-------------------------------------------------------------------*/
/*      INCREASE AND OUTPUT THE MOTOR SPEED - WAIT FOR STEADY STATE  */
/*-------------------------------------------------------------------*/

        SPEED:

        if(kk==0) goto INIT;
```

```
        for (de=0; de<3; de=de+1) {

        km=km+35;

        INIT:

        ++kk;
        aous(adapt,device,chan1,ctrl,&km,&stat);
        delay(adapt,counttttt,&stat);

                        }

        delay(adapt,countttttt,&stat);

/*-------------------------------------------------------------------*/
/*      SELECT SET OF VARIABLES                                      */
/*-------------------------------------------------------------------*/

        for (dem=0; dem<2; dem=dem+1) {

        sum0=sum1=sum2=sum3=0;

/*-------------------------------------------------------------------*/
/*      First set of variables                                       */
/*-------------------------------------------------------------------*/

        value=2;

/*-------------------------------------------------------------------*/
/*      Second set of variables                                      */
/*-------------------------------------------------------------------*/

        if (dem==1) value=58;

/*-------------------------------------------------------------------*/
/*      OUTPUT MULTIPLEXER CONTROL WORD                              */
/*-------------------------------------------------------------------*/

        bous(adapt,ddevice,hndshk,&value,&stat);

/*-------------------------------------------------------------------*/
/*      READ A/D CHANNELS 0,1,2,3  AND EVALUATE AVERAGE VALUE        */
/*-------------------------------------------------------------------*/

                for (ave=0; ave<10; ave=ave+1) {

                ainsc(adapt,device,chanlo,chanhi,ctrl,mode,
                stor,count,rate,&rawdata[0],&stat);
```

```
                delay(adapt,counttt,&stat);

                sum0=sum0+rawdata[0];
                sum1=sum1+rawdata[1];
                sum2=sum2+rawdata[2];
                sum3=sum3+rawdata[3];

                }

/*-------------------------------------------------------------------*/
/*      RECORD AVERAGE READINGS                                      */
/*-------------------------------------------------------------------*/

                if(dem==1) goto NN;

                pn[kt] = sum0/10.0*0.24414;
                speed[kt] = sum1/10.0*3.107;
                y[kt] = (sum2/10.0-2.661168*409.6)*0.917418;
                p1p2[kt] = sum3/10.0*0.7324;

                goto NB;

                NN:

                xx[kt] = (4.88*409.6-sum1/10.0)*0.1430511;
                flow[kt] = sum2/10.0*1.953-5.0;
                p1[kt] = sum3/10.0*0.24414;

                NB:

                }

                if(km>3000) goto  STORE;
                ++kt;
                goto SPEED;

                STORE:

        for (ks=0; ks<kt; ks=ks+1) {

        _fprintf(fp,"%d,%d,%d,%d,%d,%d,%d\n",
        speed[ks],flow[ks],pn[ks],p1[ks],p1p2[ks],y[ks],xx[ks]);
        _printf("O.K.\n");

        }
```

```
        _fprintf(fp,"\n");

        REDUC:

        km=km-50;
        if(km<300) goto AG;
        aous(adapt,device,chan1,ctrl,&km,&stat);
        delay(adapt,countttt,&stat);
        goto REDUC;

        AG:

        km=200;
        if(xx[kt]>230) goto STOPP;
        goto AREA;

        STOPP:

}
```

```
/*=====================================================================*/
/*     EFCU: CODE FOR TRANSIENTS (OPEN LOOP); VALIDATION               */
/*                                            PROCESS IDENTIFICATION */
/*=====================================================================*/

#include <alloc.h>
#include <stdio.h>
#include <math.h>
#include <float.h

#define absl(I) ((I)<0 ? -(I):(I))

_main()

{

/*---------------------------------------------------------------------*/
/*      VARIABLES DECLARATION                                          */
/*---------------------------------------------------------------------*/

        int rawdata[4];
        signed int tim[3000],tim1[3000];
        int xx[230],pn[230],flow[230],p1[230],p1p2[230],y[230],n[230];
        int lo,adapt,device,chanlo,chanhi,ctrl,mode,stor,stat;
        int dev,chan,setup,rawval,deact,kt,raw,ikk,kud,value,kav,hndsh!;
        int ddevice,chann,chan1,bit,bbit,second,hi,bit2,low,high;
        long int count,counttt,countt,rate,ke,sum;

        FILE *fp, *_fopen();
        fp = _fopen("trs.dat","w");

/*---------------------------------------------------------------------*/
/*      INITIALIZATION OF DATA ACQUISITION ADAPTER                     */
/*-------------------------------------------------- ------------*/

        adapt = 0 ;
        device = 9 ;
        chanlo = 0 ;
        chanhi = 3 ;
        ctrl = 0 ;
        mode = 0 ;
        stor = 0 ;
        count = 1 ;
        rate = 2000 ;
        stat = 0 ;
        bbit = 0 ;
        bit = 1 ;
        bit2 = 2 ;
        low = 0 ;
        high = 1 ;
        lo = 1 ;
        ddevice = 8 ;
```

```
        chann = 0 ;
        chan1 = 1 ;
        dev = 10 ;
        chan=0;
        setup=0;
        hndshk=0;
        rawval=-1;
        countt = 40;
        counttt=200;
        ke=2045;
        kt = 0 ;
        second=0;
        deact=0;

/*=================================================================*/
/*      MAIN CONTROL AND DATA ACQUISITION                          */
/*=================================================================*/

/*-----------------------------------------------------------------*/
/*      OUTPUT THE CONTROLLER SIGNAL                               */
/*-----------------------------------------------------------------*/

        aous(adapt,device,chann,ctrl,&ke,&stat);

/*-----------------------------------------------------------------*/
/*      INITIALIZE COUNTER FOR TIME REFERENCE                      */
/*-----------------------------------------------------------------*/

        cset (adapt,dev,chan,setup,&rawval,&stat);

/*-----------------------------------------------------------------*/
/*      OPEN LOOP CONTROL                                          */
/*-----------------------------------------------------------------*/

        BR:

/*-----------------------------------------------------------------*/
/*      SELECT CONTROL WORD FOR DEMULTIPLEXER AND STEP. MOTOR STATUS */
/*-----------------------------------------------------------------*/

        value=62;
        if(deact==1) value=58;

        if(second==1){
        value=6;
        if(deact==1) value=2;
                }
```

```
/*-------------------------------------------------------------------*/
/*      CONDITION TO DEACTIVATE STEPPER MOTOR                        */
/*-------------------------------------------------------------------*/

                if(kt==5) {
                        ke=0;
                        deact=1;
                        }

/*-------------------------------------------------------------------*/
/*      CHECK FOR TERMINATION OF DATA AQUISITION FOR TRANSIENT       */
/*-------------------------------------------------------------------*/

                if (kt>228) goto GR;

/*-------------------------------------------------------------------*/
/*      WAIT UNTIL IT IS TIME FOR NEXT DATA AQUISITION               */
/*-------------------------------------------------------------------*/
                        /*
                delay(adapt,countt,&stat);
                              */
                ++kt;

                goto BR;

        GR:

/*-------------------------------------------------------------------*/
/*      CALCULATE RESULTS, SAVE ON HARD DISK AND DISPLAY ON SCREEN   */
/*-------------------------------------------------------------------*/

        for (kt=0; kt<228; kt=kt+1) {

        flow[kt]=flow[kt]*1.953-5;
        pn[kt]=pn[kt]*0.24414;
        xx[kt]=(9*409.6-xx[kt])*0.0718;
        p1[kt]=p1[kt]*0.24414;
        y[kt]=(y[kt]-2.661168*409.6)*0.917418;
        p1p2[kt]=p1p2[kt]*0.7324;
        n[kt]=n[kt]*3.107;

        _fprintf(fp,"%d,%d,%d,%d,%d,%d,%d\n",
        flow[kt],xx[kt],pn[kt],p1[kt],y[kt],n[kt],p1p2[kt]);

        _fprintf(fp,"%d,%d,%d,%d,%d,%d,%d,%d,%d\n",
        tim[kt],tim1[kt],flow[kt],xx[kt],pn[kt],p1[kt],y[kt],n[kt],p1p2[kt]);

        _printf("t=%d t1=%d Mf=%d pn=%d xx=%d p1=%d y=%d n=%d p1p2=%d\n",
        tim[kt],tim1[kt],flow[kt],pn[kt],xx[kt],p1[kt],y[kt],n[kt],p1p2[kt]);


        }

}
```

```
/*-------------------------------------------------------------------*/
/*      OUTPUT CONTROL WORD                                          */
/*-------------------------------------------------------------------*/

        bous(adapt,ddevice,hndshk,&value,&stat);

/*-------------------------------------------------------------------*/
/*      READ A/D CHANNELS 0,1,2,3                                    */
/*-------------------------------------------------------------------*/

        ainsc(adapt,device,chanlo,chanhi,ctrl,mode,
        stor,count,rate,&rawdata[0],&stat);

/*-------------------------------------------------------------------*/
/*      READ COUNTER  (DECREMENTING AT 1000 Hz , i.e. 1 msec)        */
/*-------------------------------------------------------------------*/

        cins (adapt,dev,chan,&raw,&stat);

/*-------------------------------------------------------------------*/
/*      STORE READINGS FROM COUNTER AND A/D  0,1,2,3                 */
/*-------------------------------------------------------------------*/

        if(second==1) goto SECOND;

/*-------------------------------------------------------------------*/
/*      First Set of Variables                                       */
/*-------------------------------------------------------------------*/

                        tim[kt] = 65535-raw;
                        xx[kt] = rawdata[1];
                        flow[kt] = rawdata[2];
                        pn[kt] = rawdata[0];
                        p1[kt] = rawdata[3];

                        second=1;

                        goto BR;

/*-------------------------------------------------------------------*/
/*      Second Set of Variables                                      */
/*-------------------------------------------------------------------*/

                SECOND:

                        tim1[kt] = 65535-raw;
                        y[kt] =rawdata[2];
                        p1p2[kt]=rawdata[3];
                        n[kt]=rawdata[1];

                        second=0;
```

```
/*=====================================================================

  PROGRAMM NAME: SS-DPF2

  WRITTEN BY    : GEORGANTAS ANTONIOS

  DATE          : 19/NOV/1989

=====================================================================*/

#include <stdio.h>
#include <float.h>
#include <math.h>

/*---------------------------------------------------------------------*/

#define RAW 21
#define COLUMN 21
#define n 20

/*---------------------------------------------------------------------*/
/* GLOBAL DECLARATIONS                                                 */
/*---------------------------------------------------------------------*/

int ierror;

/*=====================================================================*/
/* THIS PROGRAM USES THE NEWTON'S METHOD TO SOLVE A SET OF NON-LINEAR */
/* EQUATIONS TO PROVIDE THE STEADY STATE SOLUTION FOR THE BENDIX      */
/* DP-F2 FUEL CONTROL UNIT FOR DIFFERENT METERING VALVE POSITIONS AND */
/* CONSTANT FUEL PUMP SPEED                                            */
/*---------------------------------------------------------------------*/

main()

{

int i,j,m,r,l,ml;
long double a[RAW][COLUMN],at[RAW][COLUMN],axat[RAW][COLUMN];
long double aaa[RAW][COLUMN];
long double f[RAW],x[RAW],atxf[RAW],dx[RAW],bbb[RAW];
long double errbbb[RAW],err[RAW];
long double cd,cdk10,cdk12,cdkanc,cdk2n,ade,kbs,kps;
long double np,pi,c1,c2,b11,b12,b21,b22,b31,b32;
long double p0,pc,np0,zmax,ymin,cc1,cc2,cc3,aa3;
long double fbo,fpo,kwbs,kwps,xmv[30],step,prel,kf1,kf2;
long double sum,sum1,lambda;
long double thb1,thb2,thb3,thp,thth,dbo,dpo,con;
long double a1,a2,a3,b1,b2,b3;

        FILE *fp, *fopen();
        fp = fopen("a:ssn.dat","w");
```

```
/*-------------------------------------------------------------------*/
/* CONSTANTS AND PARAMETERS                                          */
/*-------------------------------------------------------------------*/

pi=3.141592654;
con=360.0/(2.0*pi);
thb1=16.0/con /* rad */;
thb2=30.0/con /* rad */;
thb3=20.0/con /* rad */;
thp=30.0/con /* rad */;
dbo=0.475 /* cm */;
dpo=0.384 /* cm */;
cd=0.6;
aa3=0.7088 /* cm2 */;
ade=2.7 /* cm2 */;
kbs=50.0 /* N/cm */;
kps=166.0 /* N/cm */;
cc1=0.0414467 /* (cm3/sec)/rpm */;
cc2=-0.062288 /* cm5/N/sec */;
cc3=-23.793 /* cm3/sec */;
cdk10=280.0 /* (cm4/N/sec2)1/2 */;
cdk12=283.3 /* (cm4/N/sec2)1/2 */;
cdk2n=280.0 /* (cm4/N/sec2)1/2 */;
cdkanc=3.5 /* (cm8/N/sec2)1/2 */;
p0=20.0 /* N/cm2 */;
pc=0.0 /* N/cm2 */;
fbo=32.0 /* N */;
fpo=45 /* N */;
kf1=74.06 /* N/cm */;
kf2=10.25 /* N */;
zmax=0.04 /* cm */;
ymin=-0.14 /* cm */;

lambda=0.1;

xmv[1]=0.025;xmv[2]=0.029;xmv[3]=0.038;xmv[4]=0.044;
xmv[5]=0.048;xmv[6]=0.058;xmv[7]=0.066;xmv[8]=0.074;
xmv[9]=0.082;xmv[10]=0.090;xmv[11]=0.098;xmv[12]=0.104;
xmv[13]=0.108;xmv[14]=0.115;xmv[15]=0.120;xmv[16]=0.126;
xmv[17]=0.133;xmv[18]=0.141;xmv[19]=0.148;xmv[20]=0.157;
xmv[21]=0.164;xmv[22]=0.172;xmv[23]=0.180;xmv[24]=0.189;
xmv[25]=0.197;xmv[26]=0.205;xmv[27]=0.213;xmv[28]=0.222;
xmv[29]=0.230 /* cm */;

np0=3400 /* rpm */;
```

```
b11=-pi*pow(sin(thb1),2.0)*cos(thb1);
b12=-pi*pow(sin(thb2),2.0)*cos(thb2);
b21=pi*dbo*sin(thb1);
b22=pi*dbo*sin(thb2);
b31=0;
b32=0;
b1=b11+b12;
b2=b21+b22;
b3=b31+b32;
c1=-pi*pow(sin(thp),2.0)*cos(thp);
c2=pi*dpo*sin(thp);
thth=sin(thp)*cos(thp);

/*-------------------------------------------------------------------*/
/* ASSIGN ZEROS TO ALL ELEMENTS OF THE COEFFICIENT MATRIX A[i][j]    */
/*-------------------------------------------------------------------*/

for (i=1;i<=n;++i) {
for (j=1;j<=n;++j) {
a[i][j]=0.0;
}
}

/*-------------------------------------------------------------------*/
/* ASSIGN VALUES TO CONSTANT NON-ZERO ELEMENTS OF MATRIX A[i][j]     */
/*-------------------------------------------------------------------*/

a[1][1]=a[2][2]=a[3][3]=a[4][4]=a[5][5]=a[6][1]=a[7][2]=a[8][4]=1.0;
a[9][14]=a[9][15]=a[11][14]=a[12][15]=a[13][16]=a[14][20]=a[15][19]=1.0;
a[15][20]=a[16][17]=a[17][18]-a[18][11]=a[19][12]=a[20][13]=1.0;
a[6][2]=a[6][3]=a[7][4]=a[8][5]=a[9][16]=a[12][17]=a[12][18]=-1.0;
a[1][6]=-cc2;
a[11][6]=-ade;
a[11][7]=ade;
```

```
/*-------------------------------------------------------------------*/
/* INITIAL APPROXIMATION OF SOLUTION VECTOR X[1]                     */
/*-------------------------------------------------------------------*/

x[1]=177.0 /* Qp [cm3/sec] */;
x[2]=5.9 /* Q12 [cm3/sec] */;
x[3]=171.0 /* Q10 [cm3/sec] */;
x[4]=5.9 /* Q2mn [cm3/sec] */;
x[5]=5.9 /* Qnc [cm3/sec] */;
x[6]=105.50 /* P1 [N/cm2] */;
x[7]=92.50 /* P2 [N/cm2] */;
x[8]=3.0 /* Pn [N/cm2] */;
x[9]=0.064 /* y [cm] */;
x[10]=0.003 /* z [cm] */;
x[11]=0.00606 /* A12m [cm2] */;
x[12]=0.060 /* A10 [cm2] */;
x[13]=0.0023 /* A2mn [vm2] */;
x[14]=40.3 /* Fbp+AfP1 [N] */;
x[15]=4.5 /* Fbf-AfP1 [N] */;
x[16]=-4.5 /* Fbs [N] */;
x[17]=-4.5 /* Fbf1 [N] */;
x[18]=0.6 /* Fbf2 [N] */;
x[19]=0.6 /* A1 [cm2] */;
x[20]=0.12 /* A2 [cm2] */;

/*-------------------------------------------------------------------*/
/* SOLVE FOR DIFFERENT METERING VALVE OPENINGS                       */
/*-------------------------------------------------------------------*/

for (ml=1;ml<=29;++ml) {

        np=np0-1153.85*xmv[ml];

        a1=-0.154899; a2=0.32849; a3=0;

        if(xmv[ml]>=0.05334) {a1=-0.2615; a2=0.437616; a3=-0.00549165;}
        if(xmv[ml]>=0.1905) {a1=-0.45243; a2=0.631378; a3=-0.0354744;}
```

```
/*-------------------------------------------------------------------------*/
/* SOLVE FOR ONE POSITION OF THE METERING VALVE                            */
/*-------------------------------------------------------------------------*/

LP:

sum=0.0;
kwps=0.0;
kwbs=0.0;

b11=-pi*pow(sin(thb1),2.0)*cos(thb1);
b12=-pi*pow(sin(thb2),2.0)*cos(thb2);
b21=pi*dbo*sin(thb1);
b22=pi*dbo*sin(thb2);
b31=0;
b32=0;

if(x[10]>zmax) kwps=1000000.0;
if(x[9]<ymin) kwbs=10000.0;
if(x[9]<0.006585) {b11=b12=0;b21=b22=0.01;b31=b32=0.00385875;}

b1=b11+b12;
b2=b21+b22;
b3=b31+b32;

/*-------------------------------------------------------------------------*/
/* ASSIGN VALUES TO VARIABLE ELEMENTS OF MATRIX A[i][j]                    */
/*-------------------------------------------------------------------------*/

a[10][10]=-kps-kwps;
a[13][9]=-kbs-kwbs;

a[2][6]=-0.5*cdk12*x[11]/sqrt(fabs(x[6]-x[7]));
a[2][7]=-a[2][6];
a[2][11]=-cdk12*sqrt(fabs(x[6]-x[7]));
a[3][6]=-0.5*cdk10*x[12]/sqrt(fabs(x[6]-p0));
a[3][12]=-cdk10*sqrt(fabs(x[6]-p0));
a[4][7]=-0.5*cdk2n*x[13]/sqrt(fabs(x[7]-x[8]));
a[4][8]=-a[4][7];
a[4][13]=-cdk2n*sqrt(fabs(x[7]-x[8]));
a[5][8]=-0.5*cdkanc/sqrt(fabs(x[8]-pc));
a[10][7]=x[19];
a[10][8]=x[20];
a[10][19]=x[7];
a[10][20]=x[8];
a[14][10]=2.0*pi*thth*(dpo/2-thth*x[10]);
a[19][9]=-2.0*b1*x[9]-b2;
a[20][10]=-2*c1*x[10]-c2;
```

```
/*-------------------------------------------------------------------*/
/* EVALUATE A [i][j] TRANSPOSE = [AT]                                */
/*-------------------------------------------------------------------*/

for (i=1;i<=n;++i) {
for (j=1;j<=n;++j) {
at[i][j]=a[j][i];
}
}

/*-------------------------------------------------------------------*/
/* MULTIPLY [A]x[AT]                                                 */
/*-------------------------------------------------------------------*/

m=r=l=20;
mul(a,at,axat,m,r,l);

for (i=1;i<=n;++i) {
for (j=1;j<=n;++j) {
aaa[i][j]=axat[i][j];
}
}

/*-------------------------------------------------------------------*/
/* EVALUATE COEFFICIENT VECTOR -F[i]                                 */
/*-------------------------------------------------------------------*/

f[1]=-(x[1]-cc2*x[6]+cc2*p0-(cc1*np+cc3));
f[2]=-(x[2]-cdk12*x[11]*sqrt(fabs(x[6]-x[7])));
f[3]=-(x[3]-cdk10*x[12]*sqrt(fabs(x[6]-p0)));
f[4]=-(x[4]-cdk2n*x[13]*sqrt(fabs(x[7]-x[8])));
f[5]=-(x[5]-cdkanc*sqrt(fabs(x[8]-pc)));
f[6]=-(x[1]-x[2]-x[3]);
f[7]=-(x[2]-x[4]);
f[8]=-(x[4]-x[5]);
f[9]=-(x[14]+x[15]-x[16]);
f[10]=-(x[19]*x[7]+x[20]*x[8]-kps*x[10]-kwps*(x[10]-zmax)-aa3*p0-fpo);
f[11]=-(x[14]-ade*x[6]+ade*x[7]);
f[12]=-(x[15]-x[17]-x[18]);
f[13]=-(x[16]-kbs*x[9]-kwbs*(x[9]-ymin)-fbo);
f[14]=-(x[20]-pi*pow(dpo/2.0-thth*x[10],2.0));
f[15]=-(x[19]+x[20]-aa3);
f[16]=-(x[17]-kf1/2*xmv[ml]+kf2/2);
f[17]=-(x[18]-kf1/2*xmv[ml]+kf2/2);
f[18]=-(x[11]-a1*xmv[ml]*xmv[ml]-a2*xmv[ml]-a3);
f[19]=-(x[12]-b1*x[9]*x[9]-b2*x[9]-b3);
f[20]=-(x[13]-c1*x[10]*x[10]-c2*x[10]);
```

```
/*-------------------------------------------------------------------*/
/* MULTIPLY -[AT]x[F]                                                */
/*-------------------------------------------------------------------*/

m=r=20;
mull(at,f,atxf,m,r);

/*-------------------------------------------------------------------*/
/* CALCULATE ERROR INDEX AND CHECK FOR CONVERGENCE                   */
/*-------------------------------------------------------------------*/

for(i=1;i<=n;++i) {
sum=sum+fabs(f[i]);
}

printf(" sum=%g ",sum);

if(sum<=0.00001) goto LL;

/*-------------------------------------------------------------------*/
/* CALL FUNCTION TO SOLVE THE SYSTEM OF EQUATIONS                    */
/* APPLY CORRECTION TO SOLUTION                                      */
/*-------------------------------------------------------------------*/

for (i=1;i<=n;++i) {
for (j=1;j<=n;++j) {
aaa[i][j]=a[i][j];
}
dx[i]=0.0;
bbb[i]=f[i];
}

MM:

sum1=0.0;

gs(a,f,err);

m=r=20;
mull(aaa,err,errbbb,m,r);

for (i=1;i<=n;++i) {
f[i]=bbb[i]-errbbb[i];
bbb[i]=f[i];
}

for (i=1;i<=n;++i) {
for (j=1;j<=n;++j) {
a[i][j]=aaa[i][j];
}
}
```

```
for (i=1;i<=n;++i) {
dx[i]=dx[i]+err[i];
sum1=sum1+fabs(err[i]);
/*printf("err=%g dx=%g\n", err[i],dx[i]);  */
}

printf(" sum1=%g ",sum1);
if (sum1 <=1.0e-6) goto MMM;

goto MM;

MMM:

printf("\n");

/*-------------------------------------------------------------------*/
/* UPDATE SOLUTION VECTOR X[i+1]=X[i]+DX[i]                          */
/*-------------------------------------------------------------------*/

for(i=1;i<=n;++i) {
x[i]=x[i]+lambda*dx[i];
}

goto LP;

LL:

/*-------------------------------------------------------------------*/
/* STORE AND DISPLAY RESULTS                                         */
/*-------------------------------------------------------------------*/

fprintf(fp,"%g %g %g %g %g %g %g %g %g %g %g\n",10.0*xmv[m1],10.0*x[9],
2.88*x[1],2.88*x[2],2.88*x[3],0.1*x[6],0.1*x[7],0.1*x[8],10.0*x[10],
100*x[13],x[16],x[15]);

printf("Xmv=%g[mm] y=%g[mm] z=%g[mm]\n A12=%g[mm2] A2n=%g[mm2] A10=%g[mm2]\n",
        10.0*xmv[m1],10.0*x[9],10.0*x[10],100*x[11],100*x[13],100*x[12]);
printf("A1=%g[mm] A2=%g[mm]\n",100*x[19],100*x[20]);
printf("Mp=%g[kg/hr] M12=%g[kg/hr] M10=%g[kg/hr]\n", 2.88*x[1],2.88*x[2],
        2.88*x[3]);
printf("Mnc=%g[kg/hr]  M2n=%g[kg/hr]\n", 2.88*x[5],2.88*x[4]);
printf("P1=%g[bars] P2=%g[bars] (P1-P2)=%g[bars]", 0.1*x[6],
        0.1*x[7],0.1*(x[6]-x[7]));
printf("Pn=%g[bars]\n", 0.1*x[8]);
printf("Fp=%g Fa1=%g Fa2=%g Fa=%g Fs=%g\n\n",x[14],x[17],x[18],x[15],x[16]);

}
}
```

```
/*================================================================*/
/* THIS FUNCTION USES GAUSS ELIMINATION (WITHOUT PIVOTING) TO     */
/* SOLVE THE SYSTEM AX=B. THE CALLING PROGRAM MUST SUPPLY THE     */
/* MATRIX A, THE VECTOR B AND AN INTEGER N (WHERE A IS (NxN)).    */
/* ARRAYS A AND B ARE DESTROYED IN GAUS, THE SOLUTION IS          */
/* RETURNED IN X AND A FLAG, IERROR, IS SET TO 1 IF A IS          */
/* NON-SINGULAR AND IS SET TO 2 IF A IS SINGULAR.                 */
/*----------------------------------------------------------------*/

gs(a,b,y)

long double a[RAW][COLUMN],b[RAW],y[RAW];

{

        long double temp,q;
        int nm1,i,j,k,np1,jj,ip1,nmk,iii;

        nm1=n-1;
        for (i=1;i<=nm1;++i) {

/*----------------------------------------------------------------*/
/* SEARCH FOR NON-ZERO PIVOT ELEMENT AND INTERCHANGE ROWS IF      */
/* NECESSARY. IF NO NON-ZERO PIVOT ELEMENT IS FOUND, SET          */
/* IERROR=2 AND RETURN.                                           */
/*----------------------------------------------------------------*/


                for (j=i;j<=n;++j) {
                if(a[j][i]==0.0) goto BR;
                        for(k=i;k<=n;++k) {
                        temp=a[i][k];
                        a[i][k]=a[j][k];
                        a[j][k]=temp;
                        }
                temp=b[i];
                b[i]=b[j];
                b[j]=temp;
                goto BG;
          BR:
                }
        goto BH;
```

```
/*-----------------------------------------------------------------*/
/* ELIMINATE THE COEFFICIENTS OF X(I) IN ROWS I+1,....,N           */
/*-----------------------------------------------------------------*/

        BG:

        ip1=i+1;
                for (k=ip1;k<=n;++k) {
                q=-a[k][i]/a[i][i];
                a[k][i]=0.0;
                b[k]=q*b[i]+b[k];
                        for(j=ip1;j<=n;++j) {
                        a[k][j]=q*a[i][j]+a[k][j];
                        }
                }
                }
        if(a[n][n]==0.0) goto BH;

/*-----------------------------------------------------------------*/
/* BACKSOLVE THE EQUIVALENT TRIANGULARIZED SYSTEM, SET IERROR=1,   */
/* AND RETURN                                                      */
/*-----------------------------------------------------------------*/

        y[n]=b[n]/a[n][n];
        np1=n+1;
                for (k=1;k<=nm1;++k) {
                q=0.0;
                nmk=n-k;
                        for (j=1;j<=k; ++j) {
                        q=q+a[nmk][np1-j]*y[np1-j];
                        }
                y[nmk]=(b[nmk]-q)/a[nmk][nmk];


                }

        ierror=1;

        goto GG;
     BH:
        ierror=2;
        GG:
}
```

```
/*=================================================================*/
/* THIS SUBPROGRAM MULTIPLIES MATRIX [D]mxr BY [E]rxn AND STORES   */
/* THE RESULT IN [F]mxn                                            */
/*-----------------------------------------------------------------*/

mul(d,e,f,m,r,l)

int m,r,l;
long double d[][COLUMN],e[][COLUMN],f[][COLUMN];

{

int i,j,k;

for (i=1;i<=m;++i) {
for (j=1;j<=l;++j) {
f[i][j]=0.0;
for (k=1;k<=r;++k) {
f[i][j]=f[i][j]+d[i][k]*e[k][j];
}
}
}

}


mull(d,e,f,m,r)

int m,r;
long double d[][COLUMN],e[RAW],f[RAW];

{

int i,j,k;

for (i=1;i<=m;++i) {
f[i]=0.0;
for (k=1;k<=r;++k) {
f[i]=f[i]+d[i][k]*e[k];
}
}

}
```

```
Model File: a:tr-dpf2.sim
Date:      1 /      1 /  2060
Time:      0 :     18
Timing:  10.000E-06  ,DELTA  ;   2.0000      ,RANGE
PlotBlocks and Scales:
Format:
     BlockNo,   Plot-MINimum,   Plot-MAXimum;   Comment
Horz:      0 ,    0.0000     ,    2.0000     ; Time
  Y1:    105 ,   40.0000     ,  140.0000     ;  105 [kg/hr] Wnc
  Y2:    100 ,    0.0000     ,   50.0000     ;  100 [bar] P1
  Y3:    103 ,    0.0000     ,    0.5000000  ;  103 [mm] y
  Y4:    102 ,    1.0000     ,    1.5000     ;  102 [bar] P1-P2m


                    1 SUM      -5       9          ;   1 P1-P0
                    2 MUL       1       6          ;   2 C2(P1-P0)
                    3 SUM     200       2     150  ;   3 Qp
                    4 SUM       3     -52     -43  ;   4 Qp-Q12-Q10-ADe(dy/dt)
                              -10
 200.000E+03        5 CON                          ;   5 [P0]
  -6.229E-12        6 CON                          ;   6 [C2]
  41.450E-09        7 CON                          ;   7 [C1]
  10.000E+12        8 GAI       4                  ;   8 dP1/dt=[B/V1]{4}
   1.101E+06        9 INT       8                  ;   9 P1=INT{8}+[P1o]
 309.680E-06       10 GAI      18                  ;  10 [ADe](dy/dt)
                   11 SUM       9     -13          ;  11 P1-P2b
 270.000E-06       12 GAI      11                  ;  12 Fbp+AfP1=[ADe](P1-P2b)
 955.643E+03       13 INT      14                  ;  13 P2b=INT{14}+[P2bo]
  50.279E+12       14 GAI      15                  ;  14 d(P2b)/dt=[B/V2b]{15}
                   15 SUM      19     -53          ;  15 ADe(dy/dt)-Q2b2m
                   16 SUM      12      23     -21  ;  16 F
                             -22
    0.0180000      17 ATT      16                  ;  17 dy2/dt2=F/[Me]
    0.0000         18 INT      17                  ;  18 dy/dt=INT(F/Me)+[(dy/dt)o]
 206.450E-06       19 GAI      18                  ;  19 [ADe](dy/dt)
 403.180E-06       20 INT      18                  ;  20 y=INT(dy/dt)+[yo]
   5.000E+03       21 GAI      20                  ;  21 [Kbs]
  32.0000          22 CON                          ;  22 [Fbo]
                   23 SUM      26     -27          ;  23 Fbf-AfP1=(kf1)(xd)-Kf2
    2.0000         25 PWR      20                  ;  25 y2
    7.407E+03      26 GAI     275                  ;  26 [Kf1](xd)
   10.2500         27 CON                          ;  27 [Kf2]
                   34 SQT       1                  ;  34 SQT(P1-P0)
                   35 SUM      36      37      38  ;  35 A10=b1y2+b2y+b3
    0.0115740      36 GAI      20                  ;  36 [b2]y
   -0.9096000      37 GAI      25                  ;  37 [b1]y2
    0.0000         38 CON                          ;  38 [b3]
 660.000E-06       39 CON                          ;  39 [xo]
                   40 SUM     310    -311          ;  40 Np
```

```
                42 MUL      35      34           ; 42 (b1y2+b2y+b3)SQT(P1-P0)
  0.0280000     43 GAI      42                   ; 43 Q10=[CdR]{42}
  0.0000        44 CON                           ; 44 [Pc]
                45 SUM     185      75     -44   ; 45 Pn+PL-Pc
 35.000E-09     46 GAI      60                   ; 46 Qnc=[CdKAnc]SQT(Pn+PL-Pc)
                47 SUM      52      53    -182   ; 47 Q12m+Q2b2m-Q2mn
  4.507E+12     48 GAI      47                   ; 48 [B/V2m](Q2b2m+Q12m-Q2mn)
955.643E+03     49 INT      48                   ; 49 P2m=INT{48}+[P2mo]
                50 SUM     -49       9          ; 50 P1-P2m
                51 SQT      50                   ; 51 SQT(P1-P2m)
                52 MUL      51     215           ; 52 Q12m=(CdKA12m)SQT(P1-P2m)
                53 MUL      54      57           ; 53 Q2b2m={57}{54}
 23.226E-09     54 GAI      55                   ; 54 [CdKA2b2m]SQT(¦P2b-P2m¦)
                55 SQT      56                   ; 55 SQT(¦P2b-P2m¦)
                56 ABS      13    -49            ; 56 ¦P2b-P2m¦
                57 SGN      13    -49            ; 57 SGN(P2b,-P2m)
                60 SQT      45                   ; 60 SQT(Pn+PL-Pc)
  0.0000        75 CON                           ; 75 [PL]
                79 REM
,             INPUT
                80 SUM      81      39     82    ; 80 x
  0.0000        81 PLS                           ; 81 [D(x1)]
  2.0000
680.000E-06
  1.0000        82 PLS                           ; 82 [D(x2)]
  2.0000
 -0.0012700
 20.000E-06     89 VDT                           ; 89 Dto/[Dt size factor]
  2.0000
  0.5000000
                99 REM
,       VARIABLES FOR PLOTTING
 10.000E-06    100 GAI       9                   ; 100 [bar] P1
 10.000E-06    101 GAI      49                   ; 101 [bar] P2
 10.000E-06    102 GAI      50                   ; 102 [bar] P1-P2m
  1.000E+03    103 GAI      20                   ; 103 [mm] y
  2.880E+06    104 GAI       3                   ; 104 [kg/hr] Wp
  2.880E+06    105 GAI      46                   ; 105 [kg/hr] Wnc
  2.880E+06    106 GAI      43                   ; 106 [kg/hr] W10
  1.000E+03    107 GAI      80                   ; 107 [mm] (x)
  1.0000       108 GAI      40                   ; 108 [rpm] Np
  1.000E+03    109 GAI     275                   ; 109 [mm] (xd)
-23.793E-06    150 CON                           ; 150 [C3]
                160 REM
,       PRESSURIZING VALVE
                162 SUM     175     176    -177   ; 162 Fnet
                           -167    -330    -331
```

```
                                -355
   0.0180000      163 ATT       162                    ; 163 d2z/dt2=Fnet/Mp
   0.0000         164 INT       163                    ; 164 INT(Fnet/Mp)+(dz/dt)o
 210.190E-06      165 INT       164                    ; 165 z=INT(dz/dt)+zo
  16.600E+03      167 GAI       165                    ; 167 [kps]
                  168 MUL       165     169            ; 168 [thth]z
   0.4330000      169 CON                              ; 169 [thth]
   0.0019200      170 CON                              ; 170 [Dpo/2]
                  171 SUM       170     -168           ; 171 Dpo/2=(thth)z
   2.0000         172 PWR       171                    ; 172 {171}2
   3.1416         173 CON                              ; 173 [pi]
                  174 MUL       172     173            ; 174 A2=(pi){172]
                  175 MUL       174     185            ; 175 Fp2=(A2)Pn
                  176 MUL        49     178            ; 176 Fp1=(A1)P2m
  45.0000         177 CON                              ; 177 [Fpo]
                  178 SUM       179     -174           ; 178 A1=A3-A2
  70.880E-06      179 CON                              ; 179 [A3]
                  180 SUM        49     -185           ; 180 P2m-Pn
                  181 SQT       180                    ; 181 SQT(P2m-Pn)
                  182 MUL       181     186            ; 182 (CdKA2mn)SQT(P2m-Pn)
                  183 SUM       182     -46            ; 183 Q2mn-Qnc
   1.500E+12      184 GAI       183                    ; 184 [B/Vn](Q2mn-Qnc)
 473.131E+03      185 INT       184                    ; 185 P2m=INT{184}+[P2mo]
   0.0280000      186 GAI       190                    ; 186 [CdK2mn]A2mn
   0.0060310      187 GAI       165                    ; 187 [c2]z
   2.0000         188 PWR       165                    ; 188 z[2]
  -0.6802000      189 GAI       188                    ; 189 [c1]z2
                  190 SUM       187     189            ; 190 c1z2+c2z
                  200 MUL         7      40            ; 200 [C2]Np
                  201 REM
,       METERING VALVE AREA
   2.0000         202 PWR       275                    ; 202 [xd]2
  -0.4524300      203 GAI       202                    ; 203 [a1](xd)2
   0.0063130      204 GAI       275                    ; 204 [a2](xd)
                  205 SUM       203     204     206    ; 205 (A12m)3=a1(xd)2+a2(xd)+a3
  -3.547E-06      206 CON                              ; 206 [a3]
                  207 SUM       208     210     209    ; 207 (A12m)2=a1(xd)2+a2(xd)+a3
-549.165E-09      208 CON                              ; 208 [a3]
   0.0043760      209 GAI       275                    ; 209 [a2](xd)
  -0.2615000      210 GAI       202                    ; 210 [a1](xd)2
 533.400E-06      211 REL       216     216     212    ; 211 A12m=(A12m)1 or (A12m)2,3
                                275
                  212 SUM       213     214            ; 212 (A12m)1=a1(xd)2+a2(xd)
   0.0032840      213 GAI       275                    ; 213 [a2](xd)
  -0.1549000      214 GAI       202                    ; 214 [a1](xd)2
   0.0283300      215 GAI       211                    ; 215 [cdK12m]
   0.0019050      216 REL       205     205     207    ; 216 A12m=(A12m)2 or (A12m)3
                                275
                  258 REM
,       STEPPER MOTOR RESPONSE
                  260 TIM
   1.0000         261 REL       340     341     341    ; 261 sec/step
                                260
   1.0000         262 REL       342     343     343    ; 262 sec/step
```

```
                                260
  12.500E-06      263 ATT        80                    ;263 [STEP SIZE]
                  264 MAX      -262     -273
                  265 SUM       302     -277
   0.5000000      270 CON                              ; 270 [HALF STEP]
                  271 SUM       265      270
                  272 FIX       271                    ; 272 INTEGER No OF STEPS
                  273 SUM       263     -274
   52.8000        274 CON                              ; 274 [No]
  12.500E-06      275 GAI       272
                  276 MIN       279     -273
    0.0000        277 REL       264      264      276
                                273
  900.0900        278 CON                              ; 278 [(STEPS/SEC)2 (t2)]
                  279 SUM       262     -278
   52.8000        300 CON                              ; 300 [No]
  107.2000        301 CON                              ; 301 [No+D(x)/(STEP SIZE)]
    0.0000        302 REL       300      300      301
                                273
   4.265E+03      310 CON                              ; 310 [Npo]
                  311 MUL       312      275          ; 311 Kn(xd)
 115.385E+03      312 CON                              ; 312 [Kn]
                  330 MUL       179        5          ; 330 (A3)P0
   40.0000        331 GAI       164                   ; 331 (ZETA)p
    0.0011110     340 SPL       260                   ; 340 [SEC/STEP] for (dx/dt)2
    0.0017000     341 SPL       260                   ; 341 [SEC/STEP] for (dx/dt)1
    0.0011110     342 ATT       261                   ; 342 [SEC/STEP] for (dx/dt)2
    0.0017000     343 ATT       261                   ; 343 [SEC/STEP] for (dx/dt)1
    0.0000        350 CON                              ; 350 [kwps]
   10.000E+06     351 CON                              ; 351 [kwps]
  400.000E-06     352 REL       351      351      350  ; 352 SELECT kwps
                                165
  400.000E-06     353 CON                              ; 353 [zmax]
                  354 SUM       165     -353          ; 354 z-zmax
                  355 MUL       352      354          ; 355 kwps(z-zmax)
                  400 REM
,       BLOCKS FOR INITIAL CONDITIONS INPUT:
                  401 REM
,       9=P1,13=P2b,20=yo,39=xo,165=zo,185=Pn
                  402 REM
,       274=No,278=(STEPS/SEC)2(t2),300=No
                  403 REM
,       301=[No+D(x)/(STEP SIZE)],310=Npo
                  404 REM
,       49=P2m,340=(SEC/STEP)2,341=(SEC/STEP)1
                  405 REM
,       342=(SEC/STEP)2,343=(SEC/STEP)1
                  406 REM
,       261=t2,262=t2
```